Trafficking and surface exposure of the metalloprotease MT1-MMP in macrophages

Dissertation zur Erlangung des Doktorgrades
an der Fakultät für Mathematik Informatik, und Naturwissenschaften
Fachbereich Biologie
der Universität Hamburg

vorgelegt von
Karim EL AZZOUZI
aus Taza (Marokko)

Hamburg, 2016

Die vorliegende Arbeit wurde von März 2010 bis September 2016 unter Anleitung von Prof. Dr. Stefan Linder am Institut für Medizinische Mikrobiologie, Virologie und Hygiene am Universitätsklinikum Hamburg-Eppendorf durchgeführt.

Die vorliegende kumulative Dissertation umfasst Arbeiten aus den folgenden zwei Publikationen:

Metalloproteinase MT1-MMP islets act as memory devices for podosome reemergence.
El Azzouzi K, Wiesner C, Linder S.
J Cell Biol. 2016 Apr 11;213(1):109-25. doi: 10.1083/jcb.201510043.

A specific subset of RabGTPases controls cell surface exposure of MT1-MMP, extracellular matrix degradation and three-dimensional invasion of macrophages.
Wiesner C, El Azzouzi K, Linder S.
J Cell Sci. 2013 Jul 1;126(Pt 13):2820-33. doi: 10.1242/jcs.122358. Epub 2013 Apr 19.

Dissertation zur Erlangung des Doktorgrades
Im Fachbereich Biologie
der Universität Hamburg
vorgelegt von
Karim EL AZZOUZI (M.Sc.)
aus Taza (Marokko)

Dissertationsgutachter : Prof. Dr. Stefan Linder
Prof. Dr. Wolfgang Streit

Disputationsgutachter : Prof. Dr. Stefan Linder
Prof. Dr. Wolfgang Streit
PD Dr. Andreas Pommerening-Röser

Tag der Disputation : 21 Dezember 2016

Table of contents

I. ABSTRACT

Macrophages are immune cells capable of migration and invasion through tissues. They can also associate with metastatic cancer cells and provide support through their matrix remodeling capacities and creation of migration tracks. In both scenarios, localized proteolytic degradation of the extracellular matrix is crucial.

The major topic of my PhD thesis was the investigation of trafficking and regulation of the metalloproteinase MT1-MMP, a central regulator of matrix degradation in macrophages. This thesis shows for the first time that MT1-MMP is localized at podosomes, actin-rich matrix-degrading organelles in macrophages. Moreover, podosome dissolution induced formation of MT1-MMP dot-like structures embedded in the plasma membrane called “islets”. They are free of typical podosome-components and persist beyond podosome lifetime. Also, islets constitute a preferential site for reemergence of podosomes, revealing a new function of MT1-MMP as memory device for the reformation of podosomes. This mechanism is completely independent of the proteolytic activity of MT1-MMP. I also showed that the cytoplasmic tail of MT1-MMP and precisely the small peptide LLY^{573} is responsible for its localization at podosomes. The LLY^{573} motif ensures this localization thanks to its capacity to bind subcortical actin cytoskeleton.

In a second project, I also helped to investigate members of the RabGTPases family controlling cell surface exposure of MT1-MMP, extracellular matrix degradation and invasion of macrophages. We identified Rab5a, Rab8a and Rab14, as crucial regulators of MT1-MMP trafficking and function in human macrophages. Depletion of these RabGTPases as well as overexpression of dominant negative and positive mutants showed that Rab5a, Rab8a and Rab14 do regulate cell surface exposure of MT1-MMP, contact of MT1-MMP-positive vesicles with podosomes, matrix degradation in 2D and also 3D proteolytic cell invasion. These results provide a detailed understanding of MT1-MMP trafficking and of the molecular mechanisms regulating podosome-mediated matrix degradation and proteolytic cell invasion.

II. INTRODUCTION

1. Macrophages

Macrophages are professional phagocytic cells[1] of the immune system due to their efficiency in phagocytosis. They are derived from primary monocytes circulating in the blood stream. They are responsible for the phagocytosis of pathogens and apoptotic cells[2]. Macrophage precursors (monocytes) are recruited to tissues after infection and/or tissue damage in order to differentiate into macrophages[1]. Primary human macrophages are capable of exposing multiple receptors on their surfaces to signal tissue damages[3]. Tissue injuries induce an inflammatory response leading to the recruitment of macrophages.

The ability of cells to invade tissues is a key feature in both physiological and pathological conditions where macrophages play the role of the immune sentinel in the human body. Based on their functional phenotype and anatomical localization in the organism, macrophages can be divided into multiple subpopulations.

1.1 Tissue resident macrophages

Macrophages are present in several tissues under normal physiological conditions, in contrast to those recruited during inflammation or infection. They are found in the brain (microglia)[4], in the skin (Langerhans cells)[5], in the lung (alveolar macrophages) and in the liver (Kupffer cells)[6]. By clearing cell debris of erythrocytes and apoptotic bodies, macrophages play also an important homeostatic function beside their tissue remodeling function. They can degrade up to 3 kg of iron and haemoglobin per year[7], which is reused by the organism through catabolic pathways.
They also have the capacity of recruiting additional macrophages originating from the blood stream by secreting chemo-attractant molecules[8].

1.2 Tumor associated macrophages (TAMs)

Macrophages can associate with cancer cells to form TAMs, they are generally derived from circulating monocytes[9]. They can be recruited by a gradient of chemokines such as macrophage-colony stimulating factor (M-CSF)[10], promoting proliferation and cell survival.

TAMs have the capacity to kill tumor cells *in vitro* when stimulated. However, *in vivo*, the increase in macrophages infiltrating tumors is highly correlated with high vessel density and tumor progression[11].

Polarized and activated macrophages can be divided in 2 subgroups: M1 and M2 macrophages. This classification illustrates the plasticity of the innate immune system, and its capacity to adapt to changes in the environment and stimuli. They secrete different set of cytokines and express different receptors, as mentioned below. TAMs are poor producers of nitric oxide (NO) and reactive oxygen intermediates ROIs[12], which is a very similar pattern to M2 macrophages.

1.3 M1 macrophages

The first response to infection or tissue injury is mediated by macrophages through a pro-inflammatory response. Upon activation, these macrophages can mediate defense of the host. This response is induced by factors such as interferon-γ and Lipopolysaccharide (LPS). They intervene in the early phases of tissue repair. They initially secrete pro-inflammatory factors such as (tumor necrosis factor-α (TNF-α)), interleukins: IL-1, IL-6, and IL-23[13] and increase the concentration of oxygen and nitrogen species responsible of the M1 microbicidal activity in the innate immune response. This leads to the phagocytosis and killing of invading pathogens.

If the activation of M1 macrophages is not well regulated, this can lead to pathologies such as autoimmune diseases and chronic inflamation[13].

1.4 M2 macrophages

M2 macrophages are defined as anti-inflammatory macrophages; they tune inflammatory responses and T helper cell type 1 (Th1) immunity. M2 macrophages can be induced by interleukins (IL-13[14] and IL-4)[15]. They secrete anti-inflammatory cytokines (IL-10, transforming growth factor β (TGF-β), and IL-1 receptor antagonist (IL-1Ra))[16]. This is antagonizing the role of M1 macrophages. Indeed, M2 macrophages scavenge debris, promote tissue remodeling and angiogenesis of the damaged tissues.

M2 macrophages form a heterogeneous group that can be subdivided into M2a, M2b, and M2c[17] macrophages based on their phenotype and functional properties. M2a macrophages can be activated by exposure to IL-4 or IL-13 and possess tissue repair and immunoregulating features. M2b are stimulated by immune complexes,

Toll-like receptor (TLR), or the IL-1 receptor antagonist (IL-1ra)[18]. M2c macrophages are stimulated by IL-10 or glucocorticoids[19] (**Figure 1**).

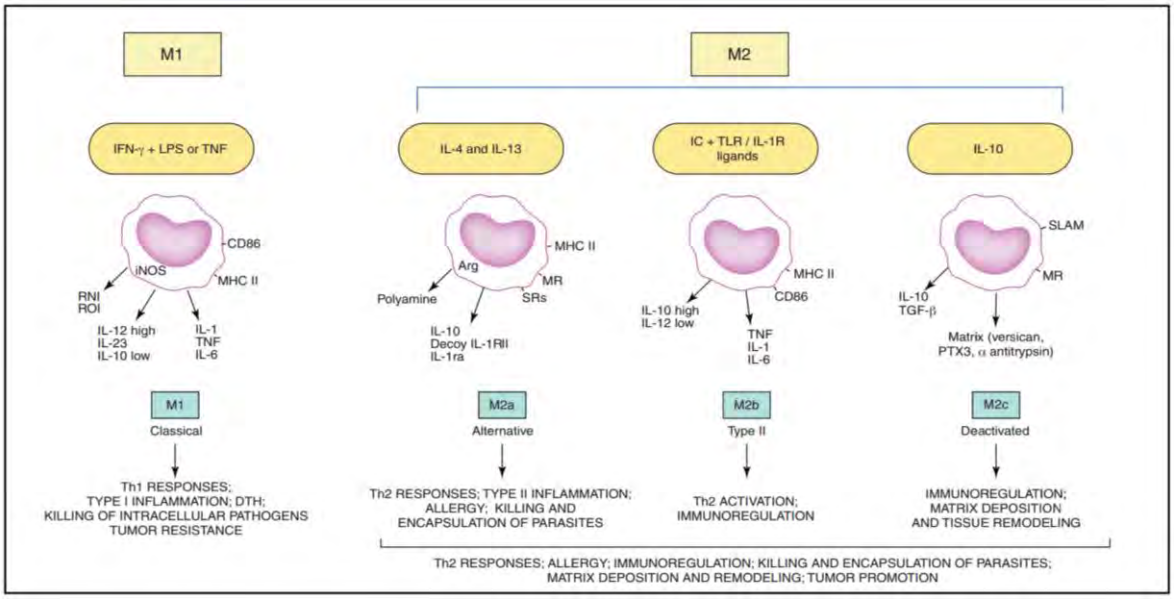

***Figure 1. Model for M1/M2 macrophages differentiation**. Mantovani and colleagues[17] proposed a model in which exposure of M1 Macrophages to IFN-γ and LPS drives M1 polarization, whereas M2 macrophages are in general more prone to immunoregulatory and protumoral activities. M2a macrophages (induced by exposure to IL-4 and IL-13) and M2b (induced by combined exposure to immune complexes and TLR or IL-1R agonists) exert immunoregulatory functions, whereas M2c macrophages (induced by IL-10) are more related to suppression of immune responses and tissue remodeling[17].*

2. Podosomes

Macrophages are able to adhere and migrate in tissues thanks to actin rich structures called podosomes. Initially described in Rous sarcoma virus transformed fibroblasts in 1985[20], podosomes have been intensley investigated since. Podosomes share similar chemical and structural characteristics with focal adhesions[21]. Podosomes and invadopodia form the group of invadosomes[22]. Podosomes can be found in macrophages[23], dendritic cells[23] and osteoclasts[24]. Upon cytokine[25] stimulation such as transforming growth factor beta (TGF-β)[26], podosomes can also be formed in endothelial cells[26].

Podosomes show a dot like pattern on the ventral side of the cell, with a diameter of 1 µm. Individual podosomes are composed of three distinct parts, an actin rich core enriched in actin-related protein2/3 (Arp2/3) complexes and F-actin associated proteins[27], a ring protein complex surrounding the core and containing the so called adhesion plaque proteins (talin, vinculin, paxillin)[28] and β2 and β3 integrins[29,22], and finally a cap on top of the F-actin core with the presence of the formin FMNL1[30] and supervillin[31] as described in **Figure 2**[32].

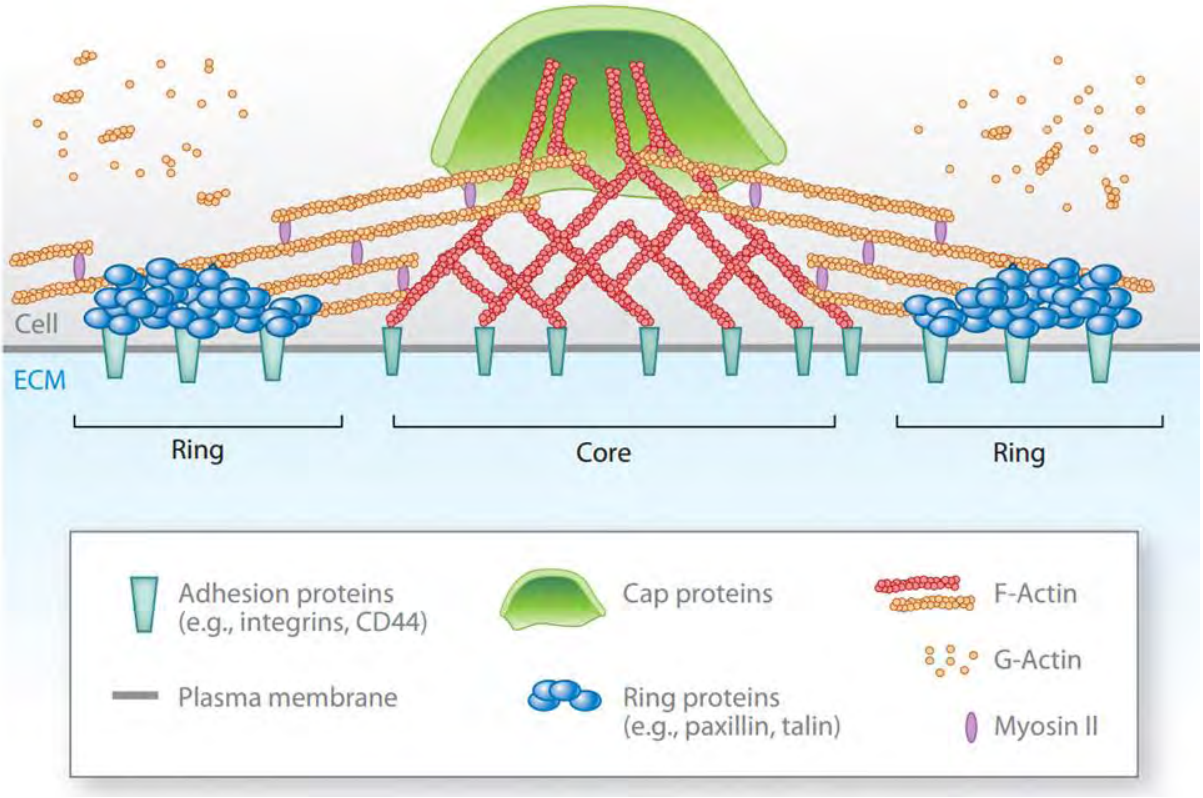

***Figure 2. Detailed model of podosome substructures**. The core contains branched F-actin (red) surrounded by possibly unbranched actin filaments (orange) bundled by myosin II (purple), a cap structure on top of the actin core (green), and the surrounding ring structure (blue). Contact to the extracellular matrix (ECM) is established by integrins and CD44 (teal). A surrounding cloud of G- and F-actin is located above the podosome*[32].

Podosomes are multifunctional organelles that combine several key functions of invasive cells, including adhesion, sensing of rigidity and topology of the substratum, as well as matrix degradation[33,32]. Podosomes are capable of degrading the underlying matrix. The presence of podosomes at the leading edge of macrophages highlights their potential involvement in the directional migration of macrophages.

2.1 Podosome regulation

Podosomes are highly dynamic organelles with a life time of 2-12 minutes[24] and they undergo constant rearrangement, including *de novo* formation, fusion and fission with the neighbouring podosomes, growth and dissolution[34]. Podosome dynamics and functions are regulated by a complex network of proteins. This necessitates spatiotemporal coordination of actin nucleation at podosome cores, growth of the actin network as well as its modulation by bundling and crosslinking proteins, and also severing of actin filaments to induce podosome turnover[32]. Moreover, even under steady state conditions, podosomes also show internal dynamics, as 1) actin in the podosome core is turned over ca. 3 times within the life span of a single podosome[24], and 2) podosomes undergo internal cycles of stiffness, which is probably based on actin bundling and myosin contractility[35]. Rigidity of the substrate can also affect podosome lifetime and density, for example, substrate rigidity positively correlates with the lifetime and stability of individual podosomes and podosome rosettes in 3T3 fibroblasts[36].

In order to degrade the matrix, cells in general and macrophages in particular need proteases capable of cleaving collagen fibers to allow free movement of the cell. To achieve this purpose, macrophages secrete matrix metalloproteases (MMPs). These enzymes are capable of cleaving a large variety of substrates including collagen, fibronectin and laminin which are present in tissues and basal membrane.

3. Matrix Metalloproteases (MMPs)

MMPs form a family of zinc-dependent endopeptidases with 23 human proteases[37](**Figure 3**). MMPs can be divided, according to their localization, into soluble versus membrane bound MMPs. Membrane MMPs or MT-MMPs form a subgroup of 6 proteases. Another distinction can be made according to their substrate specificity.

They share a broad spectrum of substrates and are thus collectively capable of degrading the basement membrane and all components of the ECM[38], but not every MMP is capable of cleaving each of the ECM substrates. MMPs can degrade collagen, laminin, elastin, fibronectin and aggregan. Among MMPs, we find specific collagenases, gelatinases (MMP-2 and MMP-9), matrilysin and elastases. ECM components are not the only substrates of MMPs. In fact, MMPs can process cellular

receptors and transmembrane proteins such as E-cadherin, integrins and cytokines involved in cell signaling pathways, angiogenesis and adherence.

MMPs play a crucial role in physiological and pathological conditions including arthritis, tumor growth and metastasis[39], which make them a perfect target for drug development, but the use of broad spectrum inhibitors of MMPs catalytic activity failed in clinical trials. In fact, several MMPs can play a paradoxical role when it comes to tumor progression[40] highlighting the necessity of a clearer understanding of the proteases' pathway.

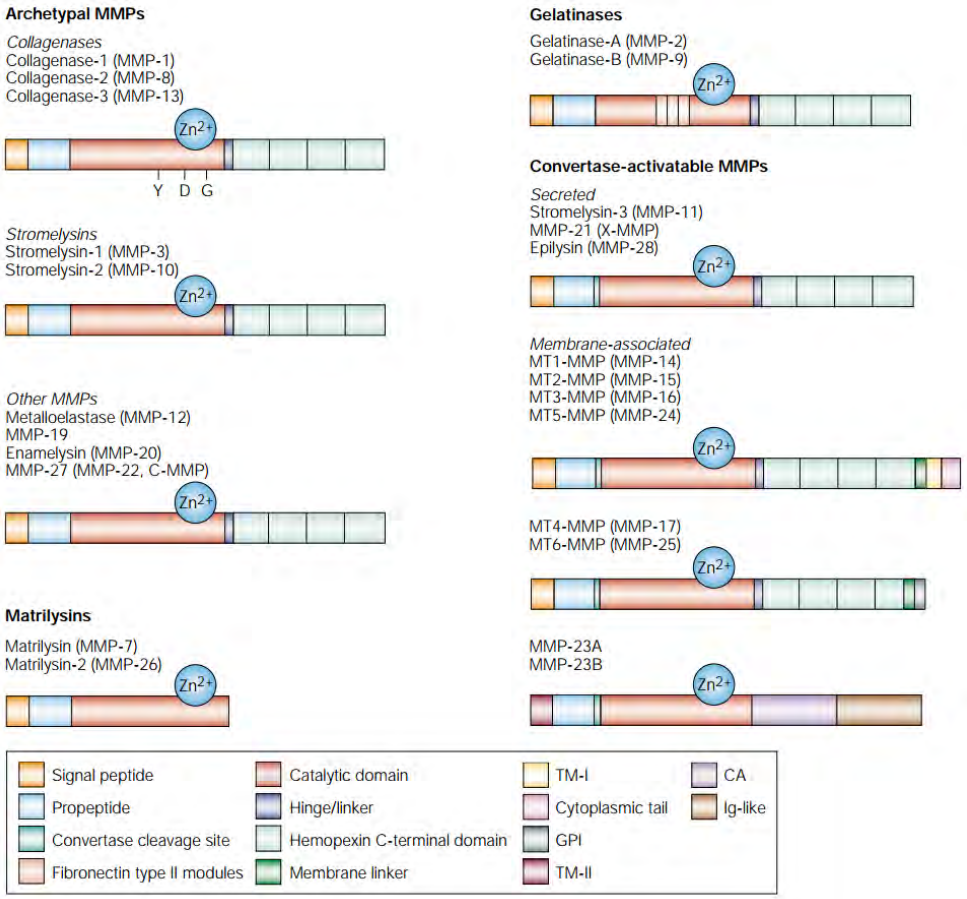

***Figure 3. Human MMPs**: Schematic representation of the structure of the 24 human matrix metalloproteases (MMPs), which are classified into four different groups on the basis of domain organization. Archetypal MMPs contain a signal peptide (necessary for secretion), propeptide, a catalytic domain that binds zinc (Zn2+) and a hemopexin carboxy (C)-terminal domain. Matrilysins contain the minimal domain organization that is required for secretion, latency and catalytic activity. Gelatinases contain fibronectin type II modules that improve collagen and gelatin degradation efficiency. Convertase-activatable MMPs contain a basic insert in the propeptide that is targeted by furin-like proteases (convertase cleavage site). MMPs that belong to this group can be secreted enzymes, or membrane-anchored via GPI (glycosylphosphatidylinositol), type I or type II transmembrane (TM) segments. MMP-23A and MMP-23B contain unique cysteine array (CA) and immunoglobulin(Ig)-like domains in their C-terminal region [41].*

3.1 Soluble MMPs and MMP activation

Secreted MMPs form the majority of MMPs with 17 members. They share the conserved zinc-binding motif in their catalytic active site. They are expressed as pro-proteins, which are the latent form of MMPs called zymogen. The zymogen is cleaved to form active MMPs as shown in **Figure 4**. In the proximity of the C-terminus of the catalytic site, the pro-protein harbours a conserved cysteine switch sequence. This cysteine switch sequence can interact with the zinc ion present in the active site inducing a change in the conformation of the protease.

This conformation change can be initiated by three mechanisms: 1) removal of the pro-domain by direct cleavage of another endoproteinase; 2) allosteric reconformation of the pro-domain; and 3) chemical modification of the free cysteine by reactive oxygen species or non physiological agents[42]. To ensure a balanced matrix turnover, cells produce tissue inhibitors of metalloproteases (TIMPs) that bind to MMPs and negatively regulate MMPs activity. The inhibition of MMP activity is operated by the chelation of the catalytic zinc atom in a molar ration of 1:1[42].

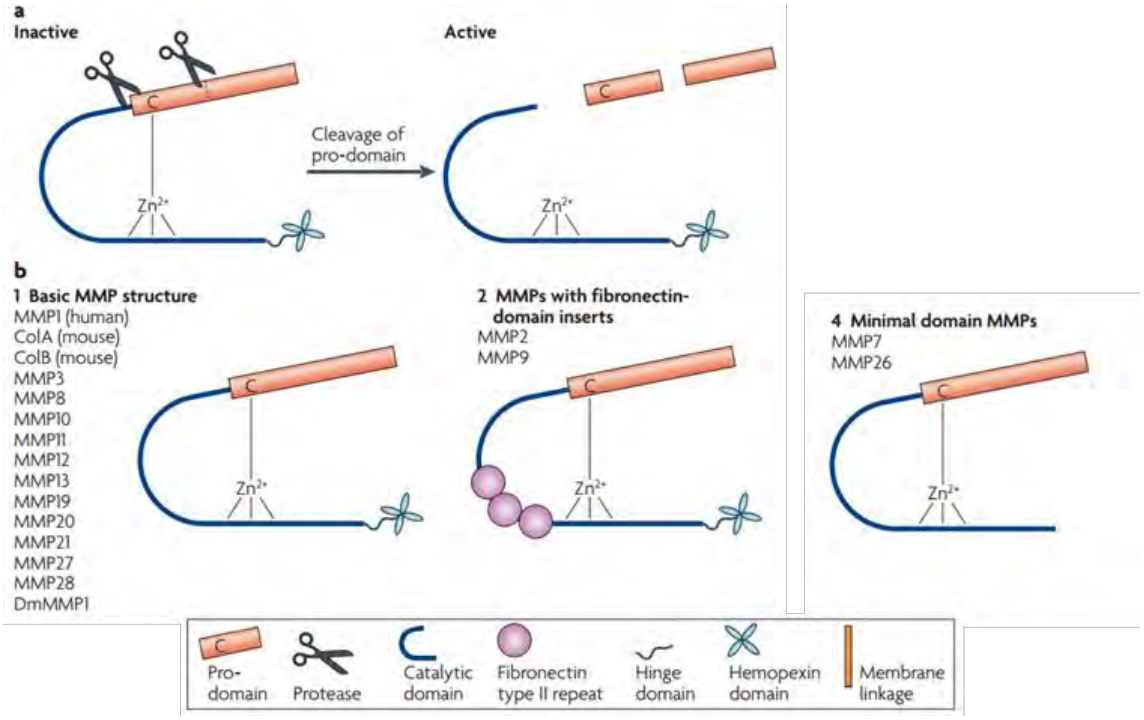

Figure 4. Schematic structure of MMPs*. a/ Matrix metalloproteases (MMPs) are expressed as pro-proteins. A conserved Cys residue in the pro-domain coordinates the zinc ion, which would otherwise be used for catalysis. The pro-domain is removed by a combination of a cleavage in the domain and a cleavage between the pro-domain and the catalytic domain. b/ Most MMPs share a conserved domain structure of pro-domain, catalytic domain, hinge region and hemopexin domain (1). All MMPs are synthesized with a signal peptide, which is cleaved during transport through the secretory pathway. MMP2 and MMP9 have three fibronectin type II repeats in their catalytic domains (2). Minimal MMPs lack the hinge and hemopexin domains (4)*[44].

3.2 Membrane anchored MMPs

Depending on the type of linker to the plasma membrane, this group can be subdivided into transmembrane tethered enzymes which are MT1-MMP, MT2-MMP, MT3-MMP, and MT5-MMP. MT4-MMP and MT6-MMP form the second group which is anchored to the membrane via a glycophosphatidylinositol (GPI) anchor. Beside their usual ECM substrates, MT-MMPs are capable of cleaving secreted MMPs and other soluble factors. For example cleavage of proMMP-2 by MT2-MMP[45], leading to an active form MMP-2.

4. Membrane Type 1-Matrix Metalloprotease (MT1-MMP)

4.1 MT1-MMP functions

MT1-MMP is a transmembrane protease, it was identified as the first membrane tethered MMP[46]. MT1-MMP was reported to be expressed in several cell types including macrophages, fibroblasts, osteoclasts[47] and endothelial cells[48].

Collagen forms the most abundant extracellular matrix in the human body and is mainly secreted by fibroblasts. Through its fibrillar form, collagen forms a scaffold that shapes the form of the ECM.

To achieve migration through the highly dense matrix and connective tissue, cleavage of collagen fibers is a necessary initial step for macrophages, to protrude and migrate toward their target. MT1-MMP create a path for cell migration by cleaving collagen I, II, III, fibronectin, and laminin I[49].

MMP-1 (collagenase I), MMP-8 (collagenase 2), MMP-13 (collagenase 3), MMP-2 (gelatinase A), and MT1-MMP are the five major human collagenases[50].

MT1-MMP is involved in the processing of the triple helical collagen type I, modulation of transmembrane receptors such as cluster of differentiation 44 (CD44), and other ECM components[51]. MT1-MMP is also capable of activation of the collagenase MMP-2[52] and MMP-13[53], which means that three out of the five major MMP collagenases are regulated by MT1-MMP, showing its capacity to trigger multiple proteinase cascades and pericellular proteolysis through its surface exposure.

The suggested model explaining the activation of proMMP-2 starts initially by the formation of a MT1-MMP homodimer. Once the homodimer is formed, MT1-MMP interacts with TIMP-2, which plays a role of a linker between MT1-MMP and proMMP-2. In fact TIMP-2 brings proMMP-2 in close contact to MT1-MMP to form a tertiary complex. Once the complex is formed, MT1-MMP processes proMMP-2, leading to the liberation of an active MMP-2 and the dissolution of the complex[54].

Unlike several individual MMPs knockout mice strains (MMP-2, MMP-3, MMP-7, MMP-9 and MMP-12) which have little effect on impairment of development and reproduction[55], MT1-MMP depletion seem to affect a wide variety of functions. MT1-MMP deficient mice suffer from craniofacial dysmorphism, arthritis, osteopenia,

dwarfism, and fibrosis of soft tissues[55] with defective angiogenesis leading to a premature death after 7 to 12 weeks[40]. This phenotype is due to the lack of MT1-MMP collagenolytic activity, which ensures the modeling of skeletal and extraskeletal connective tissues in the wildtype. These results highlight the importance of this protease during angiogenesis and embryogenesis. MT1-MMP was localized in human invasive breast carcinomas which have a tendency to form spontaneous metastasis[56]. MT1-MMP overexpression is associated in many tumor cell lines with aggressive and invasive malignancies[57].

Among the unconventional substrates of MT1-MMP is pericentrin, a centrosomal protein essential to the normal functioning of centrosomes in the mitotic spindle formation. In the pericentrosomal compartment, a fraction of cellular MT1-MMP accumulates and degrades pericentrin. MT1-MMP proteolysis of pericentrin causes chromosome instability, which is an early predictor of carcinogenesis[58]. MT1-MMP is thus not simply a protease responsible of the cleavage of collagen or other ECM components, it can be also involved in chromosome stability, neovessel formation in a collagen-based matrix[59] and can be used as a landmark for podosome reformation as it is shown in this work.

MT1-MMP is finely regulated at several levels. It is regulated at the transcriptional level, posttranscriptional level through activation by furins and inhibition by TIMPs, and also via traffic regulation where MT1-MMP vesicles can be fused, internalized and recycled depending on the type of motor proteins and Rab GTPases.

4.2 MT1-MMP domains

MT1-MMP contains a cytoplasmic tail, a single transmembrane domain and an extracellular domain containing the hemopexin (Hpx) and the catalytic domain connected by a hinge region also called linker L1. The catalytic domain contains a Glu-240 residue involved in the collagenolytic activity (**Figure 5**). Migration of epithelial cells[60] and fibroblasts[61] was reported to be severely impaired when MT1-MMP catalytic activity was inhibited.

Prior to its plasma membrane insertion, MT1-MMP is initially cleaved by furins, serine proteinases of the trans-Golgi network in order to activate MT1-MMP[62] and remove the N-terminal propeptide domain. The proprotein convertases (PCs) recognize the motif PRKR present between the pro and the catalytic domain (**Figure 5**). The hemopexin domain is involved in the formation of MT1-MMP homodimers and the interaction with CD44, a widely expressed hyaluronan receptor, especially in invasive tumor cells. CD44 is a crucial player in cell migration[63], and MT1-MMP is capable of shedding CD44 ectodomain which leads to a modification of the cell adhesion pathway mediated by this receptor[64].

MT1-MMP is known to form oligomers. The formation of such homodimeric complexes is mediated mainly by the transmembrane domain, the hemopexin domain[65,27] and a disulfide bridge involving the Cys-574 of the enzyme's cytoplasmic tail that covalently links MT1-MMP monomers[66].

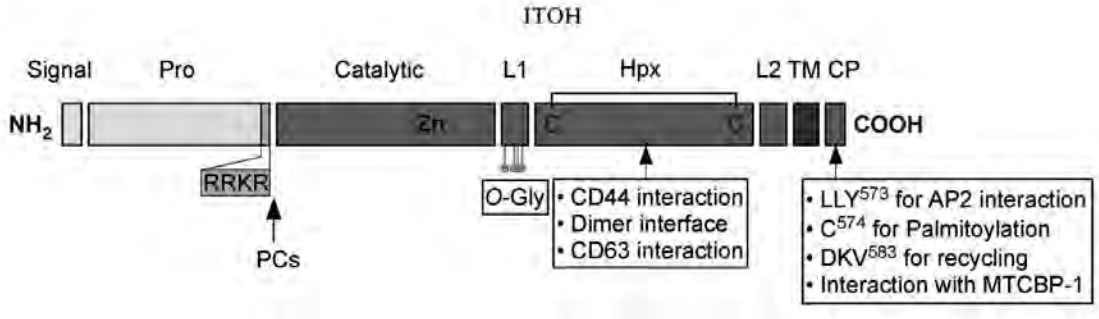

Figure 5. Domain features of MT1-MMP*. MT1-MMP is synthesized with a signal peptide (Signal), a prodomain (Pro) for latency, a catalytic domain (Catalytic) with catalytic zinc atom (Zn) for proteolytic activity, a linker-1 (L1), a hemopexin domain (Hpx), a linker-2 (L2), a transmembrane domain (TM), and a cytoplasmic tail (CP). The L1 connects Catalytic and Hpx domains. It has four O-glycosylation (O-Gly) sites which appear to be important for proMMP-2 activation. The Hpx domain has one disulfide bond connecting its N- and C-terminal Cysteines (C-C). The L2 connects Hpx and TM domains. The CP contains three defined sequences responsible for interaction with adaptor protein 2, which is important for clathrin-mediated internalization (LLY573), palmitoylation (Cys574), and recycling (DKV583)*[67]*.*

1. RabGTPases

Eukaryotic cells present a very dense cytoplasm rich in microtubules, and actin filaments network. In order to achieve accurate delivery of cargos in cells, and ensure proper communication between different cell compartments, cells need a group of proteins called RabGTPases (Ras-related proteins in brain). RabGTPases are described as the largest family of small GTPases[68], they play the role of a router of vesicles and membrane trafficking in the cell. They ensure delivery of cargoes to their correct destination in a very stringent way, despite the complexity of the interconnecting pathways.

5.1 Mechanism of RabGTPases

RabGTPases form a family of small GTPases/GTP-binding-proteins monomers. Mechanistically speaking, they ensure their functions by a conformational change. This conformational change occurs when GTP is hydrolyzed to GDP. RabGTPases activity is regulated by guanine nucleotide exchange factors (GEFs). GEFs act as a catalyzer for the exchange of GDP with GTP. The GTP hydrolysis activity is crucial for the correct routing of vesicles. Mutations affecting the GTPase activity by modifying GTP binding or hydrolysis lead to an accumulation of vesicles[69] as it was shown when dominant negative constructs were overexpressed for example in human macrophages[70].

RabGTPases are present on all compartments of the endomembrane system (endoplasmic reticulum (ER), Golgi, endosomes, lysosomes)[71]. They can be also found in the nucleus, mitochondria and the plasma membrane[72].

Among the 70 members of the RabGTPase family, each one seems to control a specific membrane transport pathway as shown in **Figure 6**. The majority of RabGTPases is localized toward a specific compartment/route. The rest of RabGTPases is present in the cytosol bound to the guanine dissociation inhibitor (GDI)[73]. The majority of RabGTPases are ubiquitously expressed in the human body, with exceptions like Rab27a, which is preferentially expressed in hematopoietic cells[74].

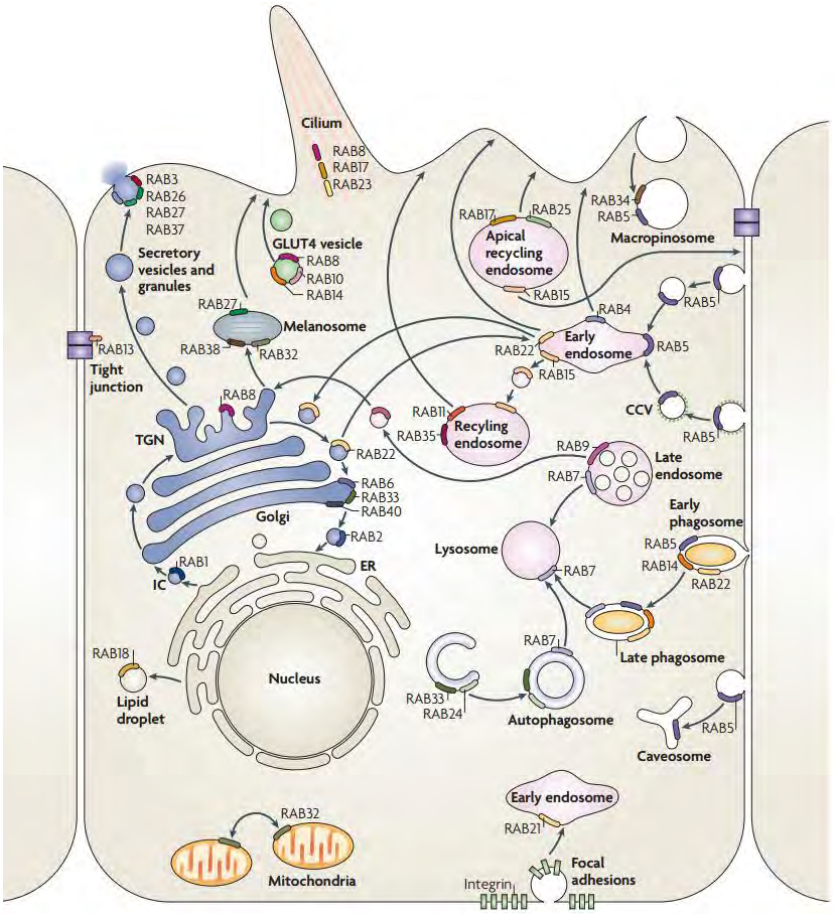

Figure 6. Localization and function of RabGTPases*. An epithelial cell with its vesicle transport pathways and the localizations of selected RabGTPases. RAB1, located at ER exit sites and the pre-Golgi intermediate compartment (IC), mediates ER–Golgi trafficking. RAB2, located at the IC, might also regulate Golgi–ER trafficking. The Golgi-localized RAB6, RAB33 and RAB40 mediate intra-Golgi trafficking. RAB33, together with RAB24, also regulates the formation of autophagosomes. RAB8 mediates constitutive biosynthetic trafficking from the trans-Golgi network (TGN) to the plasma membrane and also participates in GLUT4 vesicle translocation (with RAB10 and RAB14) and ciliogenesis (with RAB17 and RAB23). RAB3, RAB26, RAB27 and RAB37 mediate various types of regulated exocytic events and RAB27 also mediates the translocation of melanosomes to the cell periphery. RAB32 and RAB38 are involved in the biogenesis of melanosomes and RAB32 also controls mitochondrial fission. RAB13 regulates the assembly of tight junctions between epithelial cells. RAB18 controls the formation of lipid droplets. RAB22 mediates trafficking between the TGN and early endosomes (EE) and vice versa. RAB5, which is localized to early endosomes, phagosomes, caveosomes and the plasma membrane, mediates endocytosis and endosome fusion of clathrin-coated vesicles (CCVs), micropinocytosis (with RAB34) and maturation of early phagosomes (with RAB14 and RAB22). RAB21 mediates integrin endocytosis. RAB11 and RAB35 mediate slow endocytic recycling through recycling endosomes, whereas RAB4 mediates fast endocytic recycling directly from early endosomes. RAB15 is involved in the trafficking from early endosomes to recycling endosomes and in the trafficking from apical recycling endosomes to the basolateral plasma membrane. RAB17 and RAB25 control trafficking through the apical recycling endosomes to the apical plasma membrane. The late endosome-associated RAB7 mediates maturation of late endosomes and phagosomes, and their fusion with lysosomes. Another late endosomal GTPase, RAB9, mediates trafficking from late endosomes to the TGN*[68].

5.2 Functions of RabGTPases

RabGTPases regulate membrane trafficking, nuclear transport and regulation of the actin cytoskeleton. They are also involved in cell division[75], control of cell proliferation and differentiation. The role of RabGTPases in endocytosis and exocytosis is well studied. They ensure proper vesicle formation, vesicle delivery, and vesicle tethering and budding with its final destination. The specificity of targeting/routing of vesicles is achieved thanks to a post-translational addition of two C-20 geranylgeranyl groups, and to the steady state distribution of each RabGTPase within a single type of intracellular membrane[76]. The specific cellular localization of each RabGTPase ensures the correct routing of the cargo. In addition, the specificity is enhanced by the fact that even the RabGTPases that are sharing the same compartment, do localize at distinct microdomains specific for each RabGTPase called Rab domains[77,78].

The interaction between RabGTPases proteins and a set of effectors allows the regulation of a specific pathway. In general, the effectors have a higher affinity with the GTP-binding form of the RabGTPases[79]. For each step of vesicle formation, movement, tethering and fusion event, there is a different set of effectors involved in this pathway.

III. AIMS OF THE STUDY

1. Novel localization and function of MT1-MMP at podosomes.

On the ventral cell surface of macrophages, degradation of ECM appears primarily underneath podosomes[81]. MT1-MMP, a surface-anchored “master switch” protease, has been previously reported to be associated with podosomes[34]. However, its precise localization at podosomes was never demonstrated. Moreover the link between the degradative structure podosome and the collagenolytic activity of MT1-MMP needed to be clarified.

2. RabGTPases regulating MT1-MMP trafficking

This part of the study aimed to identify specific RabGTPases and their contribution to the regulation of MT1-MMP trafficking, extracellular matrix degradation and 3D invasion of macrophages. So far, Rab8a was reported to induce MT1-MMP exocytic traffic, collagen degradation and invasion in breast cancer cells[80]. However the implication of others RabGTPases remained unclear. Therefore, RabGTPases potentially regulating MT1-MMP cell surface exposure should be screened, and their impact on proteolytic activity and matrix degradation assessed.

IV. PUBLICATIONS

Metalloproteinase MT1-MMP islets act as memory devices for podosome reemergence.
El Azzouzi K, Wiesner C, Linder S.
J Cell Biol. 2016 Apr 11;213(1):109-25. doi: 10.1083/jcb.201510043.

p.21

A specific subset of RabGTPases controls cell surface exposure of MT1-MMP, extracellular matrix degradation and three-dimensional invasion of macrophages.
Wiesner C, El Azzouzi K, Linder S.
J Cell Sci. 2013 Jul 1;126(Pt 13):2820-33. doi: 10.1242/jcs.122358. Epub 2013 Apr 19.

p.49

The kinesin KIF9 and reggie/flotillin proteins regulate matrix degradation by macrophage podosomes.
Cornfine S, Himmel M, Kopp P, El Azzouzi K, Wiesner C, Krüger M, Rudel T, Linder S.
Mol Biol Cell. 2011 Jan 15;22(2):202-15. doi: 10.1091/mbc.E10-05-0394. Epub 2010 Nov 30.

p.79

Published April 11, 2016

This article has original data in the JCB Data Viewer
http://jcb-dataviewer.rupress.org/jcb/browse/11902

Metalloproteinase MT1-MMP islets act as memory devices for podosome reemergence

Karim El Azzouzi, Christiane Wiesner, and Stefan Linder

Institut für medizinische Mikrobiologie, Virologie und Hygiene, Universitätsklinikum Eppendorf, 20246 Hamburg, Germany

Podosomes are dynamic cell adhesions that are also sites of extracellular matrix degradation, through recruitment of matrix-lytic enzymes, particularly of matrix metalloproteinases. Using total internal reflection fluorescence microscopy, we show that the membrane-bound metalloproteinase MT1-MMP is enriched not only at podosomes but also at distinct "islets" embedded in the plasma membrane of primary human macrophages. MT1-MMP islets become apparent upon podosome dissolution and persist beyond podosome lifetime. Importantly, the majority of MT1-MMP islets are reused as sites of podosome reemergence. siRNA-mediated knockdown and recomplementation analyses show that islet formation is based on the cytoplasmic tail of MT1-MMP and its ability to bind the subcortical actin cytoskeleton. Collectively, our data reveal a previously unrecognized phase in the podosome life cycle and identify a structural function of MT1-MMP that is independent of its proteolytic activity. MT1-MMP islets thus act as cellular memory devices that enable efficient and localized reformation of podosomes, ensuring coordinated matrix degradation and invasion.

Introduction

Podosomes are dynamic, actin-rich adhesion structures in a variety of cell types, including macrophages (Linder et al., 1999), dendritic cells (Burns et al., 2001), osteoclasts (Destaing et al., 2003), endothelial cells (Osiak et al., 2005; Moreau et al., 2006), smooth muscle cells (Burgstaller and Gimona, 2005), and neural crest cells (Murphy et al., 2011). Together with the related invadopodia, they comprise the invadosome type of cell–matrix contacts (Linder et al., 2011; Murphy and Courtneidge, 2011).

Podosome-enabled cell invasion is thought to be involved in such diverse functions as immune cell surveillance (Wiesner et al., 2014), endothelial tubulogeneration (Obika et al., 2014), angiogenic sprouting (Rottiers et al., 2009; Seano et al., 2014), and cellular patterning during embryogenesis (Murphy et al., 2011). Accordingly, absence or impaired formation of podosomes has been implicated in a variety of diseases based on defects in cell migration and invasion such as Wiskott–Aldrich syndrome (Linder et al., 1999; Thrasher et al., 2000; Buschman et al., 2009), Frank-ter Haar syndrome (Iqbal et al., 2010), and PAPA (pyogenic arthritis, pyoderma gangrenosum and acne) syndrome (Cortesio et al., 2010; Starnes et al., 2014).

Podosomes display a bipartite architecture, with a core structure consisting of Arp2/3 complex–nucleated F-actin (Linder et al., 2000a) and actin-associated proteins (Linder and Aepfelbacher, 2003) and a ring structure containing adhesion plaque proteins such as vinculin, talin, and paxillin (Linder and Aepfelbacher, 2003). Podosomes are anchored to the substratum by cell–matrix adhesion proteins such as integrins (Zambonin-Zallone et al., 1989; Chellaiah, 2006; Luxenburg et al., 2012) and CD44 (Chabadel et al., 2007). Moreover, individual podosomes are connected by contractile actomyosin cables (Bhuwania et al., 2012; van den Dries et al., 2013a), reflecting the fact that podosomes are organized into higher-ordered groups. Podosomes are highly dynamic organelles with a lifetime of 2–12 min (Destaing et al., 2003). They can be formed de novo, through Arp2/3-dependent actin nucleation (Linder et al., 2000a), or by fission of preexisting podosomes (Evans et al., 2003; Kopp et al., 2006). Moreover, even in steady state, podosomal actin is being turned over approximately three times (Destaing et al., 2003), and the whole structure undergoes cycles of internal stiffness, based on actin turnover and actomyosin contractility (Labernadie et al., 2010).

Degradation of the ECM is a key function of podosomes. Accordingly, podosomes have been shown to recruit matrix-degrading enzymes such as matrix metalloproteinases and ADAMs (a disintegrin and metalloproteinase; Linder et al., 2011; Murphy and Courtneidge, 2011). In particular, the membrane-bound metalloproteinase MT1-MMP has emerged as a critical regulator of matrix degradation of both podosomes and invadopodia (Poincloux et al., 2009). Transport of MT1-MMP–positive vesicles along microtubules to podosomes has been demonstrated, and regulators of this transport, such as the motor proteins kinesin-1 and -2 (Wiesner et al., 2010) or the RabGTPases Rab5a, Rab8a, and Rab14 (Wiesner et al., 2013), have been identified. However, in contrast to invadopodia, actual enrichment of MT1-MMP at bona fide

Correspondence to Stefan Linder: s.linder@uke.de

Abbreviations used in this paper: PI(4)P, phosphatidylinositol 4-phosphate; TIRF, total internal reflection fluorescence.

© 2016 El Azzouzi et al. This article is distributed under the terms of an Attribution–Noncommercial–Share Alike–No Mirror Sites license for the first six months after the publication date (see http://www.rupress.org/terms). After six months it is available under a Creative Commons License (Attribution–Noncommercial–Share Alike 3.0 Unported license, as described at http://creativecommons.org/licenses/by-nc-sa/3.0/).

Supplemental Material can be found at:
http://jcb.rupress.org/content/suppl/2016/04/05/jcb.201510043.DC1.html
Original image data can be found at:
http://jcb-dataviewer.rupress.org/jcb/browse/11902

The Rockefeller University Press $30.00
J. Cell Biol. Vol. 213 No. 1 109–125
www.jcb.org/cgi/doi/10.1083/jcb.201510043

THE JOURNAL OF CELL BIOLOGY

Downloaded from jcb.rupress.org on September 1, 2016

Published April 11, 2016

podosomes, including its exposure on the ventral cell surface, has not been demonstrated yet.

Using total internal reflection fluorescence (TIRF) live-cell imaging of primary human macrophages, we now detect surface-exposed MT1-MMP at podosomes and also at dot-like "islets" that are embedded in the ventral plasma membrane. MT1-MMP islets become apparent upon podosome dissolution and are also preferred sites for podosome reemergence. Islet formation is based on the C-terminal cytoplasmic tail of MT1-MMP and its binding to the subcortical actin cytoskeleton. We propose that MT1-MMP islets constitute cellular memory devices that facilitate formation of new podosomes that are well integrated into the regular pattern of podosome groups, ensuring efficient and localized podosome formation and matrix degradation. These findings constitute a further extension of the functional repertoire of podosomes and their components. At the same time, the demonstration of a nonproteolytic function of MT1-MMP in the turnover of podosomes should also provide a new aspect for the study of other adhesion and invasion structures, most notably invadopodia, and their contribution to cell invasion and cancer progression.

Results

Cell surface–exposed MT1-MMP is present at podosomes and at podosome-free islets

To localize cell surface-exposed MT1-MMP in primary human macrophages, we used a pH-sensitive construct (MT1-MMP-pHluorin; Monteiro et al., 2013), which is fluorescent only at an extracellular pH of 7.4 (Miesenböck, 2012). (pHluorin was inserted N terminally of the transmembrane domain and is thus extracellular on the surface-exposed protease.) For visualization of total cellular MT1-MMP, cells were cotransfected with MT1-MMP-mCherry. Confocal imaging of the ventral cell side showed MT1-MMP-mCherry at a central accumulation, corresponding to the Golgi, and in vesicles (Fig. 1 B), consistent with previous results (Wiesner et al., 2010). MT1-MMP-pHluorin was detected at the ventral plasma membrane and at the cell periphery (Fig. 1 A). However, both proteins showed no localization reminiscent of podosome core or ring structures (Fig. 1, A–C). Strikingly, TIRF analysis of the same cells showed a dot-like localization of MT1-MMP-pHluorin at the substrate-attached cell side, reminiscent of podosome cores (Fig. 1, D–F; compare to Fig. 1, A–C). Indeed, MT1-MMP signals colocalized with F-actin–rich podosome cores (Fig. 1, D–F, insets). Moreover, visualization of endogenous MT1-MMP in TIRF revealed a similar dot-like staining, which mostly colocalized with F-actin–rich podosome cores (Fig. 1, G–I and M). Further analyses showed that surface-associated MT1-MMP-pHluroin is present beneath the podosome core structure and surrounded by podosome ring components such as talin (Fig. 1, J–L and N). A colocalization analysis of MT1-MMP-pHluorin and F-actin–rich podosomes (Fig. S1, A–E; n = 1,100 podosomes) showed a colocalization index of 0.57 (Fig. S1 F), with a negative correlation ($r = -0.389$) between MT1-MMP-pHluorin enrichment at podosomes and podosome core size (Fig. S1 G). This indicates that larger podosomes, such as the peripherally located subpopulation of precursor podosomes that also shows high turnover

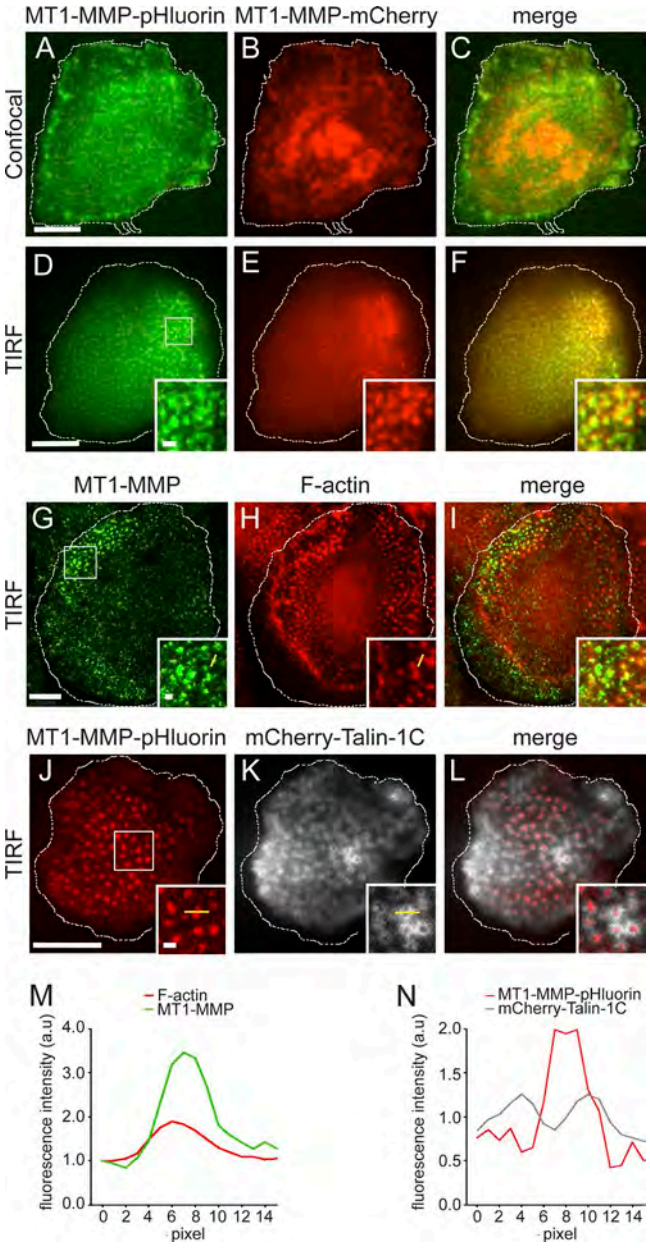

Figure 1. **TIRF microscopy reveals podosome-associated MT1-MMP.** (A and B) Micrographs of macrophage expressing MT1-MMP-pHluorin (A and D, green) and MT1-MMP-mCherry (B and E, red), with merges (C and F), with both sets of images showing the same cell. Note that in confocal mode (A–C), surface-exposed MT1-MMP, as indicated by pHluorin-based fluorescence, is not visible at distinct structures, whereas only in TIRF mode (D–F), dot-like accumulations of both MT1-MMP-pHluorin and MT1-MMP-mCherry become visible. (G–I) TIRF micrographs of endogenous MT1-MMP, stained with specific primary antibody and Alexa Fluor 488–labeled secondary antibody (G, green), and F-actin, stained with Alexa Fluor 568–labeled phalloidin (H, red), with merge (I). (J–L) TIRF micrographs of macrophage expressing MT1-MMP-pHluorin (J, red), and mCherry-Talin-1C to visualize podosome ring structures (K, white), with merge (L). White boxes (D–L) indicate detail regions shown as insets. Dotted line indicates cell circumference. Bars: 10 µm; (insets) 1 µm. (M and N) Fluorescence intensity diagrams of single podosomes. Distances are indicated by yellow lines in insets of (G and H) and (J and K). Note that peak of MT1-MMP–based fluorescence matches with that of F-actin (M) and is surrounded by peaks of talin-based fluorescence (N). Measurements are representative for the respective setup, and similar curves have been reproduced multiple times.

Downloaded from jcb.rupress.org on September 1, 2016

Published April 11, 2016

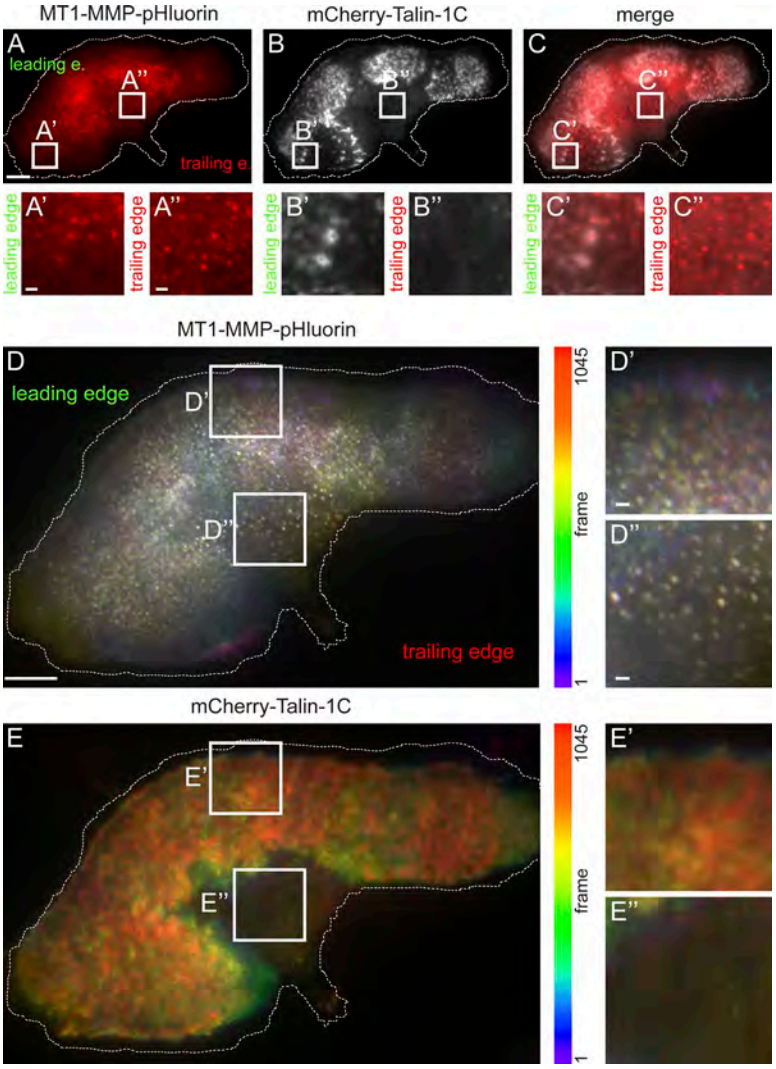

Figure 2. **Surface-exposed MT1-MMP is present at podosomes and at podosome-free islets.** (A–C) TIRF micrographs of macrophage expressing MT1-MMP-pHluorin (A, red) and mCherry-Talin-1C (B, white), with merge (C). White boxes indicate two detail regions, in which MT1-MMP is associated with podosomes (left box) and present at podosome-free islets (right box). Leading and trailing edge (e.) are indicated. (D and E). Color-coded analysis of cell shown in A–C for visualization of motile versus static structures. For both fluorescence channels (MT1-MMP-pHluorin [D] and mCherry-Talin-1C [E]), each frame was colored along the spectrum, with subsequent merge into a single image. White boxes indicate detail regions also shown enlarged below. mCherry-Talin-1C presents in varying colors, indicating regular podosome ring dynamics (E′), whereas podosome-free areas show only diffuse background (E″). Podosome-associated MT1-MMP-pHluorin also presents in varying colors, indicative of podosome core dynamics (D′). However, MT1-MMP islets present mostly in white (D″), indicating restricted lateral mobility. Dotted line indicates cell circumference. Bars: 10 µm; (insets) 1 µm.

(Bhuwania et al., 2012), are less likely to accumulate the proteinase than smaller, and generally longer-lived, podosomes.

TIRF live-cell imaging of cells coexpressing MT1-MMP-pHluorin and mCherry-Talin-1C confirmed that podosome-localized MT1-MMP-pHluorin often shows dynamic codistribution with podosomes (Fig. S1, H–J; and Video 1). However, in many cells (~35%), we also observed MT1-MMP–positive spots at the ventral surface that did not colocalize with podosome core or ring components such as F-actin or talin (Fig. 2, A–C; and Video 2). This second group of structures, termed "MT1-MMP islets," was especially evident in motile or polarized cells with pronounced trailing edges, with 60–70% of polarized cells showing islets. In these cells, podosomes were recruited to protruding areas of the cell (Burns et al., 2001; Linder et al., 2011), whereas MT1-MMP islets were mostly localized toward the trailing edge (Fig. 2, A–C).

To analyze the dynamics of podosome-associated MT1-MMP and MT1-MMP islets, TIRF live-cell videos of cells coexpressing MT1-MMP-pHluorin and mCherry-Talin-1C were acquired and color-coded using ImageJ. For both channels, each frame was colored progressively along the spectrum, with subsequent merge into a single image (Fig. 2, D and E). Dynamic structures are thus depicted in varying colors, whereas static structures are shown in white. The mCherry-Talin-1C merge presented in varying colors, indicating regular podosome ring dynamics (Fig. 2 E′), whereas podosome-free areas showed diffuse background (Fig. 2 E″). Podosome-associated MT1-MMP-pHluorin was also depicted in varying colors, indicative of podosome core dynamics (Fig. 2 D′). However, MT1-MMP islets were mostly white (Fig. 2 D″). This indicates that MT1-MMP at podosomes shows a dynamic codistribution with these structures, whereas MT1-MMP at islets displays reduced lateral dynamics.

We next performed a color-coded analysis of TIRF live-cell videos from macrophages coexpressing Lifeact-RFP and MT1-MMP-pHluorin. This analysis showed that podosome cores display variations in length and orientation of respective tracks (Fig. 3, A–A″). In contrast, podosome-associated MT1-MMP-pHluorin showed less variation (Fig. 3, B–B″), with lower lateral mobility (2.9 ± 0.6 µm during 60 min), compared with that of podosomal F-actin (4.2 ± 0.8 µm; Fig. 3 C). Also, duration of continuous tracks of Lifeact-RFP and MT1-MMP-pHluorin from podosome cores was calculated for all podosomes of five cells (n = 1,411; Fig. 4, A and B). Track duration for Lifeact-RFP signals, indicative of podosome core lifetime, was 668.4 ± 25.7 s, in agreement with earlier results (Destaing et al., 2003). In contrast, track duration for MT1-MMP-pHluorin was significantly higher at 809.6 ± 39.3 s

Downloaded from jcb.rupress.org on September 1, 2016

Published April 11, 2016

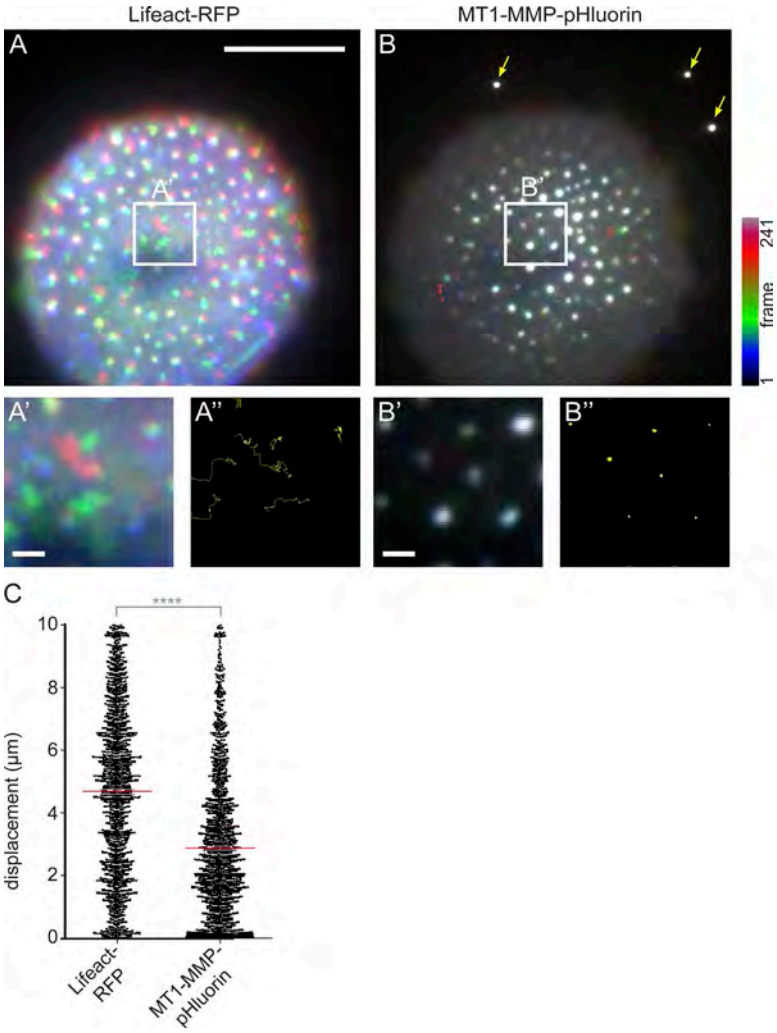

Figure 3. **Podosome-associated MT1-MMP shows reduced lateral mobility compared with podosomal F-actin.** (A and B) TIRF micrographs of macrophage expressing Lifeact-RFP to detect F-actin–rich podosome cores (A) and MT1-MMP-pHluorin (B). Images show color-coded merges of time-lapse videos with successive coloration of individual frames along the spectrum, as indicated. White boxes indicate areas of detail images shown below each panel (A′ and B′). (A″ and B″) Shown are tracks of the center of mass in yellow. Note high variability of track orientation and length of podosomes cores, whereas tracks of MT1-MMP-pHluorin are more uniform and short. Dotted line indicates cell circumference. Bar, 10 µm. Drift of the microscope stage was corrected by use of fluorescent beads, indicated by arrows in B. (C) Statistical analysis of lateral displacement of podosomal F-actin and podosomal MT1-MMP-pHluorin. Each dot represents lateral displacement of the respective center of mass of a single podosome-associated signal. Collectively, 1,411 podosomes were evaluated. Red bar indicates mean ± SEM. ****, $P < 0.0001$.

(Fig. 4 C). Interestingly, subgroups of both signals persisted throughout the whole recording period (Fig. 4 C), with 18.4 ± 10.5% of podosome cores and 49.9 ± 6.5% of MT1-MMP-pHluorin patches persisting for >50 min (Fig. 4 D).

MT-MMP islets are formed by podosome dissolution

Several lines of evidence indicated that MT1-MMP islets and podosomes could be related: (1) The mean diameter of MT1-MMP-pHluorin islets was determined as 0.83 ± 0.06 µm, and their density as 23.98 ± 1.54/100 µm^2. These values are similar to size (0.86 ± 0.06 µm) and density (24.52 ± 1.90/100 µm^2) of podosome cores (Fig. S1, K and L). (2) MT1-MMP at podosomes persists longer than the podosome structure itself (Fig. 4). (3) MT1-MMP islets are localized toward the trailing edge (Fig. 2, A–C), a preferential site of podosome dissolution (Bhuwania et al., 2012). Therefore, we next explored the potential relationship between podosomes and MT1-MMP islets and, specifically, whether MT1-MMP islets appear as a result of podosome dissolution.

To induce synchronized dissolution of a large number of podosomes, cells coexpressing MT1-MMP-pHluorin and Lifeact-RFP were treated with 100 µM of the Arp2/3 complex inhibitor CK-666 and analyzed by TIRF live-cell imaging. Podosome formation and upkeep is critically based on Arp2/3 complex–dependent actin nucleation (Linder et al., 2000a). Consequently, addition of CK-666 led to disruption of podosomes, indicated by the disappearance of the Lifeact-RFP signal from its podosomal localization. This was sometimes also accompanied by unspecific accumulation of F-actin in the cell center (Fig. 5, A–F; and Video 3). Complete disruption of the podosome structure was confirmed in parallel by dislocalization of other key components of the core, such as Arp2 and α-actinin, or of the ring structure, such as talin, vinculin, or paxillin (Table S1). In contrast, most of the dot-like, previously podosome-associated MT1-MMP-pHluorin signals persisted at their location (Fig. 5, A and D), which was especially visible in kymographs of CK-666–treated cells (Fig. 5, G–I). FRAP analysis of CK-666–induced islets (Fig. 5 J) further showed that MT1-MMP-pHluorin shows only moderate turnover in these structures, with a mobile fraction of 21.8% and a half-time of recovery of 5.2 s (Fig. 5 K).

These data indicated that MT1-MMP islets are derived from podosome-localized MT1-MMP upon podosome disruption, either induced by CK-666 addition to adherent, podosome-containing cells or during regular podosome turnover. To test whether MT1-MMP islets can also develop independently of podosomes, nonadherent macrophages were seeded under conditions that inhibit podosome formation. These included addition of the integrin-binding peptide RGD, inhibiting integrin-based adhesion (Ruoslahti, 1996), or addition of CK-666 inhibiting Arp2/3-dependent actin nucleation (Nolen et al., 2009)

Downloaded from jcb.rupress.org on September 1, 2016

Published April 11, 2016

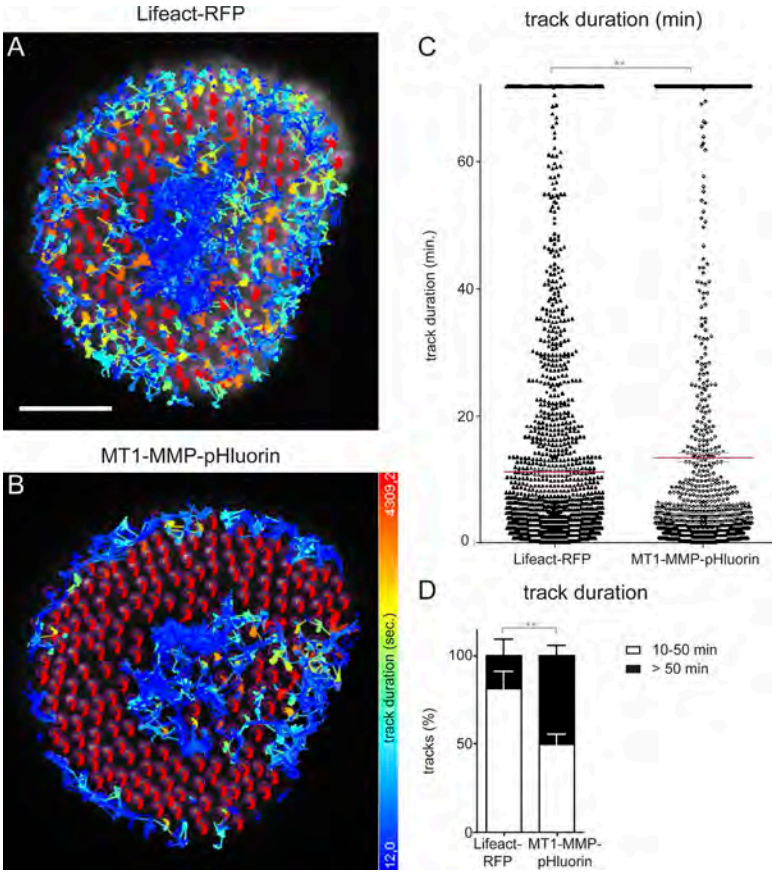

Figure 4. **MT-MMP signals at podosomes persist longer than podosomal F-actin.** (A and B) TIRF micrographs of macrophage expressing Lifeact-RFP to detect F-actin–rich podosome cores (A) and MT1-MMP-pHluorin (B). The center of mass of each podosome-associated signal was tracked, and tracks were colored according to their duration, as indicated. (C and D) Statistical analyses of track duration of podosomal F-actin and podosome-associated MT1-MMP. Each dot in C represents track duration of a single podosomal signal. Red bar indicates mean ± SEM. Note higher mean of MT1-MMP-pHluorin signals and also higher amounts of respective signals persisting for >50 min, which is plotted in D as the mean ± SEM percentage of total tracks. **, $P < 0.01$.

and thus formation of (integrin-based) podosomes, before seeding of cells. Macrophages coexpressing Lifeact-RFP and MT1-MMP-pHluorin seeded in the presence of 10 µM RGD did not attach firmly to the substratum. They also did not develop podosomes, and only a few irregularly sized accumulations of Lifeact-RFP were discernible (Fig. S2, A–C). MT1-MMP-pHluorin was mostly localized to irregularly sized patches (diameter: 2.0–3.5 µm) on the ventral cell side and also to the edges of polarized cells. Colocalization of MT1-MMP-pHluorin with Lifeact-RFP patches was only observed on few occasions. Similar results were obtained using cells treated with CK-666 before seeding (unpublished data). Collectively, these data indicate that podosome formation is a prerequisite for the genesis of MT1-MMP islets and that the appearance of islets is a result of podosome dissolution.

Molecular characterization of MT1-MMP islets

To characterize MT1-MMP islets on the molecular level, a variety of potential components were tested. Macrophages expressing respective overexpression constructs were treated with CK-666 to induce islets, fixed, stained with labeled phalloidin to ensure podosome disruption, and visualized by confocal TIRF microscopy. For detection of endogenous proteins, respective antibodies were used. Tested proteins included components of podosome core or ring structures such as Arp2 (Linder et al., 2000a), α-actinin (Gimona et al., 2003), Tks5 (Burger et al., 2011), or vinculin (Zambonin-Zallone et al., 1989), talin (Zambonin-Zallone et al., 1989), paxillin (Pfaff and Jurdic, 2001), and transmembrane proteins that link podosomes to the underlying matrix, such as β1 (Marchisio et al., 1988), β2 (Marchisio et al., 1988), and β3 (Zambonin-Zallone et al., 1989) integrins, CD44 (Chabadel et al., 2007), and integrin-associated proteins such as integrin-linked kinase (ILK; Griera et al., 2014) or kindlin-3 (Ussar et al., 2006; Table S1). All of these components localized to podosomes but were absent from islets. In case of integrins and CD44, unspecific accumulations of irregular size were observed at the ventral plasma membrane, which did not colocalize with islets. We next tested proteins associated with membrane curvature at invadosomes, such as CIP4 (Linder et al., 2000b) and FBP17 (Tsuboi et al., 2009), and vesicle regulatory proteins such as flotillin-1 and 2 that influence podosomal matrix degradation (Cornfine et al., 2011). Interestingly, CIP4 and FBP17 were absent from both podosomes and islets, whereas flotillin-2 was present at podosomes, but not at islets. Moreover, c-Src also showed no distinct localization at podosomes or islets, consistent with previous results (Linder and Aepfelbacher, 2003), and inhibition of Src activity by addition of 10 µm PP2 did not lead to discernible alterations in islet appearance.

As invadosomes are privileged membrane sites (Oikawa et al., 2008; Yu et al., 2013), we next tested a variety of membrane lipids. Indeed, comparable to invadopodia (Caldieri et al., 2009), we could show that cholesterol, stained by filipin (Gimpl and Gehrig-Burger, 2011), is also present at macrophage podosomes (Fig. S2, D–F). However, cholesterol was not detectable at MT1-MMP islets (Fig. S2, G–I). Apolipoprotein E, a regulator of cholesterol transport (Vance et al., 2006), localized to intracellular vesicles (Fig. S2, J–L) but was absent from both podosomes and islets. Interestingly, from all other probes used for the detection of lipids (Table S1), the phosphatidylinositol 4-phosphate (PI(4)P) sensor OSH2-2xPH-GFP (Balla et al., 2008) gave the clearest signal at podosomes

Downloaded from jcb.rupress.org on September 1, 2016

Published April 11, 2016

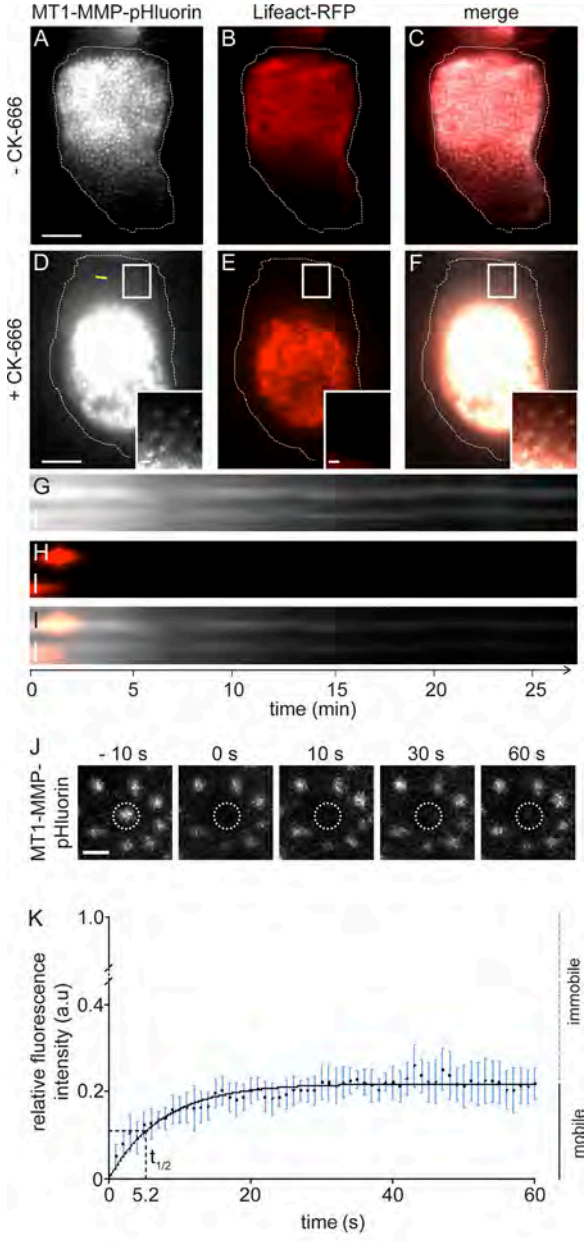

Figure 5. **MT1-MMP accumulations persist beyond disruption of podosomes.** TIRF still images of a cell expressing MT1-MMP-pHluorin (A and D, white) and Lifeact-RFP (B and E, red), with merges (C and F), before (A–C) and 30 min after (D–F) addition of Arp2/3 inhibitor CK-666. White boxes in D–F indicate detail regions shown as insets. Note that regions devoid of podosomes (E) still contain dot-like accumulations of MT1-MMP-pHluorin. Bar, 10 µm. (G–I) Kymographs of the cell shown in A–F. Time since start of the experiments is indicated in minutes. CK-666 was added at time point 0. Note that the localized MT1-MMP-pHluorin signal persists also in the absence of podosomes. Bars, 1 µm. (J) FRAP analysis of MT1-MMP-pHluorin turnover at CK-666 induced islets. Gallery shows TIRF micrographs taken from time-lapse movie of MT1-MMP-pHluorin expressing macrophage. Dashed line indicates single bleached islet. Time before and after bleaching is given above each panel. (K) Quantification of FRAP showing MT1-MMP-pHluorin-based, normalized fluorescence intensity over time, with fitted curve in black. Values are given as mean ± SD. For each value, 10 islets from three cells from three different donors were evaluated.

(Fig. S2, M–O). However, we could not detect enrichment of PI(4)P, or of any other tested lipid, at islets (Fig. S2, P–R). Collectively, these experiments pointed to MT1-MMP as the major component of islets.

The presence of MT1-MMP at islets raised the question whether these structures are able to degrade matrix. We thus performed matrix-degradation experiments in the presence of CK-666. MT1-MMP-pHluorin–expressing cells were seeded on rhodamine-labeled gelatin for 4.5 h, to allow adhesion and podosome formation, but before the onset of widespread matrix degradation, as determined by a time-course analysis (for presence of islets in untreated cells on gelatin, see Fig. S2, S–V). CK-666 was added at 4.5 h (Fig. S2 W), and cells remained on the matrix for an additional 2 h before fixation and quantification of matrix degradation (Fig. S2 X), with absence of podosomes in CK-666–treated cells being checked by staining of F-actin (Fig. S2 Y). Importantly, matrix degradation did not increase during the 2-h time period in CK-666–treated cells, when only islets were present, in contrast to control cells that contained podosomes (Fig. S2 X). We conclude from these data that islets are not degradative on gelatin matrix.

MT1-MMP islets are sites of podosome reemergence

Podosomes are often formed at sites of previous podosome localization. We therefore hypothesized that MT1-MMP islets could be sites of renewed podosome emergence. To test this, macrophages expressing MT1-MMP-pHluorin and Lifeact-RFP were imaged using TIRF live-cell microscopy and treated with CK-666 to disrupt podosomes, and thus also induce islets, with subsequent washout to allow podosome reformation. Strikingly, many of the MT1-MMP islets acquired Lifeact-RFP, indicative of podosome reformation (Fig. 6, A–C; and Video 4). Reformation of complete podosomes was confirmed in parallel by staining of markers for podosome ring (vinculin: Fig. S3, A–C; paxillin: Fig. S3, D–F) and core structures (Arp2: Fig. S2, G–I; F-actin: Fig. S2, J–L). To determine the extent of MT1-MMP islet reuse for podosome formation, we also acquired time-lapse videos during CK-666 treatment and washout. Starting with the time point of washout, all frames of the Lifeact-RFP channel were merged into one image, which was submitted to colocalization analysis with the first frame of the MT1-MMP-pHluorin channel, thus reporting renewed podosomal F-actin accumulation at islets. Quantification showed that 67.3 ± 1.1% of MT1-MMP islets were sites of renewed podosome formation within 10 min after CK-666 washout (n = 15 cells, from three donors). Interestingly, islet formation under inhibition of MT-MMP activity by addition of 100 µM of the inhibitor NSC405020 (Remacle et al., 2012) led to similar values of islet reuse (62.1 ± 3.5%), indicating that the proteolytic activity of the protease is not necessary for podosome reemergence (see also catalytically inactive MT1-MMP-E240A in Fig. 8, D and E).

Treatment of cells with CK-666 was used to generate sufficient numbers of islets for statistical analysis but is an artificial process. We thus asked whether reemergence of podosomes at islets could also be detected during regular podosome turnover. For this, cells expressing Lifeact-RFP and MT1-MMP-pHluorin were analyzed by TIRF live-cell imaging. Indeed, we found that 25–30% of MT1-MMP islets coincide with sites of

Downloaded from jcb.rupress.org on September 1, 2016

Published April 11, 2016

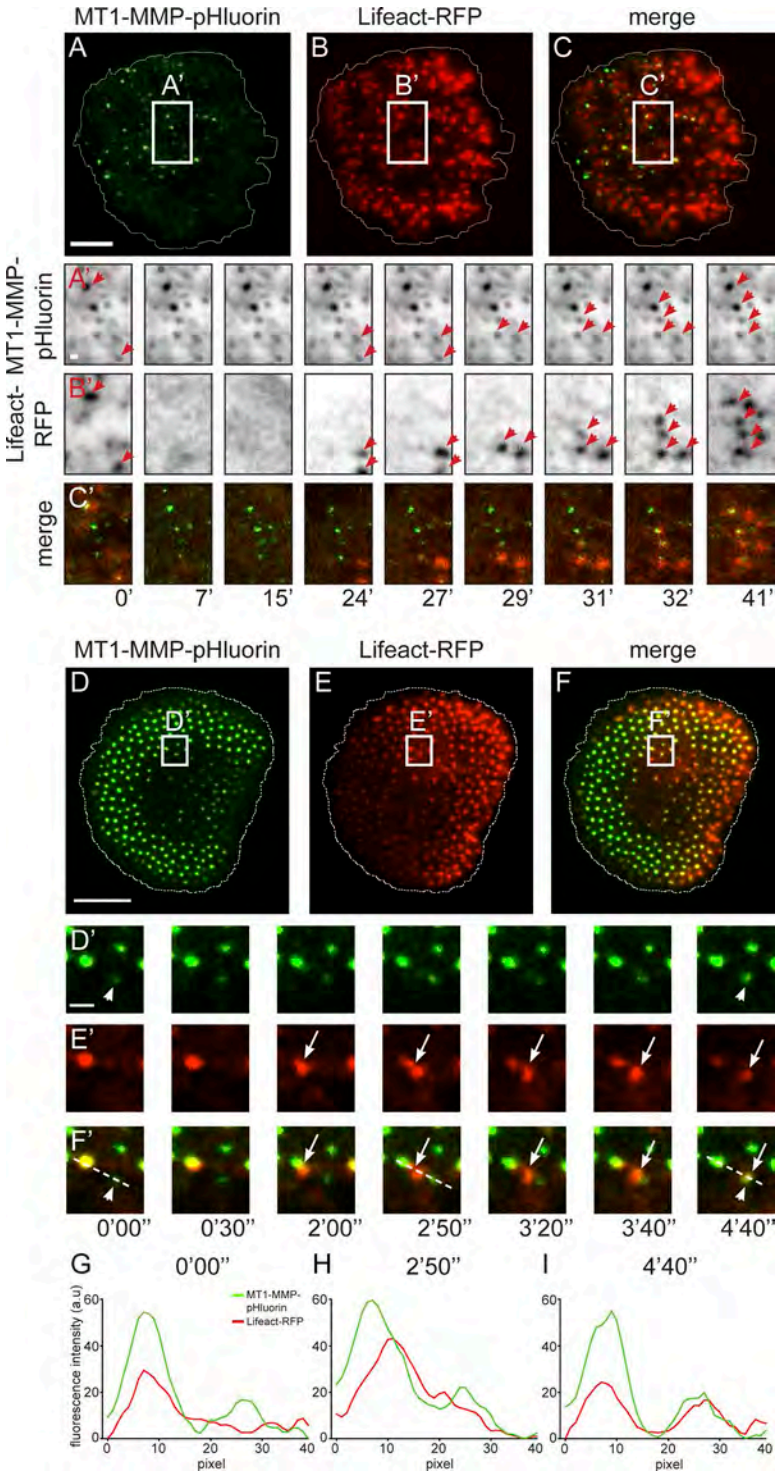

Figure 6. **MT1-MMP islets are sites of podosome reemergence.** (A–C) MT1-MMP islets are sites of de novo actin nucleation. TIRF still images of a macrophage expressing MT1-MMP-pHluorin (A, green) and Lifeact-RFP (B, red), with merge (C), treated with CK-666, with subsequent washout of the drug to allow reformation of podosomes. Cell circumference indicated by dashed line. Bars: 10 µm; (insets) 1 µm. White boxes indicate areas shown enlarged in A′–C′. Note that in A′ and B′, respective fluorescence signals have been changed to inverted grayscale. Red arrows in A′ and B′ indicate MT1-MMP islets that are also positive for Lifeact-RFP. Note absence of podosomal Lifeact-RFP signals at 7- and 15-min time points, with successive accumulation of Lifeact-RFP signals at MT1-MMP islets. Time after washout of CK-666 is indicated below (C′). (D–I) MT-MMP islets can recruit material generated by podosome fission. TIRF micrograph of macrophage expressing MT1-MMP-pHluorin (D, green) and Lifeact-RFP (E, red), with merge (F). Still images taken from Video 5. White boxes indicate detail regions shown in D′–F′. Note MT1-MMP islet (arrow) recruiting F-actin accumulation generated by fission of a podosome (white arrowheads). Time since start of the experiment is indicated in minutes and second. Bars: 10 µm; (insets) 1 µm. (G–I) Fluorescence intensity diagrams of MT1-MMP-pHluorin and Lifeact-RFP, taken along the dotted line indicated in detail images of G′–I′ at the indicated time points. Note rise of RFP-fluorescence intensity, indicative of increased actin polymerization, in the core before podosome fission, with subsequent redistribution of the daughter podosome to an MT1-MMP islet. Measurements are representative for the respective set-up, and similar curves have been reproduced multiple times.

renewed podosome reformation. Comparable to podosomes formed upon CK-666 treatment, reformation was based on actin nucleation, as indicated by increasing accumulation of Lifeact-RFP over time. In addition to de novo formation, new podosomes can also be formed by fission from preexisting podosomes and in particular from the subpopulation of precursor podosomes (Evans et al., 2003; Kopp et al., 2006). Strikingly, we observed that ∼30% of the podosomes generated by fission are recruited to nearby MT1-MMP islets (Fig. 6, D–I; and Video 5), indicating that islets can also function as anchoring points for preformed podosome cores.

The impact of other cytoskeletal components such as microtubules or dynamin on podosome reformation was determined by use of respective inhibitors, such as nocodazole and dynasore, and analysis by TIRF live imaging (Fig. S3, M–O and V–X). Addition of 1 µM nocodazole led to disruption of podosomes, as reported previously (Linder et al., 2000a), but not of islets (Fig. S3, P–R). Similar observations were made upon addition of dynasore (10 µM; Fig. S3, Y, Z, and A1). Strikingly, upon washout of nocodazole, podosomes reformed mostly between islets (Fig. S3, S–U), in contrast to washout of dynasore, with podosomes reforming mostly at islets (Fig. S3, B1, C1,

Downloaded from jcb.rupress.org on September 1, 2016

Published April 11, 2016

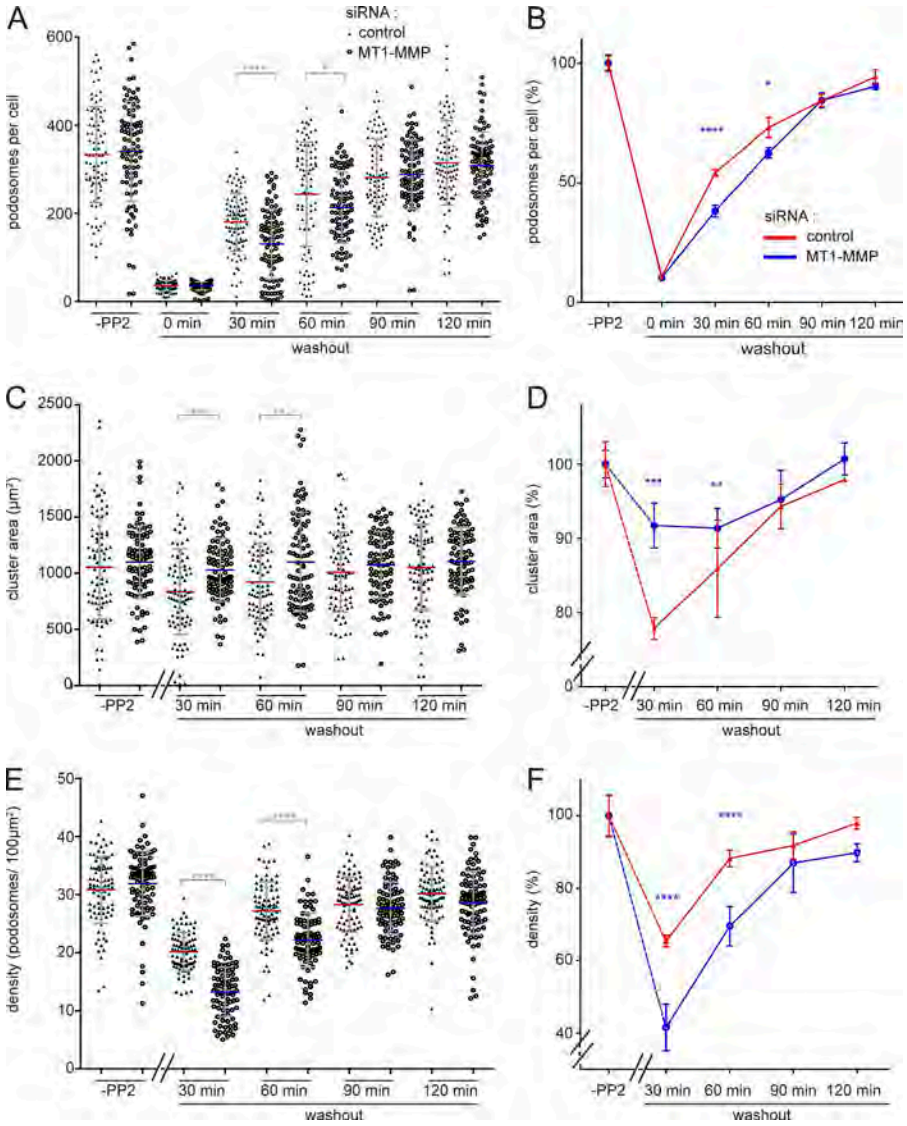

Figure 7. **Podosome reformation proceeds less efficiently in cells depleted for MT1-MMP.** Statistical evaluations of podosome numbers (A and B), area covered by podosome groups ("clusters"; C and D), or podosome density (podosomes/100 µm²; E and F) during a podosome reformation assay. Parameters were evaluated in cells before disruption of podosomes ("-PP2") or after treatment with podosome-disrupting PP2 and washout of the drug for the indicated periods, in cells treated with control siRNA (black triangles) or cells treated with MT1-MMP–specific siRNA (open circles). Each dot in A–C represents a single cell, with $n = 3 \times 30$, for cells from three different donors. Diagrams in B, D, and F show data as respective line diagrams. Podosomes are mostly absent at 0 min of the washout (A); podosome-covered area (B) and podosome density (C) were not evaluated for this time point. Note that podosome density of MT1-MMP–depleted cells is significantly different from controls at 30- and 60-min time points (C). Values are given as means ± SD. *, $P < 0.05$; **, $P < 0.01$; ***, $P < 0.001$; ****, $P < 0.0001$. For specific values, see Table S2.

and D1), indicating a differential impact of these cytoskeletal elements on the memory effect of islets.

Collectively, these data show that MT1-MMP islets can serve as sites of podosome reformation. This can be achieved by de novo Arp2/3-dependent actin nucleation or by recruiting material generated through podosome fission. This memory effect is preserved upon previous inhibition of dynamin, but not under previous disruption of microtubules.

MT1-MMP facilitates podosome reformation

As MT1-MMP islets form sites for podosome reemergence, we next investigated the consequences of MT1-MMP depletion for podosome formation. Cells treated with MT1-MMP–specific siRNA (Wiesner et al., 2013) or control siRNA were processed in a podosome reformation assay. This assay is based on disruption of podosomes by addition of the Src tyrosine kinase inhibitor PP2, with subsequent reformation of podosomes upon washout of the drug (Linder et al., 2000b), followed by semiautomated software analysis (Cervero et al., 2013). (PP2 was used for podosome dissolution as the semiautomated podosome reformation assay has been established for this inhibitor.) As expected, most (>90%) podosomes were disrupted upon PP2 treatment, in both MT1-MMP knockdown and control cells (Fig. 7, A and B). 90 min after washout of the drug, both cell populations had also recovered regular podosome numbers (Fig. 7, A and B). However, MT1-MMP–depleted cells had formed significantly fewer podosomes at time points 30 and 60 min, corresponding to relative decreases of 24% and 13%. Moreover, in control cells, the area of podosome formation was significantly decreased at these 30- and 60-min time points (Fig. 7, C and D). This probably reflects the fact that MT1-MMP islets, which are preferentially used for podosome reformation, show a restricted localization in cells (see Fig. 2). In contrast, MT1-MMP–depleted cells formed new podosomes over a larger area (Fig. 7, C and D). Podosome density, the ratio of podosome number and podosome-covered area, thus showed highly significant decreases of 34% at 30 min and of 19% at 60 min for MT1-MMP–depleted cells (Fig. 7, E and F). These results indicate that the presence of MT1-MMP is not strictly required for podosome reformation. However, MT1-MMP facilitates the generation of new podosomes, leading to faster recovery of regular podosome numbers and densities.

Downloaded from jcb.rupress.org on September 1, 2016

Published April 11, 2016

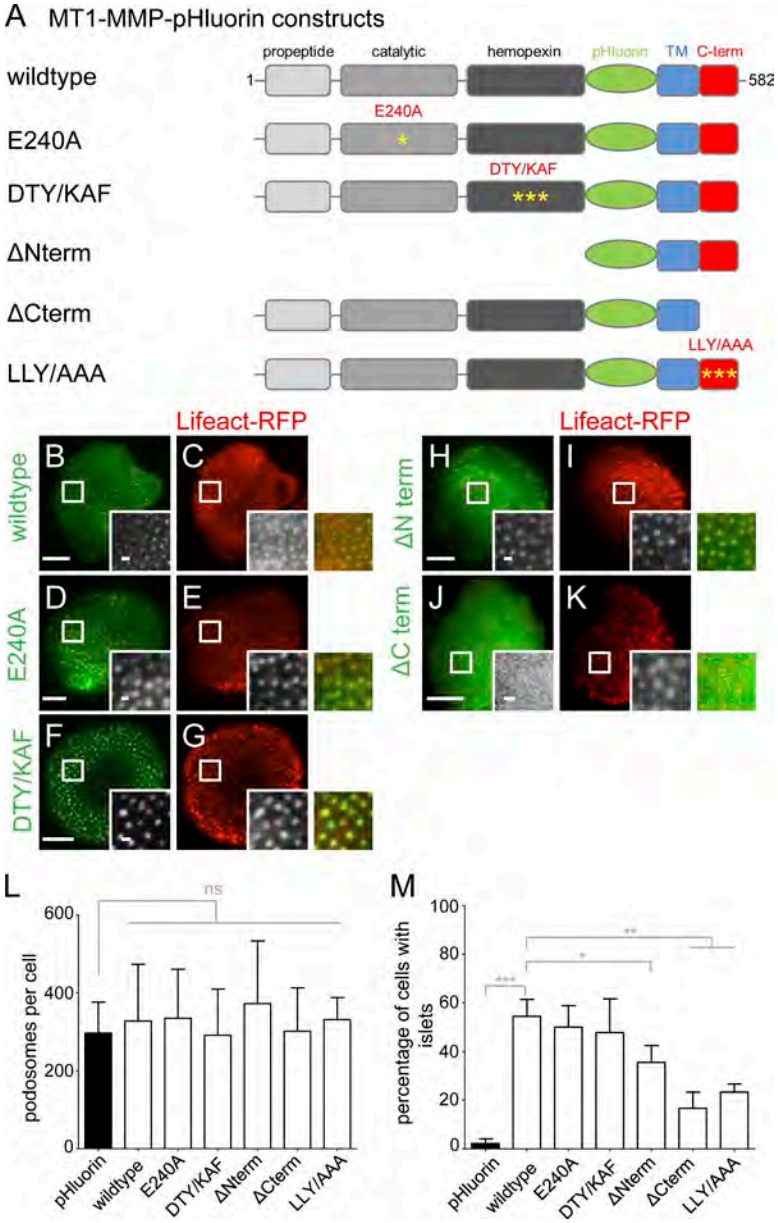

Figure 8. **The cytoplasmic tail of MT1-MMP is necessary for localization of the protease to podosomes.** (A) Domain structure of MT1-MMP, containing a propeptide domain absent in the activated protease, a catalytic domain harboring protease activity, a hemopexin domain involved in oligomerization, a transmembrane domain, and a C-terminal cytoplasmic domain. pHluorin was inserted as an intramolecular tag N terminally of the transmembrane domain and is thus extracellular on the surface-exposed protease. First and last amino acid residues are indicated. Yellow asterisks indicate respective point mutants (E240A; DTY/KAF, D385K, T412A, Y436F; LLY/AAA, L571A, L572A, L573A). (B–K) TIRF micrographs of macrophages expressing indicated MT1-MMP-pHluorin constructs (green), together with Lifeact-RFP (red). White boxes indicate areas of detail images shown in black and white insets, with colored merges on the right. Note absence of ΔCterm construct from podosomes (J and K). Bars: 10 µm; (insets) 1 µm. (L and M) Statistical evaluation of podosome numbers in cells expressing indicated MT1-MMP-pHluorin constructs (L) or of MT1-MMP-pHluorin siRNA-insensitive constructs localizing to islets in cells depleted for endogenous MT1-MMP (M). For each value, 3 × 5 cells from three different donors were evaluated. Bars represent mean ± SD. *, $P < 0.05$; **, $P < 0.001$; ***, $P < 0.0001$. For specific values, see Table S2.

Downloaded from jcb.rupress.org on September 1, 2016

Islet formation depends on the LLY motif within the MT1-MMP cytoplasmic tail

We next asked which features of MT1-MMP might enable its localization to podosomes or islets and generated a series of pHluorin-tagged mutants that are (a) deficient in either proteolytic activity (E240A; Rozanov et al., 2001) or (b) oligomerization (DTY/KAF; D385K, T412A, and Y436F; Tochowicz et al., 2011), (c) lack all extracellular domains and are thus defective in ECM binding (ΔNterm), or (d) lack the cytoplasmic tail (ΔCterm). In all cases, the transmembrane domain was included to ensure membrane embedding. (Fig. 8 A). Constructs were coexpressed with Lifeact-RFP in macrophages to assess their subcellular localization by TIRF. The E240A, DTY/KAF and ΔNterm constructs showed localization to podosomes (Fig. 8, D–I) and islets (see below; Fig. S4), comparable to the wild type (WT; Fig. 8, B and C), whereas the ΔCterm construct mostly did not localize to podosomes or islets but showed a diffuse distribution over the ventral cell surface (Fig. 8, J and K). Importantly, in all cases, the number of podosomes per cell (~350) was not significantly altered (Fig. 8 L). Collectively, these experiments indicated that the C-terminal cytoplasmic tail of MT1-MMP is necessary and sufficient to ensure localization of the protease at podosomes and islets. Indeed, podosome reformation experiments using CK-666 in cells expressing an siRNA-insensitive ΔNterm construct showed podosome reformation at respective islets comparable to WT MT1-MMP (Fig. S3, E1, F1, G1, H1, I1, J1, K1, L1, and M1), whereas an siRNA-insensitive ΔCterm construct failed to form islets (Fig. S3, N1, O1, and P1).

Several scenarios could be envisioned for the mode of action of the C-terminal domain: it could be involved in (a) localizing MT1-MMP to vesicles, (b) regulating the surface exposure of MT1-MMP, or (c) restricting the mobility of the surface-exposed protease. To distinguish between these possibilities, we generated mCherry-fused versions of the ΔCterm construct, and also of the E240A construct, for comparison. (1) Localization at vesicles was tested by coexpression of GFP-fused Rab14 Q70L (Junutula et al., 2004) or Rab22a (Weigert et al., 2004).

Published April 11, 2016

Comparable to MT1-MMP WT (Wiesner et al., 2013), both ΔCterm and E240A constructs showed prominent localization to Rab14 vesicles (Fig. S4, A–C) or Rab22a vesicles (Fig. S4, D–F). (2) The amount of surface-exposed material was determined by staining of unpermeabilized macrophages using an anti-mCherry antibody and a secondary, Alexa Fluor 647–labeled antibody. The respective surface-associated fluorescence intensity was measured and analyzed (Fig. S4, G–J). This value was not reduced in case of both the ΔCterm and E240A constructs, compared with WT, and was even slightly elevated in case of ΔCterm (Fig. S4 J). These experiments show that absence of the C-terminal domain of MT1-MMP does not influence the ability of the protease to localize to vesicles or to be exposed at the surface of macrophages.

We therefore reasoned that the localization-relevant function of the MT1-MMP C terminus could be to restrict the lateral mobility of the surface-exposed protease, possibly by anchoring it to the cortical cytoskeleton. Treatment of cells with the Arp2/3 inhibitor CK-666 leads to disruption of branched actin networks, including podosome cores, but leaving unbranched actin filaments of the cortex unaffected. We thus disrupted F-actin globally by treatment with both cytochalasin D, to inhibit actin filament elongation and latrunculin A, to sequester actin monomers. First, islets were induced by addition of CK-666 for 30 min to MT1-MMP-pHluorin–expressing cells. Next, 50 µM cytochalasin D and 10 µm latrunculin A were added, and cells were incubated for another 30 min. Strikingly, this led to complete dissolution of MT1-MMP islets, with MT1-MMP-pHluorin being distributed over the plasma membrane (Fig. 9, A–C), indicating that anchoring to the cortical unbranched actin cytoskeleton is important for MT1-MMP localization in islets.

Indeed, MT1-MMP has been reported to bind to F-actin by its C-terminal region and to thus prevent its diffusion out of invadopodia (Uekita et al., 2001; Yu et al., 2012). To test this, we generated a pHluorin-based, full-length construct of MT1-MMP, in which the three residues critical for F-actin binding were mutated to alanine (LLY/AAA; L571A, L572A, and L573A; Uekita et al., 2001; Yu et al., 2012). MT1-MMP-LLY/AAA-pHluorin was localized to podosomes (Fig. 9, D–F), and its expression did not change the number of podosomes per cell (Fig. 8 L). Subsequent to CK-666 treatment, MT1-MMP-LLY/AAA-pHluorin was also present at islets (Fig. 9, G–I). However, these experiments were performed in cells containing endogenous MT1-MMP, which might provide stabilization through oligomerization. We therefore generated a siRNA-insensitive MT1-MMP-LLY/AAA mutant, expressed it in macrophages depleted for endogenous MT1-MMP, and examined cells by TIRF microscopy. Strikingly, the LLY/AAA mutant construct failed to localize to podosomes in most cells and was diffusely localized over the ventral surface (Fig. 9, M–O), recapitulating the phenotype of the cytochalasin D/latrunculin A treatment.

Next, siRNA-insensitive MT1-MMP-pHluorin mutants were expressed in cells depleted for MT1-MMP and their localization to islets was quantified. This analysis showed that the E240A (Fig. S4, N–P) and DTY/KAF mutants (Fig. S4, Q–S) exhibit a capacity to localize to islets comparable to WT (Fig. 8 M and Fig. S4, K–M), whereas ΔCterm and LLY/AAA mutants showed strongly reduced numbers of cells with islets (Fig. 8 M). The ΔNterm mutant (Fig. S4, T–V) showed intermediate levels of islet formation (Fig. 8 M), indicating a potential influence of the MT1-MMP N terminus.

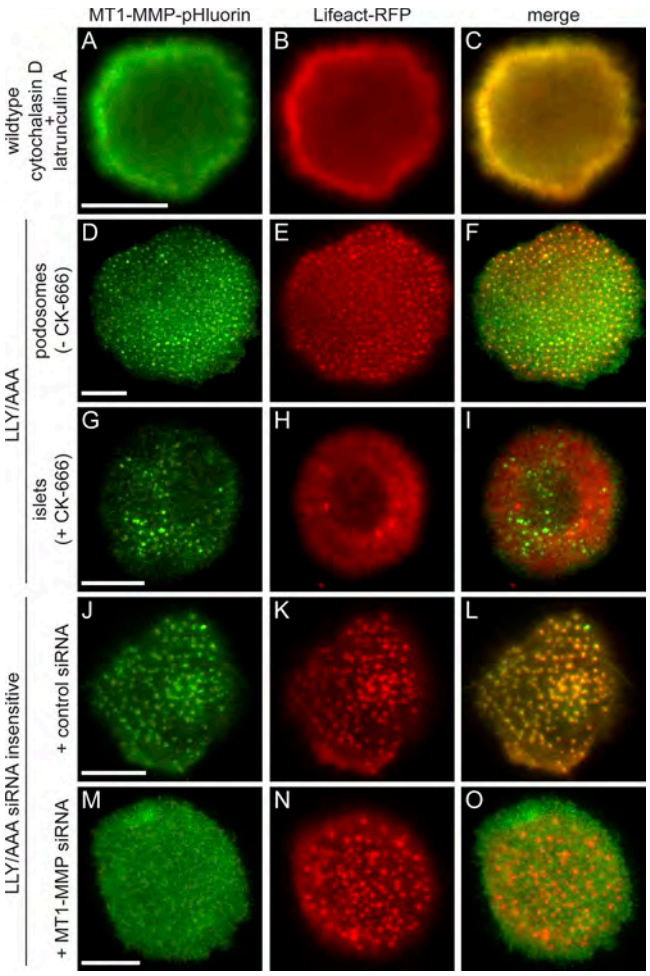

Figure 9. **The F-actin anchoring LLY motif in the MT1-MMP C terminus is critical for localization of the protease to podosomes and islets.** Confocal micrographs of macrophages expressing Lifeact-RFP (B, E, H, K, and N, red) and MT1-MMP-pHluorin constructs (green), of either WT (A) or an MT1-MMP-LLY/AAA mutant (D, G, J, and M). (A–C) Cells were treated with cytochalasin D and latrunculin A to inhibit formation of both branched and unbranched actin filaments. Note the absence of MT1-MMP islets. (D–I) Cells expressing MT1-MMP-LLY/AAA-pHluorin in a background of endogenous MT1-MMP (not labeled), without (D–F) or with (G–I) the addition of CK-666 to inhibit Arp2/3-generated branched actin filaments. Note localization of the MT1-MMP mutant construct to both podosomes (D–F) and islets (G–I). (J–O) Macrophages treated with control siRNA (J–L) or depleted of endogenous MT1-MMP (M–O) and expressing an siRNA-insensitive MT1-MMP-LLY/AAA-pHluorin construct. Note dispersed localization of the expressed protein, in contrast to enrichment at podosomes. Bars, 10 µm.

Finally, we tested the capacity of the MT1-MMP C terminus and its LLY motif to restore regular podosome reformation. For this, cells treated with control siRNA or MT1-MMP–specific siRNA were treated with PP2 to disrupt podosomes. In addition, two subsets of MT1-MMP siRNA-treated cells also expressed a pHluorin-fused construct of the MT1-MMP C terminus, including the transmembrane domain (not targeted by the siRNA; "MT1-MMP-ΔNterm"; Fig. 8 A), or of full-length MT1-MMP mutated in the LLY motif ("MT1-MMP-LLY/AAA insens"; Fig. 8 A) and rendered siRNA insensitive. Remarkably, expression of MT1-MMP-ΔNterm was sufficient to restore regular podosome numbers, podosome-covered areas (Fig. S5), and podosome densities (Fig. 10) during reformation,. In contrast, full-length MT1-MMP-LLY/AAA insens was not able to

Downloaded from jcb.rupress.org on September 1, 2016

Published April 11, 2016

restore these parameters to control values. Instead, the recovery curves closely followed those of cells depleted for MT1-MMP (Figs. 10 and S5). Collectively, these results indicate that the cytoplasmic region of MT1-MMP is crucial for its localization to podosomes. Moreover, the LLY motif within this region is able to stabilize MT1-MMP at podosome-free islets by anchoring the protease to the unbranched cortical actin network. Through this motif, MT1-MMP is able to exert its memory function and to facilitate efficient reformation of podosomes.

Discussion

The matrix metalloproteinase MT1-MMP is crucial for the ability of podosomes and invadopodia to degrade ECM (Steffen et al., 2008; Poincloux et al., 2009; Linder et al., 2011; Wiesner et al., 2014) and enables invadosome-forming cells to invade into surrounding tissues. In contrast to invadopodia, which are highly enriched in MT1-MMP (Chen and Wang, 1999; Poincloux et al., 2009), detection of MT1-MMP at bona fide podosomes has proven to be challenging. Previous work demonstrated contact of MT1-MMP–positive vesicles with podosomes (Wiesner et al., 2010), whereas siRNA-mediated knockdown of MT1-MMP in human macrophages (Wiesner et al., 2010) and endothelial cells (Varon et al., 2006) inhibited podosomal matrix degradation. However, in contrast to general assumption, detection of MT1-MMP at the ventral surface of podosomes, as well as its exact localization at podosome core or ring structures, has not been shown. Using a pH-sensitive construct of MT1-MMP in combination with TIRF microscopy, we now demonstrate enrichment of MT1-MMP at the ventral surface of primary macrophages, underneath the core structure of podosomes.

Importantly, we also describe a previously unrecognized localization of MT1-MMP at podosome-free islets that are embedded in the ventral plasma membrane of macrophages. These islets become apparent upon podosome dissolution, as shown by live-cell imaging of podosome turnover, and also by drug-induced disruption of podosomes. Podosomes can thus be viewed as organelles that imprint MT1-MMP islets in the plasma membrane, which persist beyond the lifetime of the actual podosome structure. Indeed, several lines of evidence pointed at a potential link between podosomes and islets: (a) both structures show similar sizes and spacing patterns; (b) MT1-MMP islets tend to be localized toward the trailing edge, a preferential site of podosome dissolution; (c) inhibition of podosome formation during adhesion of cells also led to absence of islets; and (d) podosome-associated MT1-MMP-pHluorin has a longer lifetime than the podosome itself.

During the course of regular podosome turnover, 49.98% of podosome-associated MT1-MMP persisted for >50 min, whereas only 18.49% of podosomes showed a comparable lifetime. Similar values were gained by measuring MT1-MMP-pHluorin fluorescence at islets formed by podosome disruption. Here, MT1-MMP islets persisted for at least 60 min. It is also noteworthy that MT1-MMP at invadopodia of breast cancer cells has previously been shown to persist for >40 min (Monteiro et al., 2013). Considering that invadopodia have a lifetime of more than 1 h, whereas podosomes are turned over within minutes (Linder, 2007), these similar values probably reflect the general ability of MT1-MMP to persist for an extended time at the plasma membrane, rather than being podosome or invadopodia specific.

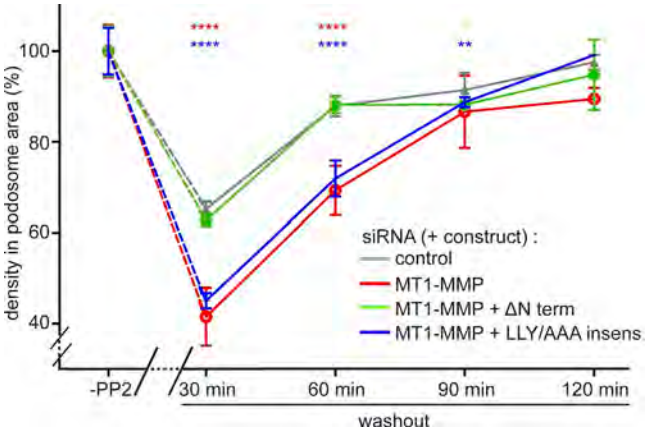

Figure 10. **The LLY motif in the MT1-MMP C terminus is crucial for the recovery of regular podosome densities during podosome reformation.** Statistical evaluation of podosome density (podosomes/100 µm²) during a podosome reformation assay. Parameters were evaluated in cells before disruption of podosomes ("-PP2") or after treatment with podosome-disrupting PP2 and washout of the drug for the indicated periods, in cells treated with control siRNA (gray) or with MT1-MMP-specific siRNA (red). Subsets of MT1-MMP–depleted cells were also expressing a construct of the MT1-MMP C terminus that is not targeted by the siRNA (ΔNterm; green) or of a full-length MT1-MMP construct mutated in the LLY motif, which was rendered siRNA insensitive (LLY/AAA insens.; blue). $n = 3 \times 30$, for cells from three different donors. Note that podosomes are mostly absent at 0 min of the washout; therefore, podosome density was not evaluated for this time point. Note also that expression of the ΔNterm constructs rescues the recovery of regular podosome density, whereas expression of the LLY/AAA mutant construct does not. Values are given as means ± SEM. *, $P < 0.05$; **, $P < 0.01$; ****, $P < 0.0001$. For dot diagrams of podosome numbers, podosome area, and podosome density, see Fig. S6. For specific values, see Table S2.

Lateral movement of podosome core structures is highly variable in the micrometer range. In contrast, podosome-localized MT1-MMP-pHluorin patches showed a more restricted mobility, which probably reflects embedding of the protease in the plasma membrane. This restricted lateral mobility of MT1-MMP was even more evident for MT-MMP islets. In this case, only the net movement of the membrane might provide the driving force for MT1-MMP islets. This could be compared with the well-known sliding of focal adhesions (Ballestrem et al., 2001), the major difference being that focal adhesions are coupled to the ECM via integrins (Wehrle-Haller and Imhof, 2003), whereas this is not a prerequisite for MT1-MMP islets, as discussed below.

An obvious question concerns the molecular composition of MT1-MMP islets. Testing both overexpressed and endogenous proteins, also at high laser power, we could not detect any of the typical podosome core or ring components at MT1-MMP islets, which argues for a complete disruption of the podosome structure. However, recruitment of MT1-MMP to invadosomes has been proposed to involve binding of MT1-MMP to other transmembrane proteins such as integrins and CD44, both of which have been shown to bind MT1-MMP in breast cancer or carcinoma cells (Deryugina et al., 2001; Marrero-Diaz et al., 2009). Therefore, we focused especially on transmembrane cell-matrix adaptors such as CD44, β1, β2, and β3 integrins, as well as integrin interactors such as talin-1 and kindlin-3. Importantly, none of the tested proteins localized to islets. This finding also indicates that the persistence of MT1-MMP at islets after podosome dissolution is not a result of its nature as a transmembrane

Downloaded from jcb.rupress.org on September 1, 2016

Published April 11, 2016

protein, but must be based on another specific property. We also explored the possibility that islets could be sites of altered membrane curvature, as dendritic cell podosomes can act as sensors of membrane topology (van den Dries et al., 2013b), and podosomes have been shown to contain membrane curvature–associated proteins such as CIP4 (Linder et al., 2000b) and FBP17 (Tsuboi et al., 2009). However, neither protein was detectable at islets. In conclusion, MT1-MMP islets present as domains at the ventral plasma membrane that are devoid of typical podosome proteins and contain MT1-MMP as a major proteinaceous component. Their exact composition should be analyzed in future experiments.

We next explored the possibility that MT1-MMP islets could be enriched in specific lipids. Indeed, the podosome-related invadopodia have been identified as specialized membrane domains enriched in cholesterol (Caldieri and Buccione, 2010; Albrechtsen et al., 2011). Moreover, phosphatidylinositols, including PI(3,4,5) (Yu et al., 2013) and PI(3,4)P (Oikawa et al., 2008) have been implicated in invadosome formation in untransformed (Yu et al., 2013) or Src-transformed (Oikawa et al., 2008) fibroblasts. Strikingly, of all lipids tested (Table S1), only cholesterol and PI(4)P showed a clear and previously unreported enrichment at podosomes. Still, no respective accumulations were found in MT1-MMP islets, reinforcing the notion that the protease itself constitutes a major component of islets.

Surprisingly, a matrix degradation assay showed that islets are not degradative on gelatin matrix. There are several possible explanations for this. (a) MT1-MMP at islets does not cleave gelatin directly and might serve only as an activator of the gelatinase MMP-2, which needs intact podosomes as docking sites for respective vesicles. However, this is unlikely, as MT1-MMP has been identified as a bona fide gelatinase. In fact, gelatin zymography is routinely used as an assay to determine MT1-MMP activity (Evans and Itoh, 2007). (b) MT1-MMP is not active at islets. This is also unlikely, as degradative podosomes are acutely disrupted by CK-666. Islets should thus contain active MT1-MMP. Also, as shown by FRAP, there is no major exchange of MT1-MMP at islets, so MT1-MMP that is active at the time of islet appearance is expected to reside for a certain time at islets. (c) MT1-MMP at islets is potentially active but does not come into contact with matrix material. Considering that islets do not contain integrins or CD44 that establish firm and close contact with the ECM, surface-exposed MT1-MMP could be covered by the cellular glycocalyx, preventing contact with the substratum, analogous to the situation in cancer cells (Paszek et al., 2014). Support in establishing matrix contact might come from the oscillatory protrusion of podosomes (van den Dries et al., 2013a), but in the absence of podosomes, islets probably represent flat, nonprotrusive parts of the plasma membrane that are not in close contact with the matrix. Combined, these effects could explain the observed absence of degradative activity at MT1-MMP islets.

Live-cell imaging of podosome reformation, both during regular podosome turnover and disruption induced by Arp2/3 complex inhibition, showed that podosomes are often formed at MT1-MMP islets. Indeed, >60% of all disruption-induced MT1-MMP islets are reused for podosome formation within 10 min after drug washout. Moreover, analysis of regular podosome turnover also allowed the identification of a second mechanism for islet reuse in podosome formation, through recruitment of material generated by fission of adjacent podosomes. Podosome fission is a process that is typically observed in macrophages, with material being split off from the mother podosome, whereas the newly formed daughter podosome is positioned at a distance that integrates it into the podosome group (Evans et al., 2003; Kopp et al., 2006). How fission-generated podosomes are integrated into the regular podosome pattern has been unclear so far. Podosomes are mostly parts of a higher-ordered group, with actin cables forming the connections between individual podosomes (Luxenburg et al., 2007; Bhuwania et al., 2012). The typical equidistant pattern of podosomes is thus thought to be based on actomyosin contractility generated by these cables (Linder et al., 2011). We now show that also MT1-MMP islets play a role in the regulation of podosome spacing, by acting as sites of podosome reemergence or as anchoring points for fission-generated material that integrate well into the existing pattern of podosome groups.

Mutation and deletion analyses showed that the localization of MT1-MMP to podosomes critically depends on its C-terminal cytoplasmic region. Constructs deficient in either catalytic ability (E240A; Rozanov et al., 2001) or oligomerization (DTY/KAF; Tochowicz et al., 2011) localized to podosomes and islets. The former result is also in line with the presence of MT1-MMP-pHluorin at islets under pharmacological inhibition of its proteolytic activity, using the inhibitor NSC405020. It is noteworthy that NSC405020 targets the hemopexin domain interaction surfaces, thus inhibiting collagenolytic activity, but not the overall catalytic activity of MT1-MMP (Remacle et al., 2012). Moreover, deletion of the MT1-MMP N terminus had no effect on its localization to podosomes or islets. Conversely, removal of the cytoplasmic region resulted in dispersal of the respective construct along the plasma membrane. At the same time, control experiments showed that absence of the MT1-MMP C terminus had no discernible effect on localization of the protease to vesicles and its exposure on the cell surface, whereas the number of podosomes per cell was also unaffected.

Importantly, the MT1-MMP C terminus has been shown to contain F-actin binding ability (Uekita et al., 2001), which also prevents diffusion of MT1-MMP out of invadopodia (Yu et al., 2012). The ability of MT1-MMP and actin to interact directly in biochemical experiments (Yu et al., 2012), however, does not rule out a more indirect mode of interaction in cells. It is also noteworthy that podosome cores contain mostly Arp2/3 complex–generated and thus branched actin networks (Linder et al., 2011), and both podosome dissolution during regular turnover or through CK666-induced inhibition of Arp2/3 complex are expected to leave the unbranched actin cytoskeleton intact. We therefore explored the possibility that the C-terminal region of MT1-MMP could anchor the protease to the unbranched subcortical actin cytoskeleton. This idea was substantiated by global inhibition of branched and unbranched F-actin using both cytochalasin D and latrunculin A, which resulted in dissolution of islets. Moreover, upon depletion of endogenous MT1-MMP, a construct of full-length MT1-MMP deficient in F-actin binding (LLY/AAA) failed to form islets. Collectively, these experiments showed that the F-actin binding ability of MT1-MMP is critical for localization of the protease to both podosomes and islets. Additional interactions with podosome components such as cortactin (Artym et al., 2006) or p130Cas (Pan et al., 2011) may support MT1-MMP localization at podosomes. However, upon podosome dissolution, MT1-MMP islets are strictly dependent for stabilization on binding of the MT1-MMP C terminus to the cortical actin cytoskeleton. In addition, oligomerization of MT1-MMP, both by N- (Tochowicz et al.,

Downloaded from jcb.rupress.org on September 1, 2016

Published April 11, 2016

2011) and C-terminal parts (Rozanov et al., 2001) of the molecule may support the coherence of islets.

F-actin binding could also explain the observed role of MT1-MMP islets in recruiting core material generated through podosome fission. F-actin binding of individual MT1-MMP C termini within islets is most likely dynamic, and a subset of binding sites are thus expected to be unoccupied at a given time point. These free binding sites could act as anchoring points for F-actin cores generated by fission. Fission-independent reformation of podosomes may be based on a similar mechanism, as MT1-MMP C termini in islets could bind short cytoplasmic actin filaments, which could act as local concentration points for Arp2/3 complex and actin-associated adaptor proteins such as Tks5 (Seals et al., 2005; Oikawa et al., 2008) or cortactin (Artym et al., 2006), thus facilitating local nucleation of branched actin networks and recruitment of further components. In addition, the MT1-MMP C terminus is also a substrate for Src kinase (Nyalendo et al., 2007) and could thus directly concentrate one of the most important upstream regulators of podosomes (Linder and Aepfelbacher, 2003; Oikawa et al., 2008). Ultimately, all of these potential mechanisms could contribute to MT1-MMP–based reformation of podosomes.

Our data thus reveal a novel function for MT1-MMP at podosomes that is independent of its proteolytic activity. MT1-MMP therefore plays crucial roles not only at the endpoint of podosome assembly, by enabling degradation of ECM material, but also by functioning as a subcellular signpost that facilitates formation or anchoring of nascent podosomes at sites of previously disassembled structures.

In conclusion, we report a previously unrecognized localization of MT1-MMP at podosome-free islets at the ventral plasma membrane of primary human macrophages. MT1-MMP islets become apparent upon dissolution of podosomes, and the existence of podosomes is a prerequisite for islet formation. Importantly, MT1-MMP islets serve as sites for podosome reemergence, either by de novo actin nucleation or by recruiting material generated through podosome fission. MT1-MMP islets enable efficient reformation of podosomes as well as upkeep of the typical equidistant pattern within podosome groups. MT1-MMP islets thus function as cellular memory devices that facilitate the continuous and coordinated ability of macrophages to locally degrade and invade the ECM.

Materials and methods

Cell isolation, cell culture, and transfection

Human peripheral blood monocytes were isolated from buffy coats (provided by F. Bentzien, University Medical Center Hamburg-Eppendorf, Hamburg, Germany) and differentiated into macrophages as described previously (Linder et al., 1999). Cells were cultured in RPMI containing 20% autologous serum at 37°C, 5% CO_2, and 90% humidity. Monocytes were differentiated for at least 7 d, under addition of 20% human autologous serum. At days 7–10 of culture, macrophages were transiently transfected using the Neon Transfection System (Thermo Fisher Scientific) with standard settings (1,000 V, 40 ms, two pulses).

Antibodies, constructs and reagents

Antibodies were purchased from the following companies: mouse monoclonal anti-MT1-MMP and anti–β-actin from EMD Millipore, rabbit polyclonal anti-Tks5, mouse anti-β3 integrin and mouse anti–α-actinin from Santa Cruz Biotechnology, Inc., mouse anti–β1 integrin from Transduction Labs, mouse anti-vinculin from Sigma-Aldrich, mouse anti-CD44 from Cell Signaling Technology, and mouse anti-Arp2 from Abcam. Rabbit polyclonal anti-Src antibody was purchased from Proteintech. Rabbit polyclonal anti-CIP-4 antibody and pEGFP-CIP4 were gifts from P. Aspenström (Karolinska Institute, Sweden). pLifeact-TagGFP2 and pLifeact-TagRFP2 were purchased from Ibidi. mCherry-flotillin-1 and -2 constructs were gifts from C. Gauthier-Rouvière (Centre de Recherche de Biochimie Macromoléculaire, Montpellier, France); Akt-PH-GFP, PLCδ1-PH-GFP, and TAPP1-PH-GFP were provided by T. Balla (National Institutes of Health, Bethesda, MD); mCherry-Talin1C was provided by W. Ziegler (Hannover Medical School, Hannover, Germany); mTagRFP-T-C-Src-7 was purchased from Addgene (plasmid #58006; deposited by M. Davidson, Florida State University, Tallahassee, FL); Tks5-GFP was a gift from S. Courtneidge (Oregon Health and Science University, Portland, OR); GFP-Rab22aQ64L was provided by J. Donaldson (National Institutes of Health, Bethesda, MD); ILK-GFP, β3 integrin-RFP, and GFP-kindlin-3 were gifts from R. Fässler (Max Planck Institute Martinsried, Munich, Germany); GFP-Rab14 Q70L was a gift from R.H. Scheller (Genentech, San Francisco, CA); ApoE-GFP was a gift from M. Kockx (University of Sydney, Sydney, Australia); and GFP–α-actinin was a gift from M. Gimona (Paracelsus University, Salzburg, Austria). MT1-MMP-mCherry and MT1-MMP-pHluorin, both based on the human MT1-MMP sequence, were provided by P. Chavrier (Institute Curie, Paris, France). Respective mutants were created by introducing point mutations (QuikChange Site-Directed Mutagenesis kit; Stratagene) with the following primers for MT1-MMP-pHluorin E240A: (forward [F]: 5′-TTCCTGGTGGCTGTGCACGCCCTGGGCCATGCCCTGGGGC-3′, reverse [R]: 5′-GCCCCAGGGCATGGCCCAGGGCGTGCACAGCCACCAGGAA-3′). MT1-MMP-pHluorin DTY/KAF was generated by introducing three successive point mutations using the following primers: F: 5′-ATTCGTCTTCTTCAAAGGAAAGAAGCATTGGGTGTTTGAT-3′, R: 5′-ATCAAACACCCAATGCTTCTTTCCTTTGAAGAAGACGAAT-3′; F: 5′-TGGGCCGAGGGCTGCCTGCCGACAAGATTGATGCTGCTCT-3′, R: 5′-AGAGCAGCATCAATCTTGTCGGCAGGCAGCCCTCGGCCCA-3′; and F: 5′-CTTCCGTGGAAACAAGTACTTCCGTTTCAACGAAGAGCTC-3′, R: 5′-GAGCTCTTCGTTGAAACGGTAGTACTTGTTTCCACGGAAG-3′. MT1-MMP ΔCterm-pHluorin was generated by the addition of a stop codon after the pHluorin tag using F: 5′-CCTTGCAGTCTTCTTCTTCTGACGCCATGGGACCCCCAGG-3′, R: 5′-CCTGGGGGTCCCATGGCGTCAGAAGAAGAAGACTGCAAGG-3′; and MT1-MMP LLY/AAA-pHluorin was generated using F: 5′-TGGGACCCCCAGGCGAGCGGCCGCCTGCCAGCGTTCCCTG-3′, R: 5′-CAGGGAACGCTGGCAGGCGGCCGCTCGCCTGGGGGTCCCA-3′. MT1-MMP ΔNterm-pHluorin was generated by the insertion of a HindIII restriction site before the pHluorin tag using F: 5′-ATATATTAAATAAGCTTCATGAGTAAAGGAGAA-3′, R: 5′-TAGATAGGGCCCTCTAGATCAGACCTTGTCC-3′; the amplified fragment was digested with HindIII and XbaI and inserted into pcDNA 3.1. NCS 405020 was purchased from APExBIO, RGD peptide was purchased from Sigma-Aldrich, and cytochalasin D and latrunculin A were purchased from EMD Millipore.

siRNA, siRNA-insensitive constructs, and podosome reformation assay

MT1-MMP-specific siRNA was 5′-AACAGGCAAGCGTGATGCAGA-3′, with control siRNA 5′-AGGTAGTGTAACCGCCTTGTT-3′ targeting firefly luciferase (Wiesner et al., 2010, 2013). siRNA-insensitive MT1-MMP ΔCterm-pHluorin and MT1-MMP LLY/AAA-pHluorin were generated by introducing two successive mutations, first with F: 5′-CTTGCAAGTAACTGGCAAAGCTG-3′, R: 5′-CAGCTTTGC

Downloaded from jcb.rupress.org on September 1, 2016

Published April 11, 2016

CAGTTACTTGCAAG-3′; followed by F: 5′-GGCAAAGCAGAT GCAGACACCAT-3′, R: 5′-ATGGTGTCTGCATCTGCTTTGCC-3′.

Podosome reformation assay

Podosome reformation was performed 72 h after siRNA transfection (Cervero et al., 2013). For live-cell imaging, siRNA transfected cells were retransfected after 48 h with both siRNA and Lifeact-GFP and seeded on glass-bottom live-cell dishes for 24 h before imaging. Podosome reformation was analyzed in the live-cell videos. Numbers were processed in Excel 2013 (Microsoft) and GraphPad Prism 6.

Immunostaining

Macrophages were seeded at a density of 10^5 cells per glass coverslip (12-mm diameter) and fixed for 10 min in 3.7% formaldehyde, washed three times in PBS, and permeabilized for 10 min in 0.5% Triton X-100. After three washes with PBS, the cells were incubated for 30 min in blocking solution (1% NHS and NGS in PBS), washed briefly in PBS, and incubated for 60 min in the primary antibody solution. Cells were washed three times in PBS and then incubated for 30 min in secondary antibody solution, supplemented with fluorescence-labeled phalloidin when indicated. After three washes in PBS, the coverslips were kept in PBS for imaging.

Microscopy

Images of fixed samples were acquired with a confocal laser-scanning microscope (DMI 6000 with a TCS SP5 AOBS confocal point scanner; Leica) equipped with a oil-immersion HCX PL APO 63× NA 1.4–0.6 objective.

Live-cell imaging

Cells were imaged in RPMI 1640 medium at 37°C. Images were acquired with a spinning disk confocal system (spinning disc CSU22) fitted on an eclipse Ti microscope (Nikon) with oil immersion Plan-Apo 63× NA 1.4 objective and a charge coupled device camera (EM-CCD C-9100-2). Acquisition and processing of images was performed with Volocity Software (Improvision). Cells were seeded on glass-bottomed dishes (35 mm; Ibidi) at a density of 2×10^5 and incubated for 20 h before the start of the experiment. TIRF imaging was performed with an iLAS TIRF unit from Visitron Systems fitted on an eclipse Ti microscope (Nikon) with oil immersion Plan-Apo 63× NA 1.45 and Plan-Apo 100× NA 1.49. To correct for drift of the microscope stage, TetraSpec Microspheres (0.1 µm, fluorescent blue/green/orange/dark red; Thermo Fisher Scientific) were used.

FRAP

Cells were transfected with MT1-MMP-pHluorin and Lifeact-RFP to visualize islets, and 20 h after transfection, single images of cells were taken every 1 s. FRAP was preceded by acquisition of 10 prebleach images; 10 circular regions of interest with individual podosomes were bleached using 20% of a 405-nm laser. Recovery images were taken for additional 120 s. FRAP analysis was performed with Volocity Software (Improvision). Data were processed with Excel 2013 and GraphPad Prism 6. Fluorescence recovery was measured for 10 individual podosomes at each time point for three cells from three donors.

Quantification of MT1-MMP surface exposure

Macrophages were seeded on glass coverslips (12-mm diameter) at a density of 10^5 and fixed with 3.7% formaldehyde solution (10 min), but not permeabilized. Surface MT1-MMP-mCherry was stained with anti-mCherry antibody followed by an Alexa Fluor 647–conjugated secondary antibody (Wiesner et al., 2010). Quantification of Alexa Fluor 647–based fluorescence intensity was performed using ImageJ. Values of control cells were set to 100%. For comparability, laser intensity was not changed between measurements. For each value, 3×30 cells were evaluated. Statistical analysis was performed with Microsoft Excel and GraphPad Prism. Differences between mean values were analyzed using the Student's *t* test.

Quantification of F-actin/MT1-MMP-pHluorin colocalization

Macrophages overexpressing MT1-MMP-pHluorin were fixed and stained with phalloidin/Alexa Fluor 647. Overlap images (actin/actin or actin/MT1-MMP-pHluorin) were generated using ImageJ (colocalization plugin), with a threshold ratio of 50%. Generated images (colocalized points 8-bit) were quantified by measuring the number of pixels per area of single podosomes with ImageJ. The colocalization index was defined as the ratio of pixels per area (actin/MT1-MMP-pHluorin) and pixels per area (actin/actin) for each podosome. In total, 1,110 podosomes from four independent cells were analyzed. Statistical analysis was performed with Microsoft Excel and GraphPad Prism software. For a correlation analysis, each podosome was measured by size (diameter of core, labeled by phalloidin/Alexa Fluor 647) using ImageJ. For each podosome, correlation between size and the respective colocalization index was calculated as described in the Statistical analysis and podosome and islet tracking section.

Matrix degradation assay

Analysis of gelatin matrix degradation was performed as described previously (Wiesner et al., 2010).

Statistical analysis and podosome and islet tracking

Podosome and islet measurements and tracking were performed using Fiji (Trackmate macro) and ImageJ version 1.49. Student's *t* test was performed using Microsoft Excel and GraphPad Prism software. Statistically significant differences are indicated by single/multiple asterisks (****, $P < 0.0001$; ***, $P < 0.001$; **, $P < 0.01$; and *, $P < 0.05$) Correlation analysis was calculated and plotted using a correlation plot and linear regression line to visualize the degree of correlation. Pearson correlation coefficient (r) and its square (r^2), slope, and significance (P) are shown on the plots.

Online supplemental material

Fig. S1 shows that acquisition of MT1-MMP-pHluorin correlates negatively with podosome size, that surface-exposed MT1-MMP codistributes dynamically with podosomes, and that podosomes and MT1-MMP islets show similar sizes and densities. Fig. S2 shows that the membrane lipids cholesterol and PI(4)P localize to podosomes, but not to MT1-MMP islets, that ApoE-GFP does not localize to podosomes or islets, and that MT1-MMP islets are not degradative on gelatin matrix. Fig. S3 shows the composition of reformed podosomes, the impact of microtubule disruption or dynamin inhibition on islets, and the localization of MT1-MMP mutants to islets. Fig. S4 shows that absence of the cytoplasmic region or catalytic inactivity does not influence MT1-MMP localization to vesicles or cell-surface exposure, and it shows the ability of MT1-MMP mutants to form islets. Fig. S5 shows that the LLY motif in the MT1-MMP C terminus is crucial for the recovery of regular podosome number, area, and density during podosome reformation. Video 1 shows dynamics of MT1-MMP-pHluorin and mCherry-talin-1C. Video 2 shows that MT1-MMP is present at podosomes and at podosome-free islets. Video 3 shows that podosomal MT1-MMP persists beyond disruption of the podosome structure itself. Video 4 shows that MT1-MMP islets are sites of podosome reemergence. Video 5 shows MT1-MMP islets can recruit material generated by podosome fission. Table S1 lists tested potential components of islets. Table S2 provides values for podosome reformation assays and MT1-MMP constructs.

Downloaded from jcb.rupress.org on September 1, 2016

Online supplemental material is available at http://www.jcb.org/cgi/content/full/jcb.201510043/DC1. Additional data are available in the JCB DataViewer at http://dx.doi.org/10.1083/jcb.201510043.dv.

Acknowledgments

We thank P. Aspenström for pEGFP-C1-CIP4 and anti-CIP4 antibody; T. Balla for Akt-PH-GFP, PLCδ1-PH-GFP, TAPP1-PH-GFP, and OSH2-2xPH-GFP; F. Bentzien for buffy coats; P. Chavrier for MT1-MMP-pHluorin; S. Courtneidge for Tks5-mCherry; J. Donaldson for GFP-Rab22-Q64L; R. Fässler for ILK, β3 integrin, and kindlin-3 constructs; C. Gauthier-Rouvière for mCherry-flotillin-1 and -2 constructs; M. Gimona for GFP–α-actinin; M. Kockx for ApoE-GFP; R.H. Scheller for GFP-Rab14-Q70L; W. Ziegler for mCherry-Talin-1C; A. Mordhorst for expert technical assistance; the Universitätsklinikum Eppendorf microscope facility for help with microscopy; and M. Aepfelbacher for continuous support. This work is part of the doctoral thesis of K. El Azzouzi.

This work has been supported by Deutsche Forschungsgemeinschaft (LI925/2-2), the Wilhelm Sander-Stiftung (2007.020.2 and 2014.135.1), and the European Union's Seventh Framework Programme (FP7/2007-2013) under grant agreement FP7-237946 (T3Net).

The authors declare no competing financial interests.

Submitted: 12 October 2015
Accepted: 2 March 2016

References

Albrechtsen, R., D. Stautz, A. Sanjay, M. Kveiborg, and U.M. Wewer. 2011. Extracellular engagement of ADAM12 induces clusters of invadopodia with localized ectodomain shedding activity. *Exp. Cell Res.* 317:195–209. http://dx.doi.org/10.1016/j.yexcr.2010.10.003

Artym, V.V., Y. Zhang, F. Seillier-Moiseiwitsch, K.M. Yamada, and S.C. Mueller. 2006. Dynamic interactions of cortactin and membrane type 1 matrix metalloproteinase at invadopodia: defining the stages of invadopodia formation and function. *Cancer Res.* 66:3034–3043. http://dx.doi.org/10.1158/0008-5472.CAN-05-2177

Balla, A., Y.J. Kim, P. Varnai, Z. Szentpetery, Z. Knight, K.M. Shokat, and T. Balla. 2008. Maintenance of hormone-sensitive phosphoinositide pools in the plasma membrane requires phosphatidylinositol 4-kinase IIIalpha. *Mol. Biol. Cell.* 19:711–721. http://dx.doi.org/10.1091/mbc.E07-07-0713

Ballestrem, C., B. Hinz, B.A. Imhof, and B. Wehrle-Haller. 2001. Marching at the front and dragging behind: differential alphaVbeta3-integrin turnover regulates focal adhesion behavior. *J. Cell Biol.* 155:1319–1332. http://dx.doi.org/10.1083/jcb.200107107

Bhuwania, R., S. Cornfine, Z. Fang, M. Krüger, E.J. Luna, and S. Linder. 2012. Supervillin couples myosin-dependent contractility to podosomes and enables their turnover. *J. Cell Sci.* 125:2300–2314. http://dx.doi.org/10.1242/jcs.100032

Burger, K.L., A.L. Davis, S. Isom, N. Mishra, and D.F. Seals. 2011. The podosome marker protein Tks5 regulates macrophage invasive behavior. *Cytoskeleton (Hoboken).* 68:694–711. http://dx.doi.org/10.1002/cm.20545

Burgstaller, G., and M. Gimona. 2005. Podosome-mediated matrix resorption and cell motility in vascular smooth muscle cells. *Am. J. Physiol. Heart Circ. Physiol.* 288:H3001–H3005. http://dx.doi.org/10.1152/ajpheart.01002.2004

Burns, S., A.J. Thrasher, M.P. Blundell, L. Machesky, and G.E. Jones. 2001. Configuration of human dendritic cell cytoskeleton by Rho GTPases, the WAS protein, and differentiation. *Blood.* 98:1142–1149. http://dx.doi.org/10.1182/blood.V98.4.1142

Buschman, M.D., P.A. Bromann, P. Cejudo-Martin, F. Wen, I. Pass, and S.A. Courtneidge. 2009. The novel adaptor protein Tks4 (SH3PXD2B) is required for functional podosome formation. *Mol. Biol. Cell.* 20:1302–1311. http://dx.doi.org/10.1091/mbc.E08-09-0949

Caldieri, G., and R. Buccione. 2010. Aiming for invadopodia: organizing polarized delivery at sites of invasion. *Trends Cell Biol.* 20:64–70. http://dx.doi.org/10.1016/j.tcb.2009.10.006

Caldieri, G., G. Giacchetti, G. Beznoussenko, F. Attanasio, I. Ayala, and R. Buccione. 2009. Invadopodia biogenesis is regulated by caveolin-mediated modulation of membrane cholesterol levels. *J. Cell. Mol. Med.* 13:1728–1740. http://dx.doi.org/10.1111/j.1582-4934.2008.00568.x

Cervero, P., L. Panzer, and S. Linder. 2013. Podosome reformation in macrophages: assays and analysis. *Methods Mol. Biol.* 1046:97–121. http://dx.doi.org/10.1007/978-1-62703-538-5_6

Chabadel, A., I. Bañon-Rodríguez, D. Cluet, B.B. Rudkin, B. Wehrle-Haller, E. Genot, P. Jurdic, I.M. Anton, and F. Saltel. 2007. CD44 and beta3 integrin organize two functionally distinct actin-based domains in osteoclasts. *Mol. Biol. Cell.* 18:4899–4910. http://dx.doi.org/10.1091/mbc.E07-04-0378

Chellaiah, M.A. 2006. Regulation of podosomes by integrin alphavbeta3 and Rho GTPase-facilitated phosphoinositide signaling. *Eur. J. Cell Biol.* 85:311–317. http://dx.doi.org/10.1016/j.ejcb.2006.01.008

Chen, W.T., and J.Y. Wang. 1999. Specialized surface protrusions of invasive cells, invadopodia and lamellipodia, have differential MT1-MMP, MMP-2, and TIMP-2 localization. *Ann. N. Y. Acad. Sci.* 878:361–371. http://dx.doi.org/10.1111/j.1749-6632.1999.tb07695.x

Cornfine, S., M. Himmel, P. Kopp, K. El Azzouzi, C. Wiesner, M. Krüger, T. Rudel, and S. Linder. 2011. The kinesin KIF9 and reggie/flotillin proteins regulate matrix degradation by macrophage podosomes. *Mol. Biol. Cell.* 22:202–215. http://dx.doi.org/10.1091/mbc.E10-05-0394

Cortesio, C.L., S.A. Wernimont, D.L. Kastner, K.M. Cooper, and A. Huttenlocher. 2010. Impaired podosome formation and invasive migration of macrophages from patients with a PSTPIP1 mutation and PAPA syndrome. *Arthritis Rheum.* 62:2556–2558. http://dx.doi.org/10.1002/art.27521

Deryugina, E.I., B. Ratnikov, E. Monosov, T.I. Postnova, R. DiScipio, J.W. Smith, and A.Y. Strongin. 2001. MT1-MMP initiates activation of pro-MMP-2 and integrin alphavbeta3 promotes maturation of MMP-2 in breast carcinoma cells. *Exp. Cell Res.* 263:209–223. http://dx.doi.org/10.1006/excr.2000.5118

Destaing, O., F. Saltel, J.C. Géminard, P. Jurdic, and F. Bard. 2003. Podosomes display actin turnover and dynamic self-organization in osteoclasts expressing actin-green fluorescent protein. *Mol. Biol. Cell.* 14:407–416. http://dx.doi.org/10.1091/mbc.E02-07-0389

Evans, R.D., and Y. Itoh. 2007. Analyses of MT1-MMP activity in cells. *Methods Mol. Med.* 135:239–249. http://dx.doi.org/10.1007/978-1-59745-401-8_15

Evans, J.G., I. Correia, O. Krasavina, N. Watson, and P. Matsudaira. 2003. Macrophage podosomes assemble at the leading lamella by growth and fragmentation. *J. Cell Biol.* 161:697–705. http://dx.doi.org/10.1083/jcb.200212037

Gimona, M., I. Kaverina, G.P. Resch, E. Vignal, and G. Burgstaller. 2003. Calponin repeats regulate actin filament stability and formation of podosomes in smooth muscle cells. *Mol. Biol. Cell.* 14:2482–2491. http://dx.doi.org/10.1091/mbc.E02-11-0743

Gimpl, G., and K. Gehrig-Burger. 2011. Probes for studying cholesterol binding and cell biology. *Steroids.* 76:216–231. http://dx.doi.org/10.1016/j.steroids.2010.11.001

Griera, M., E. Martin-Villar, I. Banon-Rodríguez, M.P. Blundell, G.E. Jones, I.M. Anton, A.J. Thrasher, M. Rodriguez-Puyol, and Y. Calle. 2014. Integrin linked kinase (ILK) regulates podosome maturation and stability in dendritic cells. *Int. J. Biochem. Cell Biol.* 50:47–54. http://dx.doi.org/10.1016/j.biocel.2014.01.021

Iqbal, Z., P. Cejudo-Martin, A. de Brouwer, B. van der Zwaag, P. Ruiz-Lozano, M.C. Scimia, J.D. Lindsey, R. Weinreb, B. Albrecht, A. Megarbane, et al. 2010. Disruption of the podosome adaptor protein TKS4 (SH3PXD2B) causes the skeletal dysplasia, eye, and cardiac abnormalities of Frank-Ter Haar Syndrome. *Am. J. Hum. Genet.* 86:254–261. http://dx.doi.org/10.1016/j.ajhg.2010.01.009

Junutula, J.R., A.M. De Maziére, A.A. Peden, K.E. Ervin, R.J. Advani, S.M. van Dijk, J. Klumperman, and R.H. Scheller. 2004. Rab14 is involved in membrane trafficking between the Golgi complex and endosomes. *Mol. Biol. Cell.* 15:2218–2229. http://dx.doi.org/10.1091/mbc.E03-10-0777

Kopp, P., R. Lammers, M. Aepfelbacher, G. Woehlke, T. Rudel, N. Machuy, W. Steffen, and S. Linder. 2006. The kinesin KIF1C and microtubule plus ends regulate podosome dynamics in macrophages. *Mol. Biol. Cell.* 17:2811–2823. http://dx.doi.org/10.1091/mbc.E05-11-1010

Labernadie, A., C. Thibault, C. Vieu, I. Maridonneau-Parini, and G.M. Charrière. 2010. Dynamics of podosome stiffness revealed by atomic force microscopy. *Proc. Natl. Acad. Sci. USA.* 107:21016–21021. http://dx.doi.org/10.1073/pnas.1007835107

Downloaded from jcb.rupress.org on September 1, 2016

Published April 11, 2016

Linder, S. 2007. The matrix corroded: podosomes and invadopodia in extracellular matrix degradation. *Trends Cell Biol.* 17:107–117. http://dx.doi.org/10.1016/j.tcb.2007.01.002

Linder, S., and M. Aepfelbacher. 2003. Podosomes: adhesion hot-spots of invasive cells. *Trends Cell Biol.* 13:376–385. http://dx.doi.org/10.1016/S0962-8924(03)00128-4

Linder, S., D. Nelson, M. Weiss, and M. Aepfelbacher. 1999. Wiskott-Aldrich syndrome protein regulates podosomes in primary human macrophages. *Proc. Natl. Acad. Sci. USA.* 96:9648–9653. http://dx.doi.org/10.1073/pnas.96.17.9648

Linder, S., H. Higgs, K. Hüfner, K. Schwarz, U. Pannicke, and M. Aepfelbacher. 2000a. The polarization defect of Wiskott-Aldrich syndrome macrophages is linked to dislocalization of the Arp2/3 complex. *J. Immunol.* 165:221–225. http://dx.doi.org/10.4049/jimmunol.165.1.221

Linder, S., K. Hüfner, U. Wintergerst, and M. Aepfelbacher. 2000b. Microtubule-dependent formation of podosomal adhesion structures in primary human macrophages. *J. Cell Sci.* 113:4165–4176.

Linder, S., C. Wiesner, and M. Himmel. 2011. Degrading devices: invadosomes in proteolytic cell invasion. *Annu. Rev. Cell Dev. Biol.* 27:185–211. http://dx.doi.org/10.1146/annurev-cellbio-092910-154216

Luxenburg, C., D. Geblinger, E. Klein, K. Anderson, D. Hanein, B. Geiger, and L. Addadi. 2007. The architecture of the adhesive apparatus of cultured osteoclasts: from podosome formation to sealing zone assembly. *PLoS One.* 2:e179. http://dx.doi.org/10.1371/journal.pone.0000179

Luxenburg, C., S. Winograd-Katz, L. Addadi, and B. Geiger. 2012. Involvement of actin polymerization in podosome dynamics. *J. Cell Sci.* 125:1666–1672. http://dx.doi.org/10.1242/jcs.075903

Marchisio, P.C., N. D'Urso, P.M. Comoglio, F.G. Giancotti, and G. Tarone. 1988. Vanadate-treated baby hamster kidney fibroblasts show cytoskeleton and adhesion patterns similar to their Rous sarcoma virus-transformed counterparts. *J. Cell. Biochem.* 37:151–159. http://dx.doi.org/10.1002/jcb.240370203

Marrero-Diaz, R., J.J. Bravo-Cordero, D. Megías, M.A. García, R.A. Bartolomé, J. Teixido, and M.C. Montoya. 2009. Polarized MT1-MMP-CD44 interaction and CD44 cleavage during cell retraction reveal an essential role for MT1-MMP in CD44-mediated invasion. *Cell Motil. Cytoskeleton.* 66:48–61. http://dx.doi.org/10.1002/cm.20325

Miesenböck, G. 2012. Synapto-pHluorins: genetically encoded reporters of synaptic transmission. *Cold Spring Harb. Protoc.* 2012:213–217. http://dx.doi.org/10.1101/pdb.ip067827

Monteiro, P., C. Rossé, A. Castro-Castro, M. Irondelle, E. Lagoutte, P. Paul-Gilloteaux, C. Desnos, E. Formstecher, F. Darchen, D. Perrais, et al. 2013. Endosomal WASH and exocyst complexes control exocytosis of MT1-MMP at invadopodia. *J. Cell Biol.* 203:1063–1079. http://dx.doi.org/10.1083/jcb.201306162

Moreau, V., F. Tatin, C. Varon, G. Anies, C. Savona-Baron, and E. Génot. 2006. Cdc42-driven podosome formation in endothelial cells. *Eur. J. Cell Biol.* 85:319–325. http://dx.doi.org/10.1016/j.ejcb.2005.09.009

Murphy, D.A., and S.A. Courtneidge. 2011. The 'ins' and 'outs' of podosomes and invadopodia: characteristics, formation and function. *Nat. Rev. Mol. Cell Biol.* 12:413–426. http://dx.doi.org/10.1038/nrm3141

Murphy, D.A., B. Diaz, P.A. Bromann, J.H. Tsai, Y. Kawakami, J. Maurer, R.A. Stewart, J.C. Izpisúa-Belmonte, and S.A. Courtneidge. 2011. A Src-Tks5 pathway is required for neural crest cell migration during embryonic development. *PLoS One.* 6:e22499. (published erratum appears in *PLoS One*. 2012;7(8))http://dx.doi.org/10.1371/journal.pone.0022499

Nolen, B.J., N. Tomasevic, A. Russell, D.W. Pierce, Z. Jia, C.D. McCormick, J. Hartman, R. Sakowicz, and T.D. Pollard. 2009. Characterization of two classes of small molecule inhibitors of Arp2/3 complex. *Nature.* 460:1031–1034. http://dx.doi.org/10.1038/nature08231

Nyalendo, C., M. Michaud, E. Beaulieu, C. Roghi, G. Murphy, D. Gingras, and R. Béliveau. 2007. Src-dependent phosphorylation of membrane type I matrix metalloproteinase on cytoplasmic tyrosine 573: role in endothelial and tumor cell migration. *J. Biol. Chem.* 282:15690–15699. http://dx.doi.org/10.1074/jbc.M608045200

Obika, M., R.B. Vernon, M.D. Gooden, K.R. Braun, C.K. Chan, and T.N. Wight. 2014. ADAMTS-4 and biglycan are expressed at high levels and co-localize to podosomes during endothelial cell tubulogenesis in vitro. *J. Histochem. Cytochem.* 62:34–49. http://dx.doi.org/10.1369/0022155413507727

Oikawa, T., T. Itoh, and T. Takenawa. 2008. Sequential signals toward podosome formation in NIH-src cells. *J. Cell Biol.* 182:157–169. http://dx.doi.org/10.1083/jcb.200801042

Osiak, A.E., G. Zenner, and S. Linder. 2005. Subconfluent endothelial cells form podosomes downstream of cytokine and RhoGTPase signaling. *Exp. Cell Res.* 307:342–353. http://dx.doi.org/10.1016/j.yexcr.2005.03.035

Pan, Y.R., C.L. Chen, and H.C. Chen. 2011. FAK is required for the assembly of podosome rosettes. *J. Cell Biol.* 195:113–129. http://dx.doi.org/10.1083/jcb.201103016

Paszek, M.J., C.C. DuFort, O. Rossier, R. Bainer, J.K. Mouw, K. Godula, J.E. Hudak, J.N. Lakins, A.C. Wijekoon, L. Cassereau, et al. 2014. The cancer glycocalyx mechanically primes integrin-mediated growth and survival. *Nature.* 511:319–325. http://dx.doi.org/10.1038/nature13535

Pfaff, M., and P. Jurdic. 2001. Podosomes in osteoclast-like cells: structural analysis and cooperative roles of paxillin, proline-rich tyrosine kinase 2 (Pyk2) and integrin alphaVbeta3. *J. Cell Sci.* 114:2775–2786.

Poincloux, R., F. Lizárraga, and P. Chavrier. 2009. Matrix invasion by tumour cells: a focus on MT1-MMP trafficking to invadopodia. *J. Cell Sci.* 122:3015–3024. http://dx.doi.org/10.1242/jcs.034561

Remacle, A.G., V.S. Golubkov, S.A. Shiryaev, R. Dahl, J.L. Stebbins, A.V. Chernov, A.V. Cheltsov, M. Pellecchia, and A.Y. Strongin. 2012. Novel MT1-MMP small-molecule inhibitors based on insights into hemopexin domain function in tumor growth. *Cancer Res.* 72:2339–2349. http://dx.doi.org/10.1158/0008-5472.CAN-11-4149

Rottiers, P., F. Saltel, T. Daubon, B. Chaigne-Delalande, V. Tridon, C. Billottet, E. Reuzeau, and E. Génot. 2009. TGFbeta-induced endothelial podosomes mediate basement membrane collagen degradation in arterial vessels. *J. Cell Sci.* 122:4311–4318. http://dx.doi.org/10.1242/jcs.057448

Rozanov, D.V., E.I. Deryugina, B.I. Ratnikov, E.Z. Monosov, G.N. Marchenko, J.P. Quigley, and A.Y. Strongin. 2001. Mutation analysis of membrane type-1 matrix metalloproteinase (MT1-MMP). The role of the cytoplasmic tail Cys(574), the active site Glu(240), and furin cleavage motifs in oligomerization, processing, and self-proteolysis of MT1-MMP expressed in breast carcinoma cells. *J. Biol. Chem.* 276:25705–25714. http://dx.doi.org/10.1074/jbc.M007921200

Ruoslahti, E. 1996. RGD and other recognition sequences for integrins. *Annu. Rev. Cell Dev. Biol.* 12:697–715. http://dx.doi.org/10.1146/annurev.cellbio.12.1.697

Seals, D.F., E.F. Azucena Jr., I. Pass, L. Tesfay, R. Gordon, M. Woodrow, J.H. Resau, and S.A. Courtneidge. 2005. The adaptor protein Tks5/Fish is required for podosome formation and function, and for the protease-driven invasion of cancer cells. *Cancer Cell.* 7:155–165. http://dx.doi.org/10.1016/j.ccr.2005.01.006

Seano, G., G. Chiaverina, P.A. Gagliardi, L. di Blasio, A. Puliafito, C. Bouvard, R. Sessa, G. Tarone, L. Sorokin, D. Helley, et al. 2014. Endothelial podosome rosettes regulate vascular branching in tumour angiogenesis. *Nat. Cell Biol.* 16:931–941: 1–8. http://dx.doi.org/10.1038/ncb3036

Starnes, T.W., D.A. Bennin, X. Bing, J.C. Eickhoff, D.C. Grahf, J.M. Bellak, C.M. Seroogy, P.J. Ferguson, and A. Huttenlocher. 2014. The F-BAR protein PSTPIP1 controls extracellular matrix degradation and filopodia formation in macrophages. *Blood.* 123:2703–2714. http://dx.doi.org/10.1182/blood-2013-07-516948

Steffen, A., G. Le Dez, R. Poincloux, C. Recchi, P. Nassoy, K. Rottner, T. Galli, and P. Chavrier. 2008. MT1-MMP-dependent invasion is regulated by TI-VAMP/VAMP7. *Curr. Biol.* 18:926–931. http://dx.doi.org/10.1016/j.cub.2008.05.044

Thrasher, A.J., S. Burns, R. Lorenzi, and G.E. Jones. 2000. The Wiskott-Aldrich syndrome: disordered actin dynamics in haematopoietic cells. *Immunol. Rev.* 178:118–128. http://dx.doi.org/10.1034/j.1600-065X.2000.17803.x

Tochowicz, A., P. Goettig, R. Evans, R. Visse, Y. Shitomi, R. Palmisano, N. Ito, K. Richter, K. Maskos, D. Franke, et al. 2011. The dimer interface of the membrane type 1 matrix metalloproteinase hemopexin domain: crystal structure and biological functions. *J. Biol. Chem.* 286:7587–7600. http://dx.doi.org/10.1074/jbc.M110.178434

Tsuboi, S., H. Takada, T. Hara, N. Mochizuki, T. Funyu, H. Saitoh, Y. Terayama, K. Yamaya, C. Ohyama, S. Nonoyama, and H.D. Ochs. 2009. FBP17 Mediates a Common Molecular Step in the Formation of Podosomes and Phagocytic Cups in Macrophages. *J. Biol. Chem.* 284:8548–8556. http://dx.doi.org/10.1074/jbc.M805638200

Uekita, T., Y. Itoh, I. Yana, H. Ohno, and M. Seiki. 2001. Cytoplasmic tail-dependent internalization of membrane-type 1 matrix metalloproteinase is important for its invasion-promoting activity. *J. Cell Biol.* 155:1345–1356. http://dx.doi.org/10.1083/jcb.200108112

Ussar, S., H.V. Wang, S. Linder, R. Fässler, and M. Moser. 2006. The Kindlins: subcellular localization and expression during murine development. *Exp. Cell Res.* 312:3142–3151. http://dx.doi.org/10.1016/j.yexcr.2006.06.030

Vance, J.E., B. Karten, and H. Hayashi. 2006. Lipid dynamics in neurons. *Biochem. Soc. Trans.* 34:399–403. http://dx.doi.org/10.1042/BST0340399

van den Dries, K., M.B. Meddens, S. de Keijzer, S. Shekhar, V. Subramaniam, C.G. Figdor, and A. Cambi. 2013a. Interplay between myosin IIA-mediated contractility and actin network integrity orchestrates podosome composition and oscillations. *Nat. Commun.* 4:1412. http://dx.doi.org/10.1038/ncomms2402

Downloaded from jcb.rupress.org on September 1, 2016

Published April 11, 2016

van den Dries, K., S.L. Schwartz, J. Byars, M.B. Meddens, M. Bolomini-Vittori, D.S. Lidke, C.G. Figdor, K.A. Lidke, and A. Cambi. 2013b. Dual-color superresolution microscopy reveals nanoscale organization of mechanosensory podosomes. *Mol. Biol. Cell.* 24:2112–2123. http://dx.doi.org/10.1091/mbc.E12-12-0856

Varon, C., F. Tatin, V. Moreau, E. Van Obberghen-Schilling, S. Fernandez-Sauze, E. Reuzeau, I. Kramer, and E. Génot. 2006. Transforming growth factor beta induces rosettes of podosomes in primary aortic endothelial cells. *Mol. Cell. Biol.* 26:3582–3594. http://dx.doi.org/10.1128/MCB.26.9.3582-3594.2006

Wehrle-Haller, B., and B.A. Imhof. 2003. Actin, microtubules and focal adhesion dynamics during cell migration. *Int. J. Biochem. Cell Biol.* 35:39–50. http://dx.doi.org/10.1016/S1357-2725(02)00071-7

Weigert, R., A.C. Yeung, J. Li, and J.G. Donaldson. 2004. Rab22a regulates the recycling of membrane proteins internalized independently of clathrin. *Mol. Biol. Cell.* 15:3758–3770. http://dx.doi.org/10.1091/mbc.E04-04-0342

Wiesner, C., J. Faix, M. Himmel, F. Bentzien, and S. Linder. 2010. KIF5B and KIF3A/KIF3B kinesins drive MT1-MMP surface exposure, CD44 shedding, and extracellular matrix degradation in primary macrophages. *Blood.* 116:1559–1569. http://dx.doi.org/10.1182/blood-2009-12-257089

Wiesner, C., K. El Azzouzi, and S. Linder. 2013. A specific subset of RabGTPases controls cell surface exposure of MT1-MMP, extracellular matrix degradation and three-dimensional invasion of macrophages. *J. Cell Sci.* 126:2820–2833. http://dx.doi.org/10.1242/jcs.122358

Wiesner, C., V. Le-Cabec, K. El Azzouzi, I. Maridonneau-Parini, and S. Linder. 2014. Podosomes in space: macrophage migration and matrix degradation in 2D and 3D settings. *Cell Adhes. Migr.* 8:179–191. http://dx.doi.org/10.4161/cam.28116

Yu, C.H., N.B. Rafiq, A. Krishnasamy, K.L. Hartman, G.E. Jones, A.D. Bershadsky, and M.P. Sheetz. 2013. Integrin-matrix clusters form podosome-like adhesions in the absence of traction forces. *Cell Reports.* 5:1456–1468. http://dx.doi.org/10.1016/j.celrep.2013.10.040

Yu, X., T. Zech, L. McDonald, E.G. Gonzalez, A. Li, I. Macpherson, J.P. Schwarz, H. Spence, K. Futó, P. Timpson, et al. 2012. N-WASP coordinates the delivery and F-actin-mediated capture of MT1-MMP at invasive pseudopods. *J. Cell Biol.* 199:527–544. http://dx.doi.org/10.1083/jcb.201203025

Zambonin-Zallone, A., A. Teti, M. Grano, A. Rubinacci, M. Abbadini, M. Gaboli, and P.C. Marchisio. 1989. Immunocytochemical distribution of extracellular matrix receptors in human osteoclasts: a beta 3 integrin is colocalized with vinculin and talin in the podosomes of osteoclastoma giant cells. *Exp. Cell Res.* 182:645–652. http://dx.doi.org/10.1016/0014-4827(89)90266-8

Downloaded from jcb.rupress.org on September 1, 2016

El Azzouzi et al., http://www.jcb.org/cgi/content/full/jcb.201510043/DC1

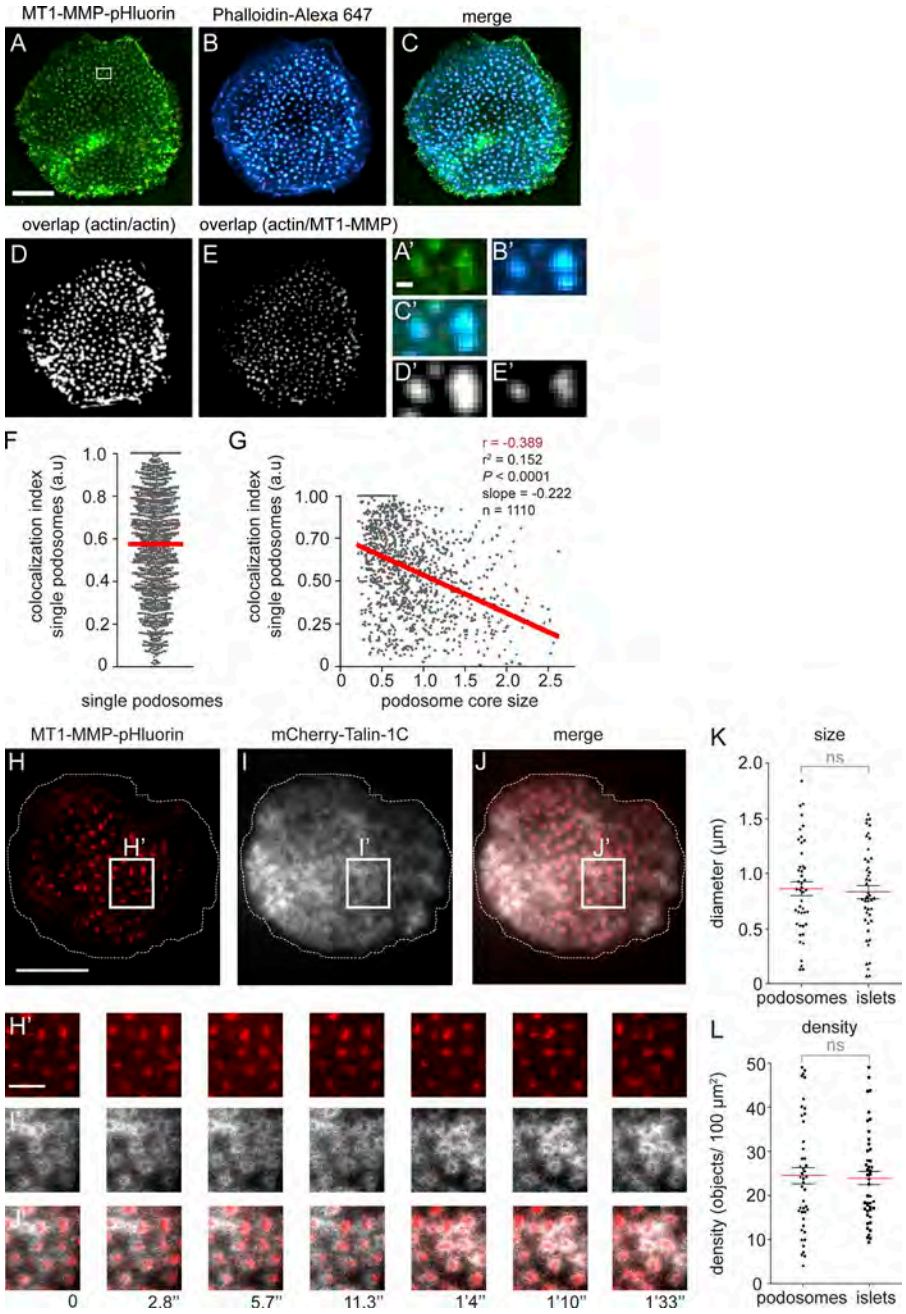

Figure S1. **Acquisition of MT1-MMP-pHluorin correlates negatively with podosome size, surface-exposed MT1-MMP codistributes dynamically with podosomes, and podosomes and MT1-MMP islets show similar sizes and densities.** (A–G) Correlation of MT1-MMP-pHluorin and F-actin at podosomes. (A–C) TIRF micrographs of macrophage expressing MT1-MMP-pHluorin (A, green) and stained for F-actin using phalloidin/Alexa Fluor 647 (B, blue), with merge (C). Bar, 10 µm. (D and E) Micrographs showing colocalizing pixels between actin/actin and actin/MT1-MMP-pHluorin, used for determination of the colocalization index. Yellow box in A indicates detail region shown in (A′–E′). Bars, 1 µm. (F) Colocalization index (0.57), as determined for 1,100 podosomes from four different cells; (G) correlation between colocalization index and podosome size. Correlation coefficient r: –0.389; r^2: 0.152, with a slope of 0.222, and P < 0.0001. (H–J) TIRF micrographs of macrophage expressing MT1-MMP-pHluorin (H, red) and mCherry-Talin-1C (I, white), to visualize podosome rings, with merge in J. Still images taken from Video 1. White boxes indicate detail regions shown in H′–J′. Time since start of the experiment is indicated in minutes and seconds. Bars: (H–J) 10 µm; (H′–J′) 2 µm. (K and L) Statistical evaluation of sizes of single podosomes and MT1-MMP islets (K) and densities (L) of podosomes and islets in macrophages. Each dot represents the respective value from a single cell. For each analysis, 3 × 15 cells from three different donors were evaluated. Red bar indicates mean ± SEM. ns, not significant.

THE JOURNAL OF CELL BIOLOGY

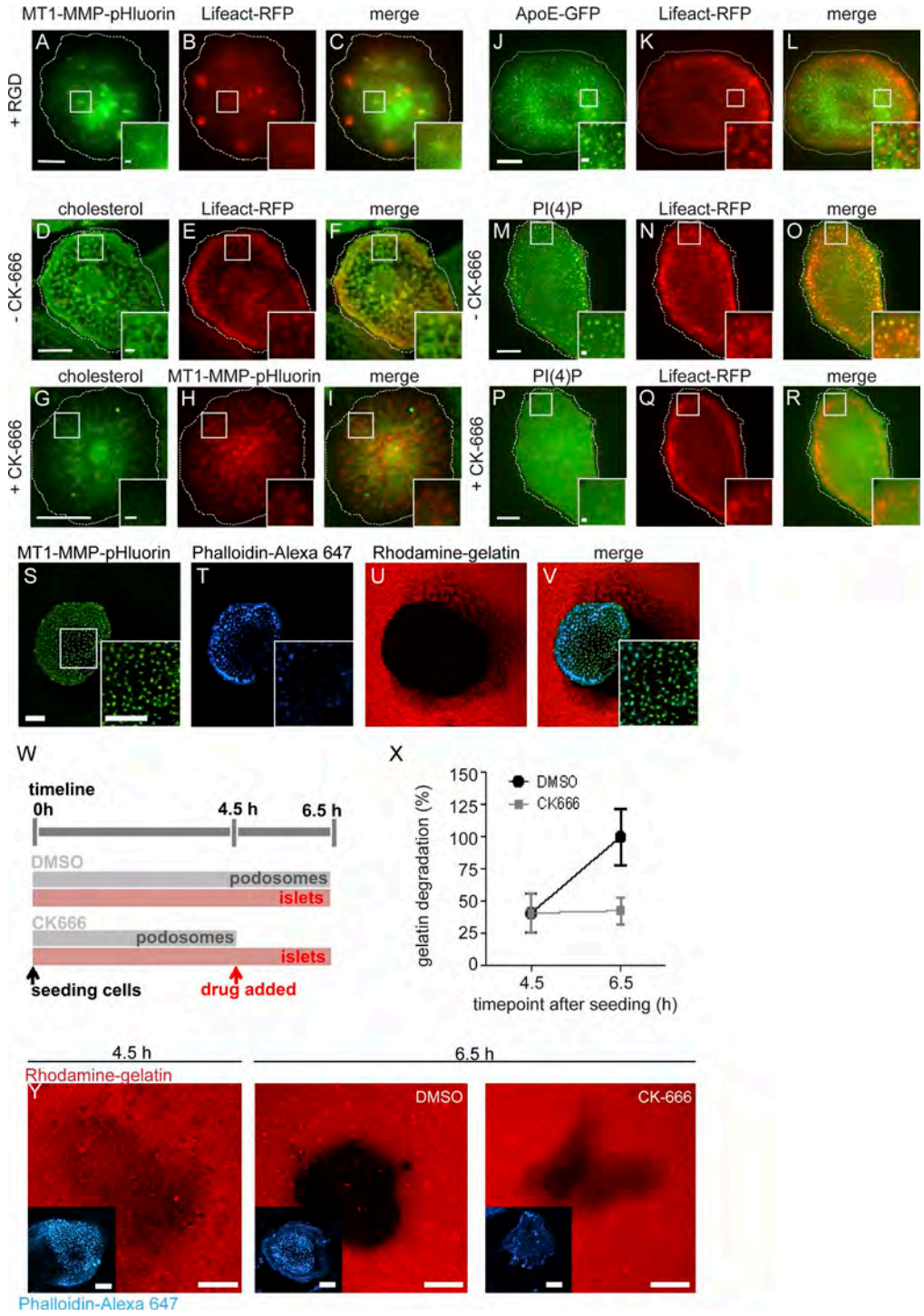

Figure S2. **The membrane lipids cholesterol and PI(4)P localize to podosomes, but not to MT1-MMP islets; ApoE-GFP does not localize to podosomes or islets; and MT1-MMP islets are not degradative on gelatin matrix.** (A–C) Immunofluorescence micrograph of macrophage expressing MT1-MMP-pHluorin (A, green) and Lifeact-RFP (B, red), seeded in the presence of integrin-binding RGD peptide (10 µM). (D–I) Immunofluorescence micrographs of macrophages expressing Lifeact-RFP (E, red) or MT1-MMP-pHluorin (H), and stained with filipin (405 nm excitation), to detect cholesterol (D and G, green). The macrophage in G–I was treated with CK-666. Note enrichment of cholesterol at F-actin–rich podosomes (F), but no enrichment at MT1-MMP islets (I). (J–L) Immunofluorescence micrographs of macrophage expressing ApoE-GFP (J, green) and Lifeact-RFP (K; red), with merge (L). Note the absence of ApoE-GFP from podosomes. (M–R) Immunofluorescence micrographs of macrophage expressing PI(4)P sensor OSH2-2xPH-GFP (M and P, green) and Lifeact-RFP (N and Q, red). Macrophage in P–R was treated with CK-666 to disrupt podosomes and induce MT1-MMP islet formation. Note enrichment of PI(4)P at podosomes, followed by dispersal after CK-666 treatment. Bars: 10 µm; (insets) 1 µm. (S–V) TIRF micrographs of macrophage expressing MT1-MMP-pHluorin (S, green), seeded on rhodamine-labeled gelatin (U, red) and stained for F-actin with phalloidin/Alexa Fluor 647 (T, blue) with merge (V). (W) Timeline of experiment for analysis of matrix degradation. Time points after seeding of cells on labeled matrix are indicated. Colored bars indicate presence of podosomes and/or islets in cell populations treated with indicated drugs. (X) Statistical evaluation of matrix degradation at 4.5- and 6.5-h time points after seeding of cells on gelatin matrix. Maximum of matrix degradation in control cells at 6.5 h was set to 100%. (Y) Representative images of matrix degradation at time points 4.5 h (left) and 6.5 h in cells treated for 2 h with DMSO as control (middle) or CK-666 (right). Insets show F-actin staining in blue. Bars: 10 µm; (insets) 1 µm.

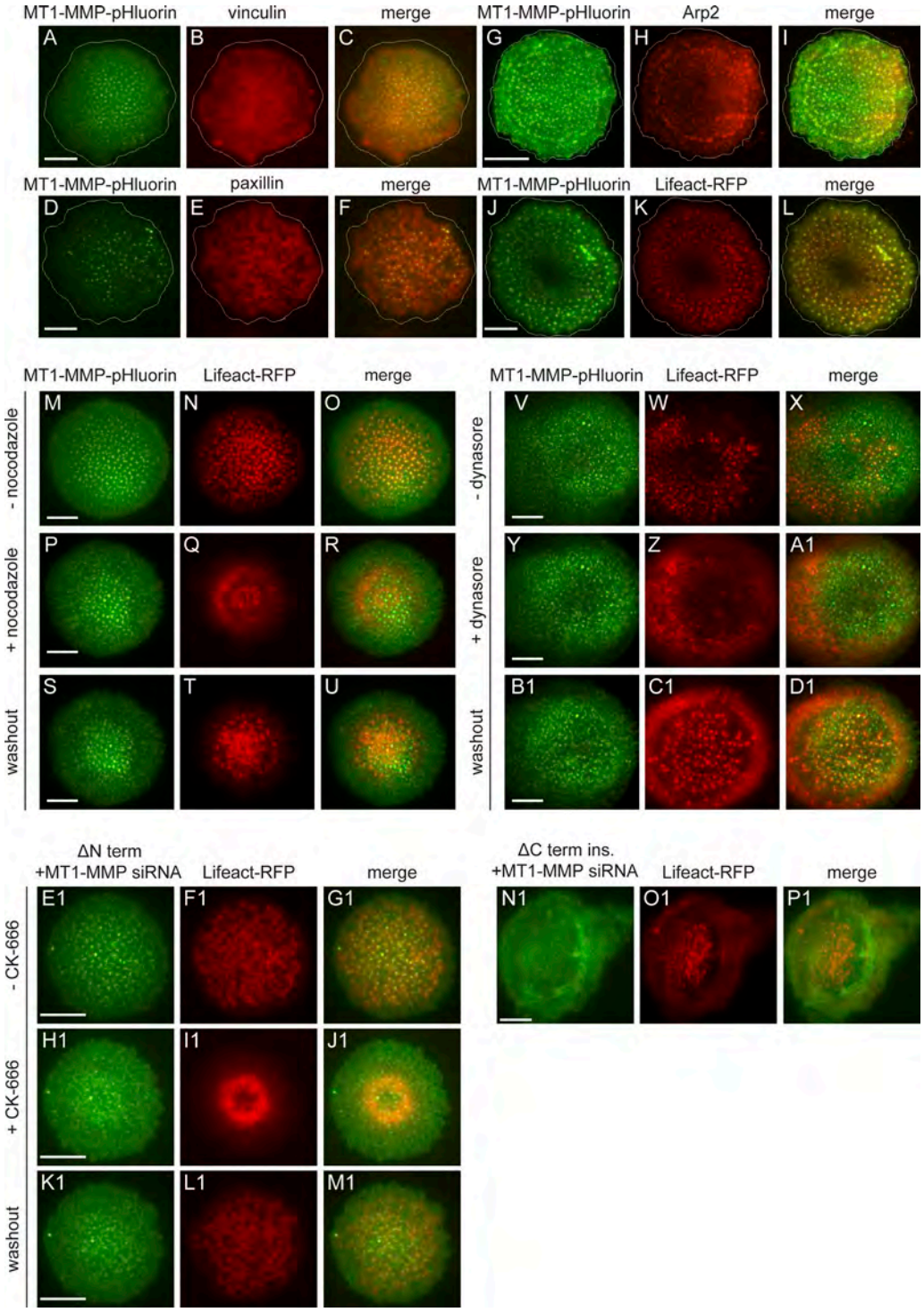

Figure S3. **Composition of reformed podosomes, impact of microtubule disruption or dynamin inhibition on islets, and localization of MT1-MMP mutants to islets.** (A–L) Composition of podosomes reformed after CK-666 washout. TIRF micrographs of macrophages expressing MT1-MMP-pHluorin (A, D, G, and J) and stained for vinculin (B), paxillin (E), and Arp2 (H) using respective antibodies or coexpressing Lifeact-RFP (K), with merges. (M–D1) Impact of microtubule disruption by nocodazole (M–U) or dynamin inhibition by dynasore (V–D1) on islet stability and podosome reformation. Stills from TIRF live-cell videos of macrophages expressing MT1-MMP-pHluorin (M, P, S, V, Y, and B1) and Lifeact-RFP (N, Q, T, WZ, and C1), with merges (O, R, U, X, A1, and D1) and treated with 1 µM nocodazole. (P–R) or 10 µM dynasore (Y-A1), with subsequent washout (S–U and B1–D1). Note disruption of podosomes in both cases (Q and Z) but reformation of podosomes mostly between islets in the nocodazole washout (U) and mostly at islets in the dynasore washout (D1). (E1–P1) Localization of MT1-MMPΔNterm and ΔCterm siRNA mutants in cells depleted of endogenous MT1-MMP by siRNA. Note that MT1-MMPΔNterm is naturally resistant to the used MT1-MMP siRNA, whereas the ΔCterm mutant was rendered insensitive by respective point mutations. Stills from TIRF live-cell videos of macrophages depleted for endogenous MT1-MMP and expressing indicated mutants. Note that MT1-MMPΔNterm localizes to islets (E1–G1), also upon disruption of podosomes by CK-666 (H1–J1), with reformation of podosomes at islets upon washout of CK-666 (K1–M1). In contrast, MT1-MMPΔCterm insensitive (insens.) does not localize to podosomes or islets (N1–P1). Bars, 10 µm.

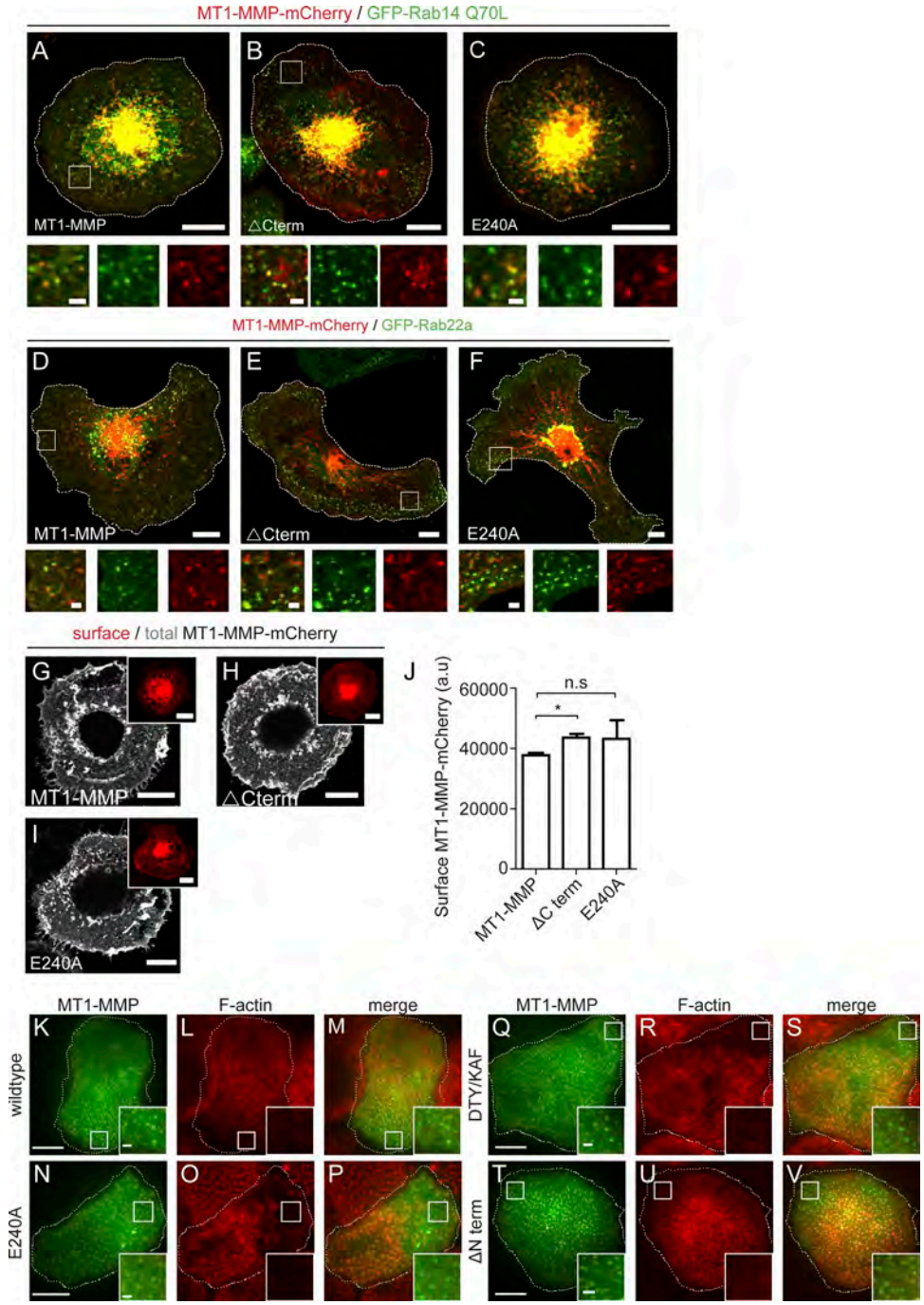

Figure S4. **Absence of the cytoplasmic region or catalytic inactivity does not influence MT1-MMP localization to vesicles or cell-surface exposure and ability of MT1-MMP mutants to form islets.** (A–F) Confocal micrographs of macrophages expressing mCherry-tagged (red) MT1-MMP WT (A and D), ΔCterm (B and E), or catalytically inactive E240A mutant (C and F), and coexpressing GFP-Rab14 Q70L (A–C) or GFP-Rab22a (D–F) to visualize vesicles. White boxes indicate areas of detail images below, with merge and each channel shown separately. Note pronounced colocalization of all three constructs to GFP-Rab14 and also to Rab22a vesicles. Dashed lines indicate cell circumference. Bars, 10 µm. (G–I). Confocal micrographs of macrophages expressing mCherry-tagged MT1-MMP WT (G), ΔCterm (H), and E240A (I) constructs. Cells were not permeabilized and stained for surface-localized MT1-MMP-mCherry using an anti-mCherry antibody (white). Insets show total cellular MT1-MMP-mCherry signals. Bars: 10 µm; (insets) 1 µm. (J). Statistical evaluation of surface-localized MT1-MMP-mCherry, based on Alexa Fluor 647 fluorescence intensity in cells expressing indicated constructs. Note that values of surface-localized ΔCterm and E240A constructs are at least as high as that of WT MT1-MMP. Bars represent mean ± SEM. *, $P < 0.05$. For specific values, see Table S2. (K–V) Localization of MT1-MMP-pHluorin constructs that were rendered siRNA insensitive and expressed in macrophages depleted for endogenous MT1-MMP and stained for F-actin. White boxes indicate detail regions shown as insets. Note localization of all constructs to F-actin/podosome-free islets.

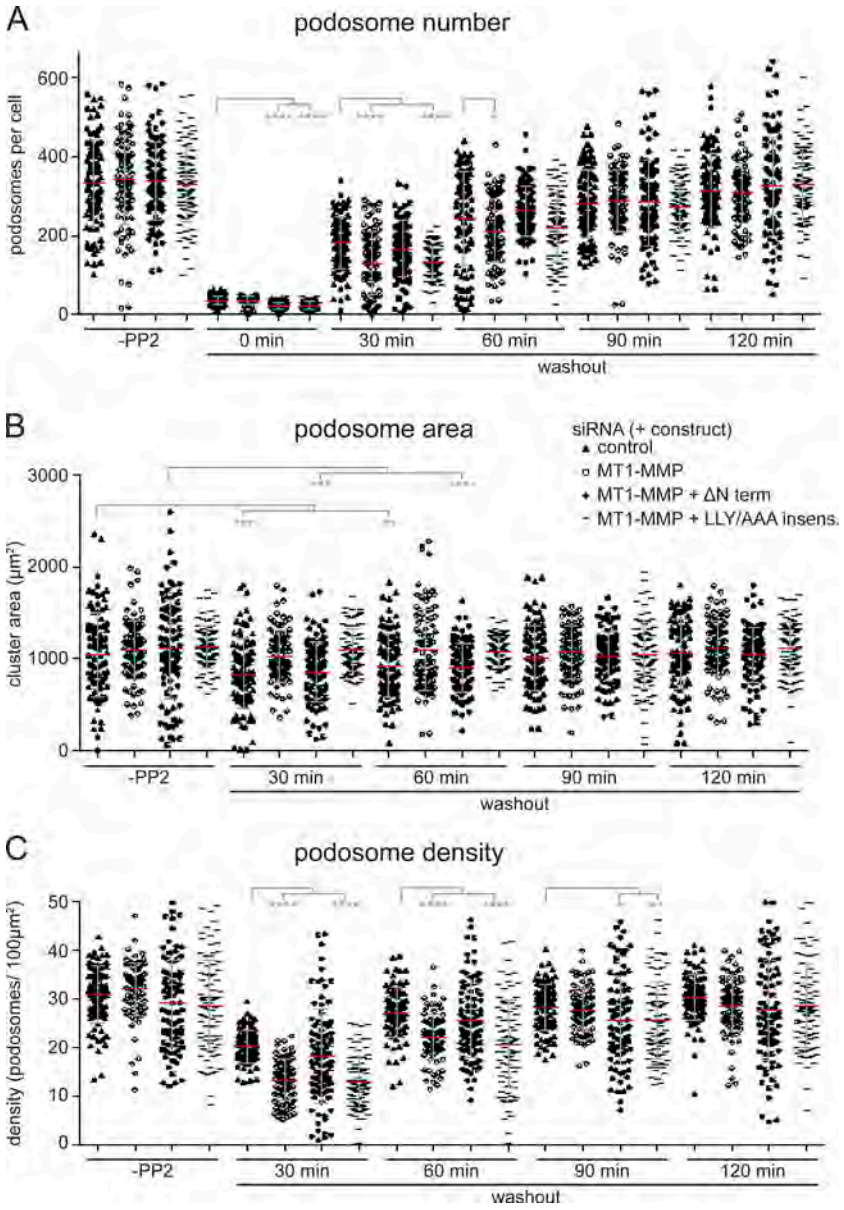

Figure S5. **The LLY motif in the MT1-MMP C terminus is crucial for the recovery of regular podosome number, area, and density during podosome reformation.** Statistical evaluations of podosome numbers (A), area covered by podosome groups ("clusters"; B), or podosome density (podosomes/100 µm²; C) during a podosome reformation assay. Parameters were evaluated in cells before disruption of podosomes ("-PP2") or after treatment with podosome-disrupting PP2 and washout of the drug for the indicated periods, in cells treated with control siRNA (black triangles) or with MT1-MMP-specific siRNA (open circles). In addition, subsets of MT1-MMP–depleted cells were also expressing a construct of the MT1-MMP C terminus that is not targeted by the siRNA (ΔNterm; filled circle) or of a full-length MT1-MMP construct mutated in the LLY motif, which was rendered siRNA insensitive (LLY/AAA insens.; line). Each dot in A–C represents a single cell, with $n = 3 \times 30$, for cells from three different donors. Note that podosomes are mostly absent at 0 min of the washout (A); podosome-covered area (B) and podosome density (C) were thus not evaluated for this time point. Values are given as means ± SD. *, $P < 0.05$; **, $P < 0.01$; ****, $P < 0.0001$. For specific values, see Table S2.

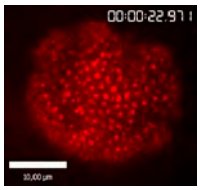

Video 1. **Dynamics of MT1-MMP-pHluorin and mCherry-talin-1C (from Fig. S1).** TIRF time-lapse video of a primary human macrophage expressing MT1-MMP-pHluorin (red; exposure time at 488 nm, 10 ms) and mCherry-Talin-1C (gray; exposure time at 568 nm, 50 ms). Acquisition rate: 20 time points/min; frame rate: 10 fps; sequence: 5 min and 21 s. Bars, 10 µm. Note that MT1-MMP-pHluorin signals are mostly surrounded by mCherry-Talin-1C, indicative of their podosomal localization.

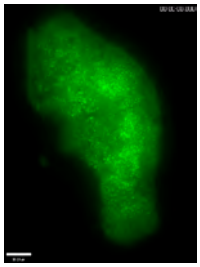

Video 2. **MT1-MMP is present at podosomes and at podosome-free islets (from Fig. 2, A–C).** TIRF time-lapse video of a primary human macrophage expressing MT1-MMP-pHluorin (red; exposure time at 488 nm, 200 ms) and mCherry-Talin-1C (gray; exposure time at 568 nm, 200 ms). Acquisition rate: 2 time points/min; frame rate: 30 fps; sequence: 2 h. Bar, 10 µm. Note the presence of MT1-MMP at podosomes and at podosome-free regions termed "islets."

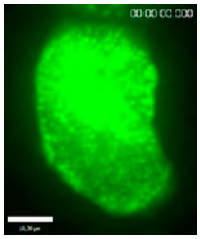

Video 3. **Podosomal MT1-MMP persists beyond disruption of the podosome structure itself (from Fig. 5, A–F).** TIRF time-lapse video of a primary human macrophage expressing MT1-MMP-pHluorin (green; exposure time at 488 nm, 600 ms) and Lifeact-RFP (red; exposure time at 568 nm, 50 ms). Acquisition rate: two time points/min; frame rate: 10 fps; sequence: 25 min and 6 s. Bar, 10 µm. Note the persistence of MT1-MMP signals even after CK-666–induced disruption of podosomes, indicated by absence of the F-actin reporter Lifeact-RFP.

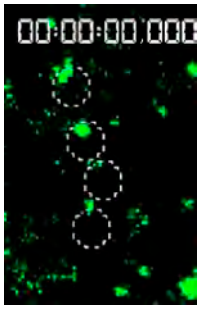

Video 4. **MT1-MMP islets are sites of podosome reemergence (from Fig. 6, A′–C′).** TIRF time-lapse video of a primary human macrophage expressing MT1-MMP-pHluorin (green; exposure time at 488 nm, 300 ms) and Lifeact-RFP (red; exposure time at 568 nm, 300 ms). Acquisition rate: six time points/min; frame rate: 10 fps; sequence: 46 min and 40 s. Bar, 10 µm. Note the successive appearance of new podosomes, indicated by Lifeact-RFP, at MT1-MMP islets.

Video 5. **MT1-MMP islets can recruit material generated by podosome fission (from Fig. S4, A′–C′).** TIRF time-lapse video of a primary human macrophage expressing MT1-MMP-pHluorin (green; exposure time at 488 nm, 300 ms) and Lifeact-RFP (red; exposure time at 568 nm, 300 ms). Acquisition rate: six time points/min; frame rate: 10 fps; sequence: 1 h. Bar, 10 µm. Note fission of podosome, resulting in the generation of a new podosome core, which is subsequently recruited to a MT-MMP islet.

Table S1. **Tested potential islet components**

Component	Characteristic	Antibody, probe, or construct	Podosomes	Islets
F-actin[a]	Podosome core component	Phalloidin	+	–
		Lifeact-RFP	+	–
Arp2[a]	Arp2/3 complex subunit	Antibody	+	–
α-Actinin[a]	Actin-binding protein	Antibody	+	–
		GFP–α-actinin	+	–
Tks5[a]	Adaptor protein	Antibody	+/–	–
		Tks5-mCherry	+	–
Vinculin[a]	Adhesion plaque protein	Antibody	+	–
Talin[a]	Adhesion plaque protein	Antibody	+	–
		mCherry–talin-1C	+	–
Paxillin[a]	Adhesion plaque protein	Antibody	+	–
kindlin-3[a]	Integrin-interacting protein	Antibody	+	–
		EGFP–kindlin-3	+	–
c-Src	Tyrosine kinase	Antibody	–	–
	Podosome regulator	mTagRFP-T-C-Src-7	–	–
ILK[b]	integrin-interacting protein	ILK-GFP	+	–
β1 integrin[a]	Cell–matrix contact protein	Antibody	+	–
β2 integrin[b]	Cell–matrix contact protein	Antibody	+/–	–
β3 integrin[a]	Cell–matrix contact protein	Antibody	+	–
		β3 integrin–RFP	+	–
CD44[a]	Cell–matrix contact protein	Antibody	+/–	–
MT1-MMP[b]	Metalloproteinase	Antibody	+	+
		MT1-MMP-pHluorin	+	+
Flotillin-1[c]	Vesicle regulatory proteins	mCherry-flotillin1	–	–
Flotillin-2[c]		mCherry-flotillin2	+	–
CIP4[b]	Membrane curvature protein	EGFP-CIP4	–	–
FBP17[b]	Membrane curvature protein	Antibody	–	–
Apolipoprotein E[c]	Cholesterin vesicle protein	ApoE-GFP	–	–
Cholesterol[b]	Membrane lipid	Filipin	+	–
PtdIns(3,4,5)P3[b] and PtdIns(3,4)P2[b]	Membrane lipid	Akt-PH	–	–
PtdIns(4,5)P2[b]	Membrane lipid	PLCδ1-PH	–	–
PtdIns(3,4)P2[b]	Membrane lipid	TAPP1-PH	–	–
PtdIns(4)P[c]	Membrane lipid	OSH2-2xPH-GFP	+	–

Shown are tested proteins or lipid components, their characteristic function, the use of antibodies or probes to detect the endogenous form, or the use of overexpression constructs. + and – indicate respective presence at or absence from podosomes or MT1-MMP islets in primary human macrophages.
[a]Tested component was previously localized to macrophage podosomes.
[b]Tested component was previously localized to invadosomes of other cells.
[c]Tested component was not known to localize to invadosomes.

Table S2. **Values for podosome reformation assay and MT1-MMP constructs**

Podosome number

Time point	Number of values	(Mean ± SD)	
		Non-specific siRNA	MT1-MMP Kd
-PP2	90	323.3 ± 108.6	340.5 ± 113.9
0 min	90	35.57 ± 11.73	35.25 ± 9.33
30 min	90	180.2 ± 66.04	136.1 ± 79.04
60 min	90	243.3 ± 118.1	212.8 ± 80.86
90 min	90	281.0 ± 87.22	287.9 ± 78.62
120 min	90	314.1 ± 95.48	307.8 ± 76.43

Podosome area (µm^2)

Time point	Number of values	(Mean ± SD)	
		Non-specific siRNA	MT1-MMP Kd
-PP2	90	1054.23 ± 462.3	1101.54 ± 324.3
30 min	90	835.12 ± 381.1	1029.35 ± 280.2
60 min	90	922.14 ± 349.2	1100.94 ± 442.1
90 min	90	1010.64 ± 356.4	1073.82 ± 295.4
120 min	90	1051.78 ± 381.2	1107.36 ± 298.7

Density (podosome/100 µm^2)

Time point	Number of values	(Mean ± SD)	
		Non-specific siRNA	MT1-MMP Kd
-PP2	90	30.84 ± 5.76	31.87 ± 5.57
30 min	90	20.15 ± 3.13	13.24 ± 4.25
60 min	90	27.16 ± 5.02	22.12 ± 4.64
90 min	90	28.26 ± 4.74	27.67 ± 4.50
120 min	90	30.16 ± 4.74	28.58 ± 5.46

Podosomes per cell

Constructs	Number of values	Podosome number (mean ± SD)
pHluorin	15	296.80 ± 79.64
MT1-MMP	15	327.7 ± 146.1
E240A	15	334.9 ± 126.0
DTY/KAF	15	291.5 ± 118.6
ΔN-term	15	372.6 ± 161.1
ΔC-term	15	301.5 ± 111.8
LLY/AAA	15	331.6 ± 56.54

MT1-MMP surface exposure (a.u.)

Construct	Number of values	Surface MT1-MMP-mCherry (mean ± SEM)
MT1-MMP	90	37460 ± 1087
ΔC-term	90	43584 ± 1280
E240A	90	43231 ± 6199

Podosome number

Time point	Number of values	(Mean ± SD)			
		Non-specific siRNA	MT1-MMP Kd	MT1-MMP Kd + ΔN-term	MT1-MMP LLY/AAA insens.
-PP2	90	321.3 ± 106.5	338.3 ± 111.7	338.6 ± 100.4	328.2 ± 94.65
0 min	90	35.22 ± 10.12	34.15 ± 9.88	20.4 ± 8.51	22.21 ± 10.43
30 min	90	178.5 ± 64.76	131.5 ± 79.54	166.2 ± 71.6	134.4 ± 41.45
60 min	90	242.7 ± 121.9	211.6 ± 83.77	262.9 ± 64.64	219.9 ± 88.25
90 min	90	282 ± 84.84	288.4 ± 80.21	283.6 ± 108.2	273.6 ± 62.22
120 min	90	312.5 ± 91.62	305.1 ± 82.31	325.7 ± 125.5	330.4 ± 91.49

Podosome area (μm^2)

Time point	Number of values	(Mean ± SD)			
		Non-specific siRNA	MT1-MMP Kd	MT1-MMP Kd + ΔN term	MT1-MMP LLY/AAA insens.
-PP2	90	1045 ± 450.7	1105 ± 315.2	1104 ± 544.2	1132 ± 230.7
30 min	90	836.4 ± 387.6	1028 ± 284.8	854.6 ± 331.1	1093 ± 230.8
60 min	90	927.5 ± 344.2	1096 ± 440.7	897.5 ± 268.8	1098 ± 166.9
90 min	90	1011 ± 354.6	1065 ± 290.9	1027 ± 262.4	1033 ± 354.3
120 min	90	1055 ± 384.6	1110 ± 312.1	1043 ± 294.2	1106 ± 293.8

Density (podosome/100 μm^2)

Time point	Number of values	(Mean ± SD)			
		Non-specific siRNA	MT1-MMP Kd	MT1-MMP Kd + ΔN-term	MT1-MMP LLY/AAA insens.
-PP2	90	30.74 ± 5.66	30.61 ± 5.49	28.95 ± 8.91	28.62 ± 9.32
30 min	90	19.24 ± 3.24	12.55 ± 4.35	18.21 ± 9.61	12.9 ± 5.29
60 min	90	26.89 ± 5.07	21.97 ± 4.25	25.58 ± 7.71	20.61 ± 8.96
90 min	90	27.89 ± 4.66	27.07 ± 4.54	25.61 ± 9.12	25.45 ± 7.95
120 min	90	29.63 ± 4.78	28.18 ± 5.29	27.53 ± 10.31	28.13 ± 8.55

Rhodamine-gelatin degradation				
Time point	Number of values	(Mean ± SEM)		
		Before drug addition	DMSO	CK-666
4.5 h	3 × 30	40.71% ± 15.48%	/	/
6.5h	3 × 30	/	100.0% ± 21.80%	42.65% ± 10.27%

Percentage of cells with islets		
Constructs	Number of values	Podosome number (mean ± SD)
pHluorin	90	2.22 ± 1.92
MT1-MMP	90	54.44 ± 6.94
E240A	90	50.00 ± 8.82
DTY/KAF	90	47.78 ± 13.88
ΔN-term	90	35.56 ± 6.94
ΔC-term	90	16.67 ± 6.67
LLY/AAA	90	23.33 ± 3.33

Declaration:

Karim El azzouzi contributed to the publication:

Metalloproteinase MT1-MMP islets act as memory devices for podosome reemergence.

El Azzouzi K, Wiesner C, Linder S.

J Cell Biol. 2016 Apr 11;213(1):109-25. doi: 10.1083/jcb.201510043.

by:

- Performing and analysing all experiments mentioned in the publication, which are not listed in the “contributed by coauthors” section below.
- Preparing figures and movies for the publication.

Published material contributed by coauthors:

- Experiment demonstrated in Figure S1 A-G
- Experiment demonstrated in Figure S2 W-X
- Experiment demonstrated in Figure S4 G-J

The experiments were designed by Karim El azzouzi and Stefan Linder.

The manuscript was written by Stefan Linder.

Hamburg, 03.11.2016

_____

Stefan Linder

A specific subset of RabGTPases controls cell surface exposure of MT1-MMP, extracellular matrix degradation and three-dimensional invasion of macrophages

Christiane Wiesner, Karim El Azzouzi and Stefan Linder*

Institut für medizinische Mikrobiologie, Virologie und Hygiene, Universitätsklinikum Eppendorf, Martinistr. 52, 20246 Hamburg, Germany

*Author for correspondence (s.linder@uke.de)

Accepted 4 April 2013
Journal of Cell Science 126, 2820–2833
© 2013. Published by The Company of Biologists Ltd
doi: 10.1242/jcs.122358

Summary

The matrix metalloproteinase MT1-MMP has a major impact on invasive cell migration in both physiological and pathological settings such as immune cell extravasation or metastasis of cancer cells. Surface-associated MT1-MMP is able to cleave components of the extracellular matrix, which is a prerequisite for proteolytic invasive migration. However, current knowledge on the molecular mechanisms that regulate MT1-MMP trafficking to and from the cell surface is limited. We have identified three members of the RabGTPase family, Rab5a, Rab8a and Rab14, as crucial regulators of MT1-MMP trafficking and function in primary human macrophages. Both overexpressed and endogenous forms show prominent colocalisation with MT1-MMP-positive vesicles, whereas expression of mutant constructs, as well as siRNA-induced knockdown, reveal that these RabGTPases are crucial in the regulation of MT1-MMP surface exposure, contact of MT1-MMP-positive vesicles with podosomes, extracellular matrix degradation in two and three dimensions, as well as three-dimensional proteolytic invasion of macrophages. Collectively, our results identify Rab5a, Rab8a and Rab14 as major regulators of MT1-MMP trafficking and invasive migration of primary human macrophages, which could be promising potential targets for manipulation of immune cell invasion.

Key words: Cell invasion, Extracellular matrix, MT1-MMP, Podosomes, RabGTPases

Introduction

Invasive migration is a key ability of cells in both physiological and pathological scenarios, including migration of immune cells to sites of infection (Ley et al., 2007) and dissemination of cancer cells during metastasis (Friedl and Wolf, 2003; Bravo-Cordero et al., 2012). To invade, cells employ two different strategies, depending on the density of the extracellular matrix (ECM): (1) amoeboid migration, a non-proteolytic form of locomotion, with cells squeezing through the gaps between matrix fibres, and (2) mesenchymal migration, which includes degradation of matrix material (Wolf and Friedl, 2011). Both forms are not mutually exclusive, and cells can switch their behaviour according to the local ECM meshwork density (Lämmermann and Sixt, 2009; Guiet et al., 2011). The fact that *in vivo*, multiple crosslinks exist between ECM fibres, however, seems to favour the mesenchymal mode of invasion (Sabeh et al., 2009).

Particularly the matrix metalloproteinase MT1-MMP has emerged as a central regulator of proteolytic cell invasion in a variety of settings, including monocyte diapedesis (Matías-Román et al., 2005; Sithu et al., 2007), T-cell homing (Itoh and Seiki, 2004) and cancer cell metastasis (Wolf et al., 2007; Friedl and Wolf, 2008). MT1-MMP cleaves multiple matrix components, including collagen (I–III), fibronectin and fibrin (Itoh and Seiki, 2004), and also matrix receptors such as CD44, osteopontin and syndecan-1 (Kajita et al., 2001; Endo et al., 2003). Moreover, it also proteolytically activates other MMPs such as MMP-2, MMP-8 and MMP-13 (Barbolina and Stack, 2008).

Considering the plethora of MT1-MMP functions, both the surface-associated pool of this protease and also its localised activity have to be exquisitely fine tuned. Regulatory mechanisms include: (1) adjustment of surface-associated activity by activation of pro-MT1-MMP through the convertase furin prior to its insertion into the plasma membrane (Sato et al., 1996) or inhibition by tissue inhibitors of metalloproteinases (TIMPs) or testican (Nakada et al., 2003); (2) degradation of MT1-MMP, which can be induced by autolysis (Lehti et al., 1998) or MMP-2 (Stanton et al.,1998); and (3) vesicle-mediated regulation of the surface-associated MT1-MMP pool, which is influenced by furin-induced uptake (Remacle et al., 2006), by PKC-dependent phosphorylation of Thr567, leading to enhanced internalisation (Williams and Coppolino, 2011), or by active Rab8, which leads to enhanced exocytosis (Bravo-Cordero et al., 2007).

In consequence, vesicle-mediated transport of MT1-MMP plays a key role in the regulation of surface-localised MT1-MMP activity, both through exocytic delivery of the proteinase and also by endocytic internalisation (Frittoli et al., 2011). Regulators of vesicle formation, transport and fusion are thus expected to have a major impact on MT1-MMP trafficking and, ultimately, on

proteolytic cell invasion. Several components of the respective molecular machineries have already been described: in primary macrophages, MT1-MMP-positive vesicles travel bidirectionally along microtubules, in a process driven by kinesin-1 and -2 motors, as well as by cytoplasmic dynein, which regulates cell surface exposure of MT1-MMP (Wiesner et al., 2010). In MDA-MB-231 breast cancer cells, trafficking of MT1-MMP to matrix-degrading invadopodia is regulated by the SNARE protein VAMP-7. Consequently, siRNA-mediated knockdown of VAMP-7 resulted in decreased invasive capacity of these cells (Steffen et al., 2008; Poincloux et al., 2009), a phenomenon that has also been observed in HeLa cells (Williams and Coppolino, 2011).

RabGTPases are central regulators of both endocytosis and exocytosis of vesicles (Schwartz et al., 2007; Stenmark, 2009; Hutagalung and Novick 2011). Depending on their nucleotide-bound state, RabGTPases act as molecular switches (Stenmark et al., 1994) that mediate specific tethering of vesicles to target organelles, thus ensuring correct compartmentalisation of cargo proteins (Zerial and McBride, 2001). Currently, more than 70 mammalian Rab proteins are known (Hutagalung and Novick, 2011). However, despite their pivotal importance for multiple aspects of intracellular transport (Stenmark, 2009; Hutagalung and Novick 2011), knowledge of the impact of RabGTPases on the trafficking of MT1-MMP is limited. The only well-documented cases concern, (1) MDA-MB-231 breast carcinoma cells, where MT1-MMP localised to Rab8-positive vesicles, and siRNA-mediated knockdown of Rab8 inhibited collagen degradation and invasion (Bravo-Cordero et al., 2007), and (2) HT1080 fibrosarcoma cells, where MT1-MMP localised to Rab5- and Rab7-positive compartments, and overexpression of dominant negative Rab7 led to a reduction of surface-associated MT1-MMP and also of cell invasion (Williams and Coppolino, 2011).

Here, we present novel data on the impact of several specific RabGTPases on MT1-MMP trafficking and function in primary human macrophages. We show that overexpression of mutants as well as siRNA-induced knockdown of Rab5a, Rab8a and Rab14 critically regulate cell surface exposure of MT1-MMP, contact of MT1-MMP-positive vesicles with podosomes, as well as podosome-localised ECM degradation in two and three dimensions, and also three-dimensional (3D) proteolytic invasion. Our results thus identify three RabGTPases with a major impact on MT1-MMP trafficking and proteolytic invasion of macrophages, which could be promising targets for therapeutic modulation of macrophage invasion.

Results

MT1-MMP vesicles are positive for Rab5a, Rab8a, Rab14, Rab21 and Rab22a

To identify RabGTPases involved in MT1-MMP trafficking in primary human macrophages, we first performed co-expression experiments with a variety of GFP-fused Rab constructs together with MT1-MMP-mCherry. In fixed cells, pronounced localisation at MT1-MMP–mCherry-positive vesicles was found for GFP–Rab5a, GFP–Rab8a, GFP–Rab14, GFP–Rab21 and GFP–Rab22a (Fig. 1). In case of GFP–Rab5a, GFP–Rab14, GFP–Rab21 and GFP–Rab22a overexpression, we also observed the formation of giant vesicles (Fig. 1A–C,G–O), as previously reported for a variety of cell types (Stenmark et al., 1994; Olkkonen et al., 1993; Junutula et al., 2004; Pellinen et al., 2006). This phenomenon also allowed higher spatial resolution of vesicle subdomains, and

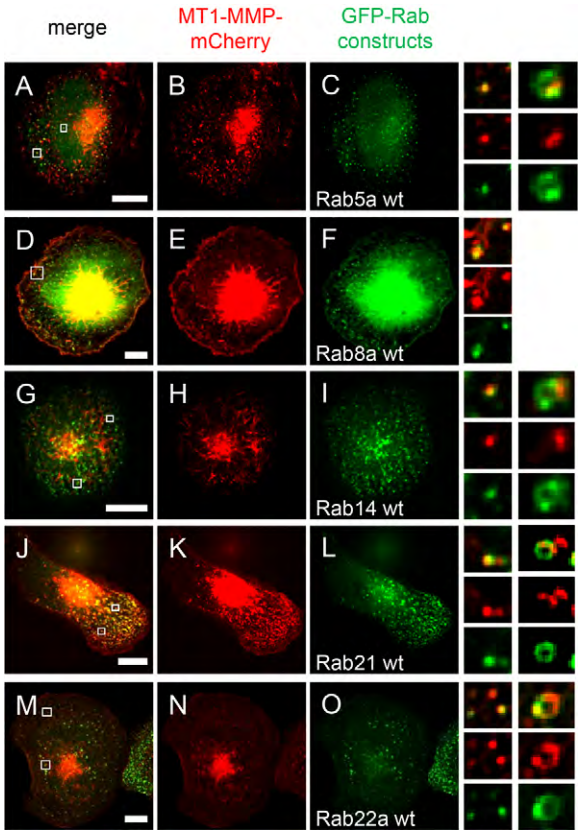

Fig. 1. MT1-MMP–mCherry vesicles partially colocalise with Rab5a, Rab8a, Rab14, Rab21 and Rab22a wild-type constructs. Confocal micrographs of macrophages expressing MT1-MMP–mCherry and GFP–Rab5a (**A–C**), GFP–Rab8a (**D–F**), GFP–Rab14 (**G–I**), GFP–Rab21 (**J–L**), or GFP–Rab22a (**M–O**). Merged images are shown in the left column, with single channel images of MT1-MMP–mCherry shown in middle column (red) and of GFP-fused Rab GTPases in right column (green). The regions in the white boxes in the merged images are shown enlarged on the right. Note localisation of MT1-MMP–mCherry together with Rab constructs on vesicles (left column of enlarged images) and giant vesicles (right column of enlarged images; fused vesicles are due to the overexpression of GFP–RabGTPase). The enlarged images in the left column show 1–4 individual vesicles; those in the right column show a single giant vesicle. Scale bars: 10 μm.

revealed that MT1-MMP and RabGTPases show distinct, although partially overlapping, localisations at these vesicles (Fig. 1A–C,G–O). (Note that localisation of RabGTPases and MT1-MMP at the same vesicles does not necessarily imply colocalisation of the respective signals, as they mostly segregate to different domains on these vesicles.)

Live cell imaging experiments in cells transfected with respective constructs confirmed that the identified RabGTPases localise to dynamic vesicles that are also positive for MT1-MMP–mCherry (supplementary material Fig. S1; Movies 1, 2). Moreover, colocalisation studies of endogenous proteins in cells stained with specific primary antibodies against MT1-MMP and RabGTPase isoforms (supplementary material Fig. S2) confirmed the results of the overexpression screen and demonstrated that Rab5, Rab8a, Rab14, Rab21 and Rab22a show substantial colocalisation with MT1-MMP vesicles. The identified RabGTPases are thus potential candidates for the regulation of MT1-MMP trafficking in primary human macrophages. (Note:

Journal of Cell Science

several other tested RabGTPases, including Rab4, Rab6a, Rab9 and Rab11, showed no colocalisation at MT1-MMP vesicles (see supplementary material Fig. S3) and were thus mostly not investigated further. (See supplementary material Fig. S9 for proof-of-principle experiments showing that the non-colocalising isoform Rab6a does not influence surface exposure of endogenous MT1-MMP, 3D collagen degradation or 3D matrix invasion.)

Cell surface exposure of MT1-MMP is regulated by Rab5a, Rab8a, Rab14 and Rab22a

In a next step, we overexpressed dominant active (DA) and negative (DN) mutants of the identified RabGTPases and analysed their potential effects on the cell surface exposure of MT1-MMP–mCherry. Non-permeabilised cells overexpressing the respective constructs were labelled with an anti-mCherry antibody, detecting the intramolecular mCherry tag of MT1-MMP–mCherry, which had been subcloned N-terminally of the MT1-MMP transmembrane domain, and is thus extracellularly accessible on the surface-exposed protein (Wiesner et al., 2010; Sakurai-Yageta et al., 2008). Fluorescence intensities were measured and the ratio of cell surface associated versus total cellular MT1-MMP–mCherry was used as a parameter for the cell surface exposure of MT1-MMP. Cells expressing respective GFP-fused wild-type constructs were used as controls. In all cases, RabGTPase expression levels, as judged by GFP-based fluorescence levels (supplementary material Fig. S4), were found to be comparable.

Pronounced deviations of the surface/total MT1-MMP–mCherry ratio were found upon expression of DN mutants of Rab5a, Rab8a, Rab14 and Rab22a. Dominant negative Rab21 and all respective DA mutants showed no or only minor effects (for specific values, see supplementary material Table S1). Interestingly, expression of GFP–Rab5aDN led to an increase of surface-associated MT1-MMP–mCherry (199.9±83.2%; Fig. 2D), whereas a decrease was measured for GFP–Rab8aDN (40.7±18.6%; Fig. 2H), GFP–Rab14DN (53.4±16.8%; Fig. 2L) and GFP–Rab22aDN (27.5±12.0%; Fig. 2T).

We next measured the impact of these RabGTPase mutants on the cell surface exposure of endogenous MT1-MMP. Cells expressing respective RabGTPase constructs were fixed, but not permeabilised, and stained for surface-associated MT1-MMP using a specific primary antibody (note that this antibody is directed against an epitope in the catalytic domain and thus recognises only unshed, but not cleaved, MT1-MMP on the cell surface). Comparable to the results gained for MT1-MMP–mCherry, we found a pronounced increase of surface-associated endogenous MT1-MMP upon expression of GFP–Rab5aDN (173.5±80.3%; supplementary material Fig. S5D), and pronounced decreases upon expression of GFP–Rab8aDN (76.8±25.0%; supplementary material Fig. S5H), GFP–Rab14DN (68.2±22.7%; supplementary material Fig. S5L) and GFP–Rab22aDN (43.9±24.9%; supplementary material Fig. S5T). Expression levels of the respective RabGTPase constructs were comparable (supplementary material Fig. S5U–Y).

To address the role of the identified Rab proteins in MT1-MMP surface exposure directly, we established respective siRNA-mediated knockdowns. For each identified RabGTPase,

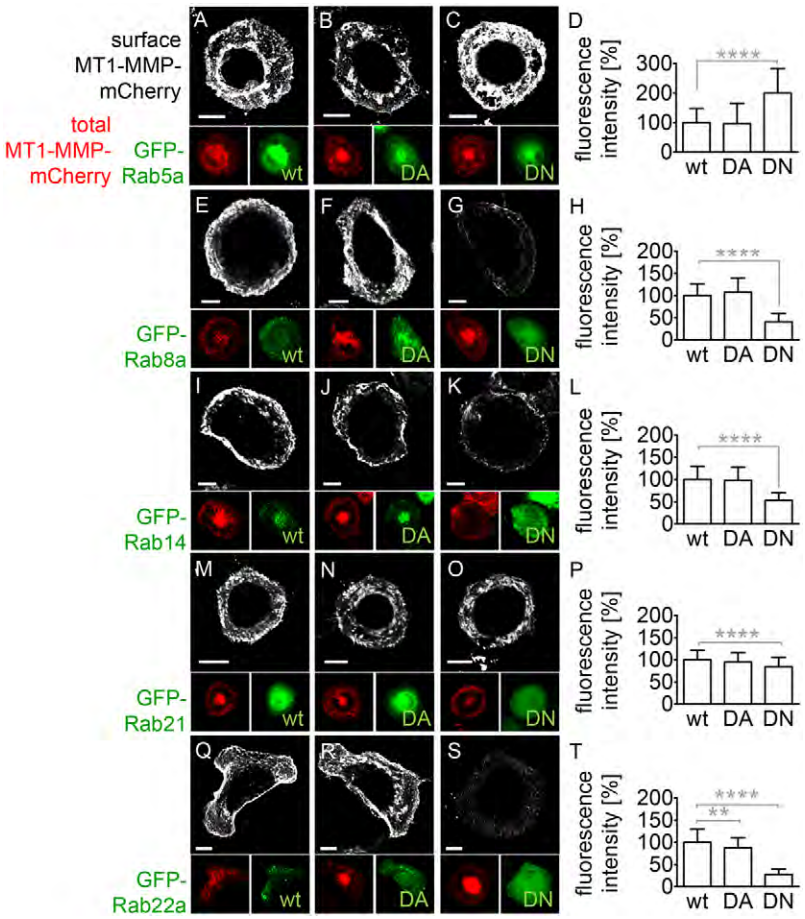

Fig. 2. Cell surface exposure of MT1-MMP–mCherry is regulated by Rab5a, Rab8a, Rab14 and Rab22a, but not Rab21. (**A–C**, **E–G**, **I–K**, **M–O**, **Q–S**) Confocal micrographs of macrophages coexpressing MT1-MMP–mCherry (red) and GFP-fused RabGTPase constructs (green): wild-type (A,E,I,M,Q; green), dominant active (DA) constructs deficient in GTP hydrolysis (B,F,J,N,R; green), or dominant negative constructs (DN) deficient in GTP binding (C,G,K,O,S; green). Cells were fixed, but not permeabilised, and stained with primary anti-mCherry antibody and secondary Alexa-Fluor-647-conjugated antibody to label surface-associated MT1-MMP–mCherry (white). Note pronounced reduction of MT1-MMP at cell surface upon overexpression of Rab8a, Rab14, Rab22a DN mutants, but less in the Rab21 DN mutant. Note also increased cell surface exposure of MT1-MMP in case of Rab5a DN and Rab7a DN overexpression. Scale bars: 10 µm for all images of the same row. (**D**,**H**,**L**,**P**,**T**) Evaluation of fluorescence intensities of surface-localised MT1-MMP–mCherry, based on Alexa Fluor 647 fluorescence, relative to the intensity of total MT1-MMP–mCherry fluorescence. Values for wild-type constructs were to 100%. 3×30 (n=90; from 3 different donors) cells were evaluated. Graphs show means + s.d. Asterisks indicate values significantly different from wild-type constructs: $^{**}P<0.002$, $^{****}P<0.0001$. For specific values, see supplementary material Table S1.

two independent siRNAs were generated (three in case of Rab5a), and the respective decrease in protein levels was shown on Western blots of macrophage lysates. Knockdown efficiencies ranged from 42% to 96%, with at least one of the two independent siRNAs leading to a knockdown of ca. 80% (supplementary material Fig. S6). Importantly, knockdown of these RabGTPase isoforms did not change the overall levels of cellular MT1-MMP (supplementary material Fig. S6). Cells treated with the respective siRNAs were fixed, but not permeabilised, and stained for surface-exposed endogenous MT1-MMP, with cells treated with luciferase- or MT1-MMP-specific siRNA (Wiesner et al., 2010) used as negative or positive controls (Fig. 3; for specific values, see supplementary material Table S1), respectively. Comparable to the expression of DN mutants, knockdown of Rab5a led to a significant increase of cell surface-exposed MT1-MMP (163.1±70.1% and 212.7±127.2%), whereas pronounced decreases were observed upon knockdown of Rab8a (35.3±24.3% and 41.3±29.5%), Rab14 (33.9±17.0% and 34.1±13.3%) and Rab22a (34.6±20.3% and 42.7±19.4%; Fig. 3M). A less pronounced but still significant effect was observed upon knockdown of Rab21 (78.6±31.0% and 72.1±22.8%). We conclude from these experiments that especially Rab5a, Rab8a, Rab14 and Rab22a are important regulators of cell surface exposure for both endogenous and overexpressed MT1-MMP in primary macrophages.

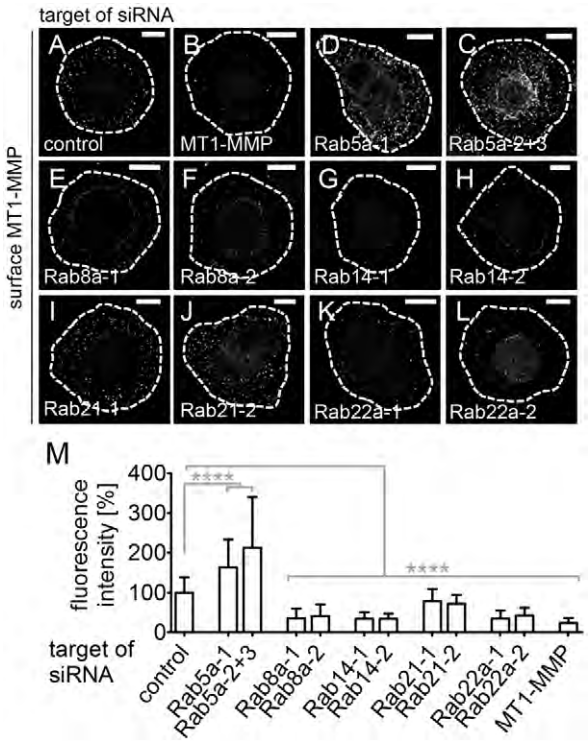

Fig. 3. Knockdown of Rab5a, Rab8a, Rab14 and Rab22a, but not of Rab21 has a major impact on the cell surface exposure of endogenous MT1-MMP. (**A–L**) Confocal micrographs of macrophages treated with siRNA specific for luciferase, as control (A), MT1-MMP (B), or RabGTPase isoforms, as indicated. Cells were fixed, but not permeabilised, and stained with primary anti-MT1-MMP and secondary Alexa-Fluor-568-conjugated antibody to label endogenous MT1-MMP on the cell surface. Scale bars: 10 µm. (**M**) Fluorescence intensities of surface-localised endogenous MT1-MMP, based on Alexa Fluor 568 fluorescence. Fluorescence intensities for control siRNA were each set to 100%. For all values, 30 cells from three different donors each were evaluated. Graph shows means + s.d. Asterisks indicate values significantly different from control values: ****$P<0.0001$. For specific values, see supplementary material Table S1.

Podosome contact of MT1-MMP vesicles and podosomal matrix degradation are regulated by Rab5a, Rab8a, Rab14 and Rab22a

A major surface-associated function of MT1-MMP is degradation of the extracellular matrix (van Hinsbergh et al., 2006; Wolf and Friedl, 2009). In monocytic cells, this is achieved by MT1-MMP-dependent, localised proteolysis of ECM material at podosomes, the major degradative organelles of macrophages and other invasive cell types (Linder et al., 2011; Murphy and Courtneidge, 2011). Delivery of MT1-MMP to podosomes is mediated by trafficking of MT1-MMP-positive vesicles along microtubules (Wiesner et al., 2010). To test the potential influence of the identified RabGTPases on this process, we evaluated contact events of MT1-MMP-positive vesicles with podosomes upon knockdown of Rab5a, Rab8a, Rab14, Rab21 and Rab22a. Three days after transfection with respective siRNAs, cells were transfected with MT1-MMP-mCherry, cultured for an additional day, fixed and stained with Alexa-Fluor-488–phalloidin to detect F-actin-rich podosome cores. The number of podosomes that were in direct contact with MT1-MMP–mCherry-positive vesicles (Fig. 4A) was counted, and set in relation to the total number of podosomes within a cell (usually >100; ratio of contacted podosomes: 25.3±8.1%). Strikingly, knockdown of Rab5a led to a higher ratio of podosomes contacted by MT1-MMP–mCherry vesicles (39.1±13.0% and 46.4±20.0%), whereas the ratios of contacted podosomes were significantly decreased upon knockdown of Rab8a (15.2±11.0% and 12.3±7.6%), Rab14 (9.1±4.4% and 11.1±7.3%) and Rab22a (11.1±5.3% and 10.4±4.1%), but not of Rab21 (21.8±7.8% and 23.6±7.3%; Fig. 4B). Importantly, overall cellular expression of MT1-MMP–mCherry as well as overall podosome number in cells were unchanged upon knockdown of the mentioned RabGTPases (supplementary material Fig. S7 and not shown).

To explore potential functional consequences, we next assessed podosome-associated matrix degradation under knockdown of specific RabGTPases. Cells were treated with respective siRNAs for 3 days re-seeded on Rhodamine-labelled gelatine matrix for 6 h, fixed and stained for F-actin to label podosome cores, and podosome-dependent ECM degradation was assessed by associated loss of the Rhodamine matrix label (Fig. 4C). Cells treated with luciferase- or MT1-MMP specific siRNAs were used as negative or positive controls, respectively, with values for luciferase-treated cells set to 100%. Knockdown of endogenous MT1-MMP led to significantly decreased levels of gelatine matrix degradation (67.9±35.5%), comparable to earlier results in macrophages (Wiesner et al., 2010). Consistent with the results gained for podosome contact of MT1-MMP vesicles, knockdown of Rab5a led to significantly enhanced levels of matrix degradation (111.9±18.7% and 125.6±59.5%), whereas pronounced decreases in matrix degradation were measured upon knockdown of Rab8a (82.9±30.6% and 86.4±38.0%), Rab14 (77.7±28.2% and 71.8±31.8%) and Rab22a (83.1±37.2% and 72.8±37.5%), but not of Rab21 (108.3±37.4% and 100.0±36.5%; Fig. 4D). Collectively, these results indicate that Rab5a acts as negative regulator of MT1-MMP vesicle contact

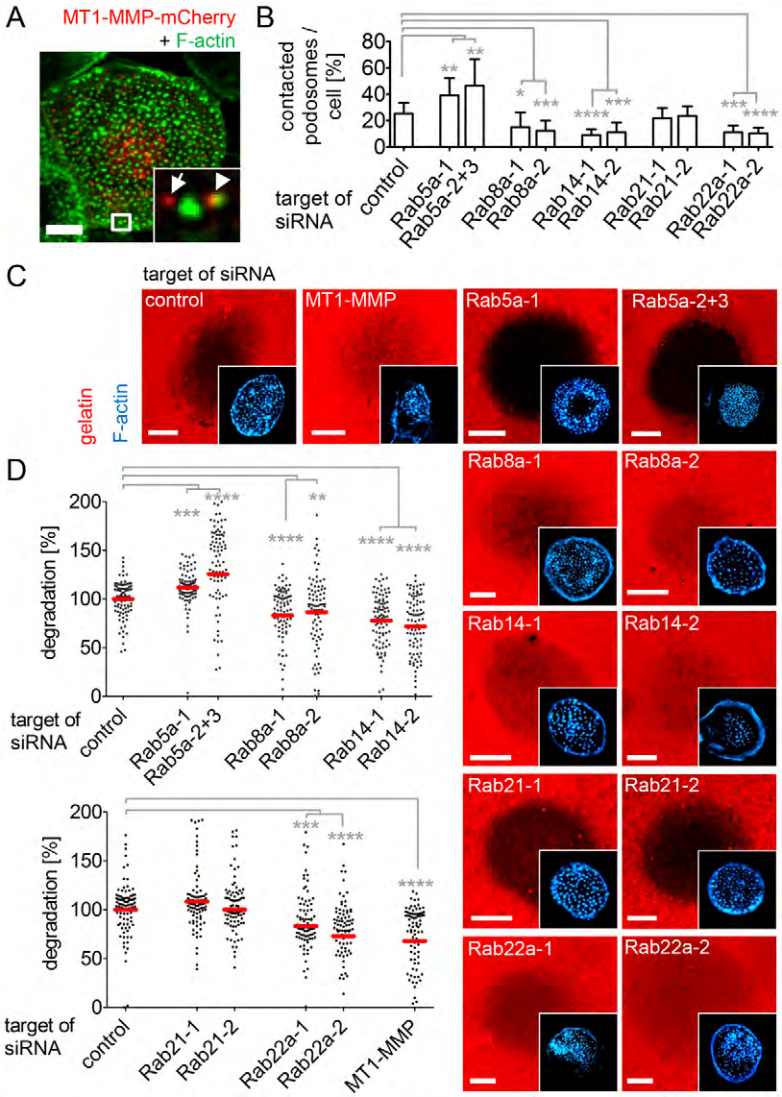

Fig. 4. Knockdown of Rab5a, Rab8a, Rab14 and Rab22a, but not of Rab21, affects contact of MT1-MMP–mCherry vesicles with podosomes and matrix degradation. (**A**) Confocal micrograph of a primary macrophage expressing MT1-MMP–mCherry and stained for F-actin using Alexa-Fluor-488–phalloidin to highlight podosome cores. The region in the white box is enlarged in the inset. Scale bar: 10 µm. White arrow or arrowhead indicate MT1-MMP–mCherry vesicles not in contact or in contact with a podosome, respectively. (**B**) Quantification of podosomes contacted by MT1-MMP–mCherry vesicles per cell. Total number of podosomes was set to 100%. For all values, five cells from three different donors each with 50–500 podosomes were evaluated. Graph shows means + s.d. Asterisks indicate values significantly different from control values: $*P<0.02$, $**P=0.005$, $***P<0.0005$, $****P<0.0001$. For specific values, see supplementary material Table S1. (**C**) Confocal micrographs of macrophages transfected with siRNA specific for RabGTPase isoforms, luciferase as negative control, or MT1-MMP as positive control, and seeded on Rhodamine-labelled gelatine matrix. Matrix degradation is visible as dark areas by concomitant loss of the fluorescent label. Insets show respective F-actin staining by Alexa-Fluor-647-labelled phalloidin. Scale bar: 10 µm. (**D**) Statistical evaluation of matrix degradation in cells treated with various siRNAs. The degree of matrix degradation was analysed by fluorescence measurements of 30 cells from three different donors each for each value. Red bars indicate mean values, black dots show single values; Mean value of matrix degradation in control was set as 100%. Asterisks indicate values significantly different from control value: $**P=0.003$, $***P<0.0009$, $****P<0.0001$. For specific values, see supplementary material Table S1.

with podosomes, and also of podosomal matrix degradation, while Rab8a, Rab14 and Rab22a are positive regulators of these processes.

Matrix degradation in 3D is localised at podosome equivalents and is regulated by Rab5a, Rab8a, Rab14 and Rab22a

Within tissues, cells are surrounded by a 3D environment. This most likely affects both regulatory pathways involved in matrix degradation as well as the matrix-degrading organelles themselves, compared to 2D situations. To date, the formation of matrix-degrading podosome equivalents in 3D is very likely (Linder et al., 2011; Van Goethem et al., 2010), although unproven. To explore the possible formation of podosome-like structures in macrophages also in a 3D context, we embedded cells expressing MT1-MMP-mCherry and LifeAct-GFP (for visualisation of F-actin) in 3D collagen I and assessed the localisation of these constructs (Fig. 5A). Consistent with previous reports (Van Goethem et al., 2010; Vérollet et al., 2011), we found formation of elongated protrusions, which showed F-actin enrichment at their tips. Strikingly, the tips were also enriched in MT1-MMP–mCherry, pointing to a potential degradative capacity of these structures (Fig. 5A). We assessed the possibility by co-staining of endogenous, surface-exposed MT1-MMP and of cleaved collagen I, using an antibody that detects a neoepitope in degraded collagen I (Wolf and Friedl, 2005). These stainings demonstrated that many of the MT1-MMP enriched protrusions are also sites of cleavage of the extracellular matrix (Fig. 5B).

We proceeded to quantify matrix degradation by macrophages in a 3D context, using a collagen dequenching assay, to evaluate the potential influence of the identified RabGTPases on this process. Macrophages were treated with RabGTPase isoform-specific siRNAs, or luciferase- or MT-MMP-specific siRNA as controls, cultured for 3 days, and embedded in quenched collagen I matrix. In this assay, collagen fibres are densely labelled by fluorophores, which effectively quenches their fluorescence. Only after proteolytic cleavage, distance between fluorophores is increased, and the matrix, and also cells that take up matrix material, become fluorescent (Fig. 5C). This increase in fluorescence can be used as a quantitative parameter for ECM degradation (Wolf et al., 2003). Matrix with embedded control cells treated with luciferase siRNA showed progressive increases in fluorescence (1129.9±111.8 a.u. at 36 h), indicative of ongoing ECM degradation. This was significantly decreased to

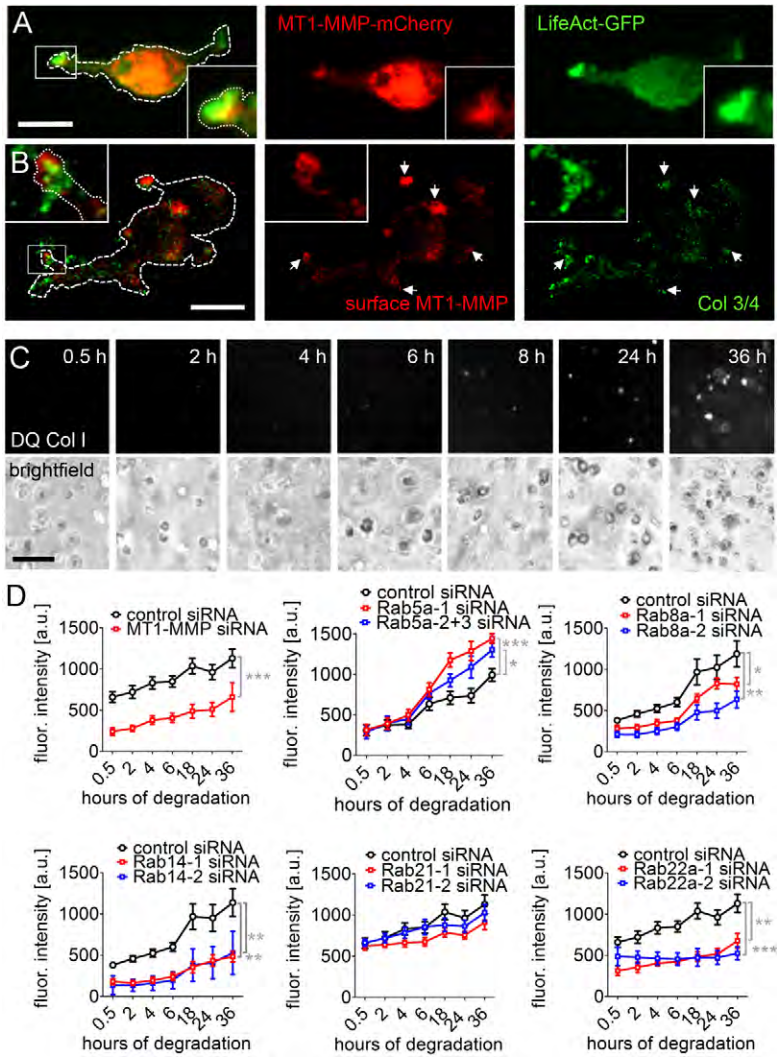

Fig. 5. 3D collagen I degradation is regulated by Rab5a, Rab8a, Rab14 and Rab22a, but not Rab21. (**A**) Confocal micrograph of a macrophage expressing MT1-MMP–mCherry (red) and LifeAct–GFP (green; to visualize F-actin) embedded in collagen I. Dashed white line indicates cell outline. White box indicates the region enlarged in the insert showing a cellular protrusion enriched in MT1-MMP–mCherry and F-actin. Scale bar: 10 µm. (**B**) Confocal 3D reconstruction of a macrophage embedded in collagen I, fixed 18 h post seeding and stained with primary antibodies against MT1-MMP (targeting surface MT1-MMP; red) and collagen 3/4 (green; to visualize degradation of ECM) and secondary antibodies coupled with Alexa Fluor 568 and Alexa Fluor 488, respectively. Dashed white lines indicate cell outline. White box indicates the region enlarged in the insert showing a cellular protrusion enriched in MT1-MMP and degradation of collagen I; further accumulations of MT1-MMP and collagen I degradation are marked by arrows. Scale bar: 10 µm. (**C**) Fluorescence (upper row) and brightfield (lower row) micrographs of macrophages embedded in quenched DQ collagen I matrix. Time after start of experiment is indicated. Scale bar: 50 µm. (**D**) Quantification of dequenched collagen I fluorescence, indicative of progressive matrix proteolysis, in cells treated with the indicated siRNAs. In all experiments, two siRNAs against each protein were used (blue and red lines and symbols), and control cells treated with luciferase siRNA were used in parallel (black lines and symbols). Cells treated with MT1-MMP-specific siRNA were used as positive control. Fluorescence intensities are given in arbitrary units (a.u.). Graphs show means + s.e.m. Time after start of experiment is indicated. Asterisks indicate values significantly different from control value at 36 h: $*P<0.018$, $**P<0.008$, $***P<0.006$. For all values, 3×48 measurements were evaluated. For specific values, see supplementary material Table S1.

ca. 50% in cells treated with MT1-MMP-specific siRNA (659.6±173.8 a.u. at 36 h; Fig. 5D). Importantly, matrix degradation was also decreased to comparable levels in case of knockdown of Rab8a (818.9±84.5 a.u. and 635.4±102.5 a.u. at 36 h), Rab14 (482.67±63.77 a.u. and 528.17±75.58 a.u. at 36 h) and Rab22a (676.1±88.7 a.u. and 524.7±76.9 a.u. at 36 h), but not of Rab21 (910.7±89.8 a.u. and 1027.6±100.3 a.u. at 36 h). In contrast, knockdown of Rab5a resulted in an increase of matrix degradation (879.3±66.5 a.u. and 762.7±78.5 a.u. at 36 h). We conclude that macrophages form F-actin rich podosome equivalents in 3D, which are enriched in MT1-MMP and are able to locally degrade ECM material. Comparable to the situation in 2D, matrix degradation in 3D is negatively regulated by Rab5a, and positively regulated by Rab8a, Rab14 and Rab22a.

3D invasion of macrophages is regulated by Rab5a, Rab8a and Rab14

Proteolytic matrix degradation is a prerequisite, but not the only determinant, for successful mesenchymal invasion (Wolf and Friedl, 2011; Petrie et al., 2012). We thus assessed the potential influence of the identified RabGTPases on this complex cellular behaviour in 3D. For this, we established a 3D invasion assay, in which cells are embedded in a plug of dense collagen I, which is surrounded by a shell of less dense collagen I. M-CSF in the outer shell acts as a chemoattractant, promoting invasion (Fig. 6A; supplementary material Fig. S10). Time lapse videomicroscopy showed that primary macrophages successfully invade the outer shell along the whole length of the plug, leading to invasive migration in several optical planes (Fig. 6B; supplementary material Movie 3). Moreover, invading macrophages developed a mesenchymal morphology, with numerous protrusions formed at the cell front and an elongated trailing edge (Fig. 6B), comparable to our earlier observations with fixed cells (Fig. 5A).

To assess the influence of RabGTPases in this assay, cells were treated with RabGTPase isoform-specific siRNAs or with luciferase- or MT1-MMP-specific siRNA as controls, cultured for 3 days, and embedded in the collagen plug. After 4 additional days, invading cells were detected by light microscopy (Fig. 6C). Invasive cells present in the outer shell were counted, with control values for luciferase siRNA-treated cells set to 100% (Fig. 6D). Cells treated with MT1-MMP siRNA showed a pronounced reduction in their invasive capacity (20.4±9.4%), consistent with the importance of this protease for mesenchymal invasion (Poincloux et al., 2009). Pronounced reductions of ca. 50% in the number of invasive cells were observed upon knockdown of Rab8a (55.5±19.0% and 51.6±25.3%) and Rab14

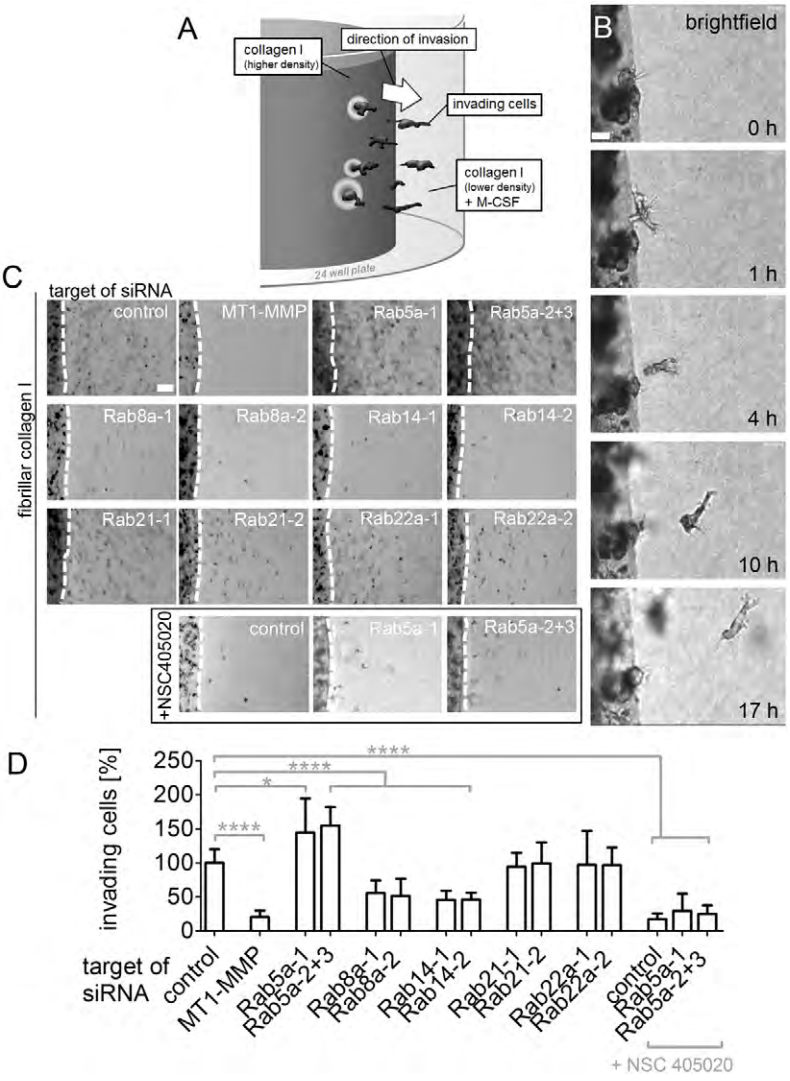

Fig. 6. Knockdown of Rab5a, Rab8a and Rab14, but not of Rab21 and Rab22a, leads to pronounced alterations in 3D invasive behaviour of macrophages. (**A**) Model of the 3D type I collagen invasion assay. Cells are embedded in a type I collagen plug (2.5 mg/ml) and invade the surrounding shell of less dense type I collagen (2 mg/ml) containing M-CSF as a chemoattractant. (**B**) Brightfield confocal micrographs of a macrophage invading fibrillar collagen I matrix. Time of image acquisition after start of experiment is indicated. Scale bar: 10 µm. Note dark zone of collagen I with embedded macrophages and brighter zone of surrounding fibrillar collagen I (for experimental set-up, see Materials and Methods), and formation of numerous protrusions of invading macrophage. (**C**,**D**) Invasion of macrophages into collagen I matrix. Cells were treated with siRNAs specific for luciferase, as a negative control, MT1-MMP, as a positive control, and for RabGTPase isoforms, and were treated with MT1-MMP inhibitor NSC405020, as indicated. (C) Brightfield micrographs of invading cells. Dashed white lines indicates border between collagen matrix with embedded macrophages and collagen matrix with invaded cells, visible as dark dots. Scale bar: 100 µm for all images. (D) Quantification of cells invading the collagen matrix, at day 4 after seeding. Values for control siRNA were set to 100%. Bars show means + s.d. Asterisks indicate values significantly different from values of control cells: $*P=0.011$, $**P=0.0056$, $***P=0.0001$, $****P<0.0001$. For all values, 16 pictures from three different donors each were evaluated. For specific values, see supplementary material Table S1.

(45.7±13.3% and 46.4±10.1%). By contrast, the levels of invasive cells were unchanged upon knockdown of Rab21 (94.4±20.4% and 99.2±31.1%) and Rab22a (97.1±50.1% and 96.8±26.0%). Strikingly, knockdown of Rab5a resulted in an increased number of invaded cells (144.6±49.7% and 154.7±49.7%). Moreover, use of MT1-MMP inhibitor NSC405020 (1 mM; Remacle et al., 2012) greatly reduced cell invasion (17.1±8.6%; Fig. 6C,D), and this effect could not be rescued by knockdown of Rab5a (29.4±25.5% and 24.7±12.9%; Fig. 6C,D), showing that Rab5a exerts its function in invasion mainly through regulation of MT1-MMP.

To further exclude MT1-MMP-independent effects of RabGTPase knockdown, we tested the viability and ECM binding by performing survival and adhesion assays of cells treated with siRNA specific for MT1-MMP, individual Rab proteins or combinations. Collectively, we find slight variations in the 10–20% range for knockdown of some RabGTPases, including Rab5a, Rab8a and Rab14 (supplementary material Fig. S8). However, considering that all alterations in cell invasion upon knockdown of these Rab proteins are pronounced (±50%; Fig. 6D), the minor, and sometimes even opposing, effects on cell viability or cell adhesion can not explain these effects. The increased invasion in case of Rab5a knockdown and the decreased invasion for Rab8a or Rab14 knockdown cells are thus most likely due to MT1-MMP-associated matrix degradation, and not, or only to a lesser degree, to changes in cell viability or matrix adhesion. We conclude from these results that Rab5a, Rab8a and Rab14 are important regulators of protease-driven mesenchymal invasion in a three-dimensional setting.

Finally, to test how the three identified RabGTPases might work together in MT1-MMP regulation, we measured surface exposure of endogenous MT1-MMP, collagen dequenching in 3D, and invasion into collagen gels, each time under double knockdown of Rab5a and Rab14 or Rab8a and Rab14. Apart from a ca. 10% increase in matrix adhesion for Rab5a/Rab14 double knockdown cells (supplementary material Fig. S8, with values given in supplementary material Table S1), no major alterations were apparent in cells depleted for the specific RabGTPases, ensuring that cell viability and matrix adhesion upon (combined) knockdown of Rab proteins were unchanged. Combined knockdown of Rab5a and Rab14 led to intermediate values in surface exposure of MT1-MMP (57.7±35.3%; Fig. 7A), in 3D collagen dequenching (1213.1±102.6 a.u. at

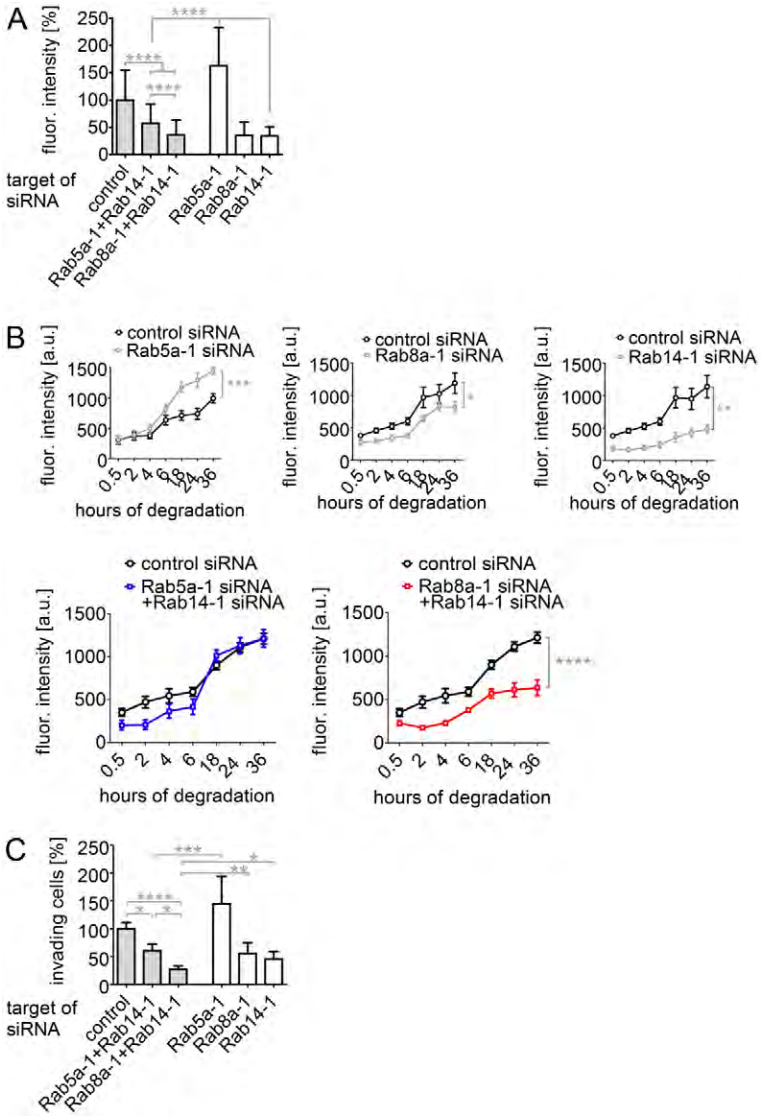

Fig. 7. Surface exposure of MT1-MMP, collagen I dequenching and 3D invasion of cells with combined knockdown of Rab5a and Rab14 or Rab8a and Rab14. (**A**) Fluorescence intensities of surface-localised endogenous MT1-MMP, based on Alexa Fluor 568 fluorescence. Fluorescence intensities for control siRNA were each set to 100%. For comparison, values for single knockdown of Rab5a, Rab8a and Rab14 are also shown (see also Fig. 3M). For all values, 30 cells from three different donors were evaluated. Graph shows means + s.d.. Asterisks indicate values significantly different from control values: ****$P<0.0001$. For specific values, see supplementary material Table S1. (**B**) Quantification of dequenched collagen I fluorescence in cells treated with indicated siRNAs. In all experiments, two siRNAs against each protein were used (blue and red), and control cells treated with luciferase siRNA were used in parallel (black). Fluorescence intensities are given in arbitrary units (a.u.). Graphs show means + s.e.m. Time after start of experiment is indicated. For comparison, graphs for single knockdown of Rab5a, Rab8a and Rab14 are also shown (see also Fig. 5D). Asterisks indicate values significantly different from control value at 36 h: *$P=0.0143$, **$P=0.0047$, ***$P=0.0003$, ****$P<0.0001$. For all values, 48 measurements from three different donors each were evaluated. For specific values, see supplementary material Table S1. (**C**) Quantification of cells invading collagen I matrix, at day 4 after seeding. Values for control siRNA were set to 100%. For comparison, values for single knockdown of Rab5a, Rab8a and Rab14 are also shown (see also Fig. 6D). Bars show means + s.d. Asterisks indicate values significantly different from values of control cells: *$P<0.0182$, **$P=0.0025$, ***$P=0.0002$, ****$P<0.0001$. For all values, 16 pictures from three different donors each were evaluated. For specific values, see supplementary material Table S1.

36 h; Fig. 7B) and collagen gel invasion (60.3±41.9%; Fig. 7C). Double knockdown of Rab8a and Rab14 led to values similar to those observed for single knockdown of Rab8a in MT1-MMP surface exposure (36.3±26.9%; Fig. 7A) and in 3D collagen dequenching (635.0±91.0 a.u. at 36 h; Fig. 7B), and to even lower values, compared to single knockdowns of either Rab8a or Rab14, in 3D invasion of macrophages (26.7±20.9%; Fig. 7C). We conclude that Rab5a, as a negative regulator of MT1-MMP trafficking, counteracts the effects of Rab14. In contrast, Rab8a and Rab14 are both positive regulators of MT1-MMP trafficking. Moreover, based on their non-additive effects on MT1-MMP cell surface exposure and collagen degradation, Rab8 and Rab14 are likely to regulate common aspects of MT1-MMP trafficking. This is in contrast to their additive effects in the plug invasion assay, suggesting that both Rab proteins regulate separate aspects of cell invasion.

Discussion

A key feature of mesenchymal cell invasion is the ability to proteolytically process extracellular matrix material, which allows cells to transmigrate through a variety of barriers including the endothelial basement membrane (Nourshargh et al., 2010) or interstitial collagen networks (Poincloux et al., 2009). The membrane-bound matrix metalloproteinase MT1-MMP plays a central role in these processes (Poincloux et al., 2009; Wolf and Friedl, 2009; Hotary et al., 2003). Consequently, therapeutic intervention on the level of MT1-MMP activity presents as an attractive option for the potential treatment of invasion-based dysfunctions such as chronic inflammation or metastasis. In order to manipulate MT1-MMP activity in a targeted manner, however, it is vital to understand the molecular mechanisms regulating MT1-MMP activity at the cell surface, which includes trafficking of MT1-MMP vesicles.

RabGTPases are major regulators of intracellular trafficking that act as molecular switches (Stenmark, 2009; Hutagalung and Novick, 2011), with their on/off regulatory function considered to be restricted to the membrane compartments where they are located (Zerial and McBride, 2001). This formed the rationale of our colocalisation screen to identify Rab proteins relevant for MT1-MMP trafficking in macrophages. We found prominent colocalisation of both GFP-fused constructs and endogenous forms of Rab5a, Rab8a, Rab14, Rab21 and Rab22a with

MT1-MMP-positive vesicles. No substantial colocalisation was found for Rab4, Rab6a, Rab9 and Rab11. Our results are consistent with a previous report showing localisation of Rab8, but not Rab11, on MT1-MMP vesicles in MDA-MB-231 adenocarcinoma cells (Bravo-Cordero et al., 2007). At the same time, these data do not exclude the possibility that other members of the extensive Rab family might also colocalise with MT1-MMP and regulate MT1-MMP functions in macrophages. Still, control experiments using dominant active/negative constructs and siRNA-mediated knockdown (supplementary material Fig. S6D) for Rab6a show that, at least for this isoform, absence of localisation to MT1-MMP vesicles is coupled to absence of a regulatory influence on MT1-MMP-dependent parameters such as surface exposure, 3D matrix degradation and 3D invasion (supplementary material Fig. S9).

Besides colocalisation with MT1-MMP vesicles, we also observed the formation of enlarged vesicles or tubules upon overexpression of Rab5a, Rab14, Rab21 and Rab22a wt constructs. Similar observations of 'giant vesicles' have been reported upon overexpression of DA Rab5 in BHK and HeLa cells (Stenmark et al., 1994), for both wt and DA Rab14 in NRK rat kidney cells (Junutula et al., 2004), of wt Rab21 in MDA-MB-231 breast cancer cells (Pellinen et al., 2006) and of wt Rab22 in BHK cells (Olkkonen et al., 1993). While this phenomenon represents an artefact of enhanced RabGTPase activity, the enlarged surface of these structures revealed that RabGTPases and MT1-MMP–mCherry often localised to distinct domains at the membrane. The common localisation to a vesicle subpopulation does, therefore, not imply colocalisation or even interaction of these proteins. These findings are also consistent with reports that RabGTPases are not randomly distributed on organelles, but are clustered in functional domains (Zerial and McBride, 2001; Sönnichsen et al., 2000).

In order to assess the relevance of the identified RabGTPases for MT1-MMP trafficking, we next determined their impact on their regulation of MT1-MMP pools at the cell surface. Out of five RabGTPases (Rab5a, Ra8a, Rab14, Rab21, Rab22a) showing prominent colocalisation with MT1-MMP-positive vesicles, four isoforms (Rab5a, Rab8a, Rab14, Rab22a) had a significant impact on the cell surface exposure of MT1-MMP, with Rab5a emerging as a negative regulator, and Rab8a, Rab14 and Rab22a as positive regulators of MT1-MMP cell surface exposure. This is in line with the key role of Rab5 during membrane fusion in endocytosis (Stenmark, 2009; Stenmark et al., 1994), and also of the Rab5 effector EEA-1 in the early endosome tethering and docking (Christoforidis et al., 1999). Rab8a has already been identified as a regulator of MT1-MMP exocytosis in MDA-MB-231 cells (Bravo-Cordero et al., 2007), and our results confirm this role for primary human macrophages, pointing to a probably general role of Rab8 in MT1-MMP exocytosis. The detected role for Rab14 in MT1-MMP surface exposure appears to be consistent with the localisation of Rab14 on early endosomes and the observed defects in transferrin recycling upon depletion of Rab14 (Yamamoto et al., 2010). Rab21 activity is clearly not required for MT1-MMP trafficking in macrophages. However, localisation of Rab21 at early endosomes, which are also positive for Rab5a (Simpson et al., 2004) may explain its localisation at MT1-MMP vesicles in this study. Rab22 also shows localisation at early endosomes (Kauppi et al., 2002) and has been implicated in the recycling of membrane proteins that are internalised independently of clathrin (Chen et al., 1994). This seems to be consistent with the finding that surface-localised MT1-MMP can be internalised by both clathrin-dependent and -independent pathways (Remacle et al., 2003). Moreover, Rab4 and Rab11, which both regulate recycling of clathrin-dependent cargo (Schlierf et al., 2000; van der Sluijs et al., 2001), did not colocalise with MT1-MMP in the screen. This suggests that uptake of MT1-MMP from the cell surface proceeds mostly via clathrin-independent pathways in primary macrophages.

Collectively, these data point to the following possible scenario of Rab-dependent trafficking of MT1-MMP in macrophages (Fig. 8): surface-associated MT1-MMP is taken up by endocytosis, which is controlled by Rab5a. Substantial parts of this pool are recycled back to the cell surface, through processes controlled by Rab14 and Rab22a, which probably reflects their respective roles in the slow and fast recycling routes for re-internalised surface proteins (Sönnichsen et al., 2000; Yudowski et al., 2009). Rab8a impacts on MT1-MMP trafficking by regulating the biosynthetic pathway from the Golgi, which can proceed via exocytic vesicles or recycling endosomes (Henry and Sheff, 2008; Grant and Donaldson, 2009). In addition, eventual degradation by lysosomes is expected to occur, to balance synthesis of new material. This model is further substantiated by our experiments using double knockdown cells. Combined knockdown of Rab5a and Rab14 led to intermediate values in surface exposure of MT1-MMP, in 3D collagen dequenching and collagen gel invasion, arguing for opposing roles of these RabGTPases in MT1-MMP trafficking, which would be

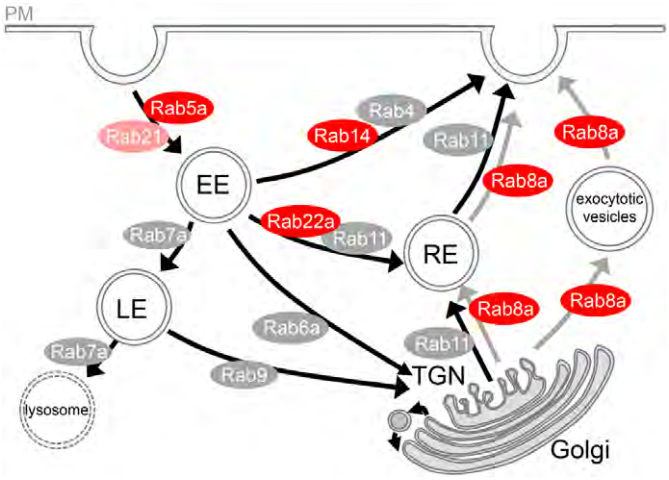

Fig. 8. Model of MT1-MMP trafficking in macrophages. Surface-associated MT1-MMP is taken up by endocytosis, which is controlled by Rab5a. Parts of this pool are recycled back to the cell surface, either by fast recycling controlled by Rab14 or by slow recycling through recycling endosomes controlled by Rab22a. Trafficking of newly synthesized MT1-MMP to the cell surface is controlled by Rab8a and may occur by exocytotic vesicles or recycling endosomes. RabGTPase isoforms colocalising with MT1-MMP in macrophages are indicated at their respective compartments. RabGTPases that are major regulators of MT1-MMP-dependent cell invasion in 3D are highlighted in deep red (Rab21, colocalising with MT1-MMP vesicles, but without major impact on MT1-MMP trafficking, in light red; other major RabGTPases, including tested isoforms without impact on recycling or biosynthetic trafficking of MT1-MMP in grey). EE, early endosomes; LE, late endosomes; RE, recycling; PRE, perinuclear recycling endosomes; TGN, trans-Golgi network. The plasma membrane is indicated as a double line.

Table 1. Overview for MT1-MMP distribution after various treatments

	Alteration of MT1-MMP distribution*								
	Target of siRNA/GFP–Rab DN overexpression								
Assay	Rab4	Rab5a	Rab6a	Rab8a	Rab9	Rab11	Rab14	Rab21	Rab22a
Colocalisation with MT-MMP	–	+	–	+	–	–	+	+	+
Surface exposure	n.a.	↑ ↑	↔	↓ ↓	n.a.	n.a.	↓ ↓	↔	↓ ↓
Recruitment to podosomes	n.a.	↑ ↑	n.a.	↓ ↓	n.a.	n.a.	↓ ↓	↔	↓ ↓
Matrix degradation on 2D gelatin	n.a.	↑ ↑	n.a.	↓ ↓	n.a.	n.a.	↓ ↓	↔	↓ ↓
Matrix degradation in 3D collagen I	n.a.	↑	↔	↓	n.a.	n.a.	↓ ↓	↔	↓ ↓
Invasion into 3D collagen I	n.a.	↑ ↑	↔	↓ ↓	n.a.	n.a.	↓ ↓	↓	↔

*Compared with adequate control cells.
–, negative.
+, positive.
(↑) ↑ , (pronounced) increase.
(↓) ↓ , (pronounced) decrease.
↔ , no significant change.
n.a., not analysed.

consistent with roles for Rab5a in endocytosis and for Rab14 in exocytosis of MT1-MMP. Moreover, combined knockdown of Rab8a and Rab14 led to values similar to those observed for single knockdown of Rab14 in MT1-MMP surface exposure and in 3D collagen dequenching. This non-additive effect suggests that both Rab proteins address aspects of the same pathway that regulates MT1-MMP trafficking and proteolytic activity. The additive effect of their combined knockdown in 3D collagen invasion further suggests that Rab8 and Rab14 have only partially overlapping functions in cell invasion. This might reflect regulation not only of MT1-MMP trafficking during proteolytic invasion, but also of other aspects such as adhesion or de-adhesion.

To test the significance of the identified Rab proteins for MT1-MMP-dependent functions, we also analysed their impact on matrix degradation by primary macrophages in both 2D and 3D settings. Podosomes are actin-rich cell-matrix contacts, that have emerged as central structures mediating matrix degradation and cell invasion (Murphy and Courtneidge, 2011; Linder, 2007), especially by monocytic cells including macrophages (Linder et al., 1999), dendritic cells (Burns et al., 2001) and osteoclasts (Destaing et al., 2003). Podosomes are able to degrade matrix material by localised release of ECM-lytic factors, including proteinases of the matrix metalloproteinase family (Wiesner et al., 2010; Delaissé et al., 2003; Tatin et al., 2006), and especially MT1-MMP has been shown to be crucial for podosome-localised ECM degradation (Linder, 2007). Indeed, microtubule plus ends have been shown to contact podosomes (Kopp et al., 2006), which is consistent with microtubule-dependent trafficking of MT1-MMP to these structures (Wiesner et al., 2010).

We now find that knockdown of Rab5a leads to enhanced contact events of MT1-MMP–mCherry vesicles with podosomes, while knockdown of Rab8a, Rab14 and Rab22a results in a reduction of contact events. These results correlate well with respective changes upon RabGTPase knockdown in the matrix degradation assay and point to Rab5a, Rab8a, Rab14 and Rab22a as important regulators of matrix degradation in macrophages, most probably by mediating the vesicular delivery of the key proteinase MT1-MMP to the main degradative structures of these cells. Direct involvement of RabGTPases in MT1-MMP-mediated ECM degrading processes has so far only been reported for Rab8, which has been shown to regulate collagen degradation by MDA-MB-231 cells (Bravo-Cordero et al., 2007). Our results confirm this role now also for gelatin degradation by primary macrophages. The only other Rab isoforms implicated in matrix degradation is Rab4a, which is involved in procathepsin L secretion in human melanoma cells (Barbarin and Frade, 2011). However, MT1-MMP does not localise to Rab4-positive vesicles in human macrophages.

It is important to consider that cell culture on 2D matrices creates a polarisation of the cell, resulting in basal and apical surfaces. This is useful for the experimental study of different outputs such as apical surface exposure of MT1-MMP or matrix degradation at the basal cell side. Moreover, it is most probably also a relevant process *in vivo*, as invasive cells do encounter two-dimensional barriers, including contact of monocytic cells with the endothelium or attachment of osteoclasts to bone surfaces (Linder et al., 2011). Within tissues, however, cells are surrounded by a three-dimensional environment, which is expected to influence both regulatory pathways involved in matrix degradation as well as the matrix-degrading organelles themselves. Indeed, primary human macrophages in gelled collagen I matrix have been shown to form long, dynamic protrusions that enriched are at their tips in podosome components such as F-actin, cortactin, talin, vinculin and CD44 (Van Goethem et al., 2010; Vérollet et al., 2011). Colocalisation of these structures with matrix defects and also with fluorescence signals in the collagen dequenching assay support the idea that these structures exhibit degradative capacity (Van Goethem et al., 2010). This is further underlined by our finding that these tip structures are also enriched in MT1-MMP. Collectively, these structures, (1) possess the typical composition of podosomes, if arranged in a different architecture, (2) recruit the major matrix-degrading protease MT1-MMP, and (3) colocalise with sites of matrix degradation, which qualifies them as bone fide 3D equivalents of 2D podosomes.

Of note, 3D invasion is a complex multi-step process involving adhesion to matrix, proteolytic cleavage of matrix components, as well as de-adhesion and pulling of the cell body (Friedl and Wolf, 2009). The impact of the identified Rab proteins on this process may thus not only reflect MT1-MMP dependent matrix degradation, but may also involve other MT1-MMP functions such as integrin processing at the cell surface (Barbolina and Stack, 2008) or cleavage of matrix receptors such as syndecan-1

(Endo et al., 2003; Wiesner et al., 2010). The complex nature of cell invasion may also explain the different influence of Rab5 on invasion of macrophages and cancer cells. In HeLa and human cervical carcinoma cells, Rab5a positively regulates focal adhesion formation (Liu et al., 2011). Decreased invasion of these cells is thus likely based on defects in cell de-/adhesion. In contrast, Rab5 negatively influences matrix degradation in primary macrophages, which transmits as a negative influence on 3D invasion of these cells. The influence of Rab5a particularly on MT1-MMP in macrophages is also evident from experiments using the MT1-MMP inhibitor NSC405020 in the 3D cell invasion assay. Here, use of NSC405020 completely reverted the invasion-promoting effect of Rab5a knockdown and decreased it to control levels (Fig. 6D), demonstrating that Rab5a exerts its function in macrophage invasion mainly through MT1-MMP.

Different functions of surface-associated MT1-MMP may be differentially influenced by the recycling route the protease takes within cells, which could offer an explanation why Rab22a, which is involved in regulating the surface pool of MT1-MMP, has no apparent impact on 3D invasion of macrophages, in contrast to Rab8a and Rab14. Indeed, the potential association of different pools of MT1-MMP with distinct intracellular trafficking routes has been speculated upon earlier (Schlierf et al., 2000). Of course, this does not exclude that Rab-dependent trafficking of other cargo molecules, for example integrins or other metalloproteinases such as ADAMs, impact on 3D invasion of macrophages. However, we consistently found, (1) strong functional correlation between inhibition of specific Rab isoforms and knockdown of MT1-MMP, (2) Rab14, which regulates ADAM10 trafficking in epithelial cells (Linford et al., 2012), does not colocalise with MT1-MMP vesicles in macrophages, and (3) Rab4, Rab11 and Rab21, major regulatory Rabs for integrin trafficking (Pellinen et al., 2006; Caswell et al., 2009), showed no pronounced influence on MT1-MMP trafficking or function in this study.

Collectively, our data identify three specific RabGTPases, Rab5a, Rab8a and Rab14, as major regulators of MT1-MMP trafficking and function in primary human macrophages. We show that these RabGTPases control the pericellular activity of MT1-MMP by regulating the cell surface exposure of MT1-MMP, modulating contact of MT1-MMP-positive vesicles with podosomes and thus impact on extracellular matrix degradation and ultimately on proteolytic invasion of macrophages. At the same time, our results show that the relevance of potential MT1-MMP regulators should be tested in a variety of experimental set ups, and that neither colocalisation nor influence on matrix degradation in 2D alone is sufficient to correctly predict an influence on proteolytic cell invasion in 3D. This appears to be consistent with recent findings in breast cancer cells that many parameters of 2D migration have only limited prognostic value for 3D invasion (Meyer et al., 2012).

Alterations in RabGTPase expression or activity can cause defects in cell adhesion, motility and invasion, leading to neurologic diseases, lipid storage disorders or cancer (Agola et al., 2011). Accordingly, Rab5a is hyperactivated in lung adenocarcinoma (Stein et al., 2003), Rab5 and Rab8 have been implicated in Parkinson's disease by affecting α-synuclein transport (Gitler et al., 2008), and Rab22a is upregulated in hepatocellular carcinoma (Agola et al., 2011). Consequently, these RabGTPases are being considered as target molecules for therapeutic intervention (Stein et al., 2003). Our results now implicate Rab5a, Rab8a and Rab14 as potential targets for therapeutic modulation of macrophage invasion and may thus indicate alternative, if challenging, routes for the treatment of invasion-based immune cell dysfunctions.

Material and Methods

Cell preparation, culture and transfection

Human peripheral blood monocytes were isolated from buffy coats and differentiated into macrophages, as described previously (Kopp et al., 2006). Cells were cultured in RPMI containing 20% autologous serum at 37℃, 5% CO_2 and 90% humidity. Transient transfections were performed using the Neon® Transfection System (Life technologies, Invitrogen, Darmstadt, Germany) with standard settings (1000 V, 40 ms, 2 pulses) and appropriate amounts of siRNA (650 ng) and plasmids (0.5–1.5 µg/10 000 cells), respectively.

Antibodies and constructs

Mouse monoclonal antibody (mAb) anti-MT1-MMP and anti-α actin were purchased from Millipore (Billerica, MA), rabbit mAb anti-Rab5 from Cell Signaling (Danvers, MA), mouse mAb anti-Rab8 (used for immunoblotting) from BD (Franklin Lakes, NJ), rabbit polyclonal antibody (pAb) anti-Rab8a (used for immunostaining) from Sigma (St. Louis, MO), rabbit pAb anti-Rab14 from Abcam (Cambridge, UK) and rabbit pAb anti-Rab22a from ProteinTech (Group, Chicago, IL). Rabbit pAb anti-Rab21 was a kind gift from J. Fransen (University of Nijmegen, Netherlands). mCherry antibody was kindly provided by J. Faix (Hannover medical school, Germany). Collagen 3/4 antibody was a kind gift from P. Friedl (Radboud University Nijmegen, Netherlands). All fluorochrome-conjugated secondary antibodies were purchased from Molecular Probes (Eugene, OR). MT1-MMP-mCherry was kindly provided by P. Chavrier (Institute Curie, Paris, France); pGreenlantern-Rab5wt (wild type), pGreenlantern-Rab5 S34N (dominant negative, DN) and pGreenlantern-Rab5 Q79L (dominant active, DA) were generously provided by Craig Roy (Yale University, New Haven, CT); GFP-Rab6awt, GFP-Rab6a Q72L (DA) and GFP-Rab6a T27N (DN) were kind gifts from J. Kremerskothen (University Hospital Muenster, Germany); GFP-Rab8awt, GFP-Rab8aQ67L (DA) and GFP-Rab8aT22N (DN) were kindly provided by D. Sheff (Carver College of Medicine, Iowa City, IA); GFP-Rab14wt, GFP-Rab14 S25N (DN) and GFP-Rab14 Q70L (DA) were gifts from R. H. Scheller (Genentech Inc., San Francisco, CA), GFP-Rab21wt, GFP-Rab21 T33N (DN), GFP-Rab21 Q78L (DA) were gifts from J.C. Simpson (University College Dublin, Ireland), GFP-Rab22awt, GFP-Rab22a S19N (DN), GFP-Rab22a Q64L (DA) were gifts from J. Donaldson (National Institutes of Health, Bethesda, MD).

Microscopy

Images of fixed samples were acquired with a confocal laser-scanning microscope (Leica DM IRE2 with a Leica TCS SP2 AOBS confocal point scanner) equipped with an oil-immersion HCX PL APO 63× NA 1.4 λ_{blue} objective. Detailed fluorescence images of cells in 3D collagen were acquired with a confocal laser-scanning microscope (Leica DMI 6000 with a Leica TCS SP5 AOBS confocal point scanner) equipped with a water-immersion HCX PL APO 63× NA 1.4-0.6 objective.

Immunoblotting

Immunolabelling was performed by standard procedure (Kopp et al., 2006), using the above mentioned anti-MT1-MMP, Rab5, Rab8, Rab14, Rab21, Rab22a, or α-actin antibodies and horseradish peroxidase-coupled anti-mouse or anti-rabbit IgG (Dianova, Hamburg, Germany) as secondary antibodies. Protein bands were visualised by using Super Signal kit (Pierce Chemical, Rockford, IL) and X-Omat AR film (Kodak, Stuttgart, Germany).

Live cell imaging

Images were acquired with a spinning disc confocal system (Spinning disc CSU22, Yokogawa, Japan) fitted on a Zeiss Axiovert 200M microscope with a temperature- and CO_2-controllable environmental chamber (Solent Scientific, Regensworth, UK), oil immersion Plan-Apo 63× NA 1.4 objective and a CCD camera (EM-CCD C-9100-2, Hamamatsu, Japan). Acquisition and processing of images was performed with Volocity Software (Improvision, Coventry, UK). Cells were seeded on glass-bottomed dishes (ibidi) at a density of 2×10^5 and incubated for 20 h before the start of the experiment.

SiRNA-induced knockdown

Specific targeting duplex siRNA were generated (MWG, Ebersberg, Germany) as follows: 5′-AACCAGGAATCAGTGTTGTAG-3′ (Rab5a-1); 5′-AAGCACAGT-CCTATGCAGATG-3′ (Rab5a-2) and 5′-GAAGAGGAGTAGACCTTAC-3′ (Rab5a-3); 5′-GACATCTTTGATCACCAGA-3′ (Rab6a-1); 5′-CACCTA-TCAGGCAACAATT-3′ (Rab6a-2); 5′-AAGAGACAAGTTTCCAAGGAA-3′

Journal of Cell Science

(Rab8a-1); 5′-CGCATTTTTCACTCTCGCC-3′ (Rab8a-2); 5′-AAGGAATCTCACCAATCCAAA-3′ (Rab14-1); 5′-AAGAAGTACATATAACCACTT-3′ (Rab14-2); 5′-AAGTTTAACGACAAGCACATC-3′ (Rab21-1); 5′-AAGAGAGATTCCATGCATTGG-3′ (Rab21-2); 5′-AAGGACTACGCCGACTCTATT-3′ (Rab22a-1); 5′-CTGCAGCTATAATCGTTT ATG-3′ (Rab22a-2); 5′-AACAGGCAAGCGTGATGCAGA-3′ (MT1-MMP); firefly luciferase targeting siRNA 5′-AGGTAGTGTAACCGCCTTGTT-3′ was used as negative control. MT1-MMP siRNA was tested in primary human macrophages and led to a reduction of ca. 95% 3 days after transfection.[24] Primary human macrophages were transfected with siRNA (650 ng) twice at 0 h and 48 h, and evaluated after a further incubation period of 18 h.

Cell survival assay

Cells were transfected with siRNA twice at 0 h and 48 h. On day 7 after initial transfection, cell survival was determined by staining the cells with Crystal Violet (5 mg/ml), resolving the stain with 2% SDS, and measuring the absorbance at 550 nm. For each value, nine points evenly distributed within one well of a 96-well plate were measured. In total, triplicates from three different donors were evaluated. Mean value of control cells was set as 100%. Statistical analysis was performed with Microsoft Excel and GraphPad Prism software. For specific values, see supplementary material Table S1.

Cell adhesion to ECM assay (Collagen I)

Cells were transfected with siRNA twice at 0 h and 48 h. On day 7, cells were detached and left to adhere for 20 min in a 96-well plate, coated with collagen I (Biochrome AG, Berlin, Germany). Cell adherence was determined as described previously (Humphries, 2009) using Crystal Violet as used to determine the survival of the cells. For each value, nine points evenly distributed within one well of a 96-well plate were measured. In total, triplicates from three different cell donors were evaluated. Mean value of control cells was set as 100%. Statistical analysis was performed with Microsoft Excel and GraphPad Prism software. For specific values, see supplementary material Table S1.

Surface exposure of MT1-MMP

Macrophages were seeded on non-coated glass coverslips in a density of 1×10^5, or seeded in Collagen I (2.5 µg/ml; from rat tail, Becton Dickinson), fixed with 3.7% formaldehyde solution, but not permeabilised. Surface MT1-MMP–mCherry and endogenous surface MT1-MMP was stained with specific antibodies (anti-mCherry and anti-MT1-MMP, respectively), followed by Cy5- and Alexa-Fluor-568-conjugated secondary antibodies, respectively, as also described previously (Wiesner et al., 2010). Quantification of Cy5- or Alexa-Fluor-568-based fluorescence intensity was performed using ImageJ software for measurement of the cell surface exposure of MT1-MMP. In the case of overexpressed MT1-MMP, values of surface-exposed MT1-MMP–mCherry were set relative to values of total overexpressed MT1-MMP–mCherry for normalisation. Values of control cells were set to 100%. For comparability, laser intensity was not changed between measurements. For each value, 3×30 cells were evaluated. Statistical analysis was performed with Microsoft Excel and GraphPad Prism software. When indicated, differences between mean values were analysed using the Student's *t*-test.

2D gelatin degradation assay

Gelatin (from swine, Roth, Karlsruhe, Germany) was fluorescently labelled with NHS-Rhodamine (ThermoScientific, Rockford, IL), according to (Chen et al., 1994). Coverslips were coated with labelled matrix solution, fixed in 0.5% glutaraldehyde (Roth) and washed with 70% ethanol and medium. Cells were seeded on coated coverslips with a density of 8×10^4, fixed and permeablised 6 h post seeding and stained with Alexa-Fluor-647-conjugated phalloidin. Values of matrix degradation were determined by a loss of fluorescence intensity relatively to non-degraded matrix, using ImageJ software. Values of control cells were set to 100%. For comparability, laser intensity was not changed between measurements. For each value, 3×30 cells were evaluated. Values were analysed using Windows Excel software. Statistical analysis was performed with GraphPad Prism software. When indicated, differences between mean values were analysed using the Student's *t*-test.

3D collagen i degradation assay

To measure 3D collagen I matrix degradation, primary human macrophages were copolymerised with rat tail collagen (2.5 mg/ml; Becton Dickinson), containing 2% quenched DQ™ collagen I (fluorescein conjugated, from bovine skin, Molecular Probes). Emitted light was measured and quantified by spectrofluorometry at a wavelength of 530 nm. Background fluorescence was analysed by measuring the fluorescence intensity of matrix without cells. For each value, 16 points evenly distributed within one well of a 96-well plate were measured; in total, three wells from three different cell donors were evaluated ($n=144$). Statistical analysis was performed with GraphPad Prism software. When indicated, differences between mean values over the whole time of measurement were analysed using the Student's *t*-test.

3D collagen i invasion assay

To measure invasive capacity of cells into a 3D collagen I matrix, primary human macrophages were copolymerised with rat tail collagen (2.5 mg/ml; Becton Dickinson) and embedded in rat tail collagen I (2 mg/ml) containing 10 ng/ml Macrophage-Colony Stimulating Factor (M-CSF, Relia Tech, Wolfenbüttel, Germany). When indicated, MT1-MMP inhibitor (NSC405020, 1 mM, Millipore) was added to the collagen I prior to polymerisation. The lower concentration of collagen I in the outer gel (2 mg/ml) was chosen to facilitate invasion outwards from the inner plug. This was based on initial testing of several different combinations of collagen concentrations for inner and outer gels. The one presented here is the one that allowed invasion in principal but hindered it under knockdown of MT1-MMP. M-CSF was chosen as a known chemoattractant for macrophages (Pixley, 2012). We found that addition of M-CSF to the outer gel enhances the number of outwardly invading cells approximately twofold (supplementary material Fig. S10A,B), without influencing cell viability (supplementary material Fig. S10C) and thus provides a clearer readout of cell invasion. The number of cells that invaded the surrounding matrix was counted after 4 days of invasion, using ImageJ cell counter. Four wells per donor and three donors in total were analysed ($n=16$). Statistical analysis was performed with GraphPad Prism software. When indicated, differences between mean values of measurement were analysed using the Student's *t*-test.

Acknowledgements

We thank Frank Bentzien (UKE transfusion medicine) for buffy coats, Philippe Chavrier for MT1-MMP-mCherry, Julie Donaldson for GFP-Rab22a, Jan Faix for anti-mCherry antibody, J. A. Fransen for anti-Rab21 antibody, Peter Friedl for collagen ¾ antibody, Joachim Kremerskothen for GFP-Rab6a constructs, Craig Roy for GFP-Rab5a constructs, R.H. Scheller for GFP-Rab14, J.C. Simpson for GFP-Rab21, Michael Sixt and Roland Wedlich-Söldner for LifeAct-GFP, Boris Hinz for technical discussions, the UKE Microscope Imaging Facility (UMIF) for technical support, Jens Cornils and Andrea Mordhorst for expert technical assistance, and Martin Aepfelbacher for continuous support.

Author Contributions

C.W. designed and performed experiments as part of the doctoral thesis, K.A. performed experiments, and S.L. designed experiments and wrote the manuscript.

Funding

This work was supported by Wilhelm Sander Stiftung [grant number 2007.020.02 to S.L.]; the Deutsche Forschungsgemeinschaft [grant number LI925/3-1, LI925/2-2 to S.L.]; and the European Union Seventh Framework Programme (FP7/2007–2013) [grant agreement number FP7-237946 (T3Net) to S.L.].

Supplementary material available online at
http://jcs.biologists.org/lookup/suppl/doi:10.1242/jcs.122358/-/DC1

References

Agola, J. O., Jim, P. A., Ward, H. H., Basuray, S. and Wandinger-Ness, A. (2011). Rab GTPases as regulators of endocytosis, targets of disease and therapeutic opportunities. *Clin. Genet.* **80**, 305-318.

Barbarin, A. and Frade, R. (2011). Procathepsin L secretion, which triggers tumour progression, is regulated by Rab4a in human melanoma cells. *Biochem. J.* **437**, 97-107.

Barbolina, M. V. and Stack, M. S. (2008). Membrane type 1-matrix metalloproteinase: substrate diversity in pericellular proteolysis. *Semin. Cell Dev. Biol.* **19**, 24-33.

Bravo-Cordero, J. J., Marrero-Diaz, R., Megías, D., Genís, L., García-Grande, A., García, M. A., Arroyo, A. G. and Montoya, M. C. (2007). MT1-MMP proinvasive activity is regulated by a novel Rab8-dependent exocytic pathway. *EMBO J.* **26**, 1499-1510.

Bravo-Cordero, J. J., Hodgson, L. and Condeelis, J. (2012). Directed cell invasion and migration during metastasis. *Curr. Opin. Cell Biol.* **24**, 277-283.

Burns, S., Thrasher, A. J., Blundell, M. P., Machesky, L. and Jones, G. E. (2001). Configuration of human dendritic cell cytoskeleton by Rho GTPases, the WAS protein, and differentiation. *Blood* **98**, 1142-1149.

Caswell, P. T., Vadrevu, S. and Norman, J. C. (2009). Integrins: masters and slaves of endocytic transport. *Nat. Rev. Mol. Cell Biol.* **10**, 843-853.

Chen, W. T., Yeh, Y. and Nakahara, H. (1994). An in vitro cell invasion assay: determination of cell surface proteolytic activity that degrades extracellular matrix. *J. Tissue Cult. Methods* **16**, 177-181.

Christoforidis, S., McBride, H. M., Burgoyne, R. D. and Zerial, M. (1999). The Rab5 effector EEA1 is a core component of endosome docking. *Nature* **397**, 621-625.
Delaissé, J. M., Andersen, T. L., Engsig, M. T., Henriksen, K., Troen, T. and Blavier, L. (2003). Matrix metalloproteinases (MMP) and cathepsin K contribute differently to osteoclastic activities. *Microsc. Res. Tech.* **61**, 504-513.
Destaing, O., Saltel, F., Géminard, J. C., Jurdic, P. and Bard, F. (2003). Podosomes display actin turnover and dynamic self-organization in osteoclasts expressing actin-green fluorescent protein. *Mol. Biol. Cell* **14**, 407-416.
Endo, K., Takino, T., Miyamori, H., Kinsen, H., Yoshizaki, T., Furukawa, M. and Sato, H. (2003). Cleavage of syndecan-1 by membrane type matrix metalloproteinase-1 stimulates cell migration. *J. Biol. Chem.* **278**, 40764-40770.
Friedl, P. and Wolf, K. (2003). Tumour-cell invasion and migration: diversity and escape mechanisms. *Nat. Rev. Cancer* **3**, 362-374.
Friedl, P. and Wolf, K. (2008). Tube travel: the role of proteases in individual and collective cancer cell invasion. *Cancer Res.* **68**, 7247-7249.
Friedl, P. and Wolf, K. (2009). Proteolytic interstitial cell migration: a five-step process. *Cancer Metastasis Rev.* **28**, 129-135.
Frittoli, E., Palamidessi, A., Disanza, A. and Scita, G. (2011). Secretory and endo/exocytic trafficking in invadopodia formation: the MT1-MMP paradigm. *Eur. J. Cell Biol.* **90**, 108-114.
Gitler, A. D., Bevis, B. J., Shorter, J., Strathearn, K. E., Hamamichi, S., Su, L. J., Caldwell, K. A., Caldwell, G. A., Rochet, J. C., McCaffery, J. M. et al. (2008). The Parkinson's disease protein alpha-synuclein disrupts cellular Rab homeostasis. *Proc. Natl. Acad. Sci. USA* **105**, 145-150.
Grant, B. D. and Donaldson, J. G. (2009). Pathways and mechanisms of endocytic recycling. *Nat. Rev. Mol. Cell Biol.* **10**, 597-608.
Guiet, R., Van Goethem, E., Cougoule, C., Balor, S., Valette, A., Al Saati, T., Lowell, C. A., Le Cabec, V. and Maridonneau-Parini, I. (2011). The process of macrophage migration promotes matrix metalloproteinase-independent invasion by tumor cells. *J. Immunol.* **187**, 3806-3814.
Henry, L. and Sheff, D. R. (2008). Rab8 regulates basolateral secretory, but not recycling, traffic at the recycling endosome. *Mol. Biol. Cell* **19**, 2059-2068.
Hotary, K. B., Allen, E. D., Brooks, P. C., Datta, N. S., Long, M. W. and Weiss, S. J. (2003). Membrane type I matrix metalloproteinase usurps tumor growth control imposed by the three-dimensional extracellular matrix. *Cell* **114**, 33-45.
Humphries, M. J. (2009). Cell adhesion assays. *Methods Mol. Biol.* **522**, 203-210.
Hutagalung, A. H. and Novick, P. J. (2011). Role of Rab GTPases in membrane traffic and cell physiology. *Physiol. Rev.* **91**, 119-149.
Itoh, Y. and Seiki, M. (2004). MT1-MMP: an enzyme with multidimensional regulation. *Trends Biochem. Sci.* **29**, 285-289.
Junutula, J. R., De Maziére, A. M., Peden, A. A., Ervin, K. E., Advani, R. J., van Dijk, S. M., Klumperman, J. and Scheller, R. H. (2004). Rab14 is involved in membrane trafficking between the Golgi complex and endosomes. *Mol. Biol. Cell* **15**, 2218-2229.
Kajita, M., Itoh, Y., Chiba, T., Mori, H., Okada, A., Kinoh, H. and Seiki, M. (2001). Membrane-type 1 matrix metalloproteinase cleaves CD44 and promotes cell migration. *J. Cell Biol.* **153**, 893-904.
Kauppi, M., Simonsen, A., Bremnes, B., Vieira, A., Callaghan, J., Stenmark, H. and Olkkonen, V. M. (2002). The small GTPase Rab22 interacts with EEA1 and controls endosomal membrane trafficking. *J. Cell Sci.* **115**, 899-911.
Kopp, P., Lammers, R., Aepfelbacher, M., Woehlke, G., Rudel, T., Machuy, N., Steffen, W. and Linder, S. (2006). The kinesin KIF1C and microtubule plus ends regulate podosome dynamics in macrophages. *Mol. Biol. Cell* **17**, 2811-2823.
Lämmermann, T. and Sixt, M. (2009). Mechanical modes of 'amoeboid' cell migration. *Curr. Opin. Cell Biol.* **21**, 636-644.
Lehti, K., Lohi, J., Valtanen, H. and Keski-Oja, J. (1998). Proteolytic processing of membrane-type-1 matrix metalloproteinase is associated with gelatinase A activation at the cell surface. *Biochem. J.* **334**, 345-353.
Ley, K., Laudanna, C., Cybulsky, M. I. and Nourshargh, S. (2007). Getting to the site of inflammation: the leukocyte adhesion cascade updated. *Nat. Rev. Immunol.* **7**, 678-689.
Linder, S. (2007). The matrix corroded: podosomes and invadopodia in extracellular matrix degradation. *Trends Cell Biol.* **17**, 107-117.
Linder, S., Nelson, D., Weiss, M. and Aepfelbacher, M. (1999). Wiskott-Aldrich syndrome protein regulates podosomes in primary human macrophages. *Proc. Natl. Acad. Sci. USA* **96**, 9648-9653.
Linder, S., Wiesner, C. and Himmel, M. (2011). Degrading devices: invadosomes in proteolytic cell invasion. *Annu. Rev. Cell Dev. Biol.* **27**, 185-211.
Linford, A., Yoshimura, S., Nunes Bastos, R., Langemeyer, L., Gerondopoulos, A., Rigden, D. J. and Barr, F. A. (2012). Rab14 and its exchange factor FAM116 link endocytic recycling and adherens junction stability in migrating cells. *Dev. Cell* **22**, 952-966.
Liu, S. S., Chen, X. M., Zheng, H. X., Shi, S. L. and Li, Y. (2011). Knockdown of Rab5a expression decreases cancer cell motility and invasion through integrin-mediated signaling pathway. *J. Biomed. Sci.* **18**, 58.
Matías-Román, S., Gálvez, B. G., Genís, L., Yáñez-Mó, M., de la Rosa, G., Sánchez-Mateos, P., Sánchez-Madrid, F. and Arroyo, A. G. (2005). Membrane type 1-matrix metalloproteinase is involved in migration of human monocytes and is regulated through their interaction with fibronectin or endothelium. *Blood* **105**, 3956-3964.
Meyer, A. S., Hughes-Alford, S. K., Kay, J. E., Castillo, A., Wells, A., Gertler, F. B. and Lauffenburger, D. A. (2012). 2D protrusion but not motility predicts growth factor-induced cancer cell migration in 3D collagen. *J. Cell Biol.* **197**, 721-729.
Murphy, D. A. and Courtneidge, S. A. (2011). The 'ins' and 'outs' of podosomes and invadopodia: characteristics, formation and function. *Nat. Rev. Mol. Cell Biol.* **12**, 413-426.
Nakada, M., Miyamori, H., Yamashita, J. and Sato, H. (2003). Testican 2 abrogates inhibition of membrane-type matrix metalloproteinases by other testican family proteins. *Cancer Res.* **63**, 3364-3369.
Nourshargh, S., Hordijk, P. L. and Sixt, M. (2010). Breaching multiple barriers: leukocyte motility through venular walls and the interstitium. *Nat. Rev. Mol. Cell Biol.* **11**, 366-378.
Olkkonen, V. M., Dupree, P., Killisch, I., Lütcke, A., Zerial, M. and Simons, K. (1993). Molecular cloning and subcellular localization of three GTP-binding proteins of the rab subfamily. *J. Cell Sci.* **106**, 1249-1261.
Pellinen, T., Arjonen, A., Vuoriluoto, K., Kallio, K., Fransen, J. A. and Ivaska, J. (2006). Small GTPase Rab21 regulates cell adhesion and controls endosomal traffic of beta1-integrins. *J. Cell Biol.* **173**, 767-780.
Petrie, R. J., Gavara, N., Chadwick, R. S. and Yamada, K. M. (2012). Nonpolarized signaling reveals two distinct modes of 3D cell migration. *J. Cell Biol.* **197**, 439-455.
Pixley, F. J. (2012). Macrophage migration and its regulation by CSF-1. *Int. J. Cell Biol.* **2012**, 501962.
Poincloux, R., Lizárraga, F. and Chavrier, P. (2009). Matrix invasion by tumour cells: a focus on MT1-MMP trafficking to invadopodia. *J. Cell Sci.* **122**, 3015-3024.
Remacle, A., Murphy, G. and Roghi, C. (2003). Membrane type I-matrix metalloproteinase (MT1-MMP) is internalised by two different pathways and is recycled to the cell surface. *J. Cell Sci.* **116**, 3905-3916.
Remacle, A. G., Rozanov, D. V., Fugere, M., Day, R. and Strongin, A. Y. (2006). Furin regulates the intracellular activation and the uptake rate of cell surface-associated MT1-MMP. *Oncogene* **25**, 5648-5655.
Remacle, A. G., Golubkov, V. S., Shiryaev, S. A., Dahl, R., Stebbins, J. L., Chernov, A. V., Cheltsov, A. V., Pellecchia, M. and Strongin, A. Y. (2012). Novel MT1-MMP small-molecule inhibitors based on insights into hemopexin domain function in tumor growth. *Cancer Res.* **72**, 2339-2349.
Sabeh, F., Shimizu-Hirota, R. and Weiss, S. J. (2009). Protease-dependent versus -independent cancer cell invasion programs: three-dimensional amoeboid movement revisited. *J. Cell Biol.* **185**, 11-19.
Sakurai-Yageta, M., Recchi, C., Le Dez, G., Sibarita, J. B., Daviet, L., Camonis, J., D'Souza-Schorey, C. and Chavrier, P. (2008). The interaction of IQGAP1 with the exocyst complex is required for tumor cell invasion downstream of Cdc42 and RhoA. *J. Cell Biol.* **181**, 985-998.
Sato, H., Kinoshita, T., Takino, T., Nakayama, K. and Seiki, M. (1996). Activation of a recombinant membrane type 1-matrix metalloproteinase (MT1-MMP) by furin and its interaction with tissue inhibitor of metalloproteinases (TIMP)-2. *FEBS Lett.* **393**, 101-104.
Schlierf, B., Fey, G. H., Hauber, J., Hocke, G. M. and Rosorius, O. (2000). Rab11b is essential for recycling of transferrin to the plasma membrane. *Exp. Cell Res.* **259**, 257-265.
Schwartz, S. L., Cao, C., Pylypenko, O., Rak, A. and Wandinger-Ness, A. (2007). Rab GTPases at a glance. *J. Cell Sci.* **120**, 3905-3910.
Simpson, J. C., Griffiths, G., Wessling-Resnick, M., Fransen, J. A., Bennett, H. and Jones, A. T. (2004). A role for the small GTPase Rab21 in the early endocytic pathway. *J. Cell Sci.* **117**, 6297-6311.
Sithu, S. D., English, W. R., Olson, P., Krubasik, D., Baker, A. H., Murphy, G. and D'Souza, S. E. (2007). Membrane-type 1-matrix metalloproteinase regulates intracellular adhesion molecule-1 (ICAM-1)-mediated monocyte transmigration. *J. Biol. Chem.* **282**, 25010-25019.
Sönnichsen, B., De Renzis, S., Nielsen, E., Rietdorf, J. and Zerial, M. (2000). Distinct membrane domains on endosomes in the recycling pathway visualized by multicolor imaging of Rab4, Rab5, and Rab11. *J. Cell Biol.* **149**, 901-914.
Stanton, H., Gavrilovic, J., Atkinson, S. J., d'Ortho, M. P., Yamada, K. M., Zardi, L. and Murphy, G. (1998). The activation of ProMMP-2 (gelatinase A) by HT1080 fibrosarcoma cells is promoted by culture on a fibronectin substrate and is concomitant with an increase in processing of MT1-MMP (MMP-14) to a 45 kDa form. *J. Cell Sci.* **111**, 2789-2798.
Steffen, A., Le Dez, G., Poincloux, R., Recchi, C., Nassoy, P., Rottner, K., Galli, T. and Chavrier, P. (2008). MT1-MMP-dependent invasion is regulated by TI-VAMP/VAMP7. *Curr. Biol.* **18**, 926-931.
Stein, M. P., Dong, J. and Wandinger-Ness, A. (2003). Rab proteins and endocytic trafficking: potential targets for therapeutic intervention. *Adv. Drug Deliv. Rev.* **55**, 1421-1437.
Stenmark, H. (2009). Rab GTPases as coordinators of vesicle traffic. *Nat. Rev. Mol. Cell Biol.* **10**, 513-525.
Stenmark, H., Parton, R. G., Steele-Mortimer, O., Lütcke, A., Gruenberg, J. and Zerial, M. (1994). Inhibition of rab5 GTPase activity stimulates membrane fusion in endocytosis. *EMBO J.* **13**, 1287-1296.
Tatin, F., Varon, C., Génot, E. and Moreau, V. (2006). A signalling cascade involving PKC, Src and Cdc42 regulates podosome assembly in cultured endothelial cells in response to phorbol ester. *J. Cell Sci.* **119**, 769-781.
van der Sluijs, P., Mohrmann, K., Deneka, M. and Jongeneelen, M. (2001). Expression and properties of Rab4 and its effector rabaptin-4 in endocytic recycling. *Methods Enzymol.* **329**, 111-119.
Van Goethem, E., Poincloux, R., Gauffre, F., Maridonneau-Parini, I. and Le Cabec, V. (2010). Matrix architecture dictates three-dimensional migration modes of human macrophages: differential involvement of proteases and podosome-like structures. *J. Immunol.* **184**, 1049-1061.

van Hinsbergh, V. W., Engelse, M. A. and Quax, P. H. (2006). Pericellular proteases in angiogenesis and vasculogenesis. *Arterioscler. Thromb. Vasc. Biol.* **26**, 716-728.

Vérollet, C., Charrière, G. M., Labrousse, A., Cougoule, C., Le Cabec, V. and Maridonneau-Parini, I. (2011). Extracellular proteolysis in macrophage migration: losing grip for a breakthrough. *Eur. J. Immunol.* **41**, 2805-2813.

Wiesner, C., Faix, J., Himmel, M., Bentzien, F. and Linder, S. (2010). KIF5B and KIF3A/KIF3B kinesins drive MT1-MMP surface exposure, CD44 shedding, and extracellular matrix degradation in primary macrophages. *Blood* **116**, 1559-1569.

Williams, K. C. and Coppolino, M. G. (2011). Phosphorylation of membrane type 1-matrix metalloproteinase (MT1-MMP) and its vesicle-associated membrane protein 7 (VAMP7)-dependent trafficking facilitate cell invasion and migration. *J. Biol. Chem.* **286**, 43405-43416.

Wolf, K. and Friedl, P. (2005). Functional imaging of pericellular proteolysis in cancer cell invasion. *Biochimie.* **87**, 315-320.

Wolf, K. and Friedl, P. (2009). Mapping proteolytic cancer cell-extracellular matrix interfaces. *Clin. Exp. Metastasis* **26**, 289-298.

Wolf, K. and Friedl, P. (2011). Extracellular matrix determinants of proteolytic and non-proteolytic cell migration. *Trends Cell Biol.* **21**, 736-744.

Wolf, K., Mazo, I., Leung, H., Engelke, K., von Andrian, U. H., Deryugina, E. I., Strongin, A. Y., Bröcker, E. B. and Friedl, P. (2003). Compensation mechanism in tumor cell migration: mesenchymal-amoeboid transition after blocking of pericellular proteolysis. *J. Cell Biol.* **160**, 267-277.

Wolf, K., Wu, Y. I., Liu, Y., Geiger, J., Tam, E., Overall, C., Stack, M. S. and Friedl, P. (2007). Multi-step pericellular proteolysis controls the transition from individual to collective cancer cell invasion. *Nat. Cell Biol.* **9**, 893-904.

Yamamoto, H., Koga, H., Katoh, Y., Takahashi, S., Nakayama, K. and Shin, H. W. (2010). Functional cross-talk between Rab14 and Rab4 through a dual effector, RUFY1/Rabip4. *Mol. Biol. Cell* **21**, 2746-2755.

Yudowski, G. A., Puthenveedu, M. A., Henry, A. G. and von Zastrow, M. (2009). Cargo-mediated regulation of a rapid Rab4-dependent recycling pathway. *Mol. Biol. Cell* **20**, 2774-2784.

Zerial, M. and McBride, H. (2001). Rab proteins as membrane organizers. *Nat. Rev. Mol. Cell Biol.* **2**, 107-117.

Journal of Cell Science

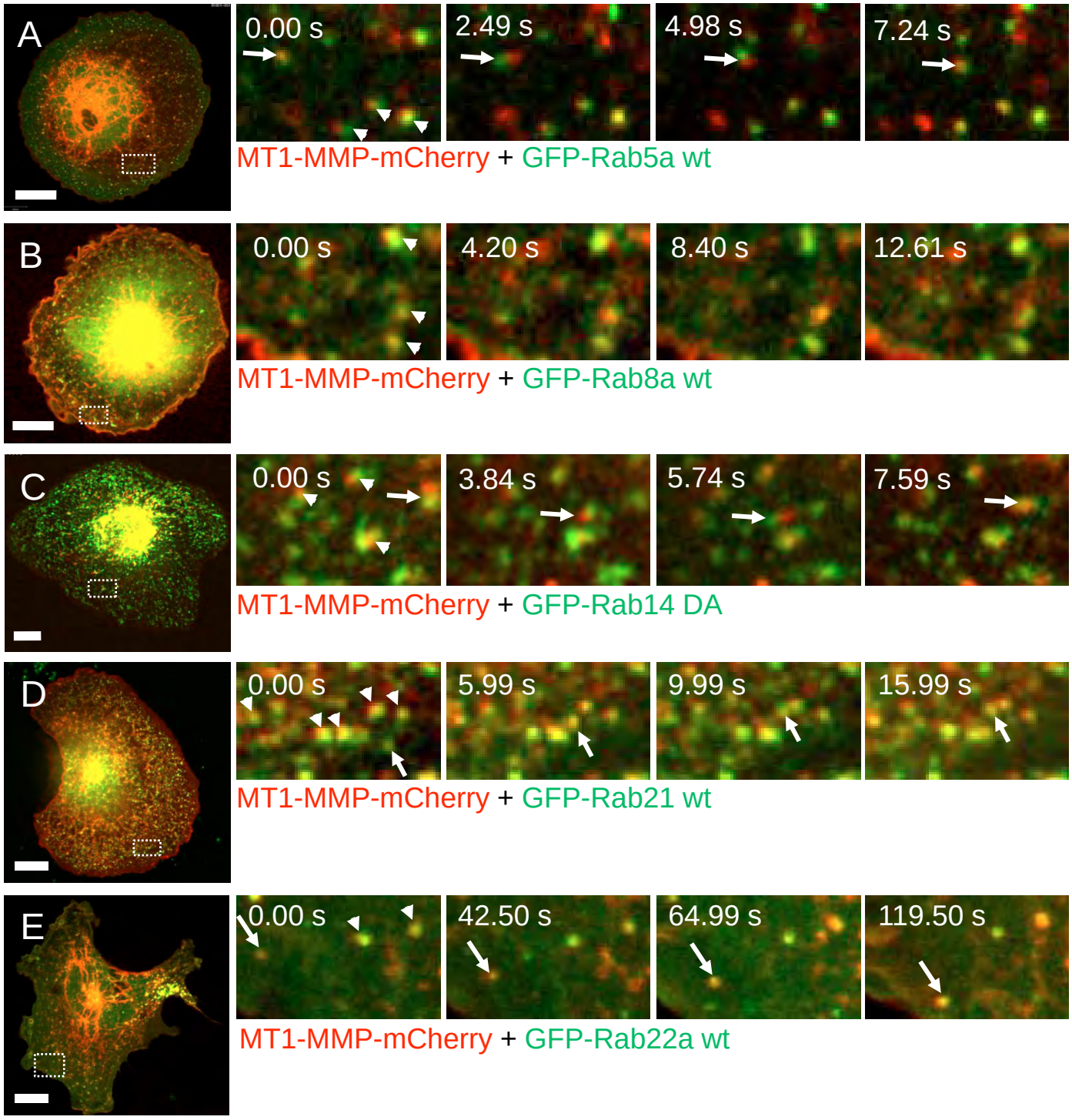

Fig. S1. RabGTPase constructs colocalising with MT-MMP-mCherry on vesicles in living macrophages. Confocal micrographs of macrophages expressing MT1-MMP-mCherry (red) and GFP-Rab5a (A), GFP-Rab8a (B), GFP-Rab14 (C), GFP-Rab21 (D), or GFP-Rab22a (E). White bars indicate 10 μm. White boxes indicate regions of interest shown enlarged on right. Time since start of experiment is indicated in seconds. White arrowheads point to stationary vesicles showing colocalisation of MT1-MMP and respective RabGTPase constructs. White arrows point to moving vesicles showing colocalisation of MT1-MMP and respective RabGTPase construct. Note that, due to delays in acquisition, red and green signals do not show perfect merge for fast-moving vesicles. Exemplary films are shown in supplementary material Movies 1 and 2.

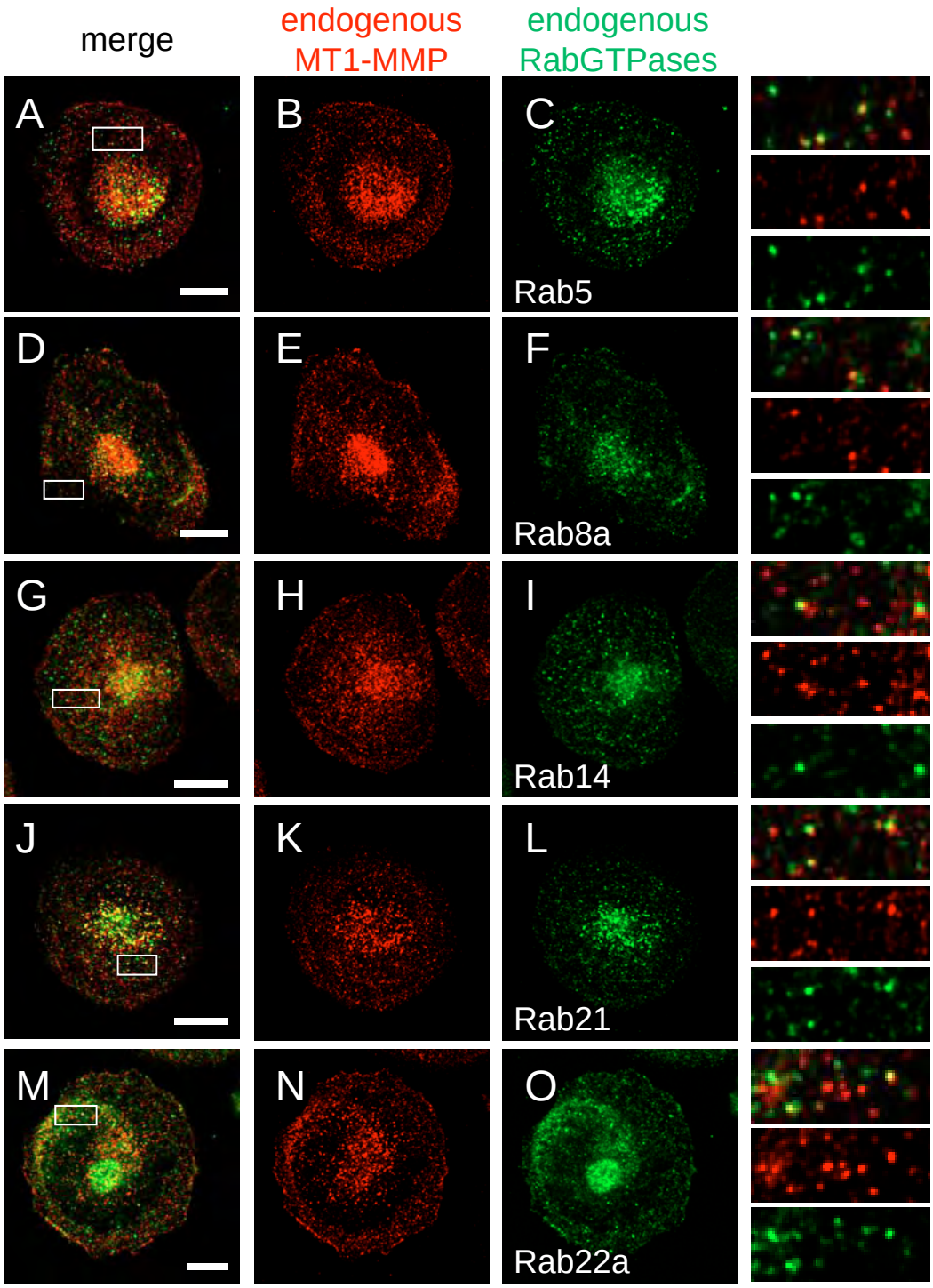

Fig. S2. Endogenous MT1-MMP at vesicles partially colocalises with endogenous Rab5, Rab8a, Rab14, Rab21, and Rab22a. Confocal micrographs of macrophages stained for endogenous MT1-MMP using specific primary and Alexa 568-labeled secondary antibody, and co-stained with specific primary and Alexa 488-labelled secondary antibody for Rab5 (A-C), Rab8a (D-F), Rab14 (G-I), Rab21 (J-L), or Rab22a (M-O). Merged images are shown in (A, D, G, J, M), with single channel images of MT1-MMP shown in (B, E, H, K, N; red) and of RabGTPases in (C, F, I, L, O; green). White boxes in (A, D, G, J, M) indicate detail images shown on the right. White bars indicate 10 μm.

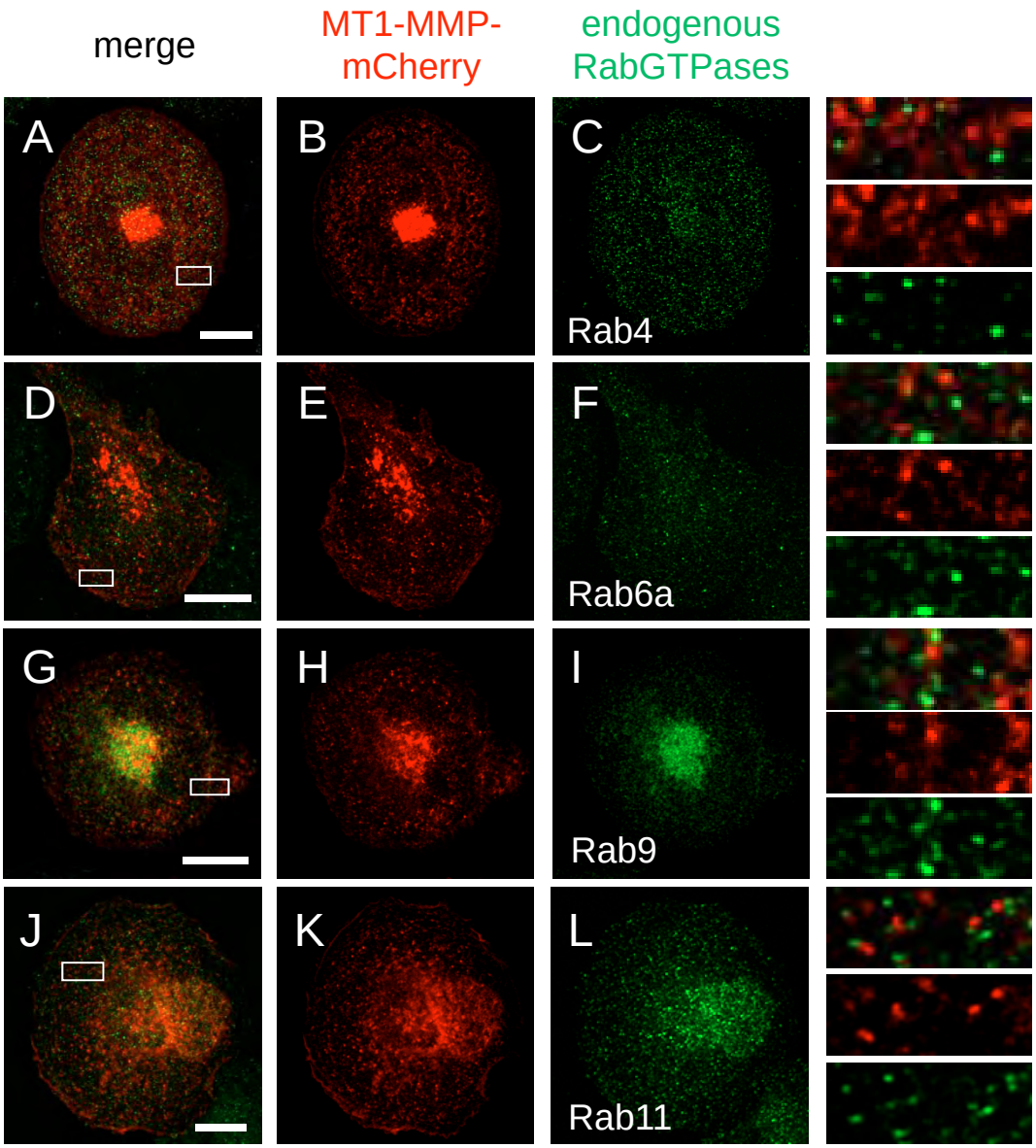

Fig. S3. MT1-MMP-mCherry does not colocalise with endogenous Rab4, Rab6a, Rab9 or Rab11. Confocal micrographs of macrophages expressing MT1-MMP-mCherry, stained with specific primary and Alexa 488-labeled secondary antibody for Rab4 (A-C), Rab6a (D-F), Rab9 (G-I), Rab11 (J-L). Merged images are shown in (A, D, G, J), with single channel images of MT1-MMP-mCherry shown in (B, E, H, K; red) and of RabGTPases in (C, F, I, L; green). White boxes in (A, D, G, J) indicate detail images shown on the right. White bars indicate 10 μm.

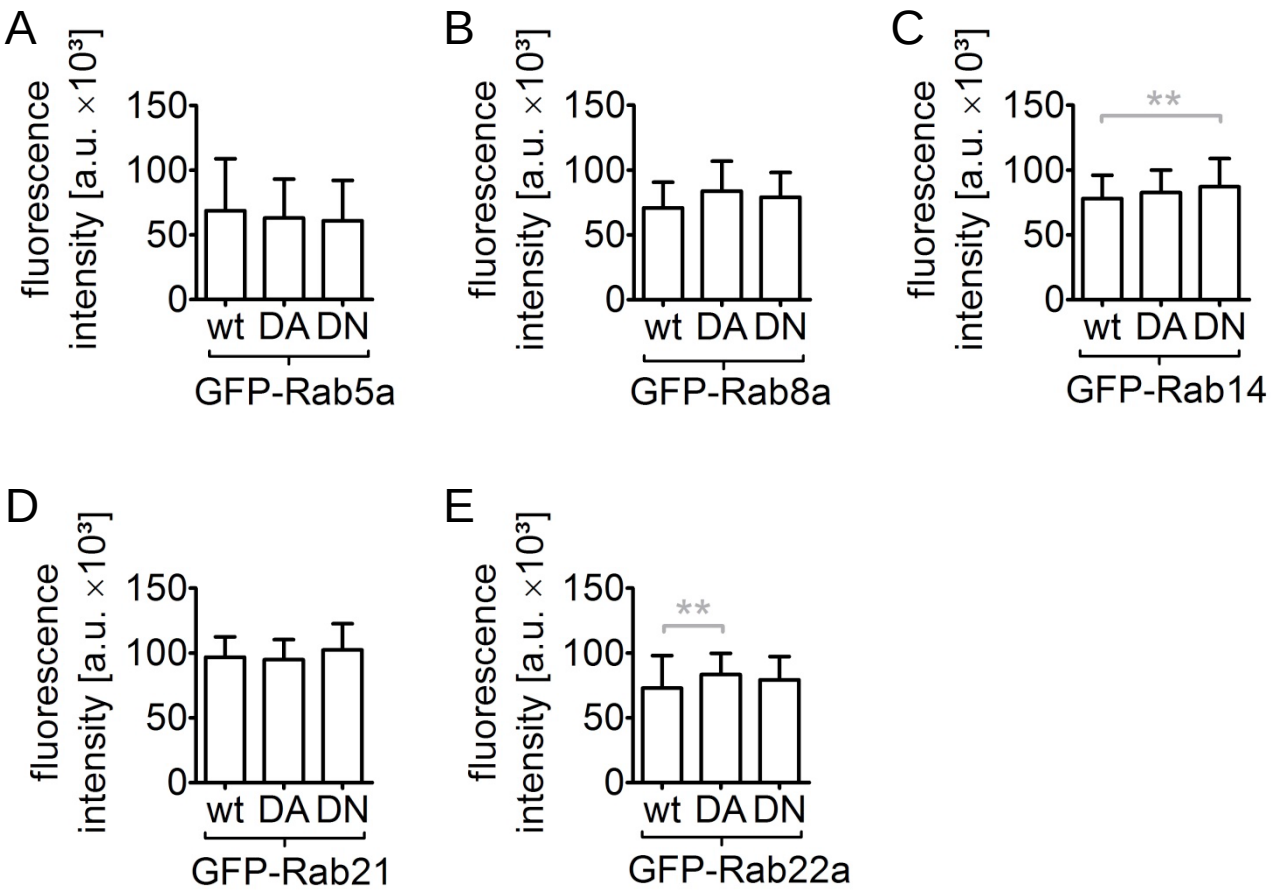

Fig. S4. Evaluation of the fluorescence intensities of expression constructs, based on GFP fluorescence. Controls for experiments shown in Fig. 2. Fluorescence intensities are indicated as arbitrary units (a.u.). Graphs show means + s.d. Note that mean expression levels are not significantly different between respective wild type, DA and DN constructs, except for GFP-Rab14 DN and GFP-Rab22a DA. Graph shows means + s.d. $^{**}P<0.004$. For all values, 3×30 cells were evaluated. For specific values, see supplementary material Table S1.

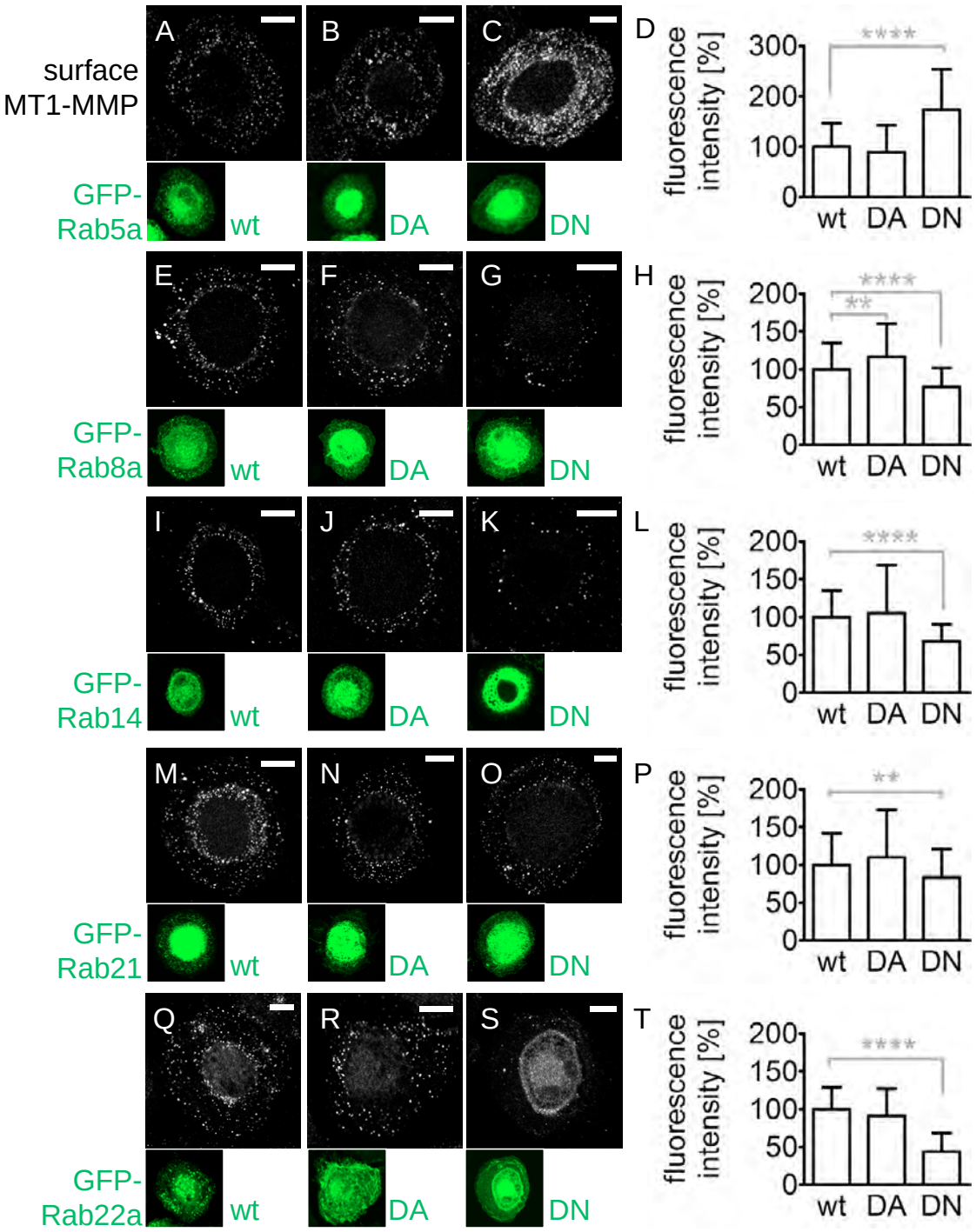

Fig. S5. Influence of dominant active or negative mutants of Rab5a, Rab8a, Rab14, Rab21 and Rab22a on cell surface exposure of endogenous MT1-MMP. (A-C, E-G, I-K, M-O, Q-S) Confocal micrographs of macrophages transfected with wild-type (A, E, I, M, Q; green) or mutant constructs (B-C, F-G, J-K, N-O, R-S; green) of RabGTPases; dominant active constructs (DA; B, F, J, N, R) deficient in GTP hydrolysis, dominant negative constructs (DN; C, G, K, O, S) deficient in GTP binding. Cells were fixed, but not permeabilised, and stained with primary anti-MT1-MMP antibody and secondary Alexa 568-conjugated antibody to label cell-surface associated MT1-MMP (white). GFP signals of expression constructs (green) are shown as small micrographs underneath respective MT1-MMP images. Note pronounced reduction of MT1-MMP at the cell surface upon overexpression of Rab8a, Rab14 and Rab22a DN mutants, which is less pronounced in case of the Rab21 DN mutant. Also note increased cell surface exposure of MT1-MMP upon GFP-Rab5a DN overexpression. White bar indicates 10 µm for all images of the same row. (D, H, L, P, T) Evaluation of the fluorescence intensities of surface-localised MT1-MMP, based on Alexa 568 fluorescence. Fluorescence intensity for wild-type constructs was set each time to 100%. Graphs show means + s.d.; Asterisks indicate values significantly different from wild-type constructs. $^{**}P<0.006$, $^{****}P<0.0001$. For all values, 3×30 cells were evaluated. For specific values, see supplementary material Table S1. (U-Y) Evaluation of fluorescence intensities of expression constructs, based on GFP fluorescence. Fluorescence intensities are indicated as arbitrary units (a.u.). Graphs show means + s.d. Note that mean expression levels are not significantly different between respective wild-type, DA and DN constructs, except for GFP-Rab22a DA. $^{**}P<0.002$. For all values, 3×30 cells were evaluated. For specific values, see supplementary material Table S1.

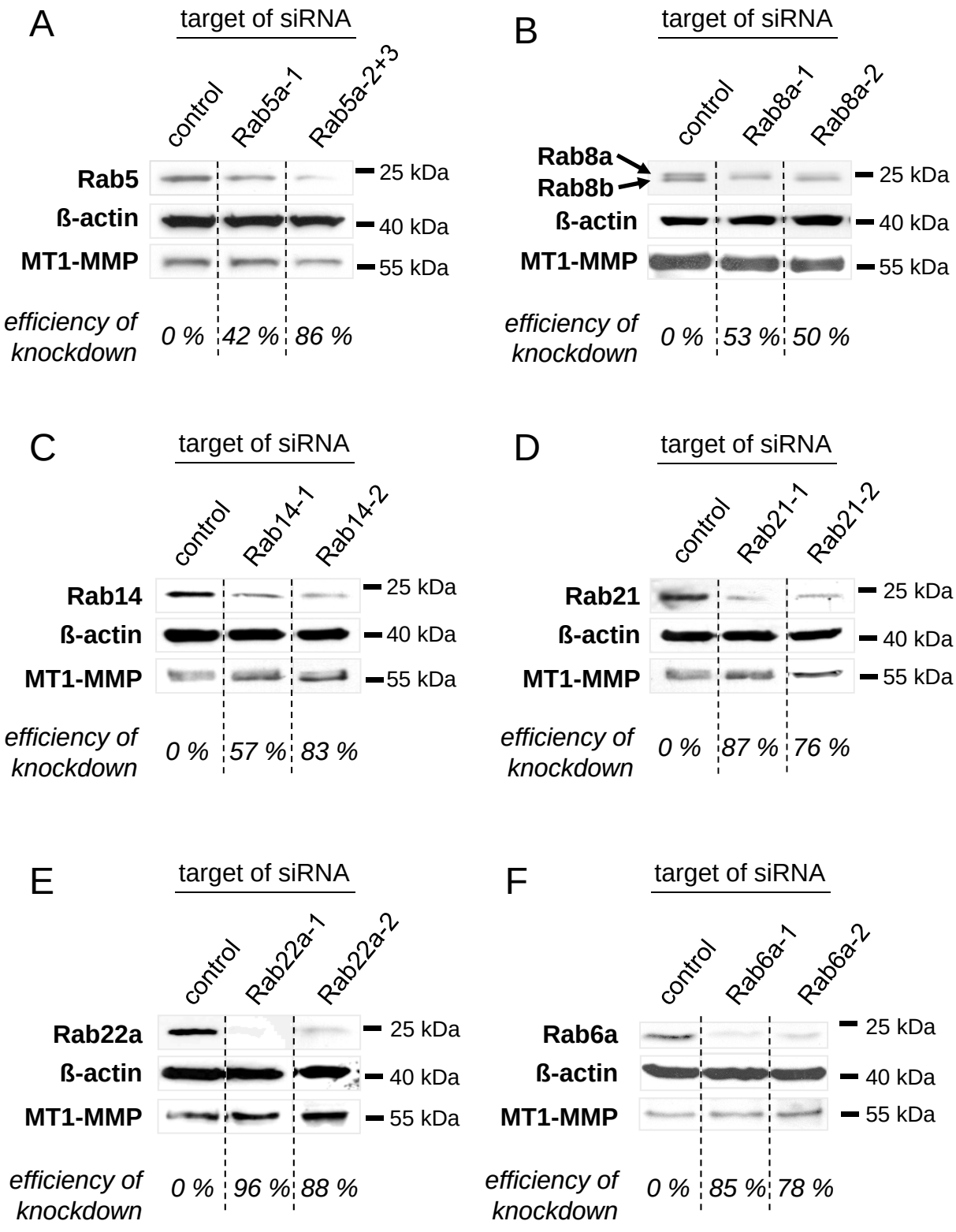

Fig. S6. Knockdown control of RabGTPases in macrophages. Western blots of whole cell lysates of primary human macrophages treated with siRNA specific for (A) Rab5a, (B) Rab8a, (C) Rab14, (D) Rab21, (E) Rab22a or (F) Rab6a. Cells were each transfected twice for 3 days in total and compared to cells transfected twice with control siRNA specific for luciferase. Comparable protein amounts were used, indicated by detection of β-actin. Note that the MT1-MMP expression is unchanged upon silencing of indicated RabGTPases. Knockdown efficiencies were calculated by measuring the band intensities using ImageJ and are indicated below respective lanes.

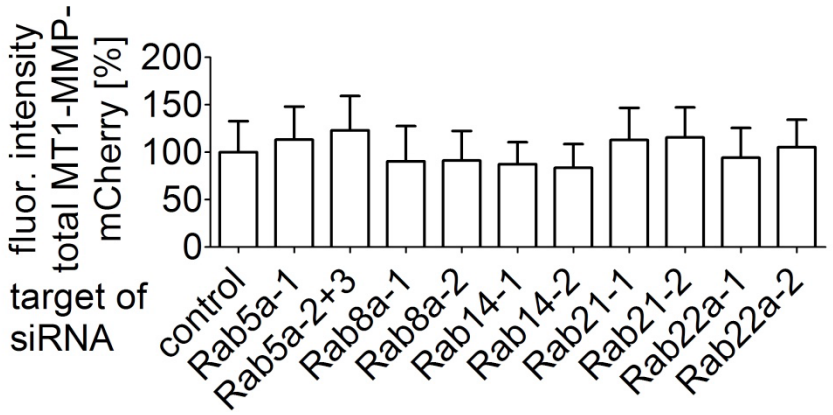

Fig. S7. Evaluation of the fluorescence intensities of total MT1-MMP-mCherry expression level, based on mCherry fluorescence. Controls for experiments shown in Fig. 4B. Fluorescence intensities were set as 100% for control cells treated with luciferase-specific siRNA. Graph shows means + s.d. Note that mean expression levels of are not significantly different to control in cells treated with indicated siRNAs. For all values, 3×30 cells were evaluated. For specific values, see supplementary material Table S1.

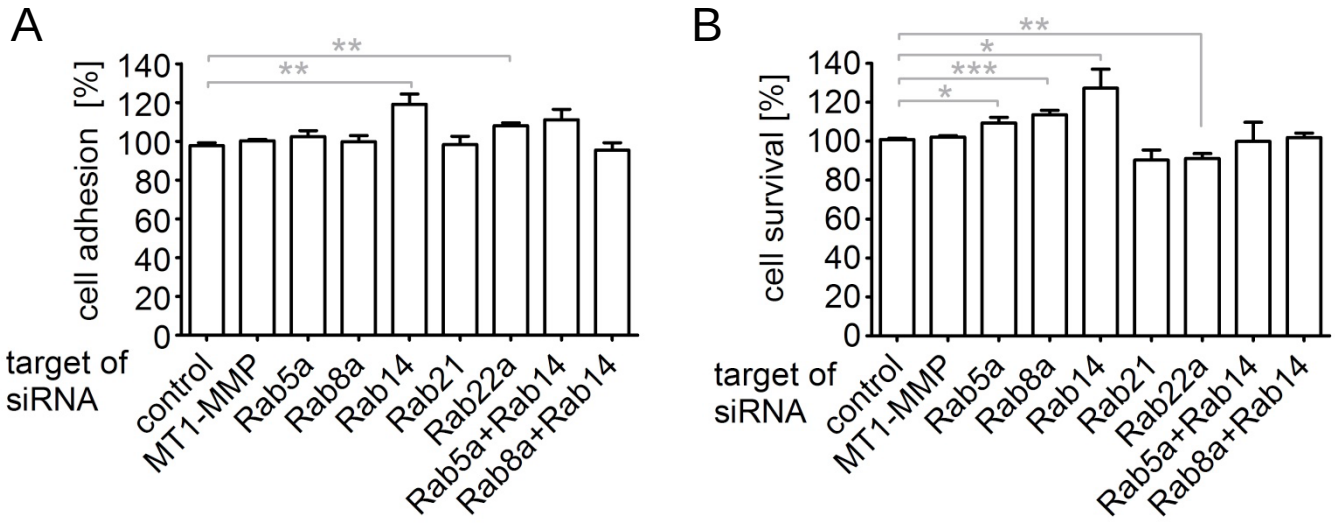

Fig. S8. Cell survival and adhesion under RabGTPase knockdown. Macrophages treated with siRNA against MT1-MMP or RabGTPases, as indicated, were seeded on culture plates coated with collagen I (A) or uncoated (B), and the number of cells surviving after 7 days post transfection (A) or cells adhering to matrix 20 min post-seeding (B) was evaluated by fluorescence measurement of Crystal Violet staining. Values for control cells treated with luciferase siRNA were set to 100%. Graph shows means + s.d.; **P*<0.0226, ***P*<0.0084, ****P*=0.0004. For all values, 3×27 values were evaluated. For specific values, see supplementary material Table S1.

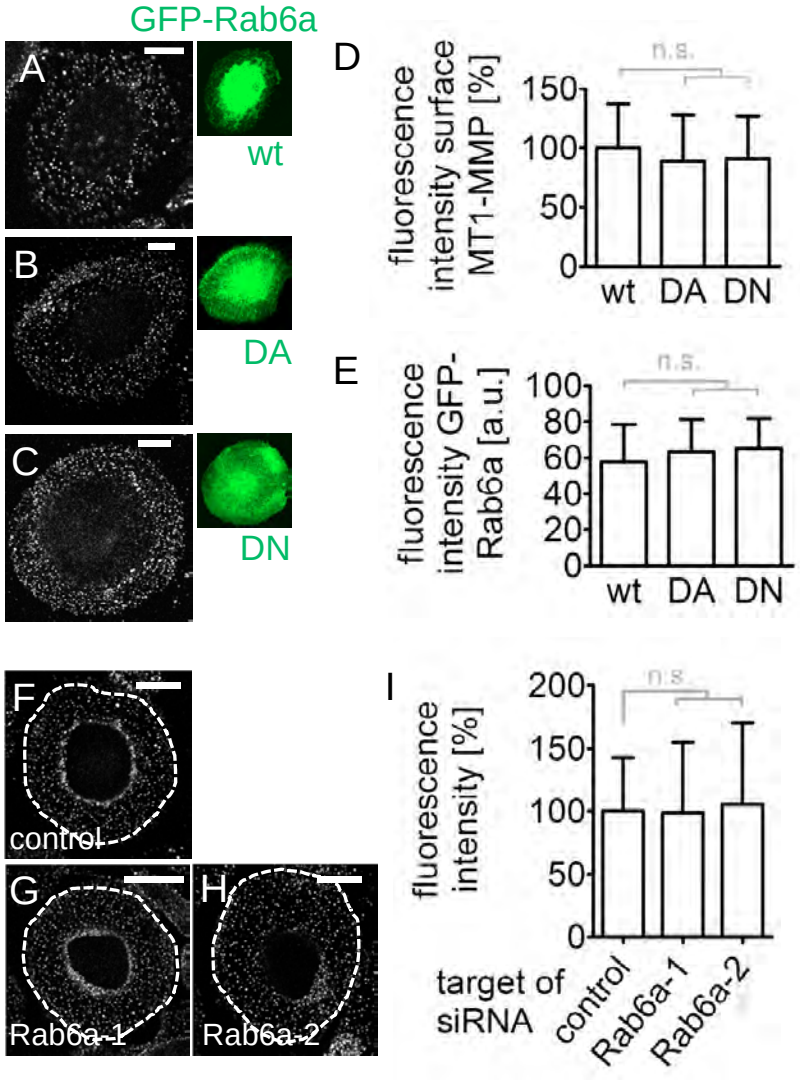

Fig. S9. Rab6a does not influence surface exposure of M1-MMP, 3D collagen dequenching or 3D invasion of macrophages. (A-E) Rab6a GFP-fused constructs do not influence surface exposure of endogenous MT1-MMP. (A-C) Confocal micrographs of macrophages stained for MT1-MMP (white) and GFP-fused RabGTPase constructs (green): wild-type (A), dominant active (DA) construct deficient in GTP hydrolysis (B), or dominant negative constructs (DN) deficient in GTP binding (C). Cells were fixed, but not permeabilised, and stained with primary anti-MT1-MMP antibody and secondary Alexa 568-conjugated antibody to label surface-associated MT1-MMP (A-C, white). White bars: 10 µm. (D) Evaluation of fluorescence intensities of surface-localised MT1-MMP based on Alexa 568 fluorescence. Values for wild-type constructs were set each time to 100%. For all values, 3×30 cells were evaluated. Graph shows means + s.d. For specific values, see supplementary material Table S1. (E) Evaluation of fluorescence intensities of Rab6a constructs, based on GFP fluorescence. Values are given in a.u.. For all values, 3×30 cells were evaluated. Graph shows means + s.d. For specific values, see supplementary material Table S1. Note that in all cases, values for surface MT1-MMP or GFP-Rab6a constructs are not statistically different from wt controls. (F-I) Knockdown of Rab6a does not influence surface exposure of endogenous MT1-MMP. (F-H) Confocal micrographs of macrophages treated with siRNA specific for luciferase as control (F), first (G) or second (H) siRNA specific for Rab6a. Cells were fixed, but not permeabilised, and stained with primary anti-MT1-MMP and secondary Alexa 568-conjugated antibody to label endogenous MT1-MMP on the cell surface. White bars: 10 µm. For demonstration of siRNA-mediated knockdown of Rab6a, see supplementary material Fig. S6F. (I) Fluorescence intensities of surface-localised endogenous MT1-MMP, based on Alexa 568 fluorescence. Fluorescence intensities for control siRNA were each set to 100%. Asterisks indicate values significantly different from control values. For all values, 3×30 cells were evaluated. Graph shows means + s.d.; ****P<0.0001. For specific values, see supplementary material Table S1. (J,K) Quantification of dequenched collagen I fluorescence in cells treated with indicated siRNAs specific for Rab6a (blue and red graphs), and control cells treated with luciferase siRNA (black graphs). Fluorescence intensities are given in arbitrary units (a.u.). Graphs show means + s.e.m. Time after start of experiment is indicated. Note that values for Rab6a knockdown cells are not significantly different from control values For all values, 3×48 measurements were evaluated. For specific values, see supplementary material Table S1. (L-O) Rab6a does not influence 3D collagen invasion. (L-N) Brightfield micrographs of invading cells. Dashed white lines indicates border between collagen matrix with embedded macrophages and collagen matrix with invaded cells, visible as dark dots. Cells were treated with siRNAs specific for luciferase as negative control (L), or two individual siRNAs specific for Rab6a (M,N) (O) Quantification of cells invading collagen matrix, at day 4 after seeding. Values for control siRNA were set to 100%. Note that values for Rab6a siRNA-treated cells are not significantly different from those of controls. For all values, 3×16 pictures were evaluated. For specific values, see supplementary material Table S1.

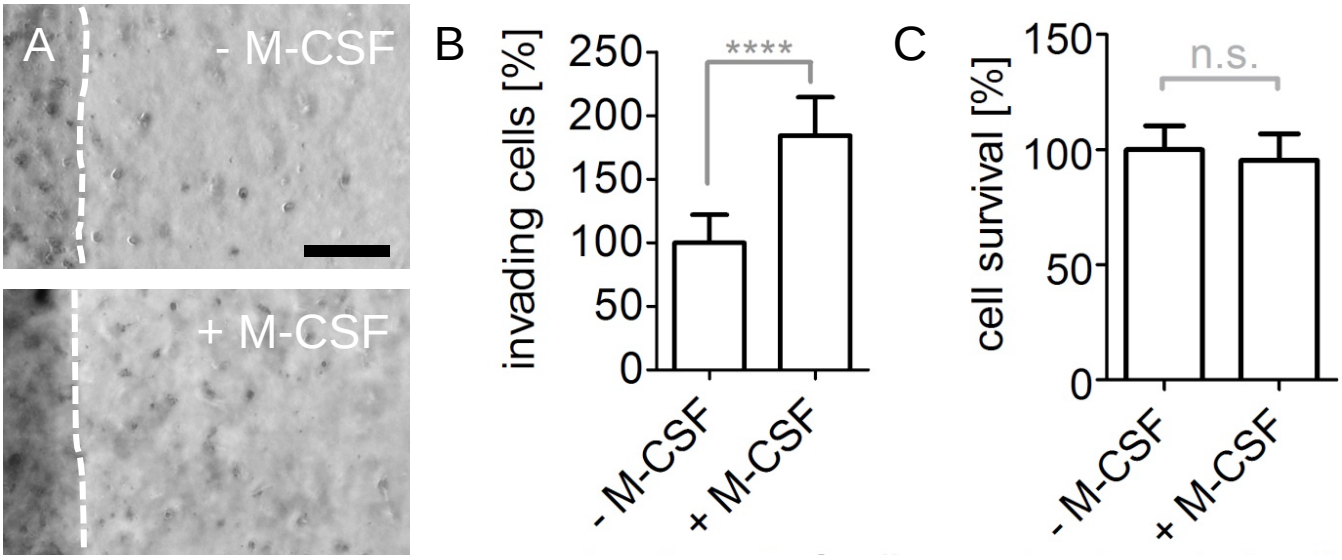

Fig. S10. Characterisation of the 3D collagen invasion assay. (A,B) Invasion of macrophages into collagen I matrix in the absence (A, upper panel) or presence (A, lower panel) of the chemoattractant M-CSF. M-CSF was added to a final concentration of 1 mg/ml to the outer gel of the 3D invasion assay, as indicated. Brightfield micrographs of invading cells. Dashed white lines indicates border between collagen matrix with embedded macrophages and collagen matrix with invaded cells, visible as dark dots. Black bar: 200 μm. (B) Quantification of cells invading into collagen matrix in the absence or presence of M-CSF, at day 4 after seeding. Values for cell invasion w/o M-CSF were set to 100% (100.0±22.1% for cells w/o M-CSF; 184.4±30.1% for cells with M-CSF). Asterisks indicate values significantly different from values of control cells. Bars show means + s.d.; ****P<0.0001. Note that addition of M-CSF to the assay leads to ca. twofold numbers of invading cells. For all values, 3×16 pictures were evaluated. (C) Survival rates of macrophages cultured in the absence or presence of M-CSF. Values for cell survival w/o M-CSF were set to 100% (100.0±10.3% for cells w/o M-CSF; 95.4±11.4% for cells with M-CSF). Note that difference between the two values is not statistically significant. Bars show mean + s.d.; For all values, 3×27 values were evaluated.

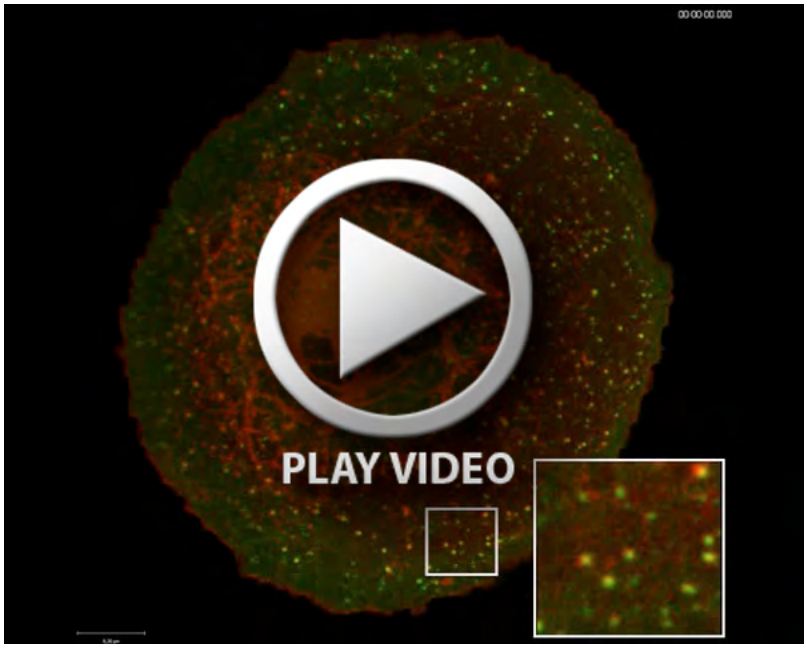

Movie 1. Colocalisation of MT1-MMP-mCherry and GFP-Rab5a in living cells. Confocal time-lapse video of a primary human macrophage expressing MT1-MMP-mCherry (red; exposure time at 568 nm: 556 ms) and GFP-Rab5a (green; exposure time at 488 nm: 330 ms). Acquisition rate: 1 image/2.5 s; frame rate: 10 f/s; sequence: 152 s. White line scales 6.5 μm; white box shows simultaneously detailed time lapse, marked within the cell. Note colocalisation of MT1-MMP-mCherry with GFP-Rab5a-positive vesicles.

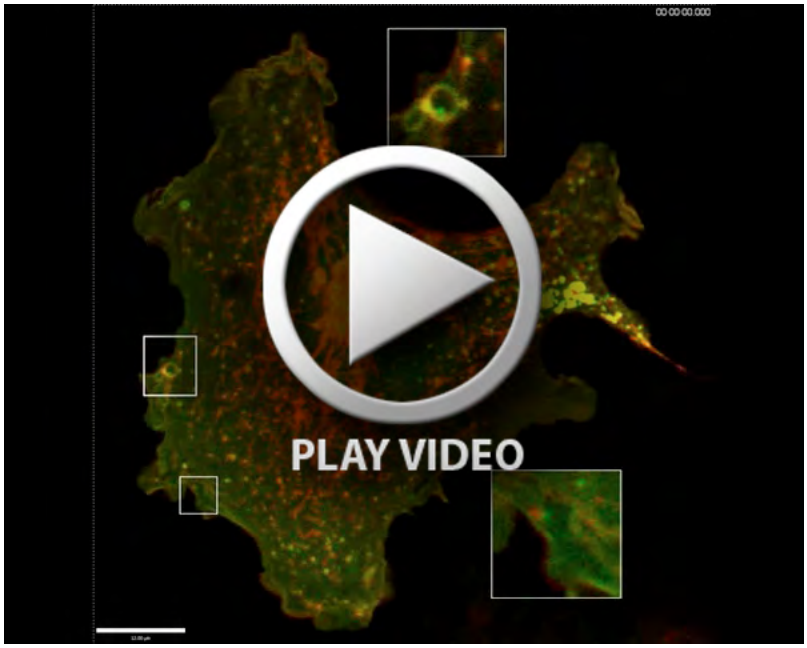

Movie 2. Colocalisation of MT1-MMP-mCherry and GFP-Rab22a in living cells. Confocal time-lapse video of a primary human macrophage expressing MT1-MMP-mCherry (red; exposure time at 568 nm: 556 ms) and GFP-Rab22a (green; exposure time at 488 nm: 232 ms). Acquisition rate: 1 image/2 s; frame rate: 10 f/s; sequence: 87 s. White bar scales 12 μm; white boxes show simultaneously detailed time lapse, marked within the cell. Note colocalisation of MT1-MMP-mCherry with GFP-Rab22a positive (small or giant) vesicles.

Movie 3. Invasion of primary human macrophages into collagen I. Time lapse video of primary human macrophages embedded in dense collagen I (2.5 mg/ml; dark area on the left), invading into less dense collagen I (2 mg/ml; lighter area on the right), which contains M-CSF as a chemoattractant. Video starts 9 h after cell seeding. Acquisition rate: 1 image/15 min; frame rate: 10 f/s; sequence: 32 h 15 min. Note mesenchymal morphology of invading cells characterised by numerous elongated protrusions.

Table S1. Values for MT1-MMP(-mCherry) distribution after various treatments

Cell surface exposure of MT1-MMP-mCherry after GFP-RabGTPase fusion construct overexpression			
Overexpression of	***Number of values***	***Fluorescence intensity surface/total MT1-MMP ratio (Mean ± SD)***	***Fluorescence intensity GFP-RabGTPase [arbitrary units] (Mean ± SD)***
GFP-Rab5a wt	90	100.00 % ± 47.54 %	68670 ± 40189
GFP-Rab5a (Q79L) DA	90	96.21 % ± 69.11 %	62956 ± 30125
GFP-Rab5a (S34N) DN	90	199.90 % ± 83.16 %	60935 ± 31131
GFP-Rab8a wt	90	100.00 % ± 26.33 %	70732 ± 19860
GFP-Rab8a (Q67L) DA	90	107.4 % ± 32.29 %	83685 ± 23221
GFP-Rab8a (T22N) DN	90	40.65 % ± 18.60 %	78946 ± 19152
GFP-Rab14 wt	90	100.00 % ± 29.61 %	77998 ± 17975
GFP-Rab14 (Q70L) DA	90	97.36 % ± 29.78 %	82572 ± 17361
GFP-Rab14 (S25N) DN	90	53.40 % ± 16.84 %	87122 ± 21709
GFP-Rab21 wt	90	100.00 % ± 21.28 %	96874 ± 15775
GFP-Rab21 (Q78L) DA	90	94.76 % ± 21.00 %	94931 ± 15513
GFP-Rab21 (T33N) DN	90	84.44 % ± 21.41 %	102185 ± 20296
GFP-Rab22a wt	90	100.00 % ± 29.58 %	72902 ± 25022
GFP-Rab22a (Q64L) DA	90	87.53 % ± 22.99 %	83393 ± 16309
GFP-Rab22a (S19N) DN	90	27.46 % ± 12.04 %	79249 ± 17926
Cell surface exposure of endogenous MT1-MMP after GFP-RabGTPase fusion construct overexpression			
Overexpression of	***Number of values***	***Fluorescence intensity endogenous surface MT1-MMP (Mean ± SD)***	***Fluorescence intensity GFP- RabGTPase [arbitrary units] (Mean ± SD)***
GFP-Rab5a wt	90	100.00 % ± 46.80 %	40630 ± 12020
GFP-Rab5a (Q79L) DA	90	89.42 % ± 53.89 %	36922 ± 13942
GFP-Rab5a (S34N) DN	90	173.50 % ± 80.29 %	37637 ± 12503
GFP-Rab6a wt	90	100.00 % ± 37.45 %	57880 ± 20582
GFP-Rab6a (Q72L) DA	90	88.95 % ± 39.41%	63321 ± 18259
GFP-Rab6a (T27N) DN	90	90.74 % ± 36.64 %	65109 ± 16759
GFP-Rab8a wt	90	100.00 % ± 34.98 %	95767 ± 41590
GFP-Rab8a (Q67L) DA	90	116.80 % ± 43.51 %	106503 ± 38115
GFP-Rab8a (T22N) DN	90	76.76 % ± 25.01 %	98714 ± 41169
GFP-Rab14 wt	90	100.00 % ± 35.27 %	62315 ± 34612

GFP-Rab14 (Q70L) DA	90	105.30 % ± 63.40 %	57322 ± 25771
GFP-Rab14 (S25N) DN	90	68.20 % ± 22.68 %	56364 ± 27224
GFP-Rab21 wt	90	100.00 % ± 41.81 %	110454 ± 40698
GFP-Rab21 (Q78L) DA	90	110.00 % ± 62.70 %	116866 ± 39384
GFP-Rab21 (T33N) DN	90	83.28 % ± 37.89 %	120643 ± 43078
GFP-Rab22a wt	90	100.00 % ± 28.65 %	68463 ± 34632
GFP-Rab22a (Q64L) DA	90	91.43 % ± 36.04 %	85533 ± 37576
GFP-Rab22a (S19N) DN	90	43.91 % ± 24.91 %	72587 ± 34097

Cell surface exposure of endogenous MT1-MMP after siRNA treatment

target of siRNA	***Number of values***	***Fluorescence intensity endogenous surface MT1-MMP (Mean ± SD)***
non-specific control	90	100.00 % ± 36.07 %
MT1-MMP	90	23.83 % ± 12.35 %
Rab5a-1	90	163.11 % ± 70.07 %
Rab5a-2+3	90	212.72 % ± 127.20 %
Rab6a-1	90	98.85 % ± 55.81 %
Rab6a-2	90	105.70 % ± 64.50 %
Rab8a-1	90	35.26 % ± 24.25 %
Rab8a-2	90	41.28 % ± 29.51 %
Rab14-1	90	33.93 % ± 17.04 %
Rab14-2	90	34.12 % ± 13.33 %
Rab21-1	90	78.55 % ± 31.04 %
Rab21-2	90	72.07 % ± 22.79 %
Rab22a-1	90	34.58 % ± 20.25 %
Rab22a-2	90	42.65 % ± 19.38 %
non-specific control	90	100.00 % ± 54.57 %
Rab5a-1 + Rab14-1	90	57.66 % ± 35.26 %
Rab8a-1 + Rab14-1	90	36.25 % ± 26.90 %

MT1-MMP-mCherry vesicles contacting podosomes

target of siRNA	***Number of values***	***Number of podosomes [%] contacted by MT1-MMP-mCherry (Mean ± SD)***	***Fluorescence intensity total MT1-MMP-mCherry (Mean ± SD)***
non-specific control	12	25.33 % ± 8.13 %	100.00 % ± 32.80 %
Rab5a-1	12	39.08 % ± 13.01 %	113.18 % ± 34.91 %
Rab5a-2+3	12	46.42 % ± 19.96 %	123.10 % ± 36.17 %
Rab8a-1	12	15.17 % ± 11.04 %	90.49 % ± 37.12 %

Rab8a-2	12	12.33 % ± 7.61 %	91.22 % ± 31.25 %
Rab14-1	12	9.08 % ± 4.44 %	87.37 % ± 23.23 %
Rab14-2	12	11.08 % ± 7.31 %	83.51 % ± 25.06 %
Rab21-1	12	21.83 % ± 7.79 %	112.98 % ± 33.70 %
Rab21-2	12	23.58 % ± 7.34 %	115.51 % ± 31.82 %
Rab22a-1	12	11.08 % ± 5.28 %	94.19 % ± 31.35 %
Rab22a-2	12	10.42 % ± 4.12 %	105.42 % ± 28.76 %

Degradation of gelatin matrix after siRNA treatment

target of siRNA	*Number of values*	*Degradation (Mean ± SD)*
non-specific control	90	100.00 % ± 18.86 %
Rab5a-1	90	111.86 % ± 18.69 %
Rab5a-2+3	90	125.57 % ± 59.50 %
Rab8a-1	90	82.94 % ± 30.64 %
Rab8a-2	90	86.42 % ± 37.96 %
Rab14-1	90	77.66 % ± 28.18 %
Rab14-2	90	71.79 % ± 31.76 %
non-specific control	90	100.00 % ± 29.47 %
Rab21-1	90	108.25 % ± 37.35 %
Rab21-2	90	99.99 % ± 36.54 %
Rab22a-1	90	83.14 % ± 37.16 %
Rab22a-2	90	72.79 % ± 37.54 %
MT1-MMP	90	67.90 % ± 35.52 %

Degradation of 3D Collagen I matrix after siRNA treatment

target of siRNA	*Number of values*	*Flourescence intensity [arbitrary units] (Mean ± SEM)*						
		0.5 hrs	*2 hrs*	*4 hrs*	*6 hrs*	*18 hrs*	*24 hrs*	*36 hrs*
non-specific control	144	275.33 ± 74.83	374.33 ± 65.19	381.89 ± 50.66	636.78 ± 78.95	711.44 ± 79.31	737.44 ± 88.71	993.11 ± 77.02
Rab5a-1	144	313.89 ± 65.87	394.00 ± 71.81	496.78 ± 70.47	813.33 ± 83.25	1176.78 ± 87.61	1289.56 ± 119.6	1443.22 ± 59.68
Rab5a-2+3	144	288.33 ± 79.34	396.56 ± 90.77	450.11 ± 71.75	765.45 ± 69.25	926.00 ± 78.02	1089.89 ± 137.6	1301.44 ± 88.06
non-specific control	144	476.00 ± 68.64	507.89 ± 51.07	642.22 ± 43.21	834.00 ± 61.00	1214.00 ± 90.84	1379.78 ± 83.54	1509.11 ± 75.17
Rab6a-1	144	336.33 ± 47.15	445.00 ± 35.46	696.56 ± 57.07	804.67 ± 43.95	1238.44 ± 86.49	1265.44 ± 86.49	1348.67 ± 86.37
Rab6a-2	144	386.45 ± 32.15	396.78 ± 46.73	577.11 ± 43.65	883.67 ± 89.59	1042.11 ± 115.7	1145.44 ± 109.6	1479.00 ± 87.41

non-specific control	144	380.88 ± 25.43	458.17 ± 38.32	524.17 ± 47.05	600.29 ± 53.75	967.75 ±155.67	1024.96 ±144.08	1187.92 ±159.29
Rab8a-1	144	279.67 ± 42.80	294.78 ± 33.68	344.56 ± 48.99	377.78 ± 32.77	649.78 ± 50.32	830.00 ± 63.99	818.89 ± 84.52
Rab8a-2	144	210.63 ± 34.80	209.08 ± 37.48	248.92 ± 40.97	303.13 ± 45.87	476.92 ± 89.30	496.29 ± 90.15	635.50 ±102.50
Rab14-1	144	179.89 ± 36.80	163.22 ± 31.44	195.33 ± 38.19	240.00 ± 46.07	356.11 ±69.34	433.00 ± 68.97	482.67 ± 63.77
Rab14-2	144	135.08 ± 32.58	133.67 ± 20.95	160.67 ± 24.71	194.92 ± 29.40	378.67 ± 56.83	409.92 ± 55.97	528.17 ± 75.58
non-specific control	144	658.56 ± 63.20	720.89 ± 76.08	831.78 ± 73.20	849.22 ± 66.92	1037.44 ± 95.06	961.67 ± 89.88	1129.89 ± 111.76
Rab21-1	144	625.00 ± 50.50	637.56 ± 33.18	664.33 ± 53.87	675.11 ± 49.31	786.67 ± 54.97	754.78 ± 47.85	910.67 ± 89.81
Rab21-2	144	662.78 ± 42.13	717.33 ± 56.76	785.44 ± 65.86	855.56 ± 93.40	880.00 ± 80.72	862.22 ± 72.80	1027.56 ± 100.30
Rab22a-1	144	312.67 ± 58.73	355.33 ± 63.53	402.00 ± 31.82	422.44 ± 27.94	486.22 ± 58.86	513.56 ± 70.78	676.11 ± 88.73
Rab22a-2	144	487.11 ±110.06	476.44 ± 73.81	462.33 ± 78.06	453.44 ± 74.20	473.56 ±107.98	472.44 ± 84.65	524.66 ± 76.89
MT1-MMP	144	242.44 ± 46.92	280.22 ± 37.45	380.33 ± 53.68	406.00 ± 56.98	487.00 ± 85.35	509.56 ± 85.19	659.56 ± 173.78
non-specific control	144	350.00 ± 44.81	472.33 ± 68.02	543.67 ± 84.51	590.56 ± 49.43	900.22 ± 49.43	1110.22 ± 53.71	1212.44 ± 63.22
Rab5a-1 + Rab14-1	144	201.00 ± 56.49	207.22 ± 54.29	365.78 ± 82.05	414.22 ± 91.63	1014.11 ± 68.25	1129.56 ± 92.71	1213.11 ± 102.63
Rab8a-1 + Rab14-1	144	227.00 ± 28.55	175.44 ± 21.99	230.11 ± 24.60	379.11 ± 22.09	568.45 ± 52.84	611.56 ± 52. 84	635.00 ± 91.02

Invasion of macrophages into 3D Collagen I matrix

target of siRNA	***Number of values***	***Number of invading cells relative to control siRNA (Mean ± SD)***
non-specific control	48	100.00 % ± 19.98 %
Rab5a-1	48	144.57 % ± 49.69 %
Rab5a-2+3	48	154.72 % ± 49.70 %
non-specific control	48	100.00 % ± 11.27 %
Rab6a-1	48	111.39 % ± 15.65 %
Rab6a-2	48	99.14 % ± 38.27 %
Rab8a-1	48	55.47 % ± 18.97 %
Rab8a-2	48	51.59 % ± 25.26 %
Rab14-1	48	45.71 % ± 13.34 %
Rab14-2	48	46.04 % ± 10.11 %
Rab21-1	48	94.35 % ± 20.43 %
Rab21-2	48	99.16 % ± 31.13 %
Rab22a-1	48	97.14 % ± 50.05 %

Rab22a-2	48	96.77 % ± 26.01 %
MT1-MMP	48	20.42 % ± 9.36 %
non-specific control +NSC405020	48	17.08 % ± 8.60 %
Rab5a-1 +NSC405020	48	29.44 % ± 25.48 %
Rab5a-2+3+NSC405020	48	24.70 % ± 12.87 %
non-specific control	48	100.00 % ± 38.98 %
Rab5a-1 + Rab14-1	48	60.26 % ± 41.89 %
Rab8a-1 + Rab14-1	48	26.74 % ± 20.94 %
Survival of macrophages after siRNA treatment		
target of siRNA	***Number of values***	***percentage of specific siRNA treated cells relative to control cells (Mean ± SD)***
non-specific control	27	100.81 % ± 0.68 %
MT1-MMP	27	102.09 % ± 0.74 %
Rab5a	27	109.31 % ± 2.94 %
Rab8a	27	113.53 % ± 2.31 %
Rab14	27	127.20 % ± 9.76 %
Rab21	27	90.32 % ± 5.12 %
Rab22a	27	91.07 % ± 2.59 %
Rab5a-1 + Rab14-1	27	99.86 % ± 9.85 %
Rab8a-1 + Rab14-1	27	101.84 % ± 2.25 %
Adhesion to collagen of macrophages after siRNA treatment		
target of siRNA	***Number of values***	***percentage of specific siRNA treated cells relative to control cells (Mean ± SD)***
non-specific control	27	97.74 % ± 1.57 %
MT1-MMP	27	100.27 % ± 0.76 %
Rab5a	27	102.42 % ± 3.07 %
Rab8a	27	99.8 % ± 3.17 %
Rab14	27	119.11 % ± 5.29 %
Rab21	27	98.31 % ± 4.29 %
Rab22a	27	108.01 % ± 1.54 %
Rab5a-1 + Rab14-1	27	111.14 % ± 5.39 %
Rab8a-1 + Rab14-1	27	95.41 % ± 3.87 %

Declaration:

Karim El azzouzi contributed to the publication:

A specific subset of RabGTPases controls cell surface exposure of MT1-MMP, extracellular matrix degradation and three-dimensional invasion of macrophages.

Wiesner C, El Azzouzi K, Linder S.

J Cell Sci. 2013 Jul 1;126(Pt 13):2820-33. doi: 10.1242/jcs.122358. Epub 2013 Apr 19.

by:

- Performing and analyzing experiments demonstrated in Figure S3 A-L.
- Performing and analyzing experiments demonstrated in Figure S8 A-B.
- Preparing figures for the publication.

The experiments were designed by Christiane Wiesner and Stefan Linder.

The manuscript was written by Stefan Linder.

Hamburg, 03.11.2016

_____

Stefan Linder

The kinesin KIF9 and reggie/flotillin proteins regulate matrix degradation by macrophage podosomes

Susanne Cornfine[a], Mirko Himmel[a,*], Petra Kopp[b,*], Karim el Azzouzi[a], Christiane Wiesner[a], Marcus Krüger[c], Thomas Rudel[d], and Stefan Linder[a,b]

[a]Institute for Medical Microbiology, Virology, and Hygiene, University Medical Center Eppendorf, 20246 Hamburg, Germany; [b]Institute for Cardiovascular Diseases, 80336 München, Germany; [c]Max-Planck-Institute for Heart and Lung Research, 61231 Bad Nauheim, Germany; [d]Biocenter, University of Würzburg, 97074 Würzburg, Germany

ABSTRACT **Podosomes are actin-based matrix contacts in a variety of cell types, most notably monocytic cells, and are characterized by their ability to lyse extracellular matrix material. Besides their dependence on actin regulation, podosomes are also influenced by microtubules and microtubule-dependent transport processes. Here we describe a novel role for KIF9, a previously little-characterized member of the kinesin motor family, in the regulation of podosomes in primary human macrophages. We find that small interfering RNA (siRNA)/short-hairpin RNA–induced knockdown of KIF9 significantly affects both numbers and matrix degradation of podosomes. Overexpression and microinjection experiments reveal that the unique C-terminal region of KIF9 is crucial for these effects, presumably through binding of specific interactors. Indeed, we further identify reggie-1/flotillin-2, a signaling mediator between intracellular vesicles and the cell periphery, as an interactor of the KIF9 C-terminus. Reggie-1 dynamically colocalizes with KIF9 in living cells, and, consistent with KIF9-mediated effects, siRNA-induced knockdown of reggies/flotillins significantly impairs matrix degradation by podosomes. In sum, we identify the kinesin KIF9 and reggie/flotillin proteins as novel regulators of macrophage podosomes and show that their interaction is critical for the matrix-degrading ability of these structures.**

Monitoring Editor
Gero Steinberg
University of Exeter

Received: May 6, 2010
Revised: Nov 8, 2010
Accepted: Nov 10, 2010

INTRODUCTION

Cells use two strategies for invasion: amoeboid, nonlytic migration through gaps in the extracellular matrix meshwork and mesenchymal, protease-dependent migration involving the cleavage of matrix components (reviewed in Friedl and Wolf, 2003). Podosomes and invadopodia, collectively called "invadosomes," are matrix contacts with the ability to lyse matrix components and are thus considered as potential key structures of proteolytic cell invasion (reviewed in Gimona *et al.*, 2008; Buccione *et al.*, 2009; Linder, 2009).

Podosomes are constitutively formed in cells that have to cross tissue boundaries, most notably monocytic cells such as monocytes, macrophages, dendritic cells, and osteoclasts (reviewed in Linder and Aepfelbacher, 2003). Comparable to focal adhesions (reviewed in Zamir and Geiger, 2001), podosomes have emerged as highly complex organelles that comprise a large variety of components ranging from matrix contact proteins such as integrins (reviewed in Gimona *et al.*, 2008) or CD44 (Chabadel *et al.*, 2007), to adhesion plaque proteins such as talin (Zambonin-Zallone *et al.*, 1989) and paxillin (Pfaff and Jurdic, 2001), to actin regulators such as Arp2/3 complex (Linder *et al.*, 2000a) or cortactin (Webb *et al.*, 2006). Podosomes are highly dynamic structures with lifetimes of 2–12 min and show an even higher internal actin turnover (Destaing *et al.*, 2003).

Besides their dependence on actin regulation, podosomes are also influenced by microtubules and microtubule-dependent transport processes (Linder *et al.*, 2000b; Cougoule *et al.*, 2005). In this

This article was published online ahead of print in MBoC in Press (http://www.molbiolcell.org/cgi/doi/10.1091/mbc.E10-05-0394) on November 30, 2010.

*These authors contributed equally to this work.

Address correspondence to: Stefan Linder (s.linder@uke.de).

Abbreviations used: FITC, fluorescein isothiocyanate; fl, full length; Ig, immunoglobulin; KIF, kinesin-like family; LC-MS/MS, liquid chromatography–tandem mass spectrometry; MMP, matrix metalloproteinases; MS, mass spectrometry; NHS, normal human serum; PAA, polyacrylamide; pEGFP, plasmid enhanced green fluorescent protein; qPCR, quantitative PCR; shRNA, short-hairpin RNA; siRNA, small interfering RNA; TGN, *trans*-Golgi network.

© 2011 Cornfine *et al.* This article is distributed by The American Society for Cell Biology under license from the author(s). Two months after publication it is available to the public under an Attribution–Noncommercial–Share Alike 3.0 Unported Creative Commons License (http://creativecommons.org/licenses/by-nc-sa/3.0).

"ASCB®," "The American Society for Cell Biology®," and "Molecular Biology of the Cell®" are registered trademarks of The American Society of Cell Biology.

Supplemental Material can be found at:
http://www.molbiolcell.org/content/suppl/2010/11/22/mbc.E10-05-0394.DC1.html

context, microtubules function as regulators of podosome dynamics (Kopp *et al.*, 2006; reviewed in Linder, 2009) and their subcellular positioning (Destaing *et al.*, 2005; Ory *et al.*, 2008; McMichael *et al.*, 2010). Moreover, microtubules also influence the matrix lytic ability of both podosomes and invadopodia (reviewed in Linder, 2007; Poincloux *et al.*, 2009), which is probably based on the transport of signaling molecules and proteases to sites of degradation (Sakurai-Yageta *et al.*, 2008; Steffen *et al.*, 2008; Wiesner *et al.*, 2010).

As podosomes are contacted by the plus ends of microtubules (Kopp *et al.*, 2006), transport of material to podosomes is likely to involve plus end–directed motors of the kinesin family. Previously, we could show that kinesin-like family 1C (KIF1C), a kinesin-3 member, is involved in the regulation of podosome dynamics in primary human macrophages (Kopp *et al.*, 2006). We have now expanded our screen for kinesins involved in podosome regulation and identified the little-characterized kinesin KIF9, a member of the kinesin-9 family (Lawrence *et al.*, 2004).

KIF9 was discovered through interaction with the GTP-binding protein Gem (Piddini *et al.*, 2001) and reported to associate with microtubules in primary glial cells (Piddini *et al.*, 2001). So far KIF9 has not been characterized further, and no cellular function has been described for this motor. Here we demonstrate a function for KIF9 as a regulator of podosomes and of podosomal matrix degradation in primary human macrophages. Furthermore, we show that its C-terminal region interacts with reggie-1/flotillin-2.

Reggie/flotillin proteins were discovered as neuronal proteins involved in axon regeneration (Schulte *et al.*, 1997; reviewed in Stuermer, 2010) and are now thought to act as ubiquitous signaling mediators between intracellular vesicles and the plasma membrane (reviewed in Langhorst *et al.*, 2008; Stuermer, 2010). To date, two isoforms have been described, reggie-1 and -2 (flotillin-2 and -1), which can form hetero-oligomers through interaction of their C-terminal regions (reviewed in Glebov *et al.*, 2006, Babuke and Tikkanen, 2007). Reggie proteins have been found both at the plasma membrane and at intracellular pools ranging from Golgi-derived vesicles and late endosomes/lysosomes to multivesicular bodies and lipid bodies (reviewed in Stuermer, 2010).

We now show that reggie-1 interacts with the C-terminal region of KIF9, that both proteins cross-precipitate from macrophage lysates, and that they dynamically colocalize in living cells. Consistent with the observed effects of KIF9 knockdown, knockdown of reggie impairs matrix degradation by podosomes. These experiments reveal both KIF9 and reggie proteins as novel regulators of matrix degradation by podosomes. (Note: The term "regulation" is used here in the broad sense of having a direct or indirect influence on the formation and/or functionality of podosomes.)

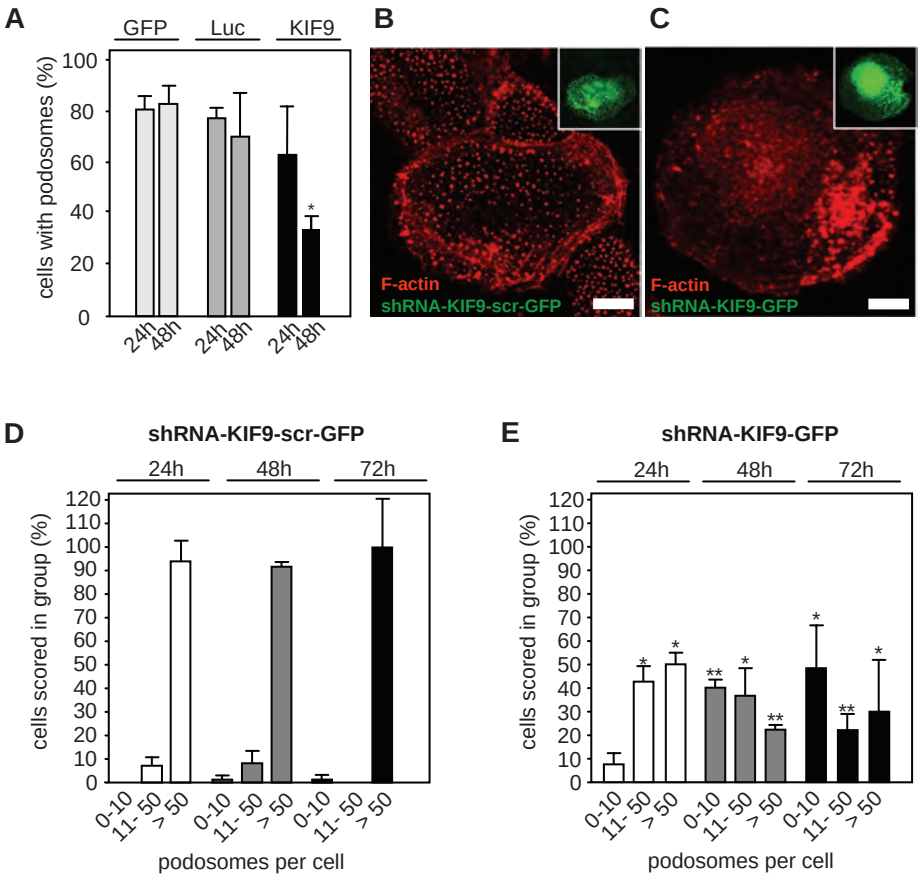

FIGURE 1: KIF9 influences podosome numbers. (A) Evaluation of podosome formation in macrophages transfected with EGFP-C1, luciferase-specific siRNA, and KIF9-specific siRNA. Influence of siRNA was analyzed 24 h (left) and 48 h (right) after transfection. For each value, 3 × 30 cells were evaluated. Cells containing less than 10 podosomes at a given time point were scored as "containing no podosomes." Values are given as mean percentage ± SD of total counts in Table 1. For differences between control values and values gained with KIF9 siRNA, a P value < 0.05 was considered significant (indicated by asterisk). (B, C) Fluorescence micrographs of primary human macrophages expressing scrambled shRNA (B) or KIF9-specific shRNA (C) 72 h after transfection. F-actin stained with rhodamine-labeled phalloidin. Inserts show respective GFP signals. White bar indicates 10 μm. (D, E) Evaluation of podosome formation in primary human macrophages transfected with psiSTRIKE vector bicistronically end encoding EGFP and scrambled shRNA, (D) or KIF9-specific shRNA (E). Influence of each shRNA was evaluated 24, 48, and 72 h after transfection. For each value, 3 × 30 cells were evaluated. Values are given as mean percentage ± SD of total counts in Table 1. For differences between control values and values gained with kinesin shRNAs, a P value < 0.05 was considered significant (indicated by asterisk).

RESULTS

KIF9 regulates podosome numbers and matrix degradation in macrophages

To identify novel kinesin isoforms involved in podosome regulation, we used a small interfering RNA (siRNA)–based knockdown approach in primary human macrophages. These cells constitutively form numerous podosomes and are thus amenable to statistical evaluation of podosome formation. Among others, an siRNA specific for KIF9 was validated in HeLa cells and found to be highly effective (>85% knockdown; see *Materials and Methods*). Primary macrophages were transfected with the respective siRNA, and the number of cells containing podosomes (i.e., ≥10 podosomes/cell) was evaluated 24 and 48 h after transfection. Compared with control cells transfected with plasmid enhanced green fluorescent

Effect on podosome numbers			
Expression of	**24 h**		**48 h**
GFP-N1	78.0% ± 7.0%		80.0% ± 7.0%
Luciferase	74.0% ± 4.0%		68.0% ± 17.0%
KIF9-specific siRNA	61.1% ± 18.4%		32.2% ± 1.9%
Effect of KIF9-specific shRNA on podosome numbers			
Podosomes/cell	**24 h**	**48 h**	**72 h**
0–10	7.4% ± 4.9%	40.0% ± 3.3%	48.2% ± 18.3%
11–50	42.6% ± 6.7%	36.7% ± 11.5%	21.8% ± 6.9%
>50	50.0% ± 4.9%	22.2% ± 1.9%	30.0% ± 21.8%
Effect of scrambled shRNA on podosome numbers			
Podosomes/cell	**24 h**	**48 h**	**72 h**
0–10	0.0% ± 0.0%	1.1% ± 1.9%	1.3% ± 2.2%
11–50	7.1% ± 3.5%	8.1% ± 5.3%	0.0% ± 0.0%
>50	92.9% ± 8.9%	90.8% ± 1.9%	98.8% ± 20.7%
Degradation of gelatin matrix after siRNA treatment			
Target of siRNA	**0–40%**		**41–100%**
Luciferase	31.1% ± 10.7%		68.9% ± 17.1%
KIF9	88.9% ± 5.1%		11.1% ± 5.1%
Microinjection of GST-KIF9-CT81			
Microinjection of	**0 h**		**1 h**
GST	6.7% ± 3.3%		72.2% ± 8.4%
GST-KIF9-CT81	7.8% ± 1.9%		32.2% ± 1.9%
Effect on podosome numbers			
Target of siRNA	**Podosomes/cell**		**72 h**
Luciferase	0–10		0.0% ± 0.0%
	11–50		1.1% ± 1.9%
	>50		95.6% ± 5.1%
Reggie-1	0–10		1.1% ± 1.9%
	11–50		3.3% ± 3.3%
	>50		95.6% ± 1.9%
Reggie-2	0–10		0.0% ± 0.0%
	11–50		1.1% ± 1.9%
	50		98.9% ± 1.9%
Reggie-1 + reggie-2	0–10		0.0% ± 0.0%
	11–50		0.0% ± 0.0%
	>50		100.0% ± 0.0%
Degradation of gelatin matrix after siRNA treatment			
Target of siRNA	**0–40%**		**41–100%**
Luciferase	14.6% ± 7.6%		85.3% ± 7.6%
Reggie-1	37.3% ± 16.6%		62.7% ± 16.6%
Reggie-2	50.6% ± 26.6%		49.4% ± 26.6%
Reggie-1 + reggie-2	60.0% ± 15.0%		40.0% ± 15.0%
Degradation of gelatin matrix after overexpression			
Construct	**0–40%**		**41–100%**
KIF9-CT402-GFP	24.3% ± 7.0%		75.7% ± 7.0%
KIF9-NT709-GFP	11.0% ± 5.0%		89.0% ± 5.0%

TABLE 1. Values for podosome formation or matrix degradation following various treatments. Statistical evaluation of podosome numbers or matrix degradation in macrophages transfected with siRNA or shRNA or microinjected with proteins. For each value, each time at least 30 randomly chosen cells from three independent experiments were evaluated. Values are given as mean percentage ± SD of total counts.

protein (pEGFP)–N1 or an siRNA specific for firefly luciferase, the number of podosome-forming cells in KIF9 siRNA-transfected macrophages was reduced to approximately 40% of controls (Figure 1A; see also Table 1). To get detailed confirmation of this effect, we next generated a KIF9-specific short-hairpin RNA (shRNA) construct, which allows bicistronic expression of EGFP. Primary macrophages transfected with this construct showed a clear reduction of podosome levels (Figure 1, B and C). A detailed evaluation of podosome

numbers in KIF9-shRNA–expressing cells at 24, 48, and 72 h post-transfection showed that the number of cells containing numerous (>50) podosomes was reduced, while the number of cells containing few (0–10) podosomes was increased, compared with cells expressing a scrambled control sequence (Figure 1, D and E; Table 1). Combined, these findings indicate that knockdown of KIF9 leads to decreased podosome numbers in primary macrophages.

To further investigate potential additional roles of KIF9, 7-d-old macrophages were transfected with siRNA specific for KIF9 or for firefly luciferase as a control. After 3 d, cells were reseeded on fluorescently labeled gelatin matrix, and their matrix-degrading ability was assessed after 5 h. Matrix degradation was evaluated only in cells containing numerous (>50) podosomes, to distinguish the potential effects of KIF9 in matrix degradation from its role in regulation of the podosome structure itself. Matrix degradation was analyzed by measuring the rhodamine-based fluorescence of the podosome-covered area, and cells were scored into groups according to the degree of matrix degradation (0–40% and 41–100%; Figure 2, A–C). Importantly, the number of cells showing low (0–40%) matrix degradation was significantly enhanced in cells transfected with siRNA specific for KIF9, compared with the control (Figure 2C; Table 1). Combined, these results indicate that KIF9 regulates not only the podosome structure itself but also the ability of podosomes to degrade matrix material.

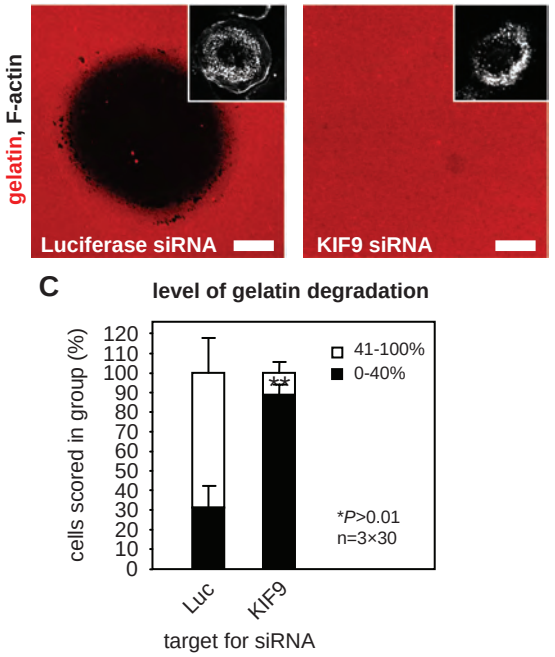

FIGURE 2: Knockdown of KIF9 influences matrix degradation. Confocal laser scanning micrographs of primary human macrophages transfected with siRNA-luciferase (A) or siRNA-KIF9 (B), seeded on rhodamine-labeled gelatin matrix (red). Matrix degradation is visible as dark areas; insets show relevant F-actin staining by Cy5-labeled phalloidin (white). White bar, 10 μm. (C) Evaluation of matrix degradation in cells treated with siRNAs. The degree of matrix degradation was analyzed by fluorescence measurements of 3×30 cells each time. Complete absence of labeled matrix beneath cells was set as 100% degradation. Cells were scored into groups according to matrix degradation (0–40% and 41–100%). For differences between control values and values gained with KIF9 siRNA, a P value < 0.01 was considered highly significant (indicated by asterisks).

KIF9-GFP vesicles associate with microtubules and contact podosomes

So that KIF9 localization and dynamics in macrophages could be visualized, both GFP- and mCherry-fusion constructs (KIF9-GFP and KIF9-mCherry) were generated and transfected into macrophages. KIF9-GFP was found to be present in vesicle-like accumulations, which were often closely associated with microtubules (Figure 3A). Live cell imaging of cells coexpressing KIF9-mCherry and GFP-α-tubulin revealed that KIF9-GFP vesicles move along microtubules (Figure 3B and Supplemental Video 1), comparable to other kinesins such as KIF1C (Kopp *et al.*, 2006).

To analyze potential interactions between KIF9-positive vesicles and podosomes, macrophages were cotransfected with KIF9-GFP and mRFP-β-actin constructs, the latter for labeling actin-rich podosome cores, and analyzed by time-lapse confocal video microscopy. KIF9-GFP–positive vesicles were found to localize at the podosome-containing ventral cell side (Figure 3C), where they dynamically and repeatedly contacted podosomes (Figure 3C and Supplemental Video 2). Interestingly, KIF9-GFP vesicles contacted mostly podosomes at the inner region of the ventral cell side, and not the larger podosome precursors at the cell periphery, which are contacted preferentially by the KIF1C kinesin (Kopp *et al.*, 2006).

KIF9 is expressed in primary macrophages and forms oligomers

To get direct proof that KIF9 is expressed in primary macrophages, reverse transcriptase PCR was performed using mRNA prepared from 7-d cultured primary human macrophages and primers specific for the KIF9 sequence comprising nucleotides 1125–1579. A band of the respective size (454 base pairs) was detected on agarose gels (Figure 4A), indicating the presence of the KIF9 transcript. To detect the KIF9 protein, a polyclonal antibody was raised against the unique C-terminal region of KIF9 comprising amino acid (aa) residues 710–790 ("CT81"; see *Materials and Methods*) as part of a GST fusion protein (GST-KIF9-CT81; see also Figure 5A) and subsequently affinity purified using the CT81 polypeptide of thrombin-cleaved GST-KIF9-CT81. On Western blots, this antibody recognized the respective KIF9 sequence both as part of the GST-KIF9-CT81 fusion protein (Figure 4B, left lane) and as the thrombin-cleaved polypeptide of the appropriate size (9 kDa; Figure 4B, right lane). Using this antibody on Western blots of macrophage lysates, we could not detect a band corresponding to endogenous KIF9 (~87 kDa), possibly owing to the relatively low abundance of kinesins in whole cell lysates, comparable to KIF1C (Kopp *et al.*, 2006).

As kinesins are present mostly as dimers (reviewed in Woehlke and Schliwa, 2000), and the KIF9 sequence contains coiled-coil sequences predicted to be involved in dimerization (Piddini *et al.*, 2001), we next tried to concentrate endogenous KIF9 protein by coprecipitation with overexpressed KIF9-GFP. Immunoprecipitations from lysates of macrophages expressing KIF9-GFP or GFP alone were performed with anti-GFP specific antibody coupled to magnetic beads. Western blots of respective fractions probed with anti-GFP antibody showed successful precipitation of both KIF9-GFP and the GFP control (Figure 4C, left blot). Comparable Western blots developed with anti-KIF9 antibody showed a band corresponding to the KIF9-GFP fusion construct, and in addition two bands in the 85–90-kDa range. Both of these bands are likely to correspond to endogenous KIF9 and may represent either splice or phosphorylation variants. These results indicate that endogenous KIF9 can be coprecipitated

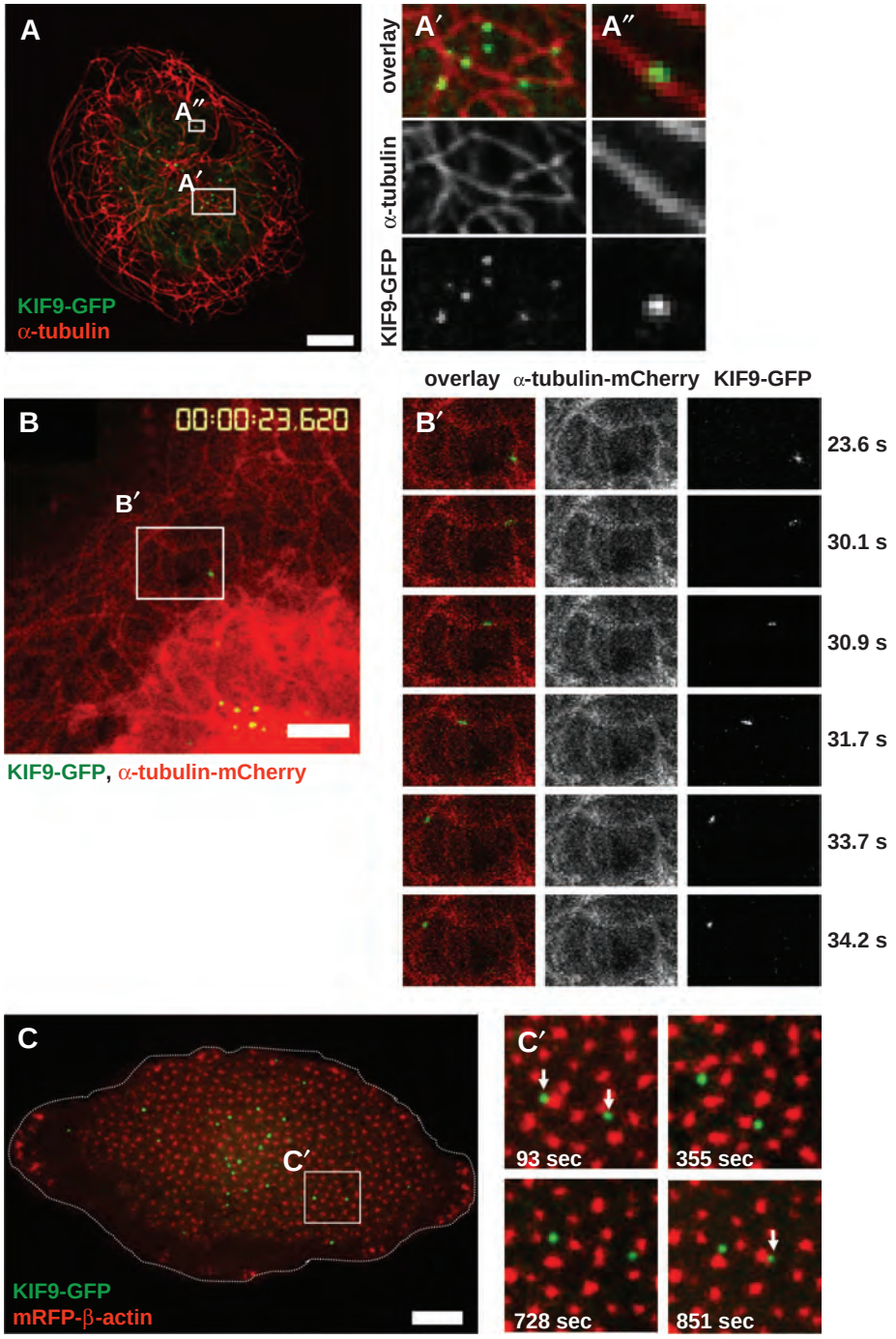

FIGURE 3: KIF9-GFP contacts microtubules and podosomes. (A) Confocal laser scanning micrographs of primary human macrophage expressing KIF9-GFP (green), labeled for α-tubulin (red). White boxes in overview image are enlarged on the right. White bar, 10 μm. (B) Image from confocal time-lapse video of a primary human macrophage expressing KIF9-GFP (green) and α-tubulin-mCherry, labeling microtubules (see Supplemental Video 1). White frame indicates detail images on the right (left panel: overlay; middle panel: α-tubulin-mCherry signal, right panel: KIF9-GFP signal). White bar, 5 μm. Elapsed time since start of the experiment is given in seconds on the right. (C) Image from confocal time-lapse video of a primary human macrophage expressing KIF9-GFP (green) and mRFP-β-actin (red), labeling podosomes (see Supplemental Video 2). Cell circumference is depicted by the dashed white line. (C) White frame indicates area of detail images on the right, elapsed time since start of the experiment is given in seconds in lower left corners. Note dynamic contact (white arrows) of KIF9-GFP particles with podosomes in the central area but not in the cell periphery.

together with overexpressed KIF9-GFP, which is probably based on the formation of heterodimers between overexpressed and endogenous forms.

The KIF9 C-terminus induces podosome disruption and Golgi dispersal

We next set out to identify domains responsible for the observed effects of KIF9 on podosomes. KIF9 shows an N-terminal motor domain with a P-loop sequence, which is involved in ATP hydrolysis of kinesins (Sack *et al.*, 1999); a stalk domain containing predicted coiled-coil sequences; and a unique tail comprising the C-terminal 81 aa residues (Figure 5A; Piddini *et al.*, 2001). We thus generated deletion constructs comprising the stalk and tail regions (KIF9-CT402-GFP; aa residues 389–790; see also Supplemental Figure 1) or the tail region (GFP-KIF9-CT81; aa residues 710–790; Figure 5A) and, vice versa, a construct lacking the tail region (KIF9-NT709-GFP). Upon expression in macrophages, KIF9-CT402-GFP localized to vesicular structures (Figure 5, E–G), comparable to full-length (fl) KIF9-GFP (Figure 5, B–D). Time-lapse videos of cells expressing KIF9-CT402-GFP together with fl KIF9-mCherry showed that this construct localizes to the same vesicle population as the full-length construct (unpublished data). Accordingly, extensive vesicle movement and contact of podosomes were observed in cells showing moderate overexpression of KIF9-CT402-GFP (Supplemental Figure 1 and Supplemental Videos 3 and 4). Upon higher overexpression, less KIF9-CT402-GFP–positive vesicles appeared to be motile, which probably reflects competitive binding of this motorless, nonprocessive construct with the endogenous and processive fl KIF9. Consistently, cells overexpressing KIF9-CT402-GFP showed reduced matrix-degrading ability, compared with controls (Supplemental Figure 2).

The construct lacking the C-terminal region (KIF9-NT709-GFP) also localized in a vesicular pattern (Figure 5, H–J). Coexpression with KIF9-mCherry confirmed that this construct colocalizes at the same vesicle population with fl KIF9 (Supplemental Figure 3, A–C). Live cell imaging further showed that these vesicles repeatedly contact podosomes (Supplemental Figure 3, D and D′; Supplemental Video 5), comparable to fl KIF9. In contrast to GFP-KIF9-CT402, however, overexpression of KIF9-NT709-GFP, also at high levels, did not influence gelatin matrix degradation (Supplemental Figure 2).

The vesicular localization of both deletion constructs may be based on the ability for dimerization with endogenous KIF9 (discussed previously), which is probably conferred by the stalk domain (Figure 5A; Piddini *et al.*, 2001). We also observed no detrimental effects on cell viability or podosome physiology upon expression of these constructs, comparable to fl KIF9-GFP

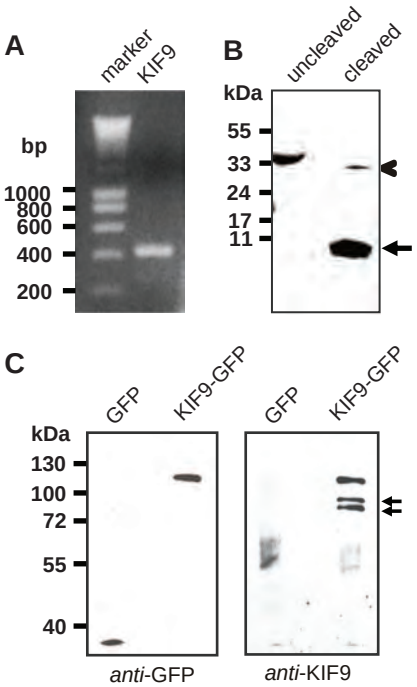

FIGURE 4: KIF9-GFP is expressed in primary human macrophages and exists as a dimer. (A) KIF9 is expressed in primary human macrophages. Reverse transcriptase-PCR using KIF9-specific primers. A band of the expected size (435 base pairs) is detected. Agarose gel stained with ethidium bromide; size in base pairs on left. (B) Western blot developed with polyclonal rabbit antibody against C-terminal tail of KIF9. GST-KIF9-CT81 fusion construct before (lane 1) and after proteolytic cleavage (lane 2). Note reactivity of anti-KIF9 antibody with the fusion construct (indicated by chevron) and the cleaved CT81 peptide (10 kDa; arrowhead), but not with the GST tag (26 kDa). (C) GFP immunoprecipitation of macrophage lysates expressing GFP (left lane) or GFP-fused KIF9 (right lane); Western blot probed with anti-GFP antibody (left blot) or anti–KIF9-CT81 (right blot). Note coprecipitated bands that react with the anti-KIF9 antibody (indicated by arrows). Molecular mass in kilodaltons is indicated on the left.

(unpublished data). By contrast, overexpressed GFP-KIF9-CT81 did not localize to vesicles and was found mostly in a perinuclear accumulation (Figure 5, K–M). Moreover, cells expressing this construct detached from coverslips 6–8 h after transfection, indicating a profound effect of GFP-KIF9-CT81 on macrophage viability.

Cells overexpressing GFP-KIF9-CT81 often showed a loss of podosomes; however, this phenomenon was inconsistent and could also have been due to a general detachment of cells. To assess potentially specific effects of the KIF9 C-terminus on podosomes, we thus generated a GST-fused version of KIF9-CT81 (GST-KIF9-CT81; Figure 5A) and used it in a microinjection-based podosome reformation assay (Linder *et al.*, 1999; Hufner *et al.*, 2001). This procedure takes advantage of a microinjection artifact, as injection of macrophages leads to initial loss of podosomes, with subsequent reformation within 1 h (Linder *et al.*, 2000b). Assessing podosome reformation after microinjection, we found that control cells injected with GST initially lost most of their podosomes, but mostly reformed them within 1 h, whereas cells injected with GST-KIF9-CT81 showed a clear reduction in podosome reformation (Figure 6, A and B; Table 1). Within the observed time period, microinjected cells showed normal spreading and no obvious loss of viability, arguing for a specific effect of GST-KIF9-CT81 on podosomes. We conclude from these experiments that the C-terminal region of KIF9 is important for the de novo formation of macrophage podosomes.

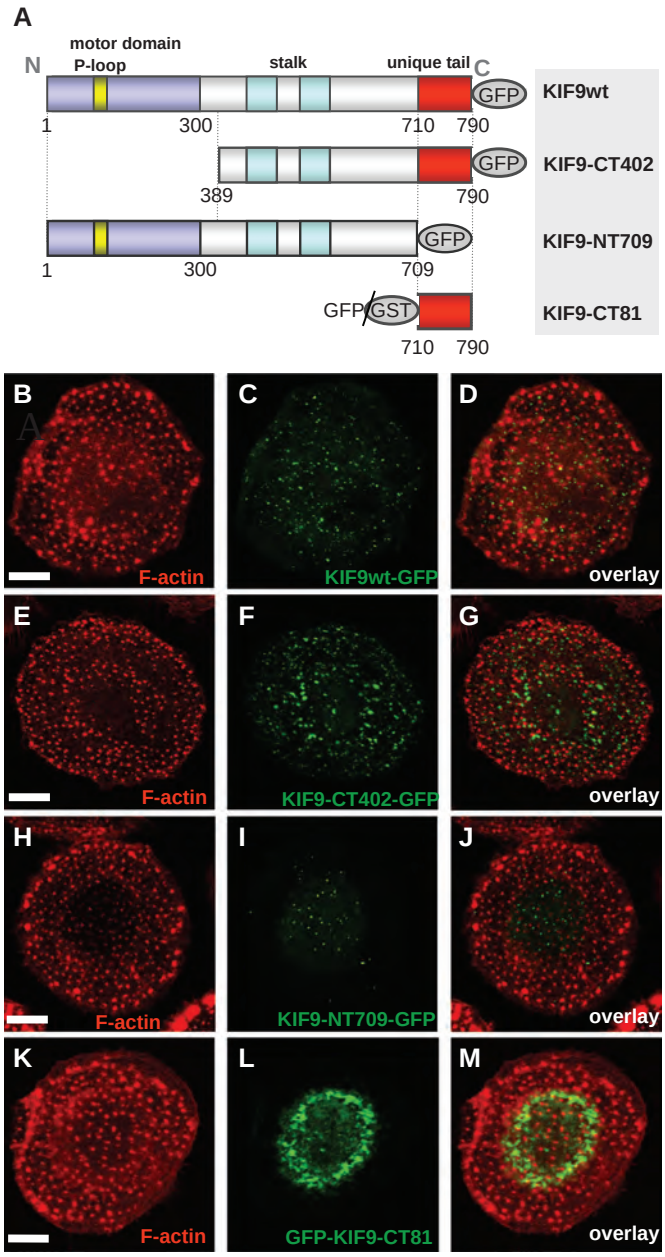

FIGURE 5: KIF9 expression constructs and their localization in cells. (A) Domain organization of KIF9 and expression constructs used in this study: P-loop sequence (aa 93–100), motor domain signature (aa 1–300), stalk (aa 301–709), and unique tail (aa 710–790). Numbers indicate first and last amino acid residues of constructs. (B–J) Confocal laser scanning micrographs of primary human macrophages expressing different GFP-fused KIF9 constructs. (B, C) Primary human macrophage expressing GFP-fused KIF9 (C), stained for F-actin (B), with overlay shown in (D). (E, F) Primary human macrophage expressing GFP-fused KIF9-CT402 (F), stained for F-actin (E), with overlay shown in (G). (H, I). Primary human macrophage expressing GFP-fused KIF9-NT709 (H), stained for F-actin (I), with overlay shown in (J). (K, L) Primary human macrophage expressing GFP-fused KIF9-CT81 (K), stained for F-actin (L), with overlay shown in (M). White bar, 10 μm.

To characterize the localization and effects of the KIF9 C-terminus in more detail, we immunostained cells expressing GFP-KIF9-CT81 for a variety of vesicular and cytoskeletal markers. We observed partial colocalization of GFP-KIF9-CT81 with Golgi proteins, such as the *trans*-Golgi marker TGN46 (Figure 7, A–F). Strikingly, cells

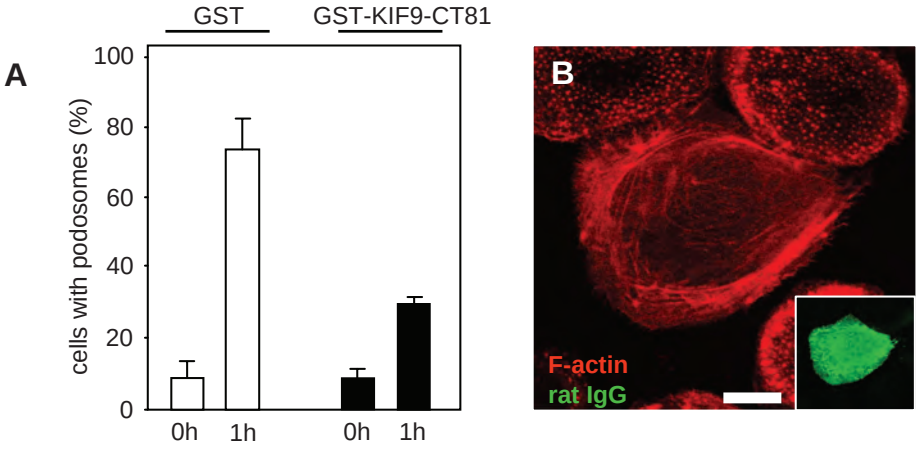

FIGURE 6: Microinjection of the KIF9 C-terminal region inhibits podosome reformation. (A) Evaluation of podosome numbers in macrophages microinjected with GST-KIF9-CT81 (0 h) and podosome reformation (1 h). For each bar, 3 × 30 cells were evaluated. Cells containing less than 10 podosomes at a given time point were scored as "containing no podosomes." Values for podosome formation are given as mean percentage ± SD of total counts in Table 1. (B) Primary human macrophage 1 h after injection of 2 µg/µl GST-KIF9-CT81, labeled for F-actin (red), confocal laser scanning micrograph of substrate-attached part of cell. Injected cells were identified by labeling coinjected rat IgG (5 mg/ml) with FITC-labeled goat anti–rat IgG antibody (green). Note absence of podosomes in cell injected with GST-KIF9-CT81. White bar, 10 µm.

expressing GFP-KIF9-CT81 also showed a dispersed localization of the Golgi (Figure 7, A–F), compared with control cells (93.3% ± 2.6% for cells expressing GFP-KIF9-CT81; 13.3% ± 8.8% for cells expressing GFP; Figure 7G). These results indicate that the KIF9 C-terminus partially colocalizes with Golgi proteins and that overexpression of GFP-KIF9-CT81 leads to Golgi dispersal, which may contribute to the observed loss of cell viability. Interestingly, siRNA-induced knockdown of KIF9 did not lead to significant alterations in Golgi architecture (Supplemental Figure 4), indicating that KIF9 per se is not involved in regulating Golgi integrity.

KIF9 interacts and colocalizes with reggie-1/flotillin-2

We next investigated potential interaction partners of the KIF9 C-terminus by overexpressing GFP-KIF9-CT81 in macrophages with subsequent anti-GFP immunoprecipitation. Silver staining of respective polyacrylamide (PAA) gels showed that additional bands coprecipitated with GFP-KIF9-CT81, compared with the GFP control (Figure 8A). Subsequent mass spectrometry (MS) and Western blot analyses revealed that a prominent band at ~45 kDa (Figure 8A) corresponded to reggie-1 and -2 (also named flotillin-2 and -1; reviewed in Stuermer, 2010).

Reggies/flotillins are known for their strong tendency toward hetero-oligomerization (Langhorst *et al.*, 2008; reviewed in Stuermer, 2010). We thus focused initially on reggie-1/flotillin-2 to verify a potential interaction of KIF9 with reggie proteins. As available antibodies against reggie-1 and KIF9 are not suitable for immunoprecipitation, we expressed GFP-tagged versions of these proteins and performed anti-GFP immunoprecipitations from macrophage lysates. Indeed, endogenous reggie-1 coprecipitated with KIF9-GFP (Figure 8B), and, vice versa, endogenous KIF9 coprecipitated with reggie-1-GFP (Figure 8C), indicating a close interaction between both proteins. Still, the construct lacking the C-terminal domain of KIF9 (KIF9-NT709-GFP) showed residual binding of reggie-1, indicating that the C-terminal 81 aa residues constitute not the only or not the complete binding site for reggie-1 in KIF9 (Figure 8C). Alternatively, this may reflect binding of reggie-1 by endogenous KIF9, which can form homodimers with GFP-fused forms of KIF9 containing the coiled-coil region (discussed previously).

To confirm the biochemical data, we next investigated whether reggie-1 and KIF9 also colocalize in fixed and living cells. Overexpression of GFP-KIF9-CT81 showed that endogenous reggie-1 partially colocalized with this construct (Figure 9, A–C) in a perinuclear accumulation, comparable to our previous observations (Figures 5 and 7). As the antibody generated against KIF9 is not suitable for immunofluorescence, KIF9-mCherry was expressed together with reggie-1-GFP in macrophages. Both proteins showed extensive colocalization in vesicle-like structures (Figure 9, D–F). However, confocal time-lapse video microscopy revealed that colocalization of reggie-1 and KIF9 is not permanent, but is a dynamic process, with two vesicle populations constantly interacting, either in a "kiss-and-run" scenario or in a more prolonged contact involving combined movement in the same direction (Figure 9, G and H; Supplemental Videos 5–7).

We conclude from these experiments that reggie-1 interacts with the KIF9 C-terminus in macrophage lysates and colocalizes with it in cells and that fl reggie-1 and KIF9 dynamically colocalize in living cells. Collectively, these data argue for a close interaction of both proteins in living cells, mainly through the KIF9 C-terminal region.

Reggie knockdown leads to reduced matrix degradation

We next investigated whether reggies/flotillins are involved in the KIF9-mediated regulation of podosomes. To assess a potential effect of reggie proteins on podosome numbers, macrophages were transfected with siRNAs specific for reggie-1 or -2 (Solis *et al.*, 2007), or a combination of both, as well as for firefly luciferase as a control, and assessed for their ability to form podosomes. However, neither knockdown of single isoforms nor a combined knockdown of reggie-1 and -2 showed effects on podosome morphology, subcellular distribution, or numbers (Supplemental Figure 5 and unpublished data), compared with controls.

To assess the potential involvement of reggie proteins in podosomal matrix degradation, siRNA-transfected cells were reseeded on fluorescently labeled gelatin matrix after 3 d and incubated for an additional 5 h. Matrix degradation was evaluated only in cells that contained numerous (>50) podosomes, by measuring the rhodamine-based fluorescence of the podosome-covered area. Each time, 3 × 30 cells were evaluated and scored into groups according to the degree of matrix degradation (0–40% or 41–100%; Figure 10). Importantly, the percentage of cells showing low matrix degradation was significantly enhanced in cells treated with siRNA specific for either reggie-1 or reggie-2 (Figure 10E; Table 1). Combined knockdown of both reggie isoforms showed a more pronounced effect, although this was not statistically significant compared with knockdown of single isoforms (Figure 10E; Table 1). We conclude from these experiments that, comparable to KIF9, reggie proteins are also important for the matrix-degrading ability of macrophage podosomes.

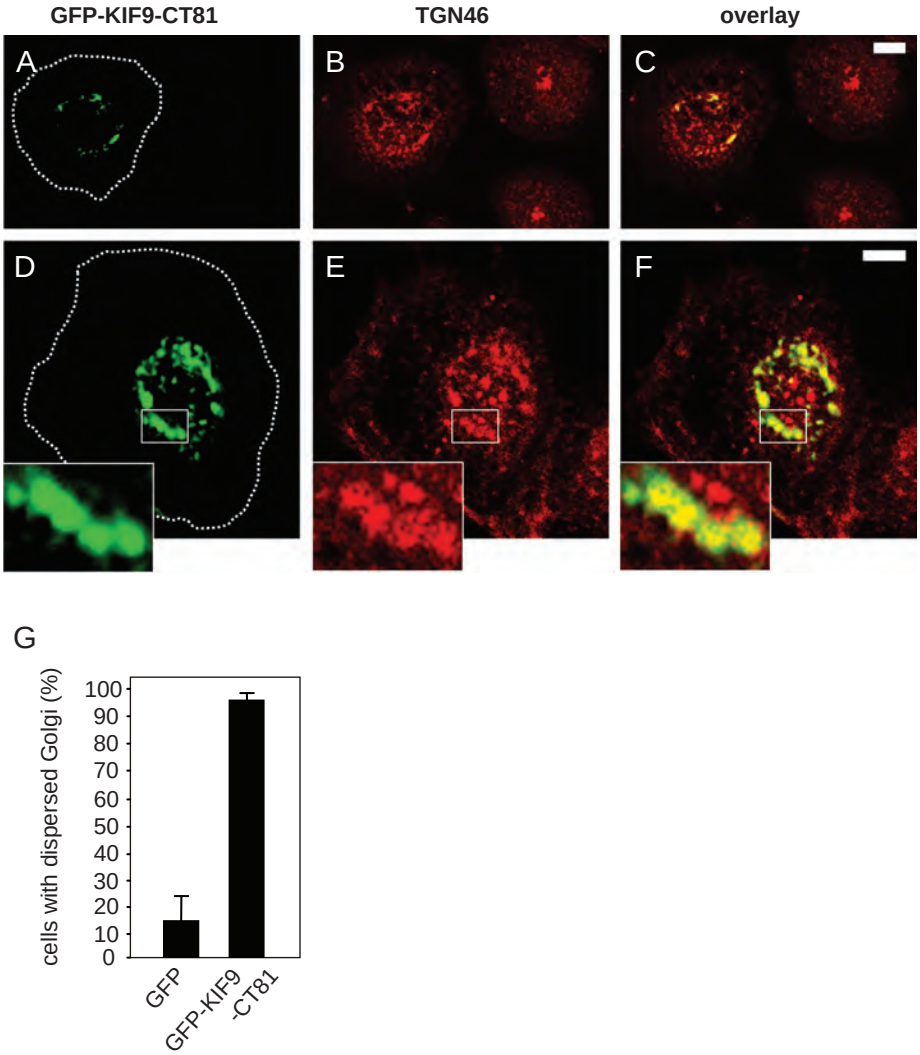

FIGURE 7: Golgi integrity is influenced by GFP-KIF9-CT81. (A–F) Confocal laser scanning micrographs of primary human macrophages expressing GPF-fused KIF9-CT81 (green, A and D), stained with specific primary antibody for TGN 46 (red, B and E) 7 h after transfection, with overlay shown in (C and F). Note compact Golgi appearance in untransfected cells, as opposed to dispersed Golgi morphology in cells expressing GFP-KIF9-CT81. White boxes in (D–F) indicate areas shown in enlarged insets. Cell circumferences are depicted by dashed white lines. White bars, 10 μm. (G) Evaluation of Golgi integrity 7 h after transfection of GFP-KIF9-CT81 or GFP as control. For each value, 3 × 30 cells were evaluated. Values are given as mean percentage ± SD of total counts in Table 1.

DISCUSSION

In this report, we focus on the microtubule-dependent regulation of podosomes in primary human macrophages. In addition to their actin-based architecture, podosomes also depend on an intact microtubule cytoskeleton and on microtubule-based transport processes (Linder *et al.*, 2000b; Cougoule *et al.*, 2005). This is most probably based on the repeated and dynamic contact between microtubule plus ends and podosomes (Kopp *et al.*, 2006) and involves the regulation of both podosome positioning (Destaing *et al.*, 2005; Ory *et al.*, 2008; McMichael *et al.*, 2010) and turnover (Kopp *et al.*, 2006).

Microtubule-based regulation, in consequence, indicates the necessity for transport processes involving plus end–directed motor proteins of the kinesin family. Indeed, KIF1C, a kinesin-3 family member, has previously been identified as an important player in the regulation of podosome dynamics (Kopp *et al.*, 2006). We have now expanded our screen for podosome-associated kinesins and report a critical role for KIF9 in the regulation of podosomal matrix degradation in macrophages.

KIF9 is a little-characterized member of the kinesin-9 family. So far, expression of KIF9 mRNA has been reported only for brain and kidney (Piddini *et al.*, 2001). We now add to these findings and show, on both mRNA and protein levels, that KIF9 is also expressed in primary human macrophages. Importantly, anti-GFP immunoprecipitation of GFP-fused KIF9 resulted in coprecipitation of endogenous KIF9. This indicates an ability of KIF9 for oligomerization, presumably as a dimer, as is typical for kinesins (reviewed in Woehlke and Schliwa, 2000). Dimer formation is likely to involve the coiled-coil regions of KIF9 (Piddini *et al.*, 2001), comparable to the general mode of kinesin dimerization (Wade and Kozielski, 2000). This is also supported by the observations that a construct lacking the motor domain (KIF9-CT402) or a construct lacking the tail region (KIF9-NT709), but in both cases containing the coiled-coil regions, localizes to vesicles, presumably through interaction with the endogenous motor. By contrast, a shorter construct lacking the coiled-coil regions (KIF9-CT81) localizes more diffusely.

Interestingly, GFP-KIF9 coprecipitates two proteins that react with the newly developed anti-KIF9 antibody and that migrate within the expected size range for KIF9 (85–90 kDa) on PAA gels. Apart from potential unspecific cross-reaction of the antibody, this 1) may be based on degradation of KIF9 in the cell lysate or 2) could indicate that KIF9 is present in two forms in macrophages, which may represent either splice or phosphorylation variants.

Knockdown of KIF9, using two independent siRNA/shRNAs, resulted in a pronounced loss of podosome numbers, indicating a role for KIF9 in the formation and/or turnover of these structures, comparable to the effect previously described for KIF1C (Kopp et al., 2006). Moreover, in KIF9 siRNA-treated cells that still form numerous podosomes, gelatin matrix degradation was almost completely blocked, pointing to an additional role of KIF9 in the regulation of podosomal matrix degradation. These effects may be independent but could also be linked through previously reported feedback loops connecting podosome formation and podosomal matrix degradation (reviewed in Linder, 2007).

Comparable to other kinesin motors, KIF9 contains an N-terminal motor domain (Piddini *et al.*, 2001), which is expected to bind to the microtubule lattice. Indeed, KIF9 has been reported to associate with the microtubule cytoskeleton in primary glial cells and to cosediment with taxol-stabilized microtubules (Piddini *et al.*, 2001). Here we show that KIF9-GFP–positive vesicles associate with microtubules and repeatedly contact podosomes, revealing a direct

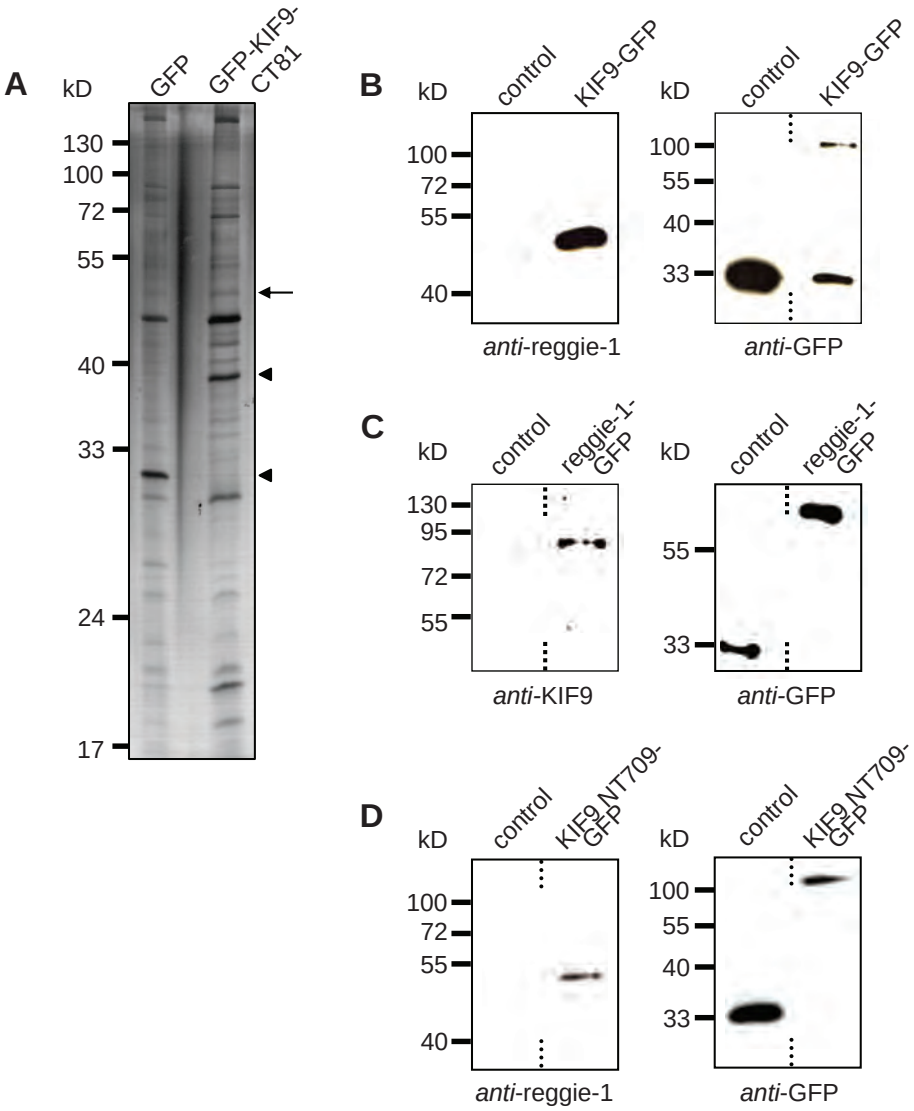

FIGURE 8: KIF9 interacts with reggie-1/flotillin-2. (A) Lysates of primary human macrophages immunoprecipitated with anti-GFP antibody coupled to magnetic beads. Silver-stained PAA gel, left lane: cells transfected with pEGFP-N1 as control; right lane: cells transfected with GFP-KIF9-CT81 construct. Arrow indicates band subsequently identified by mass spectrometry as reggie-1/2. Arrowheads indicate bands corresponding to GFP (left lane) and GFP-KIF9-CT81 (right lane), as judged by their mobility on PAA gels. Molecular mass in kilodaltons is indicated on the left. (For a comparison of immunoprecipitations performed with GFP-KIF9-CT81 and fl KIF9-GFP, see Supplemental Figure 7.) (B) GFP immunoprecipitation of KIF9-GFP–transfected macrophages, using GFP-N1 as control. Western blot developed with anti–reggie-1 antibody (left side) or with anti-GFP antibody (right side). (C) GFP immunoprecipitation of reggie-1-GFP–transfected macrophages, using GFP-N1 as control. Western blot developed with anti-KIF9 antibody (left side) or with anti-GFP antibody (right side). (D) GFP immunoprecipitation of KIF9-NT709-GFP–transfected macrophages, using GFP-N1 as control. Western blot developed with anti–reggie-1 antibody (left side) or with anti-GFP antibody (right side). Dashed lines indicate that lanes were not directly adjacent on original blots.

connection between KIF9-mediated, microtubule-based transport and actin-rich podosomes, which are regulated by KIF9.

Interestingly, KIF1C regulates the dynamics of podosome precursors in the cell periphery (Kopp *et al.*, 2006) and is not involved in the regulation of matrix degradation by podosomes (Wiesner *et al.*, 2010). By contrast, KIF9 contacts podosomes mostly in the inner region of the ventral cell surface, which are more efficient in matrix degradation (Wiesner *et al.*, unpublished observations), and has a profound effect on the matrix-degrading ability of these structures. These findings indicate that specific kinesins exert differential effects on podosomes. The molecular/structural basis of this fine-tuned regulation will be an important point to address in future studies. It may be mediated by trafficking of specific kinesins on differentially modified microtubule subsets, as shown previously for movement of kinesin-1 along acetylated (Reed *et al.*, 2006), or of KIF5c along detyrosinated, microtubules (Dunn *et al.*, 2008; reviewed in Verhey and Hammond, 2009). Furthermore, it is likely to involve differential transport of specific cargo molecules of various kinesin isoforms to podosomes.

In this context, the C-terminal regions of kinesins are of particular interest, as they are thought to function as cargo binding sites of adaptors or regulators (reviewed in Woehlke and Schliwa, 2000). Indeed, the C-terminal 81 aa residues of KIF9 comprise a unique sequence (Piddini *et al.*, 2001) that could potentially act as a hub for specific interaction partners. In a first step to investigate this, we generated a respective GFP-fused construct (GFP-KIF9-CT81). However, overexpression of GFP-KIF9-CT81 for more than 6 h resulted in cell detachment. To circumvent this problem, we microinjected a GST-fused version into macrophages, which allows for manifestation of potential effects within 1 h. This resulted in a pronounced defect of cells to reform podosomes, indicating that the C-terminal region of KIF9 is involved in podosome regulation, presumably by binding to specific interaction partners.

Immunoprecipitation of GFP-KIF9-CT81 from macrophage lysates and subsequent MS analysis revealed the presence of reggie-1 and -2 in the precipitates, indicating a potential interaction of reggie proteins with the KIF9 C-terminus. Indeed, GFP-fused full-length constructs of either KIF9 or reggie-1 were able to cross-precipitate the respective endogenous proteins, arguing for a close interaction of both proteins within cells. Interestingly, only one band of endogenous KIF9 was coprecipitated by GFP–reggie-1, indicating that reggie may interact with only one (splice or phospho) variant of the motor. Moreover, a construct lacking the unique C-terminal region of KIF9 (KIF9-NT709-GFP) still showed binding to endogenous reggie-1, although at a diminished degree. 1) This could indicate that both proteins interact through the KIF9 C-terminal region, but this region may constitute only a part or not the single reggie-1 binding site in KIF9, or 2) it may reflect recruitment of reggie-1 by endogenous KIF9, which can form dimers with KIF9-NT709-GFP. Both scenarios would be consistent with the observation that overexpression of KIF9-NT709-GFP did not reduce gelatin degradation in the matrix-degradation assay.

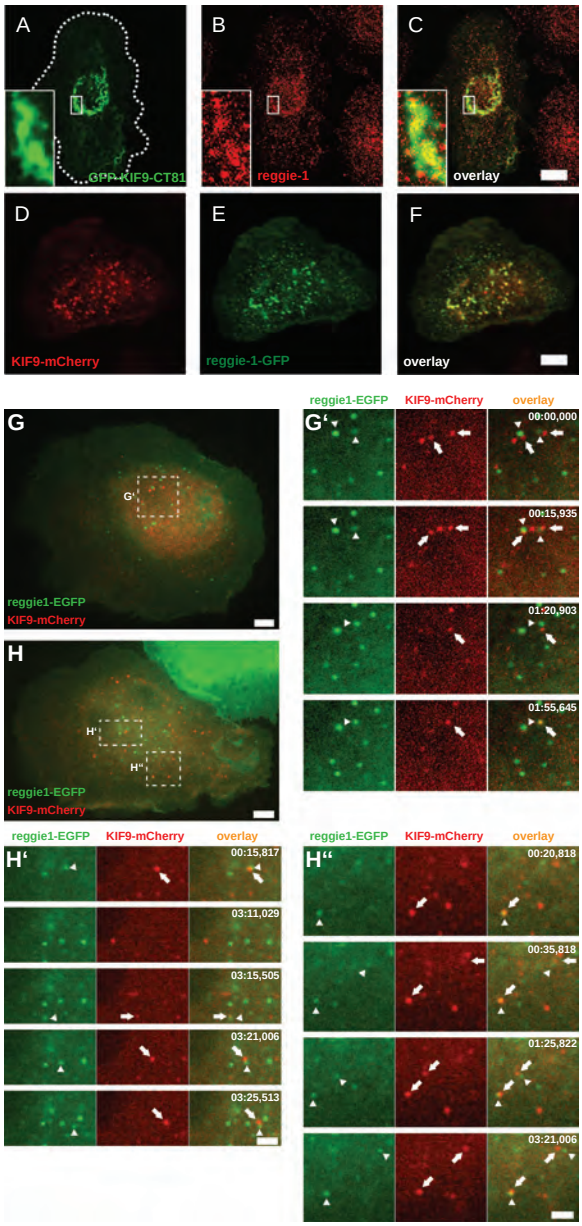

FIGURE 9: KIF9 and reggie-1 colocalize in fixed and living cells. (A–F) Confocal laser scanning micrographs of primary human macrophages expressing GFP-KIF9-CT81 (green, A), stained for reggie-1 (red, B) with specific primary antibody, with overlay shown in (C). Cell circumference is depicted by the dashed white line. White boxes indicate areas shown in detail images. (D–F) Confocal laser scanning micrographs of primary human macrophages coexpressing KIF9-mCherry (red, D) and reggie-1-GFP (green, E) with overlay shown in (F). (G, H) Images from confocal time-lapse videos of primary human macrophages expressing reggie-1-GFP (green) and KIF9-mCherry (red). White frames indicate areas of detail images. White bar, 10 μm. (G′, H′, H″) Time-lapse sequences from Supplemental Videos 6–8, taken from respective detail regions indicated in (G, H). Note close and repeated nonrandom contact between reggie-1-GFP (arrowheads) and KIF9-mCherry vesicles (arrows). Time since start of the experiments is indicated in seconds in upper right corners.

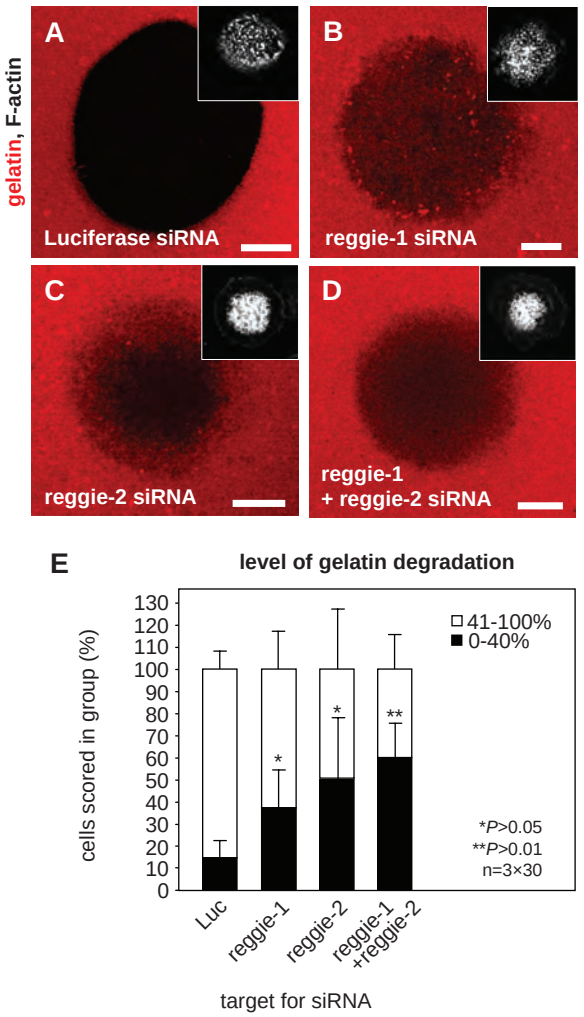

FIGURE 10: Knockdown of reggie proteins influences matrix degradation. Confocal laser scanning micrographs of primary human macrophages transfected with siRNA-luciferase (A), siRNA-reggie-1 (B), siRNA-reggie-2 (C), or a combination of both reggie siRNAs (D), seeded on rhodamine-labeled gelatin matrix (red). Matrix degradation is visible as dark areas; insets show relevant F-actin staining by Cy5-labeled phalloidin (white). White bar, 10 μm. (E) Evaluation of matrix degradation in cells treated with siRNAs. The degree of matrix degradation was analyzed by fluorescence measurements of 3 × 30 cells each time. Complete absence of labeled matrix beneath cells was set as 100% degradation. Cells were scored into groups according to matrix degradation (0–40% and 41–100%). For differences between control values and values gained with reggie siRNAs, a P value < 0.05 was considered significant, and a P value < 0.01 was considered highly significant (indicated by asterisks). Values are given as mean percentage ± SD of total counts in Table 1.

Consistent with the biochemical analysis, we observed partial colocalization of GFP-KIF9-CT81 with reggie-1 at the above-mentioned dispersed Golgi localization and colocalization of fl KIF9-mCherry with GFP-fused reggie-1 at vesicular structures in fixed cells. Both localizations are in line with earlier observations showing the presence of reggie proteins at the Golgi or at cytoplasmic vesicles (Langhorst *et al.*, 2008; Stuermer, 2010). Interestingly, live cell imaging of macrophages coexpressing reggie-1-GFP and KIF9-mCherry revealed that, although a clear overlap between reggie-1– or KIF9-positive vesicles was observed, contact between both populations is mostly transient and more reminiscent of a kiss-and-run scenario. The extensive colocalization observed in fixed specimens thus probably represents a fixation artifact.

The dispersed Golgi morphology upon overexpression of GFP-KIF9-CT81 may be due to the KIF9 polypeptide interacting with

reggie and other Golgi-localized proteins. As siRNA-induced knockdown of reggie-1 did not result in Golgi dispersal, it is unlikely that KIF9 per se is involved in the regulation of Golgi architecture. In a physiological scenario, fl KIF9, containing the motor domain, would be able to transport this cargo along microtubules. The isolated C-terminus, however, is unable to bind to and move processively along microtubules, and its overexpression may thus lead to sequestering of Golgi-derived proteins. This may result in the aberrant Golgi morphology and, ultimately, in cell detachment.

A central issue concerns the question of how the KIF9/reggie interaction affects podosomes and their function. Interestingly, siRNA-induced knockdown of reggie proteins did not influence podosome numbers but significantly impaired podosomal matrix degradation. This is in partial contrast to the results gained with knockdown of KIF9, which resulted in both reduction of podosome numbers and matrix degradation, and indicates that the KIF9 C-terminus probably binds to other regulatory factors, apart from reggie-1.

Furthermore, as reggie-1 and -2 have a pronounced tendency to form hetero-oligomers (Langhorst *et al.*, 2008), both reggie-1 and -2 are likely to form a complex together with KIF9. Consistently, knockdown of either reggie-1 or -2 had comparable effects on matrix degradation, while a combined knockdown did not show a significant enhancement over single isoform down-regulation. This indicates that 1) reggie-1 and -2 cannot compensate for each other and 2) only the reggie hetero-oligomer is functional in this regard. Interestingly, reggie proteins are not found in purified podosome fractions (our own unpublished observations), which may indicate that reggie proteins are only in transient contact with podosomes and that they are not actual components of these structures.

Reggie proteins function in the targeted delivery of membrane and membrane proteins from internal vesicle pools to privileged sites at the plasma membrane, including cell–cell contacts or growth cones (Stuermer, 2010). In this context, it is tempting to speculate that reggie proteins may be involved in the delivery of membrane material to podosomes. Involvement of membrane delivery to the related invadopodia has been demonstrated (reviewed in Caldieri and Buccione, 2010), and this mechanism may be involved in the protrusive growth of these structures. However, it is currently unclear whether podosomes are also protrusive (Gimona *et al.*, 2008; McMichael *et al.*, 2010). Alternatively, a potential reggie-dependent membrane influx at podosomes may be involved in the delivery or recycling of lytic enzymes, for example, through vesicles containing matrix metalloproteinases (MMPs), which are important for the lytic ability of podosomes (Linder, 2007). However, colocalization studies performed by staining several important MMP isoforms such as MMP-2, MMP-7, MMP-8, MMP-9, MMP-12, MT1-MMP, and MT4-MMP in reggie-1-GFP–expressing macrophages revealed no significant degree of colocalization (Supplemental Figure 6), which makes this scenario unlikely.

Reggie proteins cluster in complexes that also comprise Src family kinases and Rho GTPases (Kawase *et al.*, 2006). Interestingly, Src family members such as Src (Sounni *et al.*, 2004), Fyn (Redondo-Muñoz *et al.*, 2010), or Lyn (Zhao *et al.*, 2006) and Rho GTPase signaling (Deroanne *et al.*, 2005; Guegan *et al.*, 2008) have been shown to be involved in MMP-dependent signaling in various cell systems. The potential involvement of reggie proteins in the indirect regulation of MMPs is thus an important direction for future studies.

In sum, we show here a novel role for the kinesin KIF9 in the regulation of both numbers and matrix-degradation ability of human macrophage podosomes and demonstrate that the unique C-terminal region of KIF9 is central for these effects. KIF9 is only the second kinesin to be identified as a regulator of podosomes, while, in turn, podosome regulation is the first reported cellular function for this motor. We further show a specific interaction of the KIF9 C-terminus with reggie-1/flotillin-2. Consistently, reggie proteins also have a significant role in the regulation of podosomal matrix degradation. KIF9 thus appears to mediate several activities through interaction with distinct cargo molecules. A future challenge is thus to identify further interactors of KIF9 and to elucidate their effects on specific aspects of podosome regulation.

MATERIALS AND METHODS

Cell isolation and cell culture

Human peripheral blood monocytes were isolated from buffy coats (kindly provided by Frank Bentzien, University Medical Center Hamburg-Eppendorf, Germany) and differentiated into macrophages as described previously (Linder *et al.*, 1999).

Microinjection of proteins

Cells for microinjection experiments were cultured for 5–8 d. Proteins were expressed in *Escherichia coli* as described in Linder *et al.* (2000). For microinjection, proteins were dialyzed against microinjection buffer (50 mM Tris-HCl, pH 7.4, 150 mM NaCl, 5 mM $MgCl_2$), concentrated in Vivaspin filters (Sartorius, Göttingen, Germany), shock frozen, and stored at −80°C. Microinjection was performed using the Eppendorf Transjector 5246 and a Compic Inject micromanipulator (Cell Biology Trading, Hamburg, Germany). GST-KIF9-CT81 was injected into the cytoplasm at 2 μm/μl. Control experiments were performed with comparable concentrations of GST. Injected cells were identified by labeling coinjected rat immunoglobulin G (IgG) (5 mg/ml; Dianova, Hamburg, Germany) with fluorescein isothiocyanate transferrin (FITC)–labeled goat anti–rat IgG antibody (Dianova). Cells containing less than 10 podosomes at a given time point were scored as "containing no podosomes."

Transfection of cells

Cells were transiently transfected using the Microporator (Peqlab, Erlangen, Germany). For transfection of primary human macrophages, the following parameters were used: 1000 V, 40 ms, 2 pulses, and 0.5 μg DNA per 1×10^5 cells.

Expression vectors

For cloning of GST-KIF9-CT81, part of the coding sequence of KIF9 was amplified using the following primers: (CT81 forward) 5′-CTGGTACAATAGATCTTTTGTCATCCCTG-3′ and (CT81 reverse) 3′-ATCTGGTACGGATCCTCCTTTGTC-5′, generating 5′ *Bam*HI and 3′ *Bgl*II restriction sites, and cloned into pGEX-4T2, resulting in a construct coding for aa residues 712–793. For cloning and expression of KIF9-CT81-GFP, the same coding sequence of KIF9 was amplified using primer (CT81 forward) and primer 3′-GGCACATAGAGGATCCAACCTCATCG-5′, generating 5′ *Bam*HI and 3′ *Bgl*II restriction sites, and cloned into pEGFP-C1 (Clontech, Saint-Germain-en-Laye, France). For cloning and expression of wild-type GFP-KIF9, the KIF9 coding sequence was amplified from pBluescript-KIF9 using the primers (KIF9-GFP forward) 5′-TCGCTGCCTGGTAAGCTTAGAATGGGACTAG-3′ and (KIF9-GFP reverse) 3′-GTACTGGCGATGACCGGTTTTTTTCTATGTGC-5′, generating 5′ *Hind*III and 3′ *Age*I restriction sites. The PCR product was cleaved by using the internal *Kpn*I restriction site, and the resulting two regions were cloned successively into vector pEGFP-N1 (Clontech, Palo Alto, CA). For cloning and expression of KIF9-CT402-GFP, the fl KIF9-GFP construct was digested by *Age*I and *Kpn*I, and the region coding for aa 388–790 was cloned into pEGFP-N1. For cloning of the KIF9-NT709 tailless construct, part of the coding

sequence of KIF9 was amplified using the following primers: (KIF9-GFP NT1 forward) 5′-ATATAGTATTTAACTCGAGATGGGTAC-TAGGA-3′ and (KIF9-GFP NT709 reverse) 3′-CTGGTACAAT-GAGTCCCGGGCCCATAAAATT-5′, generating 5′ *Xho*I and 3′ *Apa*I restriction sites, and cloned into pEGFP-N1, resulting in a construct coding for aa residues 1–709. For cloning of KIF9-mCherry, GFP and mCherry sequences of KIF9-GFP and mCherry-N1 (Clontech, Mountain View, CA) were exchanged by digestion with *Age*I and *Not*I, with subsequent ligation of the mCherry sequence into the KIF9 vector backbone. For cloning of KIF9-pTagRFP, GFP and pTagRFP sequences of KIF9-GFP and pTagRFP-N (Evrogen, Moscow, Russia) were exchanged by digestion with *Age*I and *Not*I, with subsequent ligation of the pTagRFP sequence into the KIF9 vector backbone. Generation of mRFP-β-actin has been described in Osiak *et al*. (2005). Vector-based shRNAs for KIF9 and scrambled control sequences were generated using siSTRIKE U6 Hairpin Cloning System (Human)-hMGFP (Promega, Madison, WI) according to the manufacturer's instructions. The sequence for KIF9-shRNA was 5′-GAGAGGAGTTGTCAATAA-3′, targeting nucleotides 126 to 143. The sequence for scrambled control was 5′-GTACCTAAATCCAAAGAA-3′. pEGFP-N1 was purchased from Clontech, and reggie-1-GFP was a kind gift of R. Tikkanen (Universitätsklinik Frankfurt, Institute for Biochemistry, Germany).

Immunofluorescence and microscopy

Cells were fixed for 10 min in 3.7% formaldehyde solution and permeabilized for 5 min in ice-cold acetone. Actin was stained with Alexa 568–labeled phalloidin (Molecular Probes, Leiden, Netherlands), TGN 46 was stained with specific primary polyclonal antibody (AbD Serotec, Oxford, UK), and α-tubulin was stained with specific primary monoclonal antibody (Sigma, St. Louis, MO). MMPs were stained with specific primary monoclonal antibodies: MMP-2 (Calbiochem, Darmstadt, Germany), MMP-7 (Acris, Herford, Germany), MMP-8 (Millipore, Billerica, MA), MMP-9 (Calbiochem), MMP-12 (Sigma), MT1-MMP (Millipore), or MT4-MMP (Epitomics, Burlingame, CA).

Secondary antibodies were Alexa 568–labeled goat anti-mouse or goat anti-sheep (Molecular Probes). Coverslips were mounted in Mowiol (Calbiochem) containing *p*-phenylenediamine (Sigma-Aldrich, St. Louis, MO) as an antifading reagent and sealed with nail polish.

Microscopy was performed as described previously (Kopp *et al*., 2006). Images of fixed samples were acquired with a confocal laser-scanning microscope (Leica DM IRE2 with a Leica TCS SP2 AOBS confocal point scanner) equipped with an oil-immersion plan Apo 63× NA 1.4 objective. Acquisition and processing of images was performed with Leica Confocal Software (Leica, Wetzlar, Germany).

Live cell imaging

Images were acquired with a spinning disk confocal system (Spinning disk CSU22, Yokogawa, Japan) fitted on a Zeiss Axiovert 200M microscope with a temperature- and CO_2- controllable environmental chamber (Solent Scientific, Regensworth, UK), an oil immersion HCX PL Apo 63× NA 1.4–0.6 lambda blue objective, and a CCD camera (EM-CCD C-9100-2, Hamamatsu, Japan). Acquisition and processing of images were performed with Volocity Software (Improvision, Coventry, UK). Cells were seeded on 35-mm μ-dishes (ibidi, Martinsried, Germany) at a density of 2×10^5 and incubated 5 or 72 h, as indicated, before the start of the experiment.

Podosomes were counted by taking confocal images of the substrate-attached plane of macrophages and by counting separate F-actin–containing dots with a diameter of 0.5–1.5 μm. In the vast majority of cases, this allows a clear scoring of cells into the groups described (e.g., Figure 1D: containing 0–10, 11–50, and >50 podosomes). To be scored as a contact between podosomes (labeled with mRFP-actin) and KIF9-GFP vesicles, the respective mRFP and GFP signals had to be directly adjacent or overlapping for at least two pixels, without intermediate black pixels.

Immunoblotting

Immunolabeling was performed by standard procedure, using the following primary antibodies: mouse monoclonal reggie-1 was from BD Biosciences (Franklin Lakes, NJ), mouse monoclonal HA was from Cell Signaling (Danvers, MA), and mouse polyclonal GFP was a kind gift of J. Faix (Medical University Hannover, Hannover, Germany). For generating the KIF9 antibody, GST-KIF9-CT81 was thrombin cleaved, and the KIF9-CT81 peptide was separated by PAA gel electrophoresis, purified from gels, and injected into New Zealand White rabbits. Rabbit serum was affinity purified with GST-KIF9-CT81 spotted on nitrocellulose membrane. Secondary antibodies were horseradish peroxidase–coupled anti–mouse or anti–rabbit IgG (Dianova). Protein bands were visualized by using a SuperSignal kit (Pierce, Rockford, IL) and X-Omat AR film (Kodak, Stuttgart, Germany).

Quantitative real-time PCR

SiRNAs were validated by quantitative real-time PCR (qPCR) using lysates of transfected HeLa cells, as previously described (Machuy *et al*., 2005). Briefly, 0.1–0.25 μg siRNA (final concentration 80–200 nM) directed against KIF9 or luciferase as control and 2 μl TransMessenger reagent (Qiagen, Hilden, Germany) were added to 10×10^4 cells seeded in 96-well plates. RNA was isolated 48 h later using the RNeasy 96 BioRobot 8000 system (Qiagen). The relative amount of target mRNA was determined by qPCR using QuantiTect SYBR Green RT-PCR Kit following the manufacturer's instructions (Qiagen). The sequence of the KIF9-specific siRNA was 5′-CAGGACTTGGTT-TATGAGACA-3′, targeting nucleotides 196 to 216. SiRNA for firefly luciferase, used as a control, was generated as described in Kopp *et al.* (2006). siRNAs for reggie-1 and reggie-2 were generated (MWG, Ebersberg, Germany) according to Solis *et al.* (2007). Primary human macrophages were transfected with siRNA (650 ng) twice at 0 and 72 h and evaluated after a further incubation period of 5 h.

Reverse transcriptase reaction

A total of 6×10^6 cells were cultured for 7 d, and mRNA was isolated using 1 ml Trizol Reagent (Invitrogen, Carlsbad, CA). DNA was removed by DNAse digestion (Novagen, Madison, WI). For cDNA-synthesis, 1 μg random primer (Promega) was annealed to 2 μg RNA for 5 min at 70°C, and first-strand synthesis was performed using Moloney murine leukemia virus reverse transcriptase (Promega). Second-strand synthesis was performed using an oligonucleotide primer pair corresponding to nucleotides 1125–1150 and 1531–1579 of the *KIF9* coding sequence (accession number BC030657), respectively. As a control for quantitative removal of residual DNA, oligonucleotide primers specific for an exon in the human ß-*actin* gene were used, corresponding to nucleotides 1161–1142 and 716–735, respectively.

Immunoprecipitation

Immunoprecipitations of GFP-fused proteins were performed using the μMACS GFP Tagged Protein Isolation Kit (Miltenyi Biotec, Bergisch-Gladbach, Germany) according to the manufacturer's instructions. For lysis, preparation of columns, and washing, the following buffers were used: lysis buffer (150 mM NaCl, 1% Igepal

CA-630, 0.5% sodium deoxycholate, 0.1% SDS, 50 mM Tris-HCl, pH 8.0) with Complete Mini Protease Inhibitor (Roche Diagnostics, Penzberg, Germany), wash buffer 1 (150 mM NaCl, 1% Igepal CA-630, 0.5% sodium deoxycholate, 0.1% SDS, 50 mM Tris-HCl, pH 8.0), and wash buffer 2 (20 mM Tris-HCl, pH 7.5).

Mass spectrometry

After SDS–PAGE and silver staining of proteins, gel bands were excised from the gel and subjected to in-gel digest as described in Shevchenko *et al.* (2006). Extracted peptides were desalted and concentrated with "STAGE" t. Reverse-phase liquid chromatography–tandem MS (LC-MS/MS) was done by using an Agilent 1200 Nanoflow LC system (Agilent Technologies, Böblingen, Germany). The LC system was online coupled to an LTQ-Orbitrap (Thermo Scientific, Waltham, MA) equipped with a nanoelectrospray source (Proxeon, Odense, Denmark). Chromatographic separation of peptides was performed with a custom-made capillary needle packed with reverse-phase ReproSil-Pur C18 resin (Dr. Maisch GmbH, Ammerbuch-Entringen, Germany). The tryptic peptide mixtures were auto sampled at a flow rate of 0.5 µl/min and then eluted with a linear gradient at a flow rate of 0.25 µl/min. The mass spectrometers were operated in the data-dependent mode to automatically measure MS and MS/MS (Krüger *et al.*, 2008). Full-scan MS spectra were acquired with a resolution r = 60,000 at m/z 400. Raw MS spectra were processed using the MaxQuant software, which performed peak list generation and false discovery rate calculation based on search engine results (Cox and Mann, 2008). The derived peak list was searched with the Mascot search engine (Matrix Science, Boston, MA) against a concatenated database (IPI 3.54 human) (Elias and Gygi, 2007).

Matrix labeling and degradation

Gelatin (from swine; Roth, Karlsruhe, Germany) was fluorescently labeled with normal human serum (NHS)–rhodamine (Thermo Scientific, Rockford, IL) according to Chen (1996). Coverslips were coated with labeled gelatin solution, fixed in 0.5% glutaraldehyde (Roth), and washed with 70% ethanol and medium. Cells were seeded on coated coverslips with a density of 8×10^5 cells/coverslip. Cells previously transfected with siRNA and incubated for the times indicated were seeded on coated coverslips with a density of 8×10^5 cells/coverslip and incubated for a further 5 h, followed by fixation and staining.

Statistics

ImageJ software was used to analyze Cy5-labeled F-actin fluorescence intensity. Values of matrix degradation were determined by loss of fluorescence intensity, with intensity of undegraded areas set to 100%. For comparability, laser intensity was not changed between measurements. For each value, 3×30 cells were evaluated. Statistical analysis was performed with Excel software. When indicated, differences between mean values were analyzed using the Student's *t* test. $P < 0.05$ was considered as statistically significant and $P < 0.01$ as statistically highly significant.

For vesicle tracking, the ImageJ software (plug-in "manual tracking") was used to analyze vesicle movement of KIF9-GFP–transfected cells. Each vesicle was tracked manually throughout the video.

In selected time-lapse movies, line intensity profiles were determined at time points indicated using Volocity 5.3 for Mac imaging software. The resulting intensity values (gray levels of the acquired 14-bit image) of EGFP and mRFP fluorescence were offset corrected and plotted over the length of the line drawn using GraphPad Prism 5.0c for Mac.

ACKNOWLEDGMENTS

We thank Jan Faix for the anti-GFP antibody, Ritva Tikkanen for GFP-reggie-1, Jens Cornils and Barbara Böhlig for expert technical assistance, and Martin Aepfelbacher and Peter C. Weber for continuous support. This work is part of the doctoral thesis of SC. Work in the SL lab is supported by Deutsche Forschungsgemeinschaft (LI925/2-1, LI925/3-1), Wilhelm Sander-Stiftung (2007.020.02), and the European FP7 program (Marie Curie Actions, T3Net).

REFERENCES

Babuke T, Tikkanen R (2007). Dissecting the molecular function of reggie/flotillin proteins. Eur J Cell Biol 86, 525–532.

Buccione R, Caldieri G, Ayala I (2009). Invadopodia: specialized tumor cell structures for the focal degradation of the extracellular matrix. Cancer Metastasis Rev 28, 137–149.

Caldieri G, Buccione R (2010). Aiming for invadopodia: organizing polarized delivery at sites of invasion. Trends Cell Biol 20, 64–70.

Chabadel A, Banon-Rodriguez I, Cluet D, Rudkin BB, Wehrle-Haller B, Genot E, Jurdic P, Anton IM, Saltel F (2007). CD44 and beta3 integrin organize two functionally distinct actin-based domains in osteoclasts. Mol Biol Cell 18, 4899–4910.

Chen (1996). Proteases associated with invadopodia, and their role in degradation of extracellular matrix. Enzyme Protein 49, 59–71.

Cougoule C, Carreno S, Castandet J, Labrousse A, Astarie-Dequeker C, Poincloux R, Le CV, Maridonneau-Parini I (2005). Activation of the lysosome-associated p61Hck isoform triggers the biogenesis of podosomes. Traffic 6, 682–694.

Cox J, Mann M (2008). MaxQuant enables high peptide identification rates, individualized p.p.b.-range mass accuracies and proteome-wide protein quantification. Nat Biotechnol 26, 1367–1372.

Deroanne CF, Hamelryckx D, Ho TT, Lambert CA, Catroux P, Lapiere CM, Nusgens BV (2005). Cdc42 downregulates MMP-1 expression by inhibiting the ERK1/2 pathway. J Cell Sci 118, 1173–1183.

Destaing O, Saltel F, Geminard JC, Jurdic P, Bard F (2003). Podosomes display actin turnover and dynamic self-organization in osteoclasts expressing actin-green fluorescent protein. Mol Biol Cell 14, 407–416.

Destaing O, Saltel F, Gilquin B, Chabadel A, Khochbin S, Ory S, Jurdic P (2005). A novel Rho-mDia2-HDAC6 pathway controls podosome patterning through microtubule acetylation in osteoclasts. J Cell Sci 118, 2901–2911.

Dunn S, Morrison EE, Liverpool TB, Molina-Paris C, Cross RA, Alonso MC, Peckham M (2008). Differential trafficking of Kif5c on tyrosinated and detyrosinated microtubules in live cells. J Cell Sci 121, 1085–1095.

Elias JE, Gygi SP (2007). Target-decoy search strategy for increased confidence in large-scale protein identifications by mass spectrometry. Nat Methods 4, 207–214.

Friedl P, Wolf K (2003). Proteolytic and non-proteolytic migration of tumour cells and leucocytes. Biochem Soc Symp 277–285.

Gimona M, Buccione R, Courtneidge SA, Linder S (2008). Assembly and biological role of podosomes and invadopodia. Curr Opin Cell Biol 20, 235–241.

Glebov OO, Bright NA, Nichols BJ (2006). Flotillin-1 defines a clathrin-independent endocytic pathway in mammalian cells. Nat Cell Biol 8, 46–54.

Guegan F, Tatin F, Leste-Lasserre T, Drutel G, Genot E, Moreau V (2008). p190B RhoGAP regulates endothelial-cell-associated proteolysis through MT1-MMP and MMP2. J Cell Sci 121, 2054–2061.

Hufner K, Higgs HN, Pollard TD, Jacobi C, Aepfelbacher M, Linder S (2001). The verprolin-like central (vc) region of Wiskott-Aldrich syndrome protein induces Arp2/3 complex-dependent actin nucleation. J Biol Chem 276, 35761–35767.

Kawase K, Nakamura T, Takaya A, Aoki K, Namikawa K, Kiyama H, Inagaki S, Takemoto H, Saltiel AR, Matsuda M (2006). GTP hydrolysis by the Rho family GTPase TC10 promotes exocytic vesicle fusion. Dev Cell 11, 411–421.

Kopp P, Lammers R, Aepfelbacher M, Woehlke G, Rudel T, Machuy N, Steffen W, Linder S (2006). The kinesin KIF1C and microtubule plus ends regulate podosome dynamics in macrophages. Mol Biol Cell 17, 2811–2823.

Krüger M, Moser M, Ussan S, Thievessen I, Luber CA, Forner F, Schmidt S, Zanivan S, Fässler R, Mann M (2008). SILAC mouse for quantitative proteomics uncovers kindlin-3 as an essential factor for red blood cell function. Cell 134, 353–364.

Langhorst MF, Reuter A, Jaeger FA, Wippich FM, Luxenhofer G, Plattner H, Stuermer CA (2008). Trafficking of the microdomain scaffolding protein reggie-1/flotillin-2. Eur J Cell Biol 87, 211–226.
Lawrence CJ (2004). A standardized kinesin nomenclature. J Cell Biol 167, 19–22.
Linder S (2007). The matrix corroded: podosomes and invadopodia in extracellular matrix degradation. Trends Cell Biol 17, 107–117.
Linder S (2009). Invadosomes at a glance. J Cell Sci 122, 3009–3013.
Linder S, Aepfelbacher M (2003). Podosomes: adhesion hot-spots of invasive cells. Trends Cell Biol 13, 376–385.
Linder S, Higgs H, Hufner K, Schwarz K, Pannicke U, Aepfelbacher M (2000a). The polarization defect of Wiskott-Aldrich syndrome macrophages is linked to dislocalization of the Arp2/3 complex. J Immunol 165, 221–225.
Linder S, Hufner K, Wintergerst U, Aepfelbacher M (2000b). Microtubule-dependent formation of podosomal adhesion structures in primary human macrophages. J Cell Sci 113, 4165–4176.
Linder S, Nelson D, Weiss M, Aepfelbacher M (1999). Wiskott-Aldrich syndrome protein regulates podosomes in primary human macrophages. Proc Natl Acad Sci USA 96, 9648–9653.
Machuy N, Thiede B, Rajalingam K, Dimmler C, Thieck O, Meyer TF, Rudel T (2005). A global approach combining proteome analysis and phenotypic screening with RNA interference yields novel apoptosis regulators. Mol Cell Proteomics 4, 44–55.
McMichael BK, Cheney RE, Lee BS (2010). Myosin X regulates sealing zone patterning in osteoclasts through linkage of podosomes and microtubules. J Biol Chem 285, 9506–9515.
Ory S, Brazier H, Pawlak G, Blangy A (2008). Rho GTPases in osteoclasts: orchestrators of podosome arrangement. Eur J Cell Biol 87, 469–477.
Osiak AE, Zenner G, Linder S (2005). Subconfluent endothelial cells form podosomes downstream of cytokine and RhoGTPase signaling. Exp Cell Res 307, 342–353.
Pfaff M, Jurdic P (2001). Podosomes in osteoclast-like cells: structural analysis and cooperative roles of paxillin, proline-rich tyrosine kinase 2 (Pyk2) and integrin alphaVbeta3. J Cell Sci 114, 2775–2786.
Piddini E, Schmid JA, de MR, Dotti CG (2001). The Ras-like GTPase Gem is involved in cell shape remodelling and interacts with the novel kinesin-like protein KIF9. EMBO J 20, 4076–4087.
Poincloux R, Lizarraga F, Chavrier P (2009). Matrix invasion by tumour cells: a focus on MT1-MMP trafficking to invadopodia. J Cell Sci 122, 3015–3024.
Redondo-Muñoz J, Ugarte-Berzal E, Terol MJ, Van Den Steen PE, Hernandez del CM, Roderfeld M, Roeb E, Opdenakker G, Garcia-Marco JA, Garcia-Pardo A (2010). Matrix metalloproteinase-9 promotes chronic lymphocytic leukemia b cell survival through its hemopexin domain. Cancer Cell 17, 160–172.
Reed NA, Cai D, Blasius TL, Jih GT, Meyhofer E, Gaertig J, Verhey KJ (2006). Microtubule acetylation promotes kinesin-1 binding and transport. Curr Biol 16, 2166–2172.
Sack S, Kull FJ, Mandelkow E (1999). Motor proteins of the kinesin family. Structures, variations, and nucleotide binding sites. Eur J Biochem 262, 1–11.
Sakurai-Yageta M, Recchi C, Le DG, Sibarita JB, Daviet L, Camonis J, D'Souza-Schorey C, Chavrier P (2008). The interaction of IQGAP1 with the exocyst complex is required for tumor cell invasion downstream of Cdc42 and RhoA. J Cell Biol 181, 985–998.
Schulte T, Paschke KA, Laessing U, Lottspeich F, Stuermer CA (1997). Reggie-1 and reggie-2, two cell surface proteins expressed by retinal ganglion cells during axon regeneration. Development 124, 577–587.
Shevchenko A, Tomas H, Havlis J, Olsen JV, Mann M (2006). In-gel digestion for mass spectrometric characterization of proteins and proteomes. Nat Protoc 1, 2856–2860.
Solis GP, Hoegg M, Munderloh C, Schrock Y, Malaga-Trillo E, Rivera-Milla E, Stuermer CA (2007). Reggie/flotillin proteins are organized into stable tetramers in membrane microdomains. Biochem J 403, 313–322.
Sounni NE *et al*. (2004). Up-regulation of vascular endothelial growth factor-A by active membrane-type 1 matrix metalloproteinase through activation of Src-tyrosine kinases. J Biol Chem 279, 13564–13574.
Steffen A, Le DG, Poincloux R, Recchi C, Nassoy P, Rottner K, Galli T, Chavrier P (2008). MT1-MMP-dependent invasion is regulated by TI-VAMP/VAMP7. Curr Biol 18, 926–931.
Stuermer CA (2010). The reggie/flotillin connection to growth. Trends Cell Biol 20, 6–13.
Verhey KJ, Hammond JW (2009). Traffic control: regulation of kinesin motors. Nat Rev Mol Cell Biol 10, 765–777.
Wade RH, Kozielski F (2000). Structural links to kinesin directionality and movement. Nat Struct Biol 7, 456–460.
Webb BA, Eves R, Mak AS (2006). Cortactin regulates podosome formation: roles of the protein interaction domains. Exp Cell Res 312, 760–769.
Wiesner C, Faix J, Himmel M, Bentzien F, Linder S (2010). KIF5B and KIF3A/KIF3B kinesins drive MT1-MMP surface exposure, CD44 shedding and extracellular matrix degradation in primary macrophages. Blood 116, 1559–1569.
Woehlke G, Schliwa M (2000). Directional motility of kinesin motor proteins. Biochim Biophys Acta 1496, 117–127.
Zambonin-Zallone A, Teti A, Grano M, Rubinacci A, Abbadini M, Gaboli M, Marchisio PC (1989). Immunocytochemical distribution of extracellular matrix receptors in human osteoclasts: a beta 3 integrin is colocalized with vinculin and talin in the podosomes of osteoclastoma giant cells. Exp Cell Res 182, 645–652.
Zamir E, Geiger B (2001). Molecular complexity and dynamics of cell-matrix adhesions. J Cell Sci 114, 3583–3590.
Zhao Y, He D, Saatian B, Watkins T, Spannhake EW, Pyne NJ, Natarajan V (2006). Regulation of lysophosphatidic acid-induced epidermal growth factor receptor transactivation and interleukin-8 secretion in human bronchial epithelial cells by protein kinase Cdelta, Lyn kinase, and matrix metalloproteinases. J Biol Chem 281, 19501–19511.

SUPPLEMENTARY MATERIAL

Figure S1. KIF9-CT402-GFP contacts podosomes. (A) Images from confocal time lapse movie of a primary human macrophage expressing KIF9-CT402-EGFP (green) and mRFP-Lifeact (red), labelling podosomes (see marked region of interest in suppl. videos 3+4). A KIF9-CT402-GFP decorated vesicle (arrowhead) contacting several podosomes (arrow) was monitored over time. Scale bar: 2 µm. (B) Intensity profile along a line (highlighted in yellow) across a KIF9-CT402-GFP decorated vesicle, which is in close contact to a podosome; observed at time point T9. Intensity values of GFP and mRFP fluorescence were plotted over of the length of the line drawn. (C) Intensity profile along a line (highlighted in yellow) across a KIF9-CT402-EGFP decorated vesicle, which is in very close contact to a podosome; observed at time point T84. Intensity values of GFP and mRFP fluorescence were plotted over of the length of the line drawn.

Figure S2. Effects of KIF9 expression constructs on podosomal matrix degradation. Confocal laser scanning micrographs of primary human macrophages expressing EGFP (A), KIF9-CT402-GFP(B), or KIF9 NT709-GFP (C) seeded on rhodamine-labeled gelatin matrix (red). Matrix degradation is visible as dark areas, upper insets show respective F-actin stainings by Cy5-labeled phalloidin (white), lower insets show respective GFP signals (green). White bar, 10 µm. (D) Evaluation of matrix degradation in cells treated with eGFP expression constructs. The degree of matrix degradation was analyzed by fluorescence measurements of each time 5 x 30 cells. Complete absence of labeled matrix beneath cells was set as 100% degradation. Cells were scored into groups according to matrix degradation (0-40%; 41-100%). For differences betweeen control values and values gained with eGFP constructs, a p-value < 0.05 was considered significant. Values are given as mean percentage ± SD of total counts in Table 1.

Figure S3. Subcellular localization of KIF9-NT709-GFP. (A, B, C) Images from confocal time lapse movie of a primary human macrophage expressing KIF9-NT709-GFP (green) and KIF9-mCherry (red). KIF9-NT709-GFP (A) and KIF9-mCherry (B) colocalize at vesicles in living cells (C). Scale bar: 5 µm. (D, D') Images from confocal time lapse movie of a primary human macrophage expressing KIF9-NT709-GFP (green) and mRFP-Lifeact (red), labelling podosomes. In the subcellular region indicated by white box, KIF9-NT709-GFP decorated vesicles (arrowhead) contacting several podosomes (arrow) were monitored over time (see suppl. video 5). Note repeated, non-random contact of KIF9 NT709-GFP-decorated vesicles with podosomes. Scale bar: 1 µm.

Figure S4. Reggie-1 knockdown does not affect Golgi integrity. Evaluation of Golgi architecture in primary human macrophages transfected with luciferase-specific siRNA, or siRNA specific for reggie-1, siRNA. Influence of each siRNA was evaluated 72 h after transfection. For each value, 3 x 30 cells were evaluated. Values are given as mean percentage ± SD of total counts (luciferase siRNA: 85.6 % ± 1.9 % for compact Golgi,14.4 % ± 1.9 % for dispersed Golgi; reggie-1 siRNA: 84.4 % ± 3.9 % for compact Golgi, 15.6 % ± 3.9 % for dispersed Golgi).

Figure S5. Knock down of reggie proteins does not influence podosome numbers. Evaluation of podosome formation in primary human macrophages transfected with luciferase-specific siRNA, siRNA specific for reggie-1, siRNA specific for reggie-2 or a combination of both. Influence of each siRNA was evaluated 72 h after transfection. For each value, 3 x 30 cells were evaluated. Values are given as mean percentage ± SD of total counts in Table 1.

Figure S6. Reggie1-GFP does not colocalize with matrix metalloproteinases. Confocal micrographs of macrophages overexpressing reggie1-GFP and stained for endogenous MMP-2 (A-C), MMP-7 (D-F), MMP-8 (G-I), MMP-9 (J-L), MMP-12 (M-O), MT1-MMP (P-R), or MT4-MMP (S-U) using specific primary antibodies and Alexa 568-labeled secondary antibody. Merged images are shown in (A,D,G,J,M,P,S), with single channel images of reggie1-GFP shown in (B,E,H,K,N,Q,T; green) and of respective MMPs in (C,F,I,L,O,R,U; red). White boxes in (A,D,G,J,M,P,S) indicate detail images in (Ai-Ci,Di-Fi,Gi-Ii,Ji-Li,Mi-Oi,Pi-Ri,Si-Ui). White bars indicate 10 µm.

Figure S7. Immunoprecipitations of different KIF9 constructs. Lysates of primary human macrophages immunoprecipitated with anti-GFP antibody coupled to magnetic beads. Silver-stained PAA gel, left lane: cells transfected with full length KIF9-GFP; right lane: cells transfected with GFP-KIF9-CT81 construct. Arrow indicates band subsequently identified by mass spectrometry as reggie-1/-2. Arrowheads indicate bands corresponding to KIF9-GFP GFP (left lane) and GFP-KIF9-CT81 (right lane), as judged by their mobility on PAA gels. Molecular mass in kilodaltons is indicated on the left.

Video 1. video 1.mov

KIF9-GFP vesicles move along microtubules. Primary human macrophage expressing KIF9-GFP (green) and α-tubulin-mCherry (red), labeling microtubules. Confocal time lapse series of detail region indicated in Fig. 3B. (exposure time: 350 ms for green (491 nm), 350 ms for red (561 nm), frame rate: 4 f/s; sequence: 231 s).

Video 2. video 2.mov

KIF9-GFP contacts podosomes. Primary human macrophage expressing KIF9-GFP (green) and β-actin-mRFP (red), labelling podosomes. Confocal time lapse series of substrate

attached part of the cell (exposure time 1000 ms for green (491 nm), 4000 ms for red (561 nm), frame rate: 10 f/s; sequence: 1225 s).

Video 3. video 3.mov

KIF9-CT402-GFP positive vesicles contact podosomes. Primary human macrophage co-expressing KIF9-CT402-GFP (green) and mRFP-Lifeact (red). Note repeated, non-random contact of KIF9 construct-decorated vesicles with podosomes (labeled by mRFP-Lifeact). A dual channel confocal time lapse movie was acquired using an asynchronous mode as follows: exposure time 250ms for green (491nm) and 350ms for red (561nm), acquisition frame rate of 20 time points per minute for the green and 5 time points per minute for the red channel. Movie replay frame rate: 6 f/s; sequence length: 300 s.

Video 4. video 4.mov

Video of detail region shown in video-3.avi.

Video 5. video 5.mov

KIF9-NT709-GFP positive vesicles contact podosomes. Primary human macrophage co-expressing KIF9-NT709-GFP (green) and mRFP-Lifeact (red). Note repeated, non-random contact of KIF9 construct-decorated vesicles with podosomes (labeled by mRFP-Lifeact). A dual channel confocal time lapse movie was acquired using an asynchronous mode as follows: exposure time 300ms for green (491nm) and 250ms for red (561nm), acquisition frame rate of 20 time points per minute for the green and 5 time points per minute for the red channel. Movie replay frame rate: 4 f/s; sequence length: 111 s.

Video 6. video 6.mov

Reggie1-GFP and KIF9-mCherry vesicles contact each other. Primary human macrophage expressing reggie1-GFP and KIF9-mCherry. Confocal time lapse series of detail region (G´) indicated in Fig. 9G (exposure time: 500 ms for green (491nm), 1 s for red (561nm), frame rate: 6 f/s; sequence length: 10 min).

Video 7. video 7.mov

Reggie1-GFP and KIF9-mCherry vesicles contact each other. Primary human macrophage expressing reggie1-GFP and KIF9-mCherry. Confocal time lapse series of detail region (H´) indicated in Fig. 9H (exposure time: 250ms for green (491nm), 750ms for red (561nm), frame rate: 6 f/s; sequence length: 5 min).

Video 8. video 1.mov

Reggie1-GFP and KIF9-mCherry vesicles contact each other. Primary human macrophage expressing reggie1-GFP and KIF9-mCherry. Confocal time lapse series of detail region (H´´) indicated in Fig. 9H (exposure time: 250 ms for green (491nm), 750 ms for red (561nm), frame rate: 6 f/s; sequence length: 5 min).

Suppl. Fig. 1

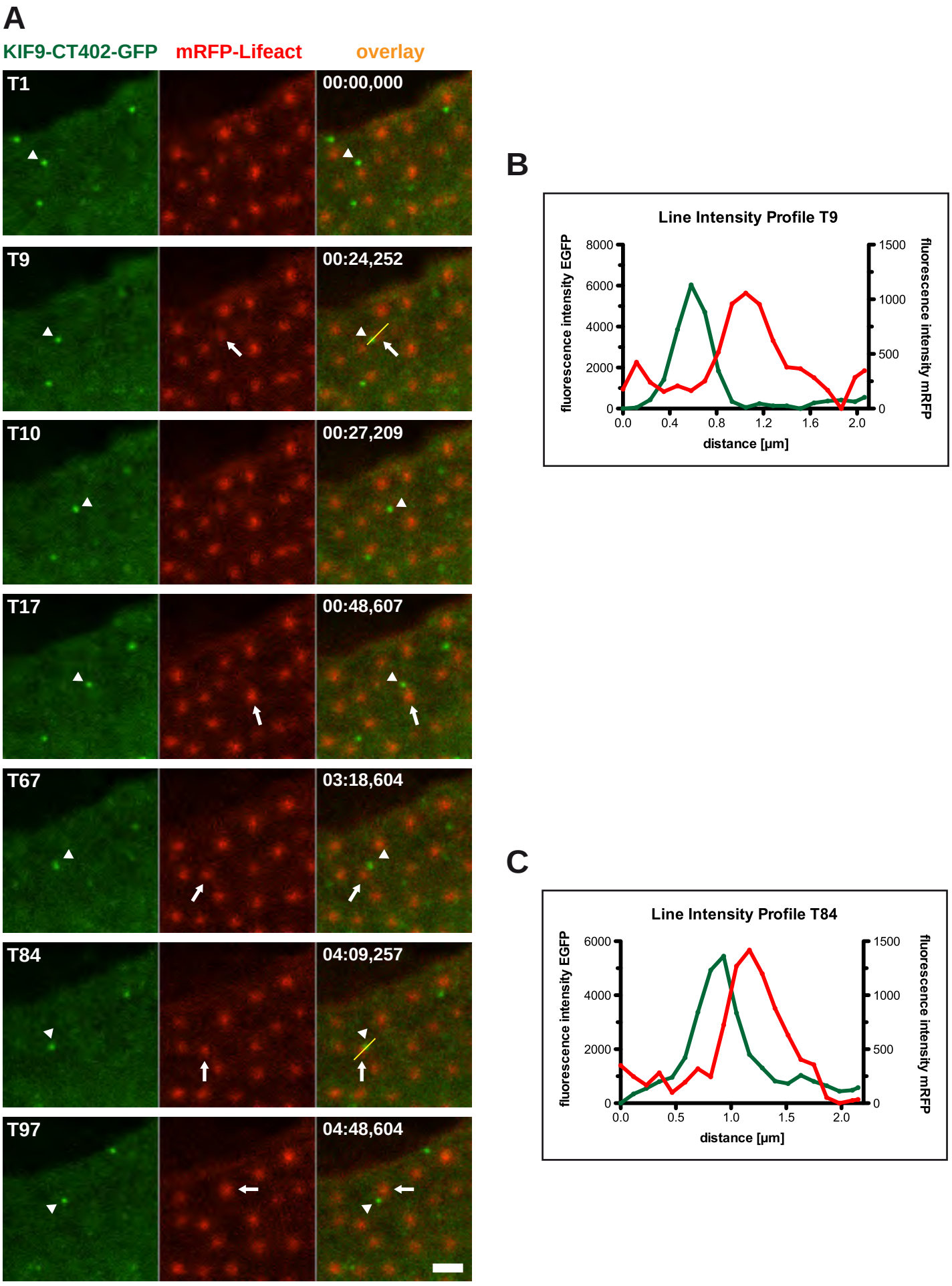
A
KIF9-CT402-GFP
mRFP-Lifeact
overlay
T1
00:00,000
T9
00:24,252
T10
00:27,209
T17
00:48,607
T67
03:18,604
T84
04:09,257
T97
04:48,604
B
Line Intensity Profile T9
fluorescence intensity EGFP
fluorescence intensity mRFP
distance [µm]
C
Line Intensity Profile T84
fluorescence intensity EGFP
fluorescence intensity mRFP
distance [µm]

Suppl. Fig. 2

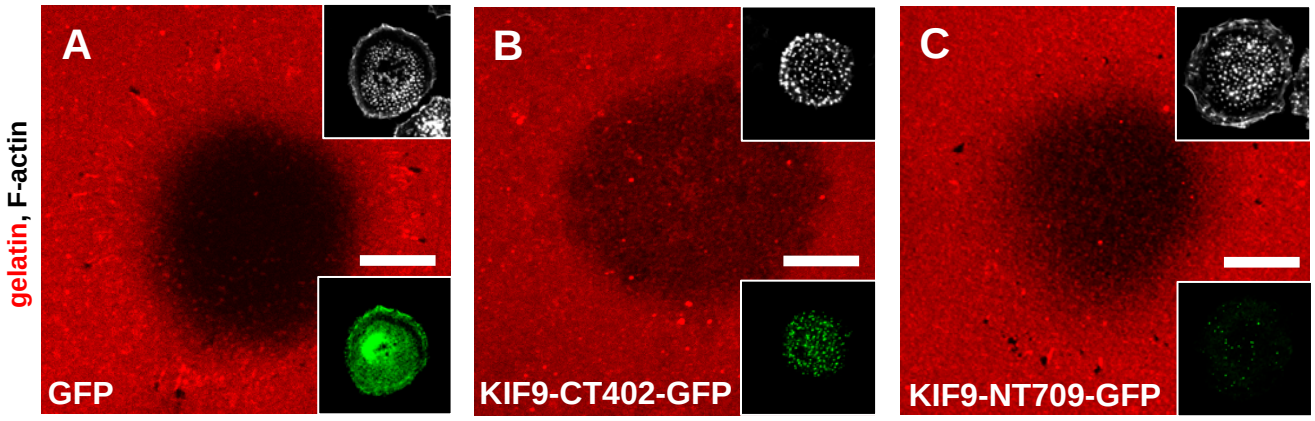
gelatin, F-actin
A
GFP
B
KIF9-CT402-GFP
C
KIF9-NT709-GFP

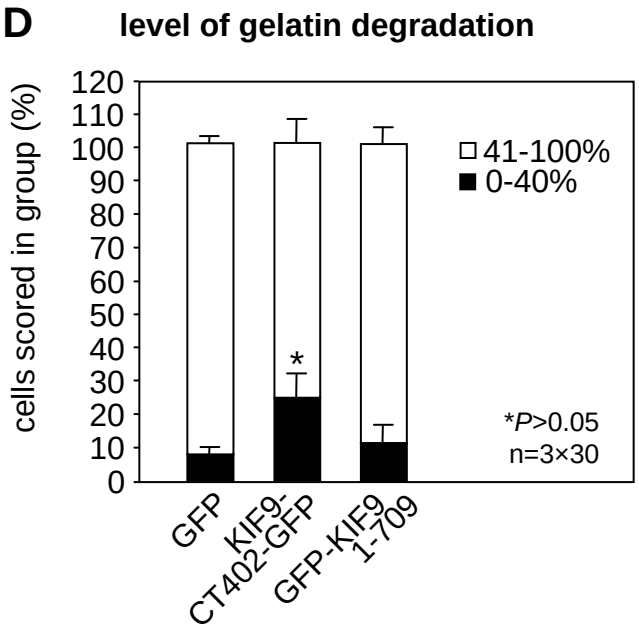
D
level of gelatin degradation
cells scored in group (%)
120
110
100
90
80
70
60
50
40
30
20
10
0
41-100%
0-40%
*
*P>0.05
n=3×30
GFP
KIF9-CT402-GFP
GFP-KIF9 1-709

Suppl. Fig. 3

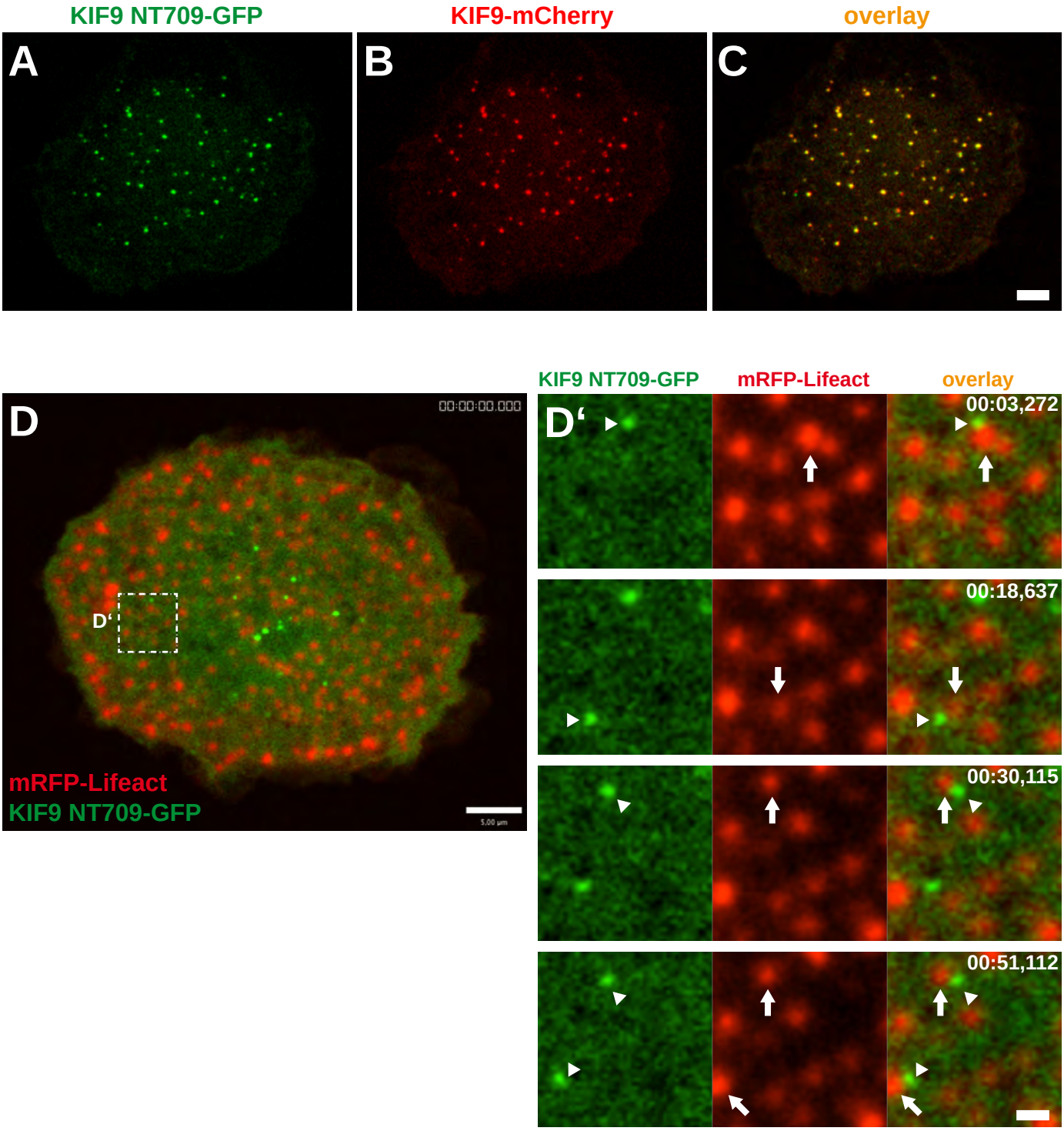
KIF9 NT709-GFP
KIF9-mCherry
overlay
A
B
C
D
00:00:00.000
D‘
mRFP-Lifeact
KIF9 NT709-GFP
5,00 µm
KIF9 NT709-GFP
mRFP-Lifeact
overlay
D‘
00:03,272
00:18,637
00:30,115
00:51,112

Suppl. Fig. 4

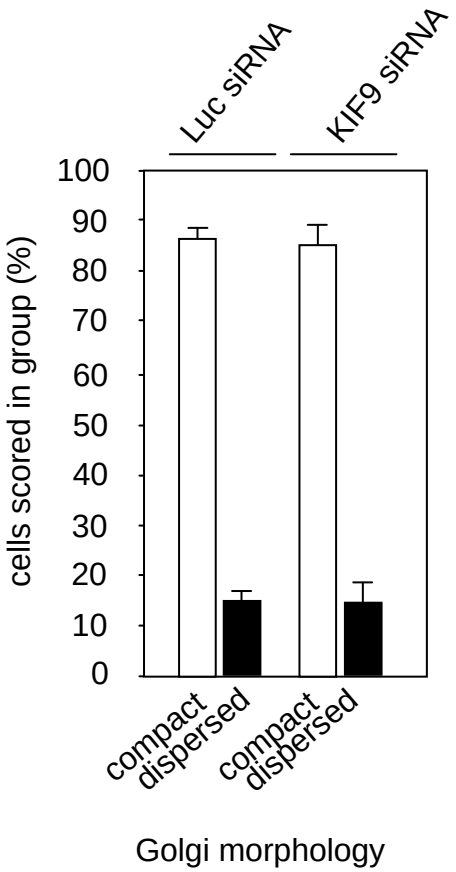
Luc siRNA
KIF9 siRNA
100
90
80
70
60
50
40
30
20
10
0
cells scored in group (%)
compact
dispersed
compact
dispersed
Golgi morphology

Suppl. Fig.5

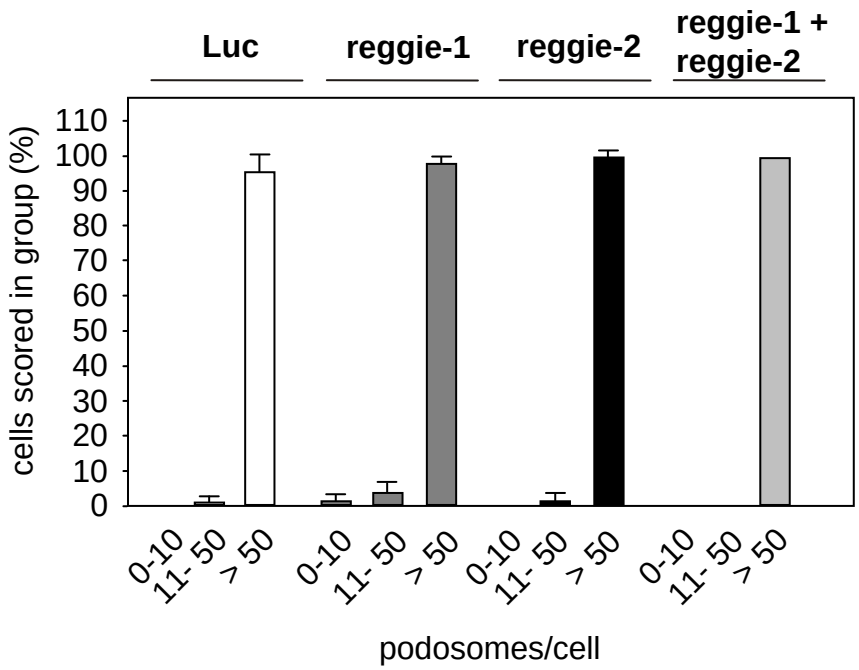
Luc
reggie-1
reggie-2
reggie-1 +
reggie-2
cells scored in group (%)
110
100
90
80
70
60
50
40
30
20
10
0
0-10
11- 50
> 50
podosomes/cell

Suppl. Fig. 6

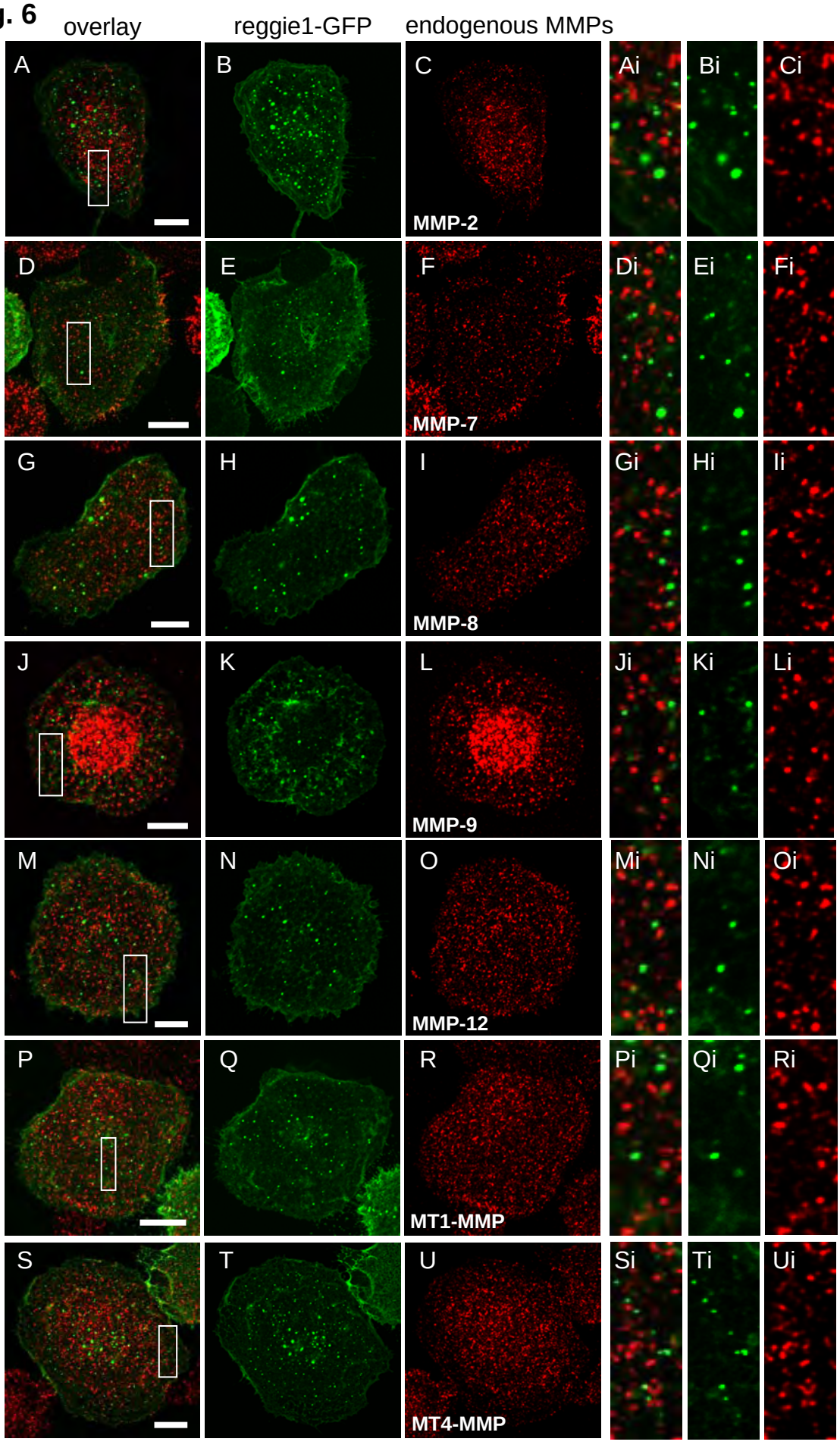
overlay
reggie1-GFP
endogenous MMPs
A
B
C
Ai
Bi
Ci
MMP-2
D
E
F
Di
Ei
Fi
MMP-7
G
H
I
Gi
Hi
Ii
MMP-8
J
K
L
Ji
Ki
Li
MMP-9
M
N
O
Mi
Ni
Oi
MMP-12
P
Q
R
Pi
Qi
Ri
MT1-MMP
S
T
U
Si
Ti
Ui
MT4-MMP

Suppl. Fig. 7

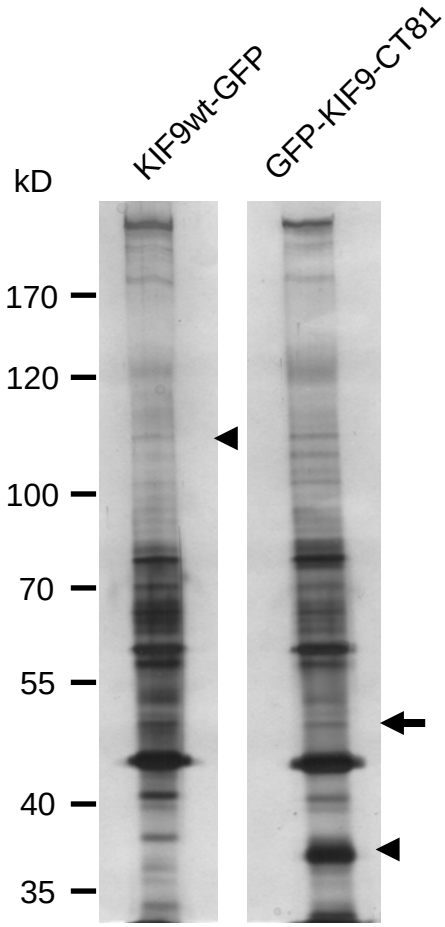

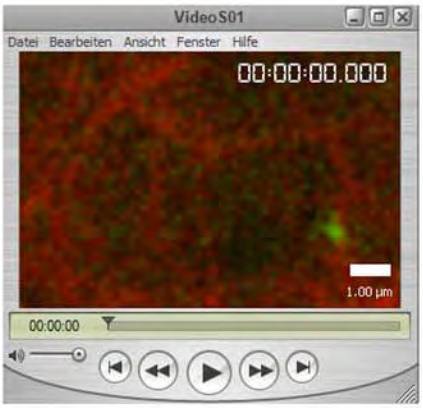

Movie S01 - KIF9-GFP vesicles move along microtubules. Primary human macrophage expressing KIF9-GFP (green) and β-tubulin-mCherry (red), labeling microtubules. Confocal time lapse series of detail region indicated in Fig. 3B. (exposure time: 350 ms for green (491 nm), 350 ms for red (561 nm), frame rate: 4 f/s; sequence: 231 s)

Movie S02 - KIF9-GFP contacts podosomes. Primary human macrophage expressing KIF9-GFP (green) and β-actin-mRFP (red), labelling podosomes. Confocal time lapse series of substrate attached part of the cell (exposure time 1000 ms for green (491 nm), 4000 ms for red (561 nm), frame rate: 10 f/s; sequence: 1225 s)

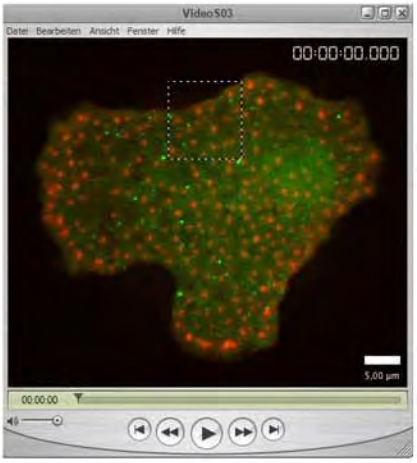

Movie S03 - KIF9-CT402-GFP positive vesicles contact podosomes. Primary human macrophage coexpressing KIF9-CT402-GFP (green) and mRFP-Lifeact (red). Note repeated, non-random contact of KIF9 construct-decorated vesicles with podosomes (labeled by mRFP-Lifeact). A dual channel confocal time lapse movie was acquired using an asynchronous mode as follows: exposure time 250ms for green (491nm) and 350ms for red (561nm), acquisition frame rate of 20 time points per minute for the green and 5 time points per minute for the red channel. Movie replay frame rate: 6 f/s; sequence length: 300 s.

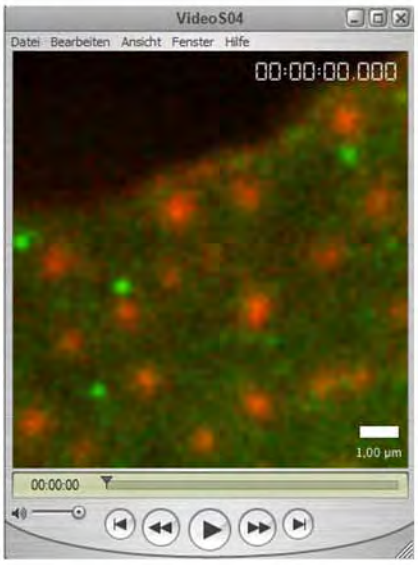

Movie S04 - Video of detail region shown in video-3.avi

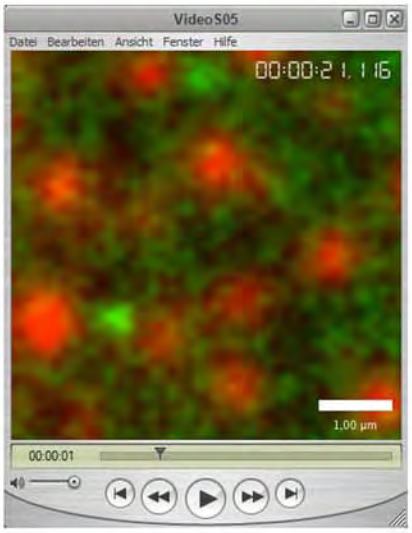

Movie S05 - KIF9-NT709-GFP positive vesicles contact podosomes. Primary human macrophage coexpressing KIF9-NT709-GFP (green) and mRFP-Lifeact (red). Note repeated, non-random contact of KIF9 construct-decorated vesicles with podosomes (labeled by mRFP-Lifeact). A dual channel confocal time lapse movie was acquired using an asynchronous mode as follows: exposure time 300ms for green (491nm) and 250ms for red (561nm), acquisition frame rate of 20 time points per minute for the green and 5 time points per minute for the red channel. Movie replay frame rate: 4 f/s; sequence length: 111 s

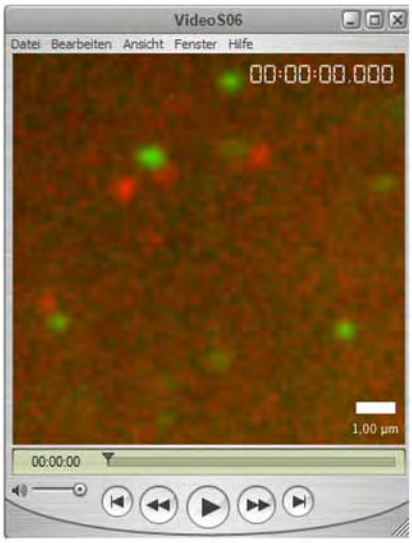

Movie S06 - Reggie1-GFP and KIF9-mCherry vesicles contact each other. Primary human macrophage expressing reggie1-GFP and KIF9-mCherry. Confocal time lapse series of detail region (G) indicated in Fig. 9G (exposure time: 500 ms for green (491nm), 1 s for red (561nm), frame rate: 6 f/s; sequence length: 10 min)

Movie S07 - Reggie1-GFP and KIF9-mCherry vesicles contact each other. Primary human macrophage expressing reggie1-GFP and KIF9-mCherry. Confocal time lapse series of detail region (H) indicated in Fig. 9H (exposure time: 250ms for green (491nm), 750ms for red (561nm), frame rate: 6 f/s; sequence length: 5 min)

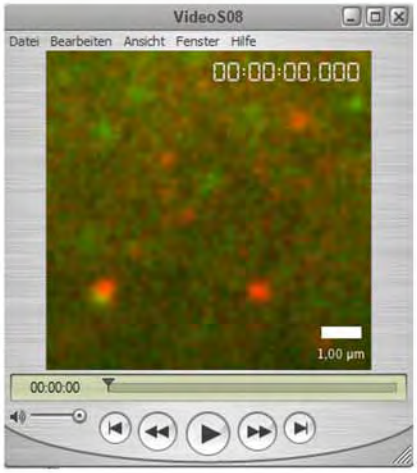

Movie S08 - Reggie1-GFP and KIF9-mCherry vesicles contact each other. Primary human macrophage expressing reggie1-GFP and KIF9-mCherry. Confocal time lapse series of detail region (H) indicated in Fig. 9H (exposure time: 250 ms for green (491nm), 750 ms for red (561nm), frame rate: 6 f/s; sequence length: 5 min).

Declaration:

Karim El azzouzi contributed to the publication:

The kinesin KIF9 and reggie/flotillin proteins regulate matrix degradation by macrophage podosomes.

Cornfine S, Himmel M, Kopp P, El Azzouzi K, Wiesner C, Krüger M, Rudel T, Linder S.

Mol Biol Cell. 2011 Jan 15;22(2):202-15. doi: 10.1091/mbc.E10-05-0394. Epub 2010 Nov 30.

by:

- Performing and analyzing experiments demonstrated in Figure 3 A-B.
- Performing and analyzing experiments demonstrated in Figure 5 A, E-G.
- Performing and analyzing experiments demonstrated in Movie S1.
- Preparing figures for the publication.

The experiments were designed by Susanne Cornfine and Stefan Linder.
The manuscript was written by Stefan Linder.

Hamburg, 03.11.2016

_____
Stefan Linder

V. DISCUSSION

1. Surface-exposed MT1-MMP localizes at podosomes and forms islets after podosome dissolution

My initial project was focusing on the study of traffic and regulation of the Matrix Metalloprotease MT1-MMP in macrophages. During the last years, podosomes, described as an actin-rich structures found on the ventral surface of the plasma membrane, have emerged as the major adhesion and invasion-relevant structures of macrophages and other monocytic cells such as dendritic cells[23]. Moreover, podosomes constitute multifunctional organelles that combine several key functions of invasive cells, including adhesion, sensing of rigidity and topology of the substratum, as well as matrix degradation[33,82,32]. MMPs in general, including MMP-2, MMP-9 and MT1-MMP, have been described previously to be enriched in invadosomes and particularly in invadopodia[83,84,85], which are specialized actin-based membrane protrusions present in invasive tumor cells. The presence of these enzymes explains how ECM degradation is achieved by podosomes and invadopodia. Despite being the “master switch” protease and the major collagenase responsible of the remodeling of the ECM, MT1-MMP traffic and regulation still need to be clarified. In fact, following MT1-MMP traffic from its synthesis in the Golgi to its delivery to the ventral surface of macrophages seems to be challenging. It was reported that MT1-MMP vesicles require an intact microtubule system[86] for the long distance range transport. The anterograde transport of this protease is powered by kinesin family-5B (KIF5B) and kinesin family-3A/3B (KIF3A/KIF3B) kinesins, ensuring an enrichment of MT1-MMP at podosomes at the ventral surface of the cell. Although MT1-MMP vesicles are able to dynamically contact podosomes with a speed deceleration in the vicinity of the podosomes ring[81], the precise localization of MT1-MMP at the plasma membrane at the level of the ventral surface was never shown.

Using total internal reflection fluorescence (TIRF) live-cell imaging of primary human macrophages and a green fluorescent protein (GFP) variant fluorophore called “pHluorin” characterized by its sensitivity to pH variation, I could show for the first time that surface-exposed MT1-MMP is present at podosomes. This observation

resolves the missing spatial connection between podosomes as a matrix degradative structure and the enzyme MT1-MMP as the actual ECM degrading machinery.
Furthermore, podosome formation and upkeep depend on actin nucleation by Arp2/3 complex[87], so I treated macrophages with CK-666 to inhibit Arp2/3 complex. Addition of CK-666 led to disruption of podosomes and showed another novel localization of surface-exposed MT1-MMP, where it localizes at dot-like “islets” that are embedded in the ventral plasma membrane, and are free of podosome components. These islets can form either naturally during dynamic formation/dissolution of podosomes or by chemical disruption of podosomes, using drugs inhibiting actin nucleation and targeting the Arp2/3 complex. The apparition of MT1-MMP islets upon podosome dissolution clearly illustrates the capacity of podosomes to imprint MT1-MMP in the plasma membrane, especially because these islets persist beyond the regular lifetime of a podosome. To assess the relation between islets and podosomes. I seeded nonadherent macrophages under conditions inhibiting podosome formation. It was reported that β1, β2 and β3 integrins were necessary to form podosomes in osteoclasts[88] also, murine dendritic cells lacking β2 integrin failed to form podosomes[89]. Cells seeded in the presence of the integrin-binding peptide RGD, inhibiting integrin-based adhesion[90], thus inhibiting formation of integrin-based podosomes, did not attach properly to the glass surface and failed to form podosomes and islets. We can conclude that podosomes are a prerequisite for islets formation, which appear as a result of podosome disruption after CK-666 treatment.

In addition, preliminary tracking of podosomes, podosome-associated MT1-MMP and MT1-MMP islets showed that podosomes and podosome-associated MT1-MMP display a dynamic co-distribution, whereas MT1-MMP islets have a more static distribution. Further advanced tracking experiments showed that podosome cores display a high variability of track orientation and length, in contrast to podosome-associated MT1-MMPs, which are displaying a more uniform distribution with extremely short tracks. The fact that podosome cores and podosome-associated MT1-MMP share the same localization, raises the question of a possible connection between these two structures. The analysis of lifetime of F-actin podosome cores and podosome-associated MT1-MMP highlight, the long lifetime of the podosome-associated MT1-MMP where approximately half of them persisted for more than 50 minutes. In contrast, only 18.49% of podosome cores persisted for such a long

period. I also observed that MT1-MMP islets can persist for over than 1 hour in comparison to the relative short lifetime of podosomes (2-12 minutes)[24]. In terms of movement, I showed that podosome-associated MT1-MMP has a restricted lateral movement of 2.9 ± 0.6 µm In comparison to podosomes (4.2 ± 0.8 µm) during 1 hour of observation, this observation was even more pronounced for MT1-MMP islets, where the small observed lateral movement is most likely driven by the global mobility of the membrane.

A model of invadopodia, another actin-rich protrusion structure associated with degradation of the ECM and cancer invasion[33], suggests that MT1-MMP affects invadopodia dynamics in the formation and stability phases. MT1-MMP knockdown (KD) leads to a decrease in the median lifetime of invadopodia from 45.5 to 35.5 minutes[91] in breast cancer cells. This result suggests a positive feedback of MT1-MMP at invadopodia. The invadopodia model places MT1-MMP downstream of adhesion ring components at a later stage of invadopodia formation (**Figure 7**), because the inhibition of adhesion signaling decreases the recruitment of MT1-MMP at invadopodia, where MT1-MMP knockdown did not reduce the number of adhesion-ringed invadopodia[91].

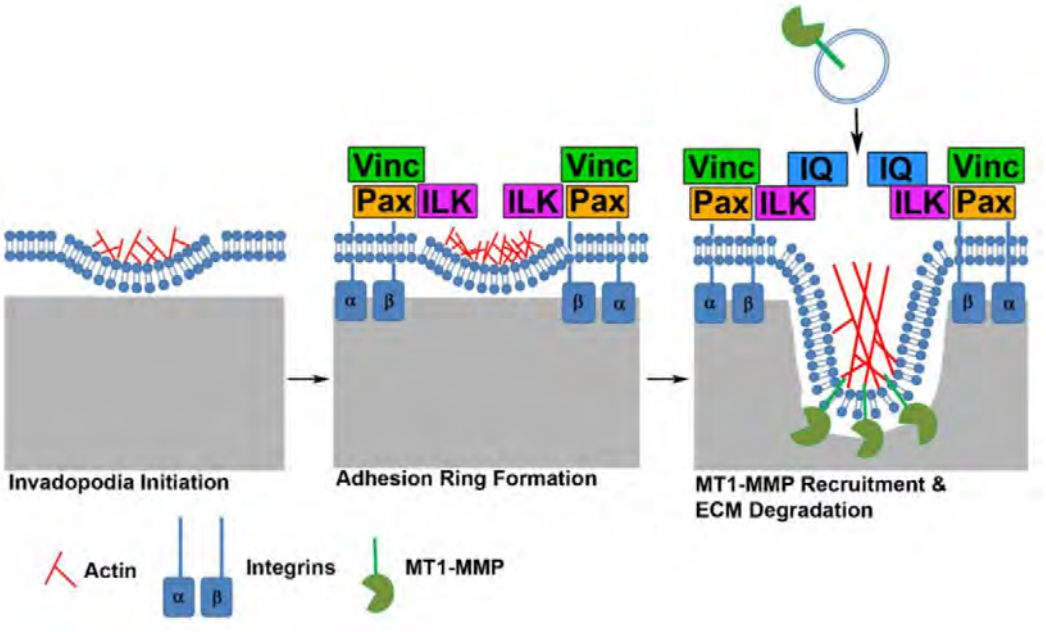

Figure 7. Model of invadopodium maturation. *Initial actin puncta appearance is followed by adhesion ring structure formation including integrins (α, β), ILK, paxillin (Pax) and vinculin (Vinc). Ring formation leads to enhanced MT1-MMP recruitment and ECM degradation by invadopodia*[91].

Despite the complete different dynamics of invadopodia and podosomes, MT1-MMP persists for a long time in both structures, which could indicate, that MT1-MMP dynamic is not specific to invadopodia or podosomes. It is still unclear if it is regulated by exocytosis, recycling endocytosis or membrane diffusion.

I showed that islets do not contain F-actin, raising the question about the existence of other podosome core or ring components at islets. Among a long list of proteins, I found neither typical core components such as Arp2, tyrosine kinase substrate 5 (Tks5) nor ring components (vinculin, talin and paxillin) in islets. However, since MT1-MMP is a transmembrane endopeptidase, I did expect the presence of transmembrane receptors and proteins that mediate cell-matrix interaction. As mentioned above, integrins can dock MT1-MMP in invadopodia and in endothelial cells, a hypothesis explaining the enhancement of invadopodia lifetime could be based on the capacity of MT1-MMP to interact with integrins via direct docking[92,93]. Also, MT1-MMP can be found associated with integrin αvβ3 in cellular microdomains called caveolae[94] characterized by enriched cholesterol plasma membrane invaginations. We looked therefore for the presence of integrins at islets. We could not detect β1, β2 and β3 integrins at these structures. Kindlin-3 and talin-1, which are integrin activators were also absent from islets. In addition, the hyaluronan receptor CD44, also a transmembrane protein, was also not colocalising with the islets, despite the fact that CD44 is important for adhesion and cell matrix interactions[63], and despite its capacity to bind MT1-MMP.
MT1-MMP is also known for its association with caveolin-1 in lipid membrane rafts in human endothelial cells[95]. Based on these observations, I investigated whether the islets present some specificities in term of membrane topography or lipid composition. It is known that lipid rafts are enriched in cholesterol, and it was also established that phosphatidylinositol 4-phosphate PI(4)P can induce curvature in biological membrane[96]. Although we found an enrichment of cholesterol and PI(4)P at podosomes, this enrichment was completely lost when podosomes were disrupted to form islets. MT1-MMP islets from this first glance seem to contain only the protease MT1-MMP. However, an extensive characterization of islets components needs to be done, to elucidate the presence of potential markers at islets using mass spectrometry.

Once I characterized the MT1-MMP islet composition, I focused on their potential function and biological significance. I observed during normal live cell imaging that podosomes tend to re-form at islets. Indeed, we and many other labs observed over the years that podosomes had a tendency to reappear at sites of previous podosome formation. However, an explanation or a molecular mechanism for this phenomenon was missing. In order to quantify this phenomenon, I artificially induced podosome disruption by inhibiting F-actin nucleation by blocking Arp2/3 complex activity using the chemical inhibitor CK-666[97]. After a 10 minutes washout of the Arp2/3 inhibitor, I found that more than 60% of islets are reused to form podosomes. This occurs by recruitment of new material (*de novo* actin nucleation) or by recruitment of actin from neighbouring pre-existing podosomes (fission). I could thus show a new mechanism of podosome reformation, where MT1-MMP functions as a landmark for podosome reformation.

I suggest a novel mechanism where MT1-MMP plays the role of a memory device capable of generating new podosomes as explained in **Figure 8**. We demonstrated that MT1-MMP is recruited after podosome formation, and we think that MT1-MMP recruitment to podosomes occurs in a similar way to invadopodia. Once the podosomes are disrupted, podosome-associated MT1-MMP becomes apparent as islets, and can then be used as a memory device for podosomes reemergence by either two mechanisms: *de novo* actin nucleation, or recruitment of fission-generated material.

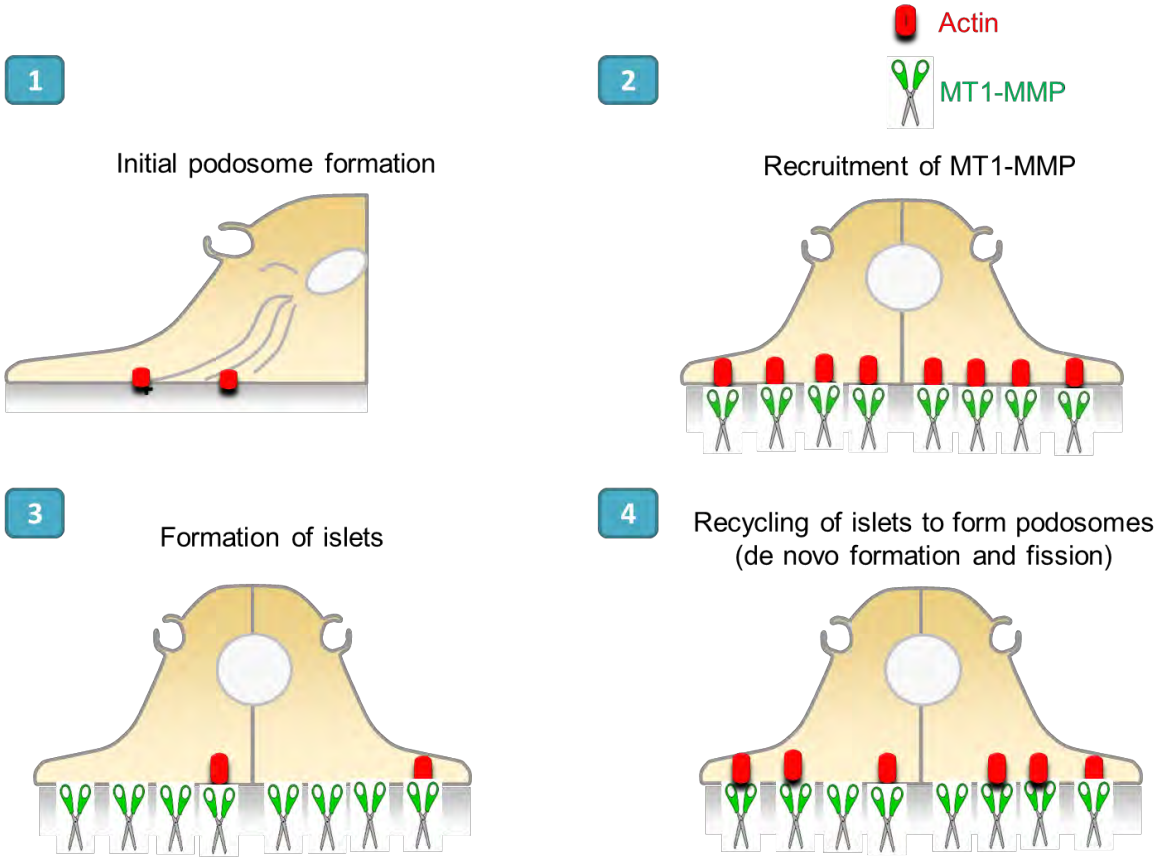

Figure 8. Suggested model for formation of podosome-associated MT1-MMP and MT1-MMP islets during formation of podosomes.
1, Cells start the initial steps of adhesion by forming the first podosomes.
2, Podosomes are formed, and subsequently enriched in MT1-MMP.
3, Podosome dissolution results in MT1-MMP islets formation.
4, MT1-MMP act as a memory device for the reformation of podosomes, either by de novo actin nucleation, or recruitment of fission generated material.

2. Islet formation depends on the cytoplasmic tail of MT1-MMP, and its actin binding activity

In order to clarify which domains of MT1-MMP are responsible for its specific localization at islets, I generated multiple deletions and mutated MT1-MMP constructs. It was clear that islets are formed by enrichment of MT1-MMP at dot like pattern, suggesting the possibility of formation of oligomers at these domains. In fact, MT1-MMP forms homodimers, which are important mainly for two functions: 1) ensuring the activation of proMMP2 through a tertiary complex (MT1-MMP, TIMP-2, and MMP-2) essential for the cleavage of type IV collagen[98] which is a component of the basal membrane and a substrate of MT1-MMP[99], 2) degradation of collagen by

MT1-MMP[100]. **Figure 9** shows how the dimerization among other positive regulators induces activation of MMP-2 and MMP-13, processing of ECM, shedding of CD44 in order to enhance cell migration and invasion.

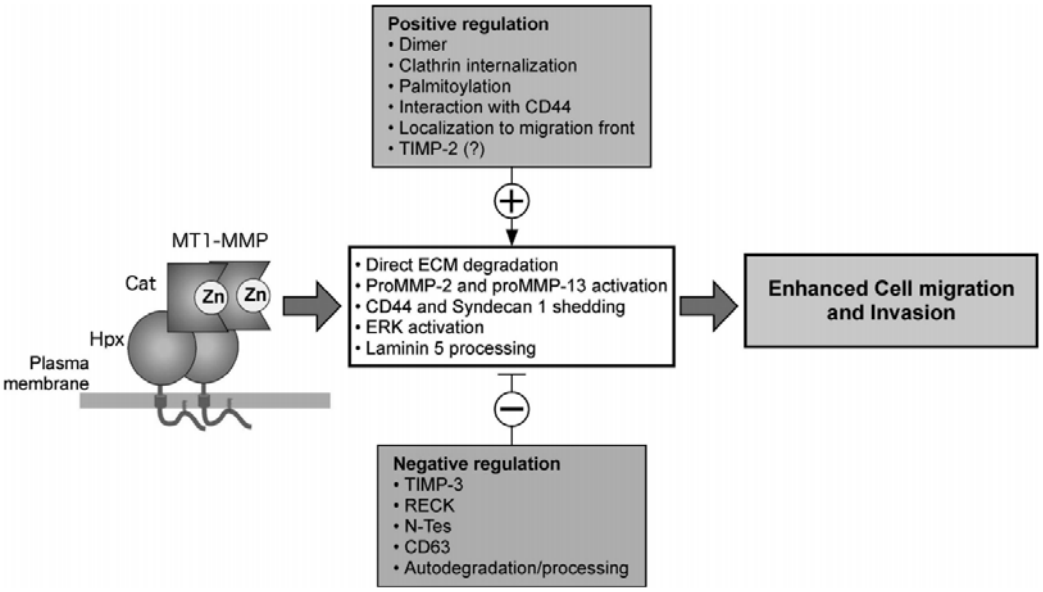

Figure 9. Biological activities of MT1-MMP and their regulation. *MT1-MMP enhances cell migration and invasion by direct ECM degradation, activation of proMMP-2 and proMMP-13, CD44 and syndecan-1 shedding. These activities are positively and negatively regulated by a variety of processes. Disturbing one of the positive regulation processes may be enough to inhibit MT1-MMP-dependent cell migration*[67]*.*

First, the analysis of mutation constructs revealed that only the cytoplasmic tail of MT1-MMP is crucial for its localization at podosomes and islets. Although oligomerization seem to be important for the activation of MT1-MMP as mentioned above, cells transfected with the mutated hemopexin domain of MT1-MMP (DTY/KAF)[101] did form podosomes and islets. The same result was obtained when macrophages were transfected with the catalytic mutated domain construct (E240A)[102].

The relevance of the hemopexin domain and collagenase activity on controlling islets formation was also assessed using chemical inhibition under NSC405020 treatment, a noncatalytic inhibitor of MT1-MMP. NSC405020 affects homodimerization by interacting directly with the hemopexin domain of MT1-MMP, which leads to an inhibition of its collagenase activity. The islets were formed normally after treatment with NSC405020, ruling out the implication of the hemopexin involved in the

oligomerization and the catalytic domain on islet formation and confirming the results obtained with the mutation constructs.

Second, the analysis of deletion mutation constructs revealed the role of the MT1-MMP C-terminus in proper localization of the protease at podosome and islets. The deletion of the C-terminus leads to a loss of the islet pattern and a diffuse localization in the plasma membrane. However, the deletion of the N-terminus, which constitutes the major part of this protease, did not perturb the localization of MT1-MMP at podosomes and islets.

The C-terminal domain is intracellular and contains only 20 amino acids. Despite its small size, the C-terminus is involved in multiple functions. It is involved in the internalization of MT1-MMP through its di-leucine ($Leu^{571-572}$ and $Leu^{578-579}$) and tyrosine ^{573} residues[103]. The LLY^{573} motif in particular binds adaptor protein 2 (AP-2), a component of clathrin coated pits [103]. This motif plays also a role in the activation of MT1-MMP by furins through the interaction with the peripheral Golgi matrix protein Golgi reassembly stacking protein 55 (GRASP55). Moreover LLY^{573} interacts *in vitro* with actin[104] in invadopodia. It's also noteworthy that MT1-MMP cytoplasmic tail can be phosphorylated at Thr^{567}, leading to an enhanced invasion in 3D type I collagen[105], making the cytoplasmic tail of MT1-MMP a target of choice for further investigations.

I previously described that podosomes, actin-rich structures do colocalize with MT1-MMP organized dot like pattern, but once podosomes are disrupted during normal podosomes turnover or chemical inhibition of actin branching (Arp2/3 complex inhibition), MT1-MMP persists in the form of islets although the podosome cores disappeared, which raises the question of the possible persistence of an interaction between MT1-MMP and the other forms of cortical F-actin. Podosome disruption was induced by the Arp2/3 inhibitor CK-666, affecting only branched actin. This leaves unbranched actin at the cell cortex as a potential interactor for the LLY motif. This hypothetic interaction might anchor the protease in the specific local dot like pattern and explain the persistence of islets independently of the presence of the F-actin podosomes cores.

Before exploring the impact of the motif LLY^{573} on islets formation, I chemically inhibited all forms of cellular actin, both branched and unbranched, by combining cytochalasin D and latrunculin A treatments. This treatment induced a total dissolution of islets, highlighting the potential involvement of the interaction of F-actin and MT-MMP in islet persistence.

I generated MT1-MMP LLY/AAA mutant, which was rendered small interfering ribonucleic acid (siRNA) insensitive. This construct has a very low actin binding activity[105]. This construct was not able to form islets when the endogenous MT1-MMP was depleted. These combined two results, highlight the crucial role of the actin binding activity of MT1-MMP in ensuring proper formation and persistence of islets, thanks to its LLY^{573} motif within its cytoplasmic tail. It seems that the actin binding activity of this motif can be divided hypothetically in two steps during islets formation. The initial step would occur during podosome-associated MT1-MMP recruitment to podosomes, where LLY^{573} binds the branched F-actin present in podosome cores. The second step would occur during podosome core dissolution, where this time LLY^{573} binds the cortical actin to stabilize MT1-MMP islets.

I observed reformation of podosomes at islets by a fission mechanism, where the newly formed daughter podosome originates from a preexisting podosome. Considering the well-organized spatial architecture of podosomes, thanks to the high turnover of cytoplasmic actin, presence of radiating actin fibers (unbranched filaments)[106,107] and interconnecting podosomes, we can suggest that the LLY^{573} motif binds F-actin filaments originating from free floating actin bundles from the vicinity of podosomes. Those filaments could potentially be used as a basic structure for actin nucleation and for the recruitment of fission material to form podosomes.

In invadopodia, the actin-associated scaffold protein palladin plays the role of a linker between the actin cytoskeleton and MT1-MMP's protease activity[108]. Palladin is required for organization of regular actin cytoskeleton and potentially influences polymerization and assembly of both filamentous and monomeric actin[109], it can also be phosphorylated by the proto-oncogene tyrosine-protein kinase (Src)[110]. Since palladin binds specifically the MT1-MMP cytoplasmic tail, we can imagine that a similar mechanism is occurring in podosomes to explain reformation of fission independent podosomes. A fraction of MT1-MMP islets is interacting through the cytoplasmic tail with cortical actin, the other free fraction of MT1-MMP islets can

easily bind palladin and start the formation of podosome cores by recruiting Src and inducing filamentous actin formation. This mechanism could be an explanation for the formation of daughter podosomes at islets originating from pre-existing podosomes by fission.

Collectively, I provide here, for the first time, the exact localization of MT1-MMP at podosomes at the ventral cell surface in primary human macrophages. Podosomes imprint the transmembrane protease MT1-MMP to form podosome-associated MT1-MMP islets in the plasma membrane. MT1-MMP become apparent especially upon podosome dissolution, and it seem to be mainly composed of MT1-MMP itself. The islets have a similar pattern to podosomes in terms of density and size, reflecting their podosome origin. Moreover, they are reused to form podosomes, either by *de novo* formation through formation of a new pool of F-actin, or capturing of daughter podosomes that are generated by fission from pre-existing podosomes. I describe here a new function of MT1-MMP, where islets play the role of a memory device that constantly ensures the formation of new podosomes at precise locations with an equidistant pattern. This newly discovered function is independent of the proteolytic activity of MT1-MMP and describes for the first time a structural role of this protein.

3. Control of cell surface exposure of MT1-MMP, ECM degradation and invasion by RabGTPases

I showed that MT1-MMP is localized at podosomes, where matrix degradation is taking place[33]. Previously, it was also shown by our lab that transport of MT1-MMP vesicles is driven by the kinesins KIF5B and KIF3A/KIF3B[81] via the microtubule system[86] toward podosomes. However, fine tuning of the intracellular traffic of MT1-MMP in macrophages still needed to be clarified. In this part of my thesis, I helped to investigate the role of the RabGTPases, which ensure regulation of biosynthesis, endocytosis, recycling and exocytosis of MT1-MMP vesicles.

We aimed initially to identify effectors involved in MT1-MMP trafficking in primary human macrophages. Co-expression of MT1-MMP and RabGTPases showed that MT1-MMP vesicles are positive for a subset of effectors, which are Rab5a, Rab8a, Rab14, Rab21 and Rab22a. Overexpression of RabGTPases leads in some cases to

the formation of artificial giant vesicles and tubules. This artefact allowed the observation of different microdomains that RabGTPases could potentially occupy in the same MT1-MMP vesicle, without necessarily perfectly colocalizing with MT1-MMP. This distribution of RabGTPases seems to be consistent with the specific routing role of each effector. In fact, despite the large number of the RabGTPases family (more than 70), delivery of cargoes to their correct destination is ensured in a very stringent way thanks to the specific localization of each RabGTPase, but also to the presence of microdomains[77] called rab domains especially for RabGTPases sharing the same compartment or routing path.
We also confirmed that endogenous Rab5a, Rab8a, Rab14, Rab21 and Rab22a vesicles are positive for MT1-MMP to exclude that colocalization is simply an overexpression artefact. In M.D. Anderson - Metastatic Breast-231 (MDA-MB-231) cells, recruitment of MMP14 to the invasive front of these adenocarcinoma cells at invadopodia, requires Rab8[111], which mobilizes MT1-MMP from the intracellular storage compartment, is consistent with the results obtained in macrophages. The specificity of the identified RabGTPases for MT1-MMP transport was underlined by the fact that other tested RabGTPases such as Rab4, Rab6a, Rab9 and Rab11 did not show localization to MT1-MMP vesicles.

Once we identified the RabGTPases present in the MT1-MMP vesicles, we focused on the regulation of the MT1-MMP pool at the cell surface, as MT1-MMP can be re-endocytosed, and then either be recycled or degraded. The outcome of the overexpression of the dominant active and negative isoforms of RabGTPases showed that cell surface exposure of MT1-MMP is mainly regulated by Rab5a, Rab8a, Rab14, and Rab22a. This subset of RabGTPases can be divided in positive regulators Rab8a, Rab14, and Rab22a and a negative regulator Rab5a, which appears to be consistent with their described roles in the regulation of the biosynthetic, recycling and endocytic trafficking routes, respectively. Similar results were obtained when these four RabGTPases were silenced by siRNA.

As mentioned before, matrix degradation appears underneath podosomes where MT1-MMP is localized at podosomes. Prior to podosome enrichment in MT1-MMP, the protease needs to be delivered to the ventral surface of macrophages. It was described that MT1-MMP vesicles contact podosomes[81], so we decided to assess

contact events between MT1-MMP vesicles and podosomes after depletion of Rab5a, Rab8a, Rab14, Rab21, and Rab22a using siRNAs. As expected, the knockdown of the positive regulators Rab8a, Rab14, and Rab22a of MT1-MMP, induced a drastic reduction of MT1-MMP-podsome contact events. Rab8a mobilizes MT-MMP from a storage compartment[80] to reach the cell surface, explaining the reduction of contact events at podosomes after Rab8a depletion. Rab14 on the other hand localizes to an intermediate compartment prior to Rab11 and after Rab5 and Rab4 for the transferrin-recycling pathway[112]. Depletion of Rab14 induces a reduction of cell surface exposure of a disintegrin and metalloproteinase domain-containing protein 10 (ADAM10)[112], another zinc-proteases of the ADAM family. Instead, ADAM10 accumulates in a transferrin-positive endocytic compartment, which is clearly similar to what occurs to MT1-MMP vesicles in macrophages. Rab22a interacts with Early Endosome Antigen 1 (EEA1)[113], which localizes to early endosomes (EE). However the knockdown of Rab5a, which is a negative regulator of MT1-MMP, increased the number of vesicles contacting podosomes. It was also shown that Rab5a depletion significantly increased basal glucose transporter type 4 (GLUT4), another transmembrane protein, on the cell surface of adipocytes[114], supporting the role of Rab5a as a negative regulator of surface exposure of transmembrane proteins.

Combining all these results, we proposed a preliminary map of RabGTPases controlling MT1-MMP trafficking (**Figure 10**). The first RabGTPase to intervene during endocytosis is Rab5a at the stage of early endosomes formation, if the vesicle is intended to be directed toward late endosomes (LE), Rab5a will ensure recruitment of Rab7a to deliver MT1-MMP toward this compartment where vesicles follow a maturation process to form lysosomes at the end, where vesicle content is degraded. On the other hand, Rab14 by its localization to EE will drive fast recycling of MT1-MMP toward the cell surface. In case MT1-MMP vesicles are directed toward slow recycling, Rab22a will direct EE to recycling endosomes (RE), and then Rab8a will ensure the surface delivery of MT1-MMP. Rab8a is also responsible of MT1-MMP delivery to the cell surface and may control the traffic of newly synthetized MT1-MMPin the biosynthetic pathway, but also from the RE compartment or from exocytotic vesicles.

A recent article reported that Rab2a, a RabGTPase essential for ER to Golgi transport controls specifically transport of post-endocytotic MT1-MMP vesicles originating from the plasma membrane[115]. Rab2a promotes 3D invasion in breast cancer cells in a proteolytic-dependant manner. Surprisingly, depletion of Rab2a does not affect surface exposure of MT1-MMP, but impairs its endosomal recycling with an accumulation of MT1-MMP vesicles around the nucleus impairing motility of MT1-MMP-positive late endosomes[115].

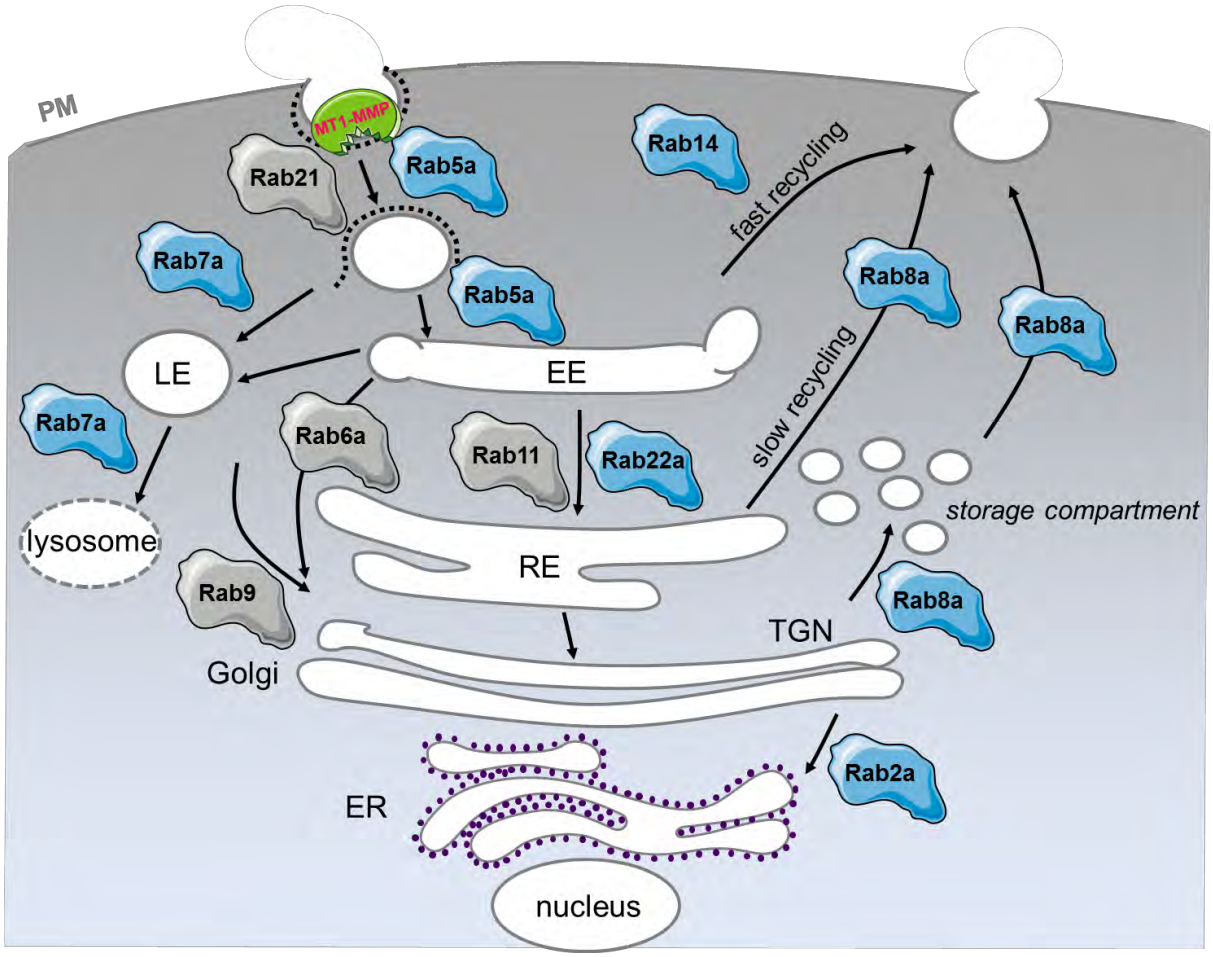

Figure 10. Proposed model of RabGTPases regulating MT1-MMP traffic. *Surface-associated MT1-MMP is uptaken by endocytosis, which is controlled by Rab5a. Parts of this pool are recycled back to the cell surface, either via fast recycling controlled by Rab14 or via slow recycling through recycling endosomes controlled by Rab22a. Trafficking of newly synthesized MT1-MMP to the cell surface is controlled by Rab8a and may occur by exocytotic vesicles or recycling endosomes. RabGTPase isoforms colocalising with MT1-MMP in macrophages are indicated at their respective compartments. In blue are represented RabGTPases that do affect either surface exposure of MT1-MMP, migration or invasion. In grey, other major RabGTPases with less impact on MT1-MMP biosynthesis and recycling pathway. MT1-MMP is represented in green.* ***EE:*** *early endosomes,* ***LE:*** *late endosomes,* ***RE:*** *recycling endosome,* ***TGN:*** *trans Golgi network.* ***PM:*** *plasma membrane*[70].

4. ECM degradation and 3D invasion are regulated by Rab5a, Rab8a, and Rab14

We identified the positive regulators Rab8a, Rab14, and Rab22a and a negative regulator Rab5a of cell surface exposure of MT1-MMP. We next wondered if the perturbation of MT1-MMP traffic and recycling by RabGTPase depletion, impacts on matrix degradation and cell invasion. On 2D gelatin and 3D collagen assays, we found a significant decrease of matrix degradation for individual knockdown of Rab8a, Rab14, and Rab22a, which is in line with the results of cell surface exposure. Rab5a was also confirmed as negative regulator since its depletion led to an increase of matrix degradation. Moreover, knockdown of Rab5a to a strong increase of invasion. This is inhibited by adding the MT1-MMP inhibitor NSC405020, thus showing that Rab5a mainly works through MT1-MMP in invasion. Interestingly, combinatory knockdown of Rab5a and Rab14 did not decrease 3D collagen dequenching. This result showed the antagonistic effect of Rab5a and agonistic effect of Rab14 with degradation levels similar to those observed in the control. On the other hand the combinatory knockdown of Rab8a and Rab14 showed a clear synergetic effect on cell invasion. However, combinatory knockdown of Rab8a and Rab14 did not show this synergy at the level of surface exposure or collagen dequenching. This could be explained by the fact that both Rab8a and Rab14 are in the same pathway regulating the traffic of MT1-MMP. It was described that proteolytic invasion involves five steps[116], including formation of leading edge protrusion, anterior formation of integrin-mediated focal interactions to the matrix, ECM breakdown, actomyosin mediated cell contraction and rear-end retraction and forward sliding of cell body[116]. The synergetic effect observed during invasion is not necessarily related to MT1-MMP traffic regulation, and could be explained by the non redundant function of Rab8a and Rab14 at one of the five described steps of proteolytic invasion. For example, in polarized HT1080 cells, large macropinosomes were reported to contain Rab8 and β1 integrins at the leading edge[117]. Also, only Rab5a[108], Rab21[118] and Rab25[79] were reported to associate with integrins, in contrast to Rab14.

We identified three effectors, Rab5a, Rab8a, and Rab14 as key players in MT1-MMP traffic. They ensure control of cell surface exposure and modulation of contact events between MT1-MMP vesicles and podosomes. Rab8a and Rab14 were identified as positive regulators of MT1-MMP traffic, while Rab5a ensures negative regulation. They are also regulating ECM degradation in 2D conditions similar to those found in barriers in physiological conditions and in 3D collagen where invasion is taking place.

For the past decade, cancer research faced disillusion with broad spectrum inhibitors blocking the proteolytic activity of MMPs. The recent findings of novel functions of MMPs, their complex interconnectivity, and the lack of understanding of their regulation, are all possible explanations for such a failure. For example, marimastat, an inhibitor targeting the catalytic zinc activity was used for treatment of metastatic breast cancer and failed because of its musculoskeletal toxicity[119]. The reason of musculoskeletal pain was the off-targeting of non-MMP metalloproteinases, such as ADAM and ADAMTS family members[120].

In this thesis, I reveal part of the RabGTPase networks regulating MT1-MMP traffic in macrophages. I also show how a small peptide present in the cytoplasmic tail of MT1-MMP is governing MT1-MMP localization at podosomes. Novel strategies could be explored to target MT1-MMP-dependent dysfunction. Due to its plethoric physiological functions, MT1-MMP needs to be targeted wisely by combining novel approaches targeting for example exocytosis, with Rab8a, Rab14, and the cytoplasmic tail of MT1-MMP as potential molecular targets.

VI. REFERENCES

1. Murray, P. J. & Wynn, T. a. Protective and pathogenic functions of macrophage subsets. *Nat. Rev. Immunol.* **11,** 723–37 (2011).
2. Wynn, T. A. & Vannella, K. M. Macrophages in Tissue Repair, Regeneration, and Fibrosis. *Immunity* **44,** 450–462 (2016).
3. Kaplan, G. Differences in the mode of phagocytosis with Fc and C3 receptors in macrophages. *Scand. J. Immunol.* **6,** 797–807 (1977).
4. Yona, S. *et al.* Fate Mapping Reveals Origins and Dynamics of Monocytes and Tissue Macrophages under Homeostasis. *Immunity* **38,** 79–91 (2013).
5. Merad, M. *et al.* Langerhans cells renew in the skin throughout life under steady-state conditions. *Nat. Immunol.* **3,** 1135–1141 (2002).
6. Schulz, C. *et al.* A Lineage of Myeloid Cells independent of Myb and Hematopoietic Stem Cells. *Science (80-.).* **336,** 86–90 (2012).
7. Mosser, D. M. & Edwards, J. P. Exploring the full spectrum of macrophage activation. *Nat. Rev. Immunol.* **8,** 958–69 (2008).
8. Deshmane, S. L., Kremlev, S., Amini, S. & Sawaya, B. E. Monocyte Chemoattractant Protein-1 (MCP-1): An Overview. *J. Interf. Cytokine Res.* **29,** 313–326 (2009).
9. Mantovani, A., Bottazzi, B., Colotta, F., Sozzani, S. & Ruco, L. The origin and function of tumor-associated macrophages. *Immunol Today* **13,** 265–270 (1992).
10. Lin, E. Y., Nguyen, A. V, Russell, R. G. & Pollard, J. W. Colony-stimulating factor 1 promotes progression of mammary tumors to malignancy. *J. Exp. Med.* **193,** 727–40 (2001).
11. Sica, A., Schioppa, T., Mantovani, A. & Allavena, P. Tumour-associated macrophages are a distinct M2 polarised population promoting tumour progression: Potential targets of anti-cancer therapy. *Eur. J. Cancer* **42,** 717–727 (2006).
12. Klimp, A. H. *et al.* Expression of cyclooxygenase-2 and inducible nitric oxide synthase in human ovarian tumors and tumor-associated macrophages. *Cancer Res.* **61,** 7305–9 (2001).
13. Sindrilaru, A. *et al.* An unrestrained proinflammatory M1 macrophage population induced by iron impairs wound healing in humans and mice. *J. Clin. Invest.* **121,** 985–997 (2011).
14. Coussens, L. M., Zitvogel, L. & Palucka, a K. Neutralizing tumor-promoting chronic inflammation: a magic bullet? *Science* **339,** 286–91 (2013).
15. Allavena, P., Sica, A., Solinas, G., Porta, C. & Mantovani, A. The inflammatory micro-environment in tumor progression: The role of tumor-associated macrophages. *Critical Reviews in Oncology/Hematology* **66,** 1–9 (2008).
16. Gordon, S. Alternative activation of macrophages. *Nat Rev Immunol* **3,** 23–35 (2003).
17. Mantovani, A. *et al.* The chemokine system in diverse forms of macrophage activation and polarization. *Trends in Immunology* **25,** 677–686 (2004).
18. Cassol, E., Cassetta, L., Rizzi, C., Alfano, M. & Poli, G. M1 and M2a polarization of human monocyte-derived macrophages inhibits HIV-1 replication by distinct mechanisms. *J. Immunol.* **182,** 6237–46 (2009).
19. Martinez, F. O., Sica, A., Mantovani, A. & Locati, M. Macrophage activation

and polarization. *Front. Biosci.* **13,** 453–61 (2008).
20. Tarone, G., Cirillo, D., Giancotti, F. G., Comoglio, P. M. & Marchisio, P. C. Rous sarcoma virus-transformed fibroblasts adhere primarily at discrete protrusions of the ventral membrane called podosomes. *Exp. Cell Res.* **159,** 141–157 (1985).
21. Marchisio, P. C., Cirillo, D., Teti, A., Zambonin-Zallone, A. & Tarone, G. Rous sarcoma virus-transformed fibroblasts and cells of monocytic origin display a peculiar dot-like organization of cytoskeletal proteins involved in microfilament-membrane interactions. *Exp. Cell Res.* **169,** 202–214 (1987).
22. Linder, S. Invadosomes at a glance. *J. Cell Sci.* **122,** 3009–3013 (2009).
23. Burns, S., Thrasher, A. J., Blundell, M. P., Machesky, L. & Jones, G. E. Configuration of human dendritic cell cytoskeleton by Rho GTPases, the WAS protein, and differentiation. *Blood* **98,** 1142–1149 (2001).
24. Destaing, O., Saltel, F., Géminard, J.-C., Jurdic, P. & Bard, F. Podosomes Display Actin Turnover and Dynamic Self- Organization in Osteoclasts Expressing Actin-Green Fluorescent Protein □ V. *Mol. Biol. Cell* **14,** 407–416 (2003).
25. Osiak, A. E., Zenner, G. & Linder, S. Subconfluent endothelial cells form podosomes downstream of cytokine and RhoGTPase signaling. *Exp. Cell Res.* **307,** 342–353 (2005).
26. Varon, C. *et al.* Transforming growth factor beta induces rosettes of podosomes in primary aortic endothelial cells. *Mol. Cell. Biol.* **26,** 3582–3594 (2006).
27. Lehti, K., Lohi, J., Juntunen, M. M., Pei, D. & Keski-Oja, J. Oligomerization through Hemopexin and Cytoplasmic Domains Regulates the Activity and Turnover of Membrane-type 1 Matrix Metalloproteinase*. (2002). doi:10.1074/jbc.M109128200
28. Linder, S. & Aepfelbacher, M. Podosomes: Adhesion hot-spots of invasive cells. *Trends in Cell Biology* **13,** 376–385 (2003).
29. Dovas, A. & Cox, D. Signaling networks regulating leukocyte podosome dynamics and function. *Cellular Signalling* **23,** 1225–1234 (2011).
30. Mersich, A. T., Miller, M. R., Chkourko, H. & Blystone, S. D. The formin FRL1 (FMNL1) is an essential component of macrophage podosomes. *Cytoskeleton* **67,** 573–585 (2010).
31. Bhuwania, R. *et al.* Supervillin couples myosin-dependent contractility to podosomes and enables their turnover. *J. Cell Sci.* jcs.100032- (2012). doi:10.1242/jcs.100032
32. Linder, S., Wiesner, C. & Himmel, M. Degrading Devices: Invadosomes in Proteolytic Cell Invasion. *Annu. Rev. Cell Dev. Biol.* **27,** 185–211 (2011).
33. Murphy, D. A. & Courtneidge, S. A. The 'ins' and 'outs' of podosomes and invadopodia: characteristics, formation and function. *Nat. Rev. Mol. Cell Biol.* **12,** 413–26 (2011).
34. Linder, S. The matrix corroded: podosomes and invadopodia in extracellular matrix degradation. *Trends Cell Biol.* **17,** 107–17 (2007).
35. Labernadie, A. *et al.* Protrusion force microscopy reveals oscillatory force generation and mechanosensing activity of human macrophage podosomes. *Nat. Commun.* **5,** 5343 (2014).
36. Collin, O. *et al.* Spatiotemporal dynamics of actin-rich adhesion microdomains: influence of substrate flexibility. *J. Cell Sci.* **119,** 1914–25 (2006).
37. Kessenbrock, K., Plaks, V. & Werb, Z. Matrix Metalloproteinases: Regulators of

the Tumor Microenvironment. *Cell* **141,** 52–67 (2010).
38. Mott, J. D. & Werb, Z. Regulation of matrix biology by matrix metalloproteinases. *Current Opinion in Cell Biology* **16,** 558–564 (2004).
39. Holmbeck, K., Bianco, P., Yamada, S. & Birkedal-Hansen, H. MT1-MMP: A tethered collagenase. *Journal of Cellular Physiology* **200,** 11–19 (2004).
40. Folgueras, A. R., Pendás, A. M., Sánchez, L. M. & López-Otín, C. Matrix metalloproteinases in cancer: From new functions to improved inhibition. *International Journal of Developmental Biology* **48,** 411–424 (2004).
41. Overall, C. M. & López-Otín, C. Strategies for MMP inhibition in cancer: innovations for the post-trial era. *Nat. Rev. Cancer* **2,** 657–672 (2002).
42. Löffek, S., Schilling, O. & Franzke, C.-W. Series 'matrix metalloproteinases in lung health and disease': Biological role of matrix metalloproteinases: a critical balance. *Eur. Respir. J.* **38,** 191–208 (2011).
43. Broadus, J. & Doe, C. Q. Evolution of neuroblast identity: seven-up and prospero expression reveal homologous and divergent neuroblast fates in Drosophila and Schistocerca. *Development* **121,** 3989–3996 (1995).
44. Page-McCaw, A., Ewald, A. J. & Werb, Z. Matrix metalloproteinases and the regulation of tissue remodelling. *Nat. Rev. Mol. Cell Biol.* **8,** 221–33 (2007).
45. Butler, G. S., Will, H., Atkinson, S. J. & Murphy, G. Membrane-type-2 matrix metalloproteinase can initiate the processing of progelatinase A and is regulated by the tissue inhibitors of metalloproteinases. *Eur. J. Biochem.* **244,** 653–7 (1997).
46. Sato, H. *et al.* A matrix metalloproteinase expressed on the surface of invasive tumour cells. *Nature* **370,** 61–65 (1994).
47. Sato, T. *et al.* Identification of the membrane-type matrix metalloproteinase MT1-MMP in osteoclasts. *J. Cell Sci.* **110 (Pt 5,** 589–96 (1997).
48. Hiraoka, N., Allen, E., Apel, I. J., Gyetko, M. R. & Weiss, S. J. Matrix metalloproteinases regulate neovascularization by acting as pericellular fibrinolysins. *Cell* **95,** 365–377 (1998).
49. Itoh, Y. & Nagase, H. Matrix metalloproteinases in cancer. *Essays Biochem.* **38,** 21–36 (2002).
50. Visse, R. & Nagase, H. Matrix metalloproteinases and tissue inhibitors of metalloproteinases: Structure, function, and biochemistry. *Circulation Research* **92,** 827–839 (2003).
51. Gonzalo, P., Moreno, V., Gálvez, B. G. & Arroyo, A. G. MT1-MMP and integrins: Hand-to-hand in cell communication. *BioFactors* **36,** 248–254 (2010).
52. Tokuraku, M., Sato, H., Watanabe, Y. & Seiki, M. Expression of membrane-type matrix metalloproteinase (MT-MMP) and activation of MMP-2 in lung cancer. *Nippon rinsho. Japanese journal of clinical medicine* **53,** 1822–1826 (1995).
53. Knäuper, V. *et al.* Cellular mechanisms for human procollagenase-3 (MMP-13) activation. Evidence that MT1-MMP (MMP-14) and gelatinase A (MMP-2) are able to generate active enzyme. *J. Biol. Chem.* **271,** 17124–17131 (1996).
54. Itoh, Y. Membrane-type matrix metalloproteinases: Their functions and regulations. *Matrix Biol.* **44–46,** 207–223 (2015).
55. Holmbeck, K. *et al.* MT1-MMP-deficient mice develop dwarfism, osteopenia, arthritis, and connective tissue disease due to inadequate collagen turnover. *Cell* **99,** 81–92 (1999).
56. Ohkawara, H., Ikeda, K., Ogawa, K. & Takeishi, Y. MEMBRANE TYPE 1-MATRIX METALLOPROTEINASE (MT1-MMP) IDENTIFIED AS A

MULTIFUNCTIONAL REGULATOR OF VASCULAR RESPONSES. *Fukushima J. Med. Sci.* (2015). doi:10.5387/fms.2015-15
57. Egeblad, M. & Werb, Z. New functions for the matrix metalloproteinases in cancer progression. *Nat Rev Cancer* **2,** 161–74 (2002).
58. Golubkov, V. S. *et al.* Membrane type-1 matrix metalloproteinase (MT1-MMP) exhibits an important intracellular cleavage function and causes chromosome instability. *J. Biol. Chem.* **280,** 25079–25086 (2005).
59. Chun, T. H. *et al.* MT1-MMP-dependent neovessel formation within the confines of the three-dimensional extracellular matrix. *J. Cell Biol.* **167,** 757–767 (2004).
60. Hotary, K., Allen, E., Punturieri, A., Yana, I. & Weiss, S. J. Regulation of cell invasion and morphogenesis in a three-dimensional type I collagen matrix by membrane-type matrix metalloproteinases 1, 2, and 3. *J. Cell Biol.* **149,** 1309–23 (2000).
61. Sabeh, F. *et al.* Tumor cell traffic through the extracellular matrix is controlled by the membrane-anchored collagenase MT1-MMP. *J. Cell Biol.* **167,** 769–781 (2004).
62. Pei, D. & Weiss, S. J. Transmembrane-deletion mutants of the membrane-type matrix metalloproteinase-1 process progelatinase A and express intrinsic matrix-degrading activity. *J. Biol. Chem.* **271,** 9135–9140 (1996).
63. Naor, D., Sionov, R. V & Ish-Shalom, D. CD44: structure, function, and association with the malignant process. *Adv. Cancer Res.* **71,** 241–319 (1997).
64. Kajita, M. *et al.* Membrane-type 1 matrix metalloproteinase cleaves CD44 and promotes cell migration. *J. Cell Biol.* **153,** 893–904 (2001).
65. Itoh, Y. *et al.* Homophilic complex formation of MT1-MMP facilitates proMMP-2 activation on the cell surface and promotes tumor cell invasion. *EMBO J.* **20,** 4782–4793 (2001).
66. Deryugina, E. I. *et al.* MT1-MMP initiates activation of pro-MMP-2 and integrin αvβ3 promotes maturation of MMP-2 in breast carcinoma cells. *Exp. Cell Res.* **263,** 209–223 (2001).
67. Itoh, Y. MT1-MMP: a key regulator of cell migration in tissue. *IUBMB Life* **58,** 589–96 (2006).
68. Stenmark, H. Rab GTPases as coordinators of vesicle traffic. *Nat. Rev. Mol. Cell Biol.* **10,** 513–25 (2009).
69. Zerial, M. & McBride, H. Rab proteins as membrane organizers. *Nat. Rev. Mol. Cell Biol.* **2,** 107–117 (2001).
70. Wiesner, C., El Azzouzi, K. & Linder, S. A specific subset of RabGTPases controls cell surface exposure of MT1-MMP, extracellular matrix degradation and three-dimensional invasion of macrophages. *J. Cell Sci.* **126,** 2820–33 (2013).
71. Zhen, Y. & Stenmark, H. Cellular functions of Rab GTPases at a glance. *J. Cell Sci.* **128,** 3171–3176 (2015).
72. Bhuin, T. & Roy, J. K. Rab proteins: The key regulators of intracellular vesicle transport. *Experimental Cell Research* **328,** 1–19 (2014).
73. Ullrich, O. *et al.* Rab GDP dissociation inhibitor as a general regulator for the membrane association of rab proteins. *J. Biol. Chem.* **268,** 18143–18150 (1993).
74. Hume, A. N. *et al.* Rab27a regulates the peripheral distribution of melanosomes in melanocytes. *J. Cell Biol.* **152,** 795–808 (2001).
75. Militello, R. & Colombo, M. I. Small GTPases as regulators of cell division.

Commun. Integr. Biol. **6,** e25460 (2013).
76. Hammer, J. A. & Wu, X. S. Rabs grab motors: Defining the connections between Rab GTPases and motor proteins. *Current Opinion in Cell Biology* **14,** 69–75 (2002).
77. Sönnichsen, B., De Renzis, S., Nielsen, E., Rietdorf, J. & Zerial, M. Distinct membrane domains on endosomes in the recycling pathway visualized by multicolor imaging of Rab4, Rab5, and Rab11. *J. Cell Biol.* **149,** 901–14 (2000).
78. Gorvel, J. P., Chavrier, P., Zerial, M. & Gruenberg, J. rab5 controls early endosome fusion in vitro. *Cell* **64,** 915–25 (1991).
79. Hutagalung, A. H. & Novick, P. J. Role of Rab GTPases in membrane traffic and cell physiology. *Physiol. Rev.* **91,** 119–49 (2011).
80. Bravo-Cordero, J. J. *et al.* MT1-MMP proinvasive activity is regulated by a novel Rab8-dependent exocytic pathway. *EMBO J.* **26,** 1499–1510 (2007).
81. Wiesner, C., Faix, J., Himmel, M., Bentzien, F. & Linder, S. KIF5B and KIF3A/KIF3B kinesins drive MT1-MMP surface exposure, CD44 shedding, and extracellular matrix degradation in primary macrophages. *Blood* **116,** 1559–1569 (2010).
82. Wiesner, C., Le-Cabec, V., El Azzouzi, K., Maridonneau-Parini, I. & Linder, S. Podosomes in space: Macrophage migration and matrix degradation in 2D and 3D settings. *Cell Adhesion and Migration* **8,** 179–191 (2014).
83. Poincloux, R., Lizárraga, F. & Chavrier, P. Matrix invasion by tumour cells: a focus on MT1-MMP trafficking to invadopodia. *J. Cell Sci.* **122,** 3015–24 (2009).
84. Clark, E. S. & Weaver, A. M. A new role for cortactin in invadopodia: Regulation of protease secretion. *Eur. J. Cell Biol.* **87,** 581–590 (2008).
85. Artym, V. V., Zhang, Y., Seillier-Moiseiwitsch, F., Yamada, K. M. & Mueller, S. C. Dynamic interactions of cortactin and membrane type 1 matrix metalloproteinase at invadopodia: Defining the stages of invadopodia formation and function. *Cancer Res.* **66,** 3034–3043 (2006).
86. Remacle, A. G. *et al.* The transmembrane domain is essential for the microtubular trafficking of membrane type-1 matrix metalloproteinase (MT1-MMP). *J. Cell Sci.* **118,** 4975–4984 (2005).
87. Linder, S. *et al.* The polarization defect of Wiskott-Aldrich syndrome macrophages is linked to dislocalization of the Arp2/3 complex. *J. Immunol.* **165,** 221–5 (2000).
88. Schmidt, S. *et al.* Kindlin-3-mediated signaling from multiple integrin classes is required for osteoclast-mediated bone resorption. *J. Cell Biol.* **192,** 883–897 (2011).
89. Gawden-Bone, C. *et al.* A critical role for beta2 integrins in podosome formation, dynamics and TLR-signaled disassembly in dendritic cells. *J. Cell Sci.* 4213–4224 (2014). doi:10.1242/jcs.151167
90. Ruoslahti, E. RGD and Other Recognition Sequences for Integrins. *Annu. Rev. Cell Dev. Biol.* **12,** 697–715 (1996).
91. Branch, K. M., Hoshino, D. & Weaver, A. M. Adhesion rings surround invadopodia and promote maturation. *Biol. Open* **1,** 711–722 (2012).
92. Mueller, S. C. *et al.* A novel protease-docking function of integrin at invadopodia. *J. Biol. Chem.* **274,** 24947–24952 (1999).
93. Gálvez, B. G., Matías-Román, S., Yáñez-Mó, M., Sánchez-Madrid, F. & Arroyo, A. G. ECM regulates MT1-MMP localization with β1 or αvβ3 integrins at distinct cell compartments modulating its internalization and activity on human

endothelial cells. *J. Cell Biol.* **159,** 509–521 (2002).
94. Puyraimond, A., Fridman, R., Lemesle, M., Arbeille, B. & Menashi, S. MMP-2 colocalizes with caveolae on the surface of endothelial cells. *Exp. Cell Res.* **262,** 28–36 (2001).
95. Galvez, B. G. *et al.* Caveolae are a novel pathway for membrane-type 1 matrix metalloproteinase traffic in human endothelial cells. *Mol Biol Cell* **15,** 678–687 (2004).
96. Furse, S. *et al.* Lipid membrane curvature induced by distearoyl phosphatidylinositol 4-phosphate. *Soft Matter* **8,** 3090–3093 (2012).
97. Nolen, B. J. *et al.* Characterization of two classes of small molecule inhibitors of Arp2/3 complex. *Nature* **460,** 1031–1034 (2009).
98. Strongin, a. Y. *et al.* Mechanism Of Cell Surface Activation Of 72-kDa Type IV Collagenase. *Journal of Biological Chemistry* **270,** 5331–5338 (1995).
99. Ohuchi, E. *et al.* Membrane type 1 matrix metalloproteinase digests interstitial collagens and other extracellular matrix macromolecules. *J. Biol. Chem.* **272,** 2446–2451 (1997).
100. Itoh, Y. *et al.* Cell surface collagenolysis requires homodimerization of the membrane-bound collagenase MT1-MMP. *Mol. Biol. Cell* **17,** 5390–9 (2006).
101. Tochowicz, A. *et al.* The dimer interface of the membrane type 1 matrix metalloproteinase hemopexin domain: crystal structure and biological functions. *J. Biol. Chem.* **286,** 7587–7600 (2011).
102. Rozanov, D. V. *et al.* Mutation analysis of membrane type-1 matrix metalloproteinase (MT1-MMP): The role of the cytoplasmic tail Cys574, the active site Glu 240, and furin cleavage motifs in oligomerization, processing, and self-proteolysis of MT1-MMP expressed in breast carcinoma cells. *J. Biol. Chem.* **276,** 25705–25714 (2001).
103. Uekita, T., Itoh, Y., Yana, I., Ohno, H. & Seiki, M. Cytoplasmic tail-dependent internalization of membrane-type 1 matrix metalloproteinase is important for its invasion-promoting activity. *J. Cell Biol.* **155,** 1345–1356 (2001).
104. Yu, X. *et al.* N-WASP coordinates the delivery and F-actin-mediated capture of MT1-MMP at invasive pseudopods. *J. Cell Biol.* **199,** 527–544 (2012).
105. Moss, N. M., Wu, Y. I., Liu, Y., Munshi, H. G. & Stack, M. S. Modulation of the membrane type 1 matrix metalloproteinase cytoplasmic tail enhances tumor cell invasion and proliferation in three-dimensional collagen matrices. *J. Biol. Chem.* **284,** 19791–9 (2009).
106. Akisaka, T., Yoshida, H., Suzuki, R. & Takama, K. Adhesion structures and their cytoskeleton-membrane interactions at podosomes of osteoclasts in culture. *Cell Tissue Res.* **331,** 625–641 (2008).
107. Burgstaller, G. & Gimona, M. Podosome-mediated matrix resorption and cell motility in vascular smooth muscle cells. *Am. J. Physiol. Heart Circ. Physiol.* **288,** H3001–H3005 (2005).
108. von Nandelstadh, P. *et al.* Actin-associated protein palladin promotes tumor cell invasion by linking extracellular matrix degradation to cell cytoskeleton. *Mol. Biol. Cell* **25,** 2556–70 (2014).
109. Mykkänen, O. M. *et al.* Characterization of human palladin, a microfilament-associated protein. *Mol. Biol. Cell* **12,** 3060–73 (2001).
110. Rönty, M. *et al.* Palladin interacts with SH3 domains of SPIN90 and Src and is required for Src-induced cytoskeletal remodeling. *Exp. Cell Res.* **313,** 2575–2585 (2007).
111. Bravo-Cordero, J. J. *et al.* MT1-MMP proinvasive activity is regulated by a

novel Rab8-dependent exocytic pathway. *EMBO J.* **26,** 1499–1510 (2007).
112. Linford, A. *et al.* Rab14 and Its Exchange Factor FAM116 Link Endocytic Recycling and Adherens Junction Stability in Migrating Cells. *Dev. Cell* **22,** 952–966 (2012).
113. Kauppi, M. *et al.* The small GTPase Rab22 interacts with EEA1 and controls endosomal membrane trafficking. *J. Cell Sci.* **115,** 899–911 (2002).
114. Tessneer, K. L., Jackson, R. M., Griesel, B. A. & Olson, A. L. Rab5 activity regulates GLUT4 sorting into insulin-responsive and non-insulin-responsive endosomal compartments: A potential mechanism for development of insulin resistance. *Endocrinology* **155,** 3315–3328 (2014).
115. Kajiho, H. *et al.* RAB2A controls MT1-MMP endocytic and E-cadherin polarized Golgi trafficking to promote invasive breast cancer programs. *EMBO Rep.* **17,** 1061–80 (2016).
116. Friedl, P. & Wolf, K. Proteolytic interstitial cell migration: A five-step process. *Cancer and Metastasis Reviews* **28,** 129–135 (2009).
117. Hattula, K. *et al.* Characterization of the Rab8-specific membrane traffic route linked to protrusion formation. *J. Cell Sci.* **119,** 4866–77 (2006).
118. Subramani, D. & Alahari, S. K. Integrin-mediated function of Rab GTPases in cancer progression. *Mol. Cancer* **9,** 312 (2010).
119. Sparano, J. A. *et al.* Randomized phase III trial of marimastat versus placebo in patients with metastatic breast cancer who have responding or stable disease after first-line chemotherapy: Eastern Cooperative Oncology Group Trial E2196. *J. Clin. Oncol.* **22,** 4631–4638 (2004).
120. Fingleton, B. MMPs as therapeutic targets-Still a viable option? *Seminars in Cell and Developmental Biology* **19,** 61–68 (2008).
121. Huotari, J. & Helenius, A. Endosome maturation. *EMBO J.* **30,** 3481–3500 (2011).
122. Junutula, J. R. *et al.* Rab14 Is Involved in Membrane Trafficking between the Golgi Complex and Endosomes □ V. *Mol. Biol. Cell* **15,** 2218–2229 (2004).
123. Jacob, A. & Prekeris, R. The regulation of MMP targeting to invadopodia during cancer metastasis. *Front. cell Dev. Biol.* **3,** 4 (2015).

VII. LIST OF FIGURES

VIII. LIST OF ABBREVIATIONS

ADAM10	A disintegrin and metalloproteinase domain-containing protein 10
AP-2	Adaptor protein 2
Arp2/3	Actin-Related Protein2/3
CD44	Cluster of differentiation 44
CK-666	2-Fluoro-N-[2-(2-methyl-1H-indol-3-yl)ethyl]-benzamide
ECM	Extracellular matrix
EE	Early endosomes
EEA1	Early Endosome Antigen 1
ER	Endoplasmic reticulum
ER	Endoplasmic reticulum
GDI	Guanine dissociation inhibitor
GEFs	Guanine nucleotide exchange factors
GFP	Green fluorescent protein
GLUT4	Glucose transporter type 4
GRASP55	Golgi matrix protein Golgi reassembly stacking protein 55
GTPases	Guanine tyrosine phosphatases
Hpx	Hemopexin
IL-1	Interleukin 1
IL-10	Interleukin 10
IL-13	Interleukin 13
IL-1ra	IL-1 receptor antagonist
IL-23	Interleukin 23
IL-4	Interleukin 4
IL-6	Interleukin 6
KD	Knock down
KIF3A/KIF3B	Kinesin family-3A/3B
KIF5B	Kinesin family-5B
LE	Late endosomes
LPS	Lipopolysaccharide
M2a	Macrophages 2a
M2b	Macrophages 2b
M2c	Macrophages 2c
M-CSF	Macrophage colony stimulating factor
MDA-MB-231	M.D. Anderson - metastatic breast-231
NO	Nitric oxide
NSC405020	3,4-dichloro-N-pentan-2-ylbenzamide
PCs	Proprotein convertases
PI(4)P	Phosphatidylinositol 4-phosphate
Rab	Ras-related proteins in brain
RE	Recycling endosomes

ROIs	Reactive oxygen intermediates
siRNA	Small interfering ribonucleic acid
Src	Proto-oncogene tyrosine-protein kinase
TGF-β	Transforming growth factor β
TGF-β	Transforming growth factor beta
TIMPs	Tissue inhibitor of metalloproteinases
TIRF	Total internal reflection fluorescence
Tks5	Tyrosine kinase substrate 5
TLR	Toll-like receptor
TNF-α	Tumor necrosis factor α

IX. DECLARATION ON OATH

I hereby declare, on oath, that I have written the present dissertation on my own and have not used other than the acknowledged resources and aids.

Hamburg, 03.11.2016

_____
Karim EL AZZOUZI